N-24659

NOISE AND VIBRATION CONTROL FOR WIND TUNNELS

A Thesis

Presented to

the Faculty of the Department of Engineering

The University of Virginia

In Partial Fulfillment

of the Requirements for the Degree

Master of Applied Mechanics

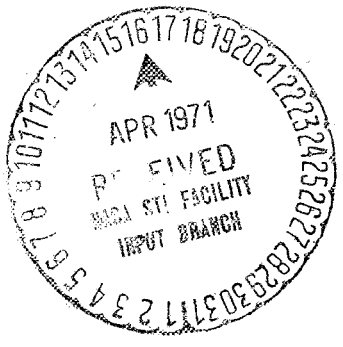

by

William C. Sperry

June 1953

NOISE AND VIBRATION CONTROL FOR WIND TUNNELS

A Thesis

Presented to

the Faculty of the Department of Engineering

The University of Virginia

In Partial Fulfillment

of the Requirements for the Degree

Master of Applied Mechanics

---

by

William C. Sperry

June 1953

APPROVAL SHEET

This thesis is submitted in partial fulfillment of
the requirements for the degree of
Master of Applied Mechanics

_____
Author

Approved:

_____
Faculty Advisor

_____
For Subcommittee

_____
Chairman, Committee on Graduate Studies
in Engineering

June 1953

TABLE OF CONTENTS

CHAPTER		PAGE
I.	INTRODUCTION	1
	Purpose	1
	Quantitative and qualitative control	2
	Noise control defined	3
	Noise and vibration control related	4
	Effects of noise upon human auditors	5
	Planning control measures	6
	Generation of noise	11
	Control methods (types and uses)	13
	Turbulence damping screens	13
	Acoustic baffles	13
	Test section noise	14
	Rigid connections for turning vanes	15
	Airborne noise	15
	Structure-borne energy	16
	Vibration break and helical springs	16
	Stiffening tunnel structure	17
	Insulating blanket	18
	Resonators	18
	Discussion of some control measures at Langley Field	19
	16-foot transonic tunnel	19
	8-foot transonic pressure tunnel	26

CHAPTER PAGE

8-foot transonic tunnel 26

Unitary Plan 4- by 4-foot supersonic tunnel . 26

7- by 10-foot high-speed tunnel 31

Symbols 34

II. ACOUSTIC BAFFLES 38

Description 38

Uses 39

Case 1: Surface lined rectangular duct . . . 39

Case 2: Rectangular duct with baffles, all surfaces lined 41

Case 3: Rectangular duct with baffles, top and bottom surfaces unlined 43

Case 4: Surface lined circular duct 45

Case 5: Unlined circular duct with baffles . 47

Absorption coefficient 53

Drag losses and friction factors 57

III. NOISE INSULATION 63

Definition 63

Random incidence mass law 64

Basic principles for design 66

Comments for use of mass law graph 67

Attenuation of noise through partitions 68

Partitions with openings (noise leaks) 75

CHAPTER PAGE

IV. EXAMPLE - 7- BY 10-FOOT HIGH-SPEED TUNNEL 78

Existing problems 78

Corrective measures 78

Method of noise analysis 83

Detailed analysis and computations 88

V. CONCLUDING REMARKS 98

REFERENCES 100

APPENDIX A - TURNING VANE SUPPORT FOR ELLIPTICAL CORNER RINGS 102

Discussion 102

Symbols 106

References 108

Geometry 109

General loading 115

Pressure loading 120

Pressure plating loading 128

APPENDIX B - HELICAL COMPRESSION SPRINGS SUBJECTED TO COMBINED LOADING 138

Discussion 138

Symbols 143

References 147

Spring geometry 148

General loading 159

CHAPTER PAGE

Axial loading 163
Lateral loading 170
Bending moment 178
Combined loading 183
Deflections 185
Unit stresses 222
Design 232
Example 275

CHAPTER I

INTRODUCTION

The design of a modern wind tunnel together with its shops, offices, and laboratories such as the 8-foot transonic tunnel or the Unitary Plan 4- by 4-foot supersonic tunnel designed by and built for the National Advisory Committee for Aeronautics located at Langley Field, Va., requires the combined efforts of scores of engineering and scientific personnel. Civil, structural, mechanical, electrical, and aeronautical engineers, physicists, metallurgists, architects, mathematicians, and chemists pool their scientific abilities to produce this gigantic, high powered, multimillion dollar research facility necessary to the development of modern and future aircraft.

Although scientific achievements today, at the beginning of the atomic age, are phenomenal compared with 50 or even 25 years ago, it is still impossible, apparently, to produce something that fulfills its purpose, completely and efficiently, within the laws of the universe, without unwanted or detrimental byproducts. Wind tunnels are no exception. One important, unwanted byproduct of wind tunnels is noise.

It is the purpose of this thesis to record results of experience, investigations, and theoretical development, for

noise and vibration control for wind tunnels, by the author while acting in the capacity of structural designer for the National Advisory Committee for Aeronautics at Langley Field, Va. The material contained herein is offered as an aid to the structural engineer in the original design of the main structure and its appurtenances or, in part, as modifications to a completed structure.

Noise and vibration control for wind tunnels is a specialized subject. However, most of the material contained herein, if considered individually, has much more general application as will be noted. In fact, two of the topics, helical springs and turning vane support, are arranged as self-contained units in the appendix due as much to their general application as to their lengths of context.

The following material offered as noise and vibration control may be classified into two parts; quantitative and qualitative control. Quantitative control is the treatment for which predictions can be made that can be reasonably verified by testing. Qualitative control is the treatment which logically and by experience has merit but cannot easily be verified by testing. Although the degree of merit is unknown, so far as noise and vibration control are concerned, other advantages, resulting in increased strength

and economy, make the qualitative control measures discussed herein worth consideration.

Noise control shall be defined as: the acoustic treatment necessary to reduce the noise level, at a specific location, a predetermined amount without inhibiting the functions of the noise source and the auditors by more than a predetermined acceptable amount. The term auditor refers to a person, instrument, or piece of equipment that is concerned with noise. Noise control, as defined above, is not merely noise reduction but includes reasonable predictions for the noise reduction and the loss of efficiency, if any, of the noise source and the auditors. The problem is frequently complicated by the existence of several noise sources or one or more primary sources or one or more secondary sources. Therefore, the noise control problem may include the evaluation of the primary and secondary noise sources, the relative importance of each, and the application of acoustic treatment for one or more of the noise sources. In special cases, the acoustic treatment may neglect the noise sources and be applied to the auditors in such form as sound proof rooms, booths, or containers, helmets, and earplugs.

In general, the noise control problem is not simple. Very few problems are similar but most problems contribute useful experience for future application. Paradoxically,

noise reduction may be quite simple in concept. Given sufficient material and labor, most noises may be effectively eliminated before reaching the auditors. However, the expenditure of material and labor may be impractical in the sense that an acceptable reduction in noise level and efficiency might be accomplished with much less expenditure. Thus noise control may be simply defined as practical noise reduction.

Since noise represents dynamic or vibrational energy having amplitude and frequency within the audible range, the problems of noise control and vibration control are related. For, if vibration is eliminated, noise is nonexistent. However, the converse does not necessarily follow. While a noise generator has vibration, control of the noise, so far as the auditors are concerned, may have little or no effect upon the vibration. Only if noise and vibration have detrimental effects, do control problems arise. The detrimental effects may or may not be obvious since the sensitivity of the auditors, equipment and supporting structure is dependent upon many factors. The noise intensity and quality that can be tolerated by auditors, especially human beings, generally is more determinant than the vibrational intensity and quality that can be tolerated by machinery, supporting structure, and instruments. This is

due, principally, to the fact that human beings, as auditors, are able to register complaints and so indicate sensitivity.

The detrimental effects of noise upon the average human auditor are dependent upon, primarily, the intensity and frequency of the noise reaching the auditor and, secondarily, the function of the auditor. The effects vary, in increasing order, from minor annoyance, loss of efficiency, headaches, nausea, to actual pain and possibly permanent physical damage. Annoyance and loss of efficiency are dependent upon the auditor's function. For instance, if the function of the human auditor is to sleep or recuperate from illness, his tolerance to noise may be considerably less than otherwise. Furthermore, the annoying or distracting effects of noise are greater for those human auditors engaged in skilled and professional duties than for those engaged in unskilled or routine duties. Figures 1, 2, and 3 illustrate the effects of noise upon human auditors. These figures are the results of hundreds of tests and represent averages; consequently, any particular auditor may deviate from the average. However, these figures are useful in predicting the detrimental effects that may be produced by a noise generator.

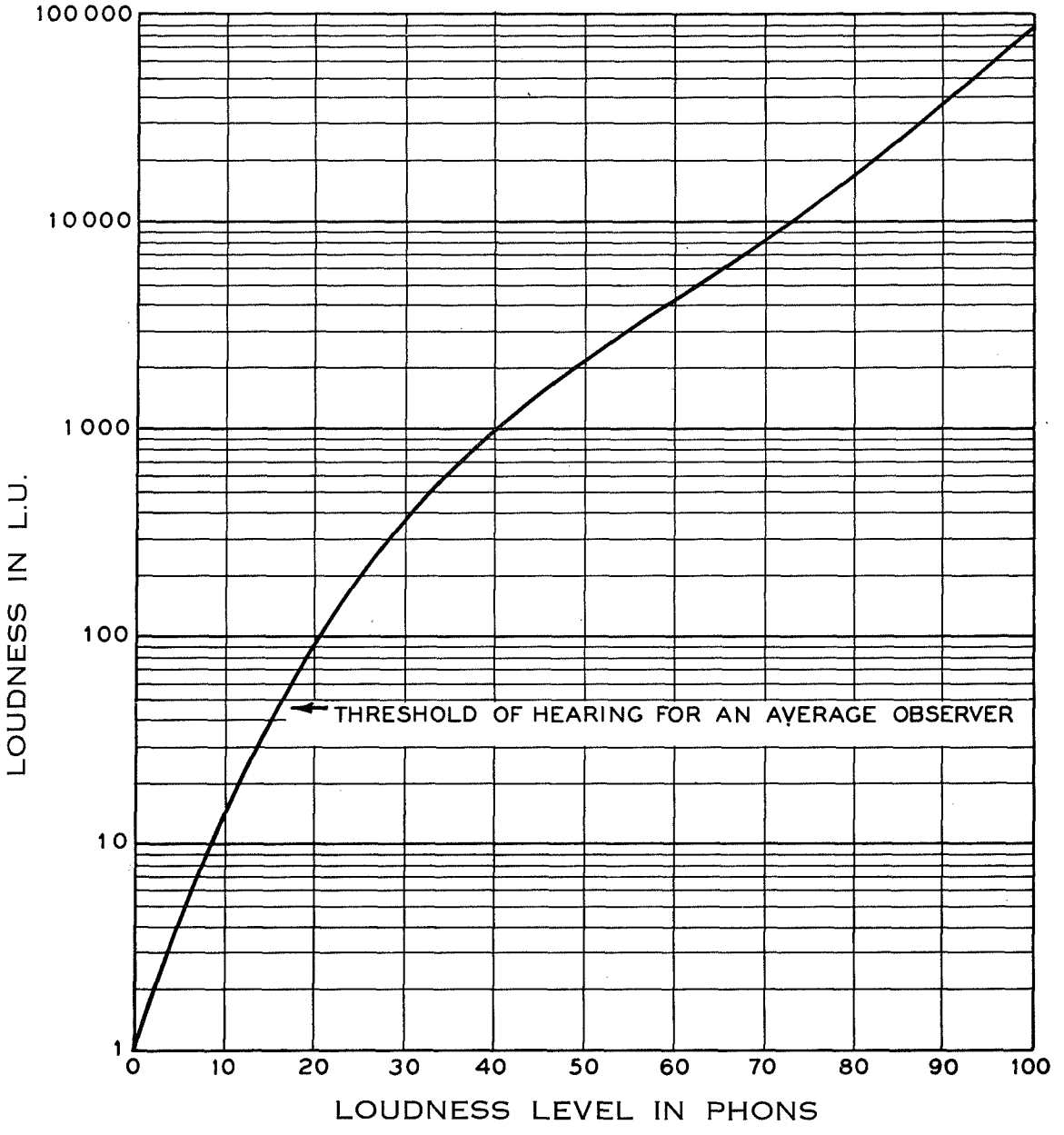

FIG. 1. Relation between Loudness and Loudness Level.

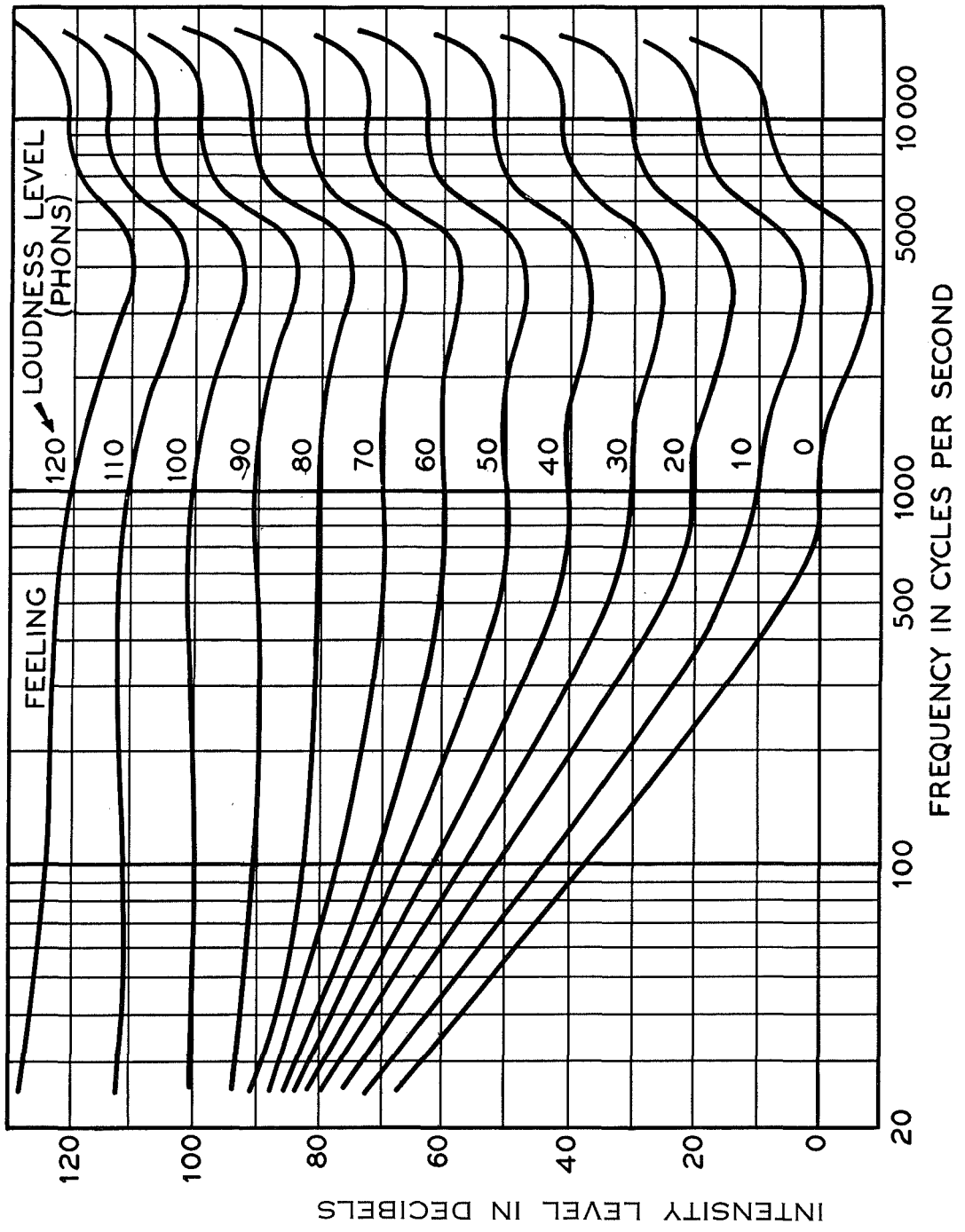

FIG. 2. Loudness Contours.

HUMAN HEARING

SCHEMATIC REPRESENTATION OF INTENSITY AND FREQUENCY CHARACTERISTICS OF THE HUMAN EAR AND LOUDNESS OF SOUNDS

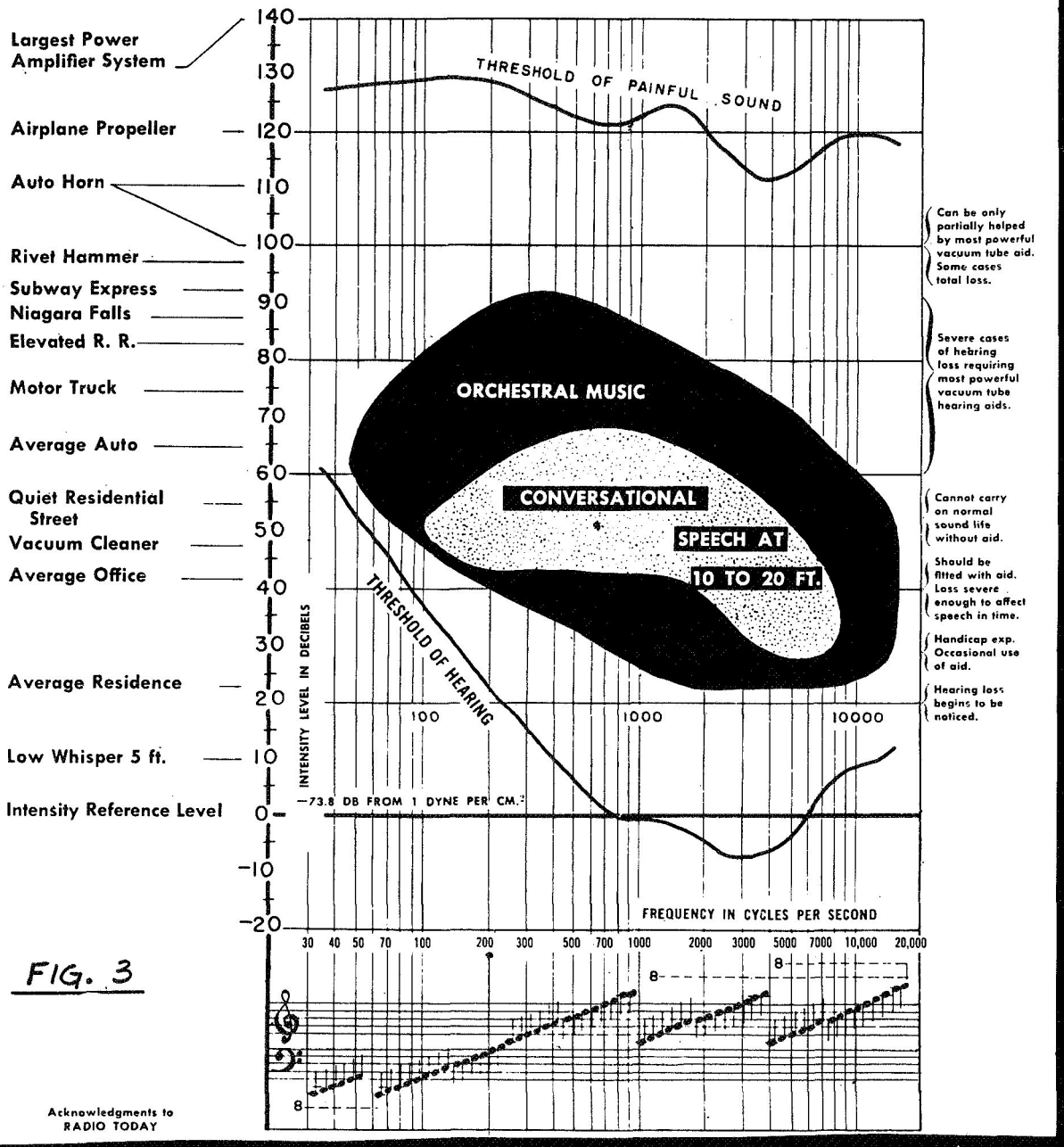

FIG. 3

Acknowledgments to RADIO TODAY

Generally, the detrimental effects of vibration are even more difficult to predict than noise. Frequently, it isn't until failure of some sort or malfunctioning of machinery or equipment occurs that harmful vibratory motion is apparent. However, in most cases, vibration control is less difficult than noise control.

Since noise and vibration are related, it is advantageous, from the standpoint of economy, to provide treatment that will control both. Any treatment that decreases the amplitude of vibration will have a corresponding effect upon noise. It is sometimes possible, by structural modification, to change the vibrational frequency spectrum of a wind tunnel so that both noise and vibration control result.

Careful consideration should be given to the type and amount of acoustic treatment to be applied to a wind tunnel. It is expensive and impractical to attempt to reduce the noise level below an acceptable maximum amount which will be governed by the average existing background noises and the comfort and efficiency of the auditors. This should be determined in advance and then noise control measures planned to reach that objective. Many features can be incorporated in the design of a wind tunnel that have other advantages as well as noise and vibration control and effort

should be made to include as many of these in the original design as is feasible.

If a wind tunnel exists, is in operation, and proves to be a noise generator to an objectionable degree, the problem of noise control may be less complicated than if the wind tunnel is still in the design stage. A noise survey of the existing wind tunnel can be made, the frequencies analyzed, the location of the primary and possibly several secondary noise sources determined and then modifications made for controlling the noise. For the case of the wind tunnel in the design stage, considerable difficulty may arise in making reasonable predictions for the noise level, frequencies, and primary and secondary sources, but if this can be accomplished, then the noise control measures can be more easily incorporated in the original design and construction than as modifications after completion. It follows, therefore, that predetermination of primary and secondary noise sources and their intensity and quality has great advantage for noise control and considerable effort should be expended for that achievement. There is no general method, to the author's knowledge, of predicting the general noise characteristics of a wind tunnel other than a comparison with similar existing structures. Experience has shown, however, that while a quantitative analysis may not be accomplished, qualitative measures for noise control may

be incorporated in the original design, and allowances made for additional acoustic treatment after completion and operation of the wind tunnel, at which time, noise measurements can be obtained to determine the extent of the additional treatment required.

In general, the noise energy of a wind tunnel is generated principally by the fan or compressor and has a spectrum with major components corresponding to the first several harmonics of the fan. The first harmonic of the fan, in cycles per second, will be the revolutions per second times the number of blades. However, the noise spectrum may not correspond to the fan harmonics as defined above if the fan blades pass in close proximity to objects in the air stream such as supporting members, counter vanes, and other fan blades but may contain components of higher intensities and frequencies than those if the air stream obstructions were nonexistent. From the standpoint of qualitative noise control, it is advantageous to keep air stream obstructions as far removed from the fan as structural and aerodynamic requirements will permit.

The function of a wind tunnel is to impart kinetic energy to the air stream in the form of a mass movement of air and to direct this movement by structural configuration so that controlled velocities are obtained at the test section. The fan imparts kinetic energy to the air stream

consisting of two parts; energy of motion of the air as a whole, and dynamic or oscillatory energy. The dynamic energy is valueless and generally objectionable, for that part of the dynamic energy with amplitude and frequency within the audible range is noise. Furthermore, since the energy output of the fan is limited, the dynamic energy within the air stream represents a functional loss for the wind tunnel, for from the law of conservation of energy, less mass flow energy is available. Dynamic energy, in addition to that directly imparted by the fan, is created within the air stream by turbulent air flow conditions. Usually, turbulent flow results from changes in configuration of the tunnel structure and the presence of obstructions in the air stream such as structural supporting members and turning and counter vanes. The dynamic turbulent energy, like that imparted by the fan represents a functional energy loss and is a noise generator as well. From the standpoint of qualitative noise control, it is advantageous to eliminate or prevent the creation of as much dynamic energy within the air stream as is feasible, which, of course, is desirable for tunnel efficiency as well and usually consideration is given to turbulence prevention in wind tunnel design.

In the original design, if more consideration were given to the prevention and elimination of dynamic energy, it is quite possible that the required amount of acoustic

treatment, of the type that has no other function than acoustic treatment, would be appreciably lessened with the added advantage of a more efficient tunnel. The design of a multistage fan system with low rotational velocities compared with conventional fan systems, would have a great effect in reducing the dynamic energy at its source. A satisfactory system of this type might not prove feasible but might well be worth investigating.

Experience at Langley Field has shown that installation of turbulence damping screens in the wind tunnel settling chamber has had excellent results in decreasing turbulence in the test section. The turbulence damping screens consist of several, closely woven, small diameter wire screens, preloaded and elastically supported by helical springs and installed parallel to each other and perpendicular to the tunnel axis. The drag losses through properly designed screens may be all or in part regained by the conversion of turbulent dynamic energy to mass flow energy. While quantitative acoustic data are not available at present, it is reasonable to assume that the turbulence damping screens have merit for noise control.

A method of partially absorbing the dynamic energy of the air stream is to install absorption material in the form of acoustic baffles at convenient locations in the tunnel circuit. This method is discussed in chapter II. The

acoustic baffles effect an appreciable noise reduction by converting a portion of the dynamic energy to heat. Like the turbulence damping screens, the drag losses through the baffles may be partially regained by conversion of turbulent dynamic energy to mass flow energy.

Two sources of noise energy within the wind tunnel air stream have been discussed; the dynamic energy generated by the fan, and the dynamic energy due to turbulence. Additional sources of noise may exist, particularly in the vicinity of the test section, such as the noise generated by shock waves, the induced noise due to model configuration, and the noise due to the fact that the model may be a powered source. Since the author has gathered very little information concerning test section noise, no recommendations will be made in this paper for noise control measures to be incorporated in the original design of the test section. However, after completion and operation of the tunnel, if the test section noise is objectionable, a noise insulating blanket, as discussed in chapter III may prove effective.

Another source of noise within the tunnel air stream is that generated by obstructions not rigidly fastened. For instance, it is common practice to rigidly fasten the turning vanes at one end and provide guided supports at the other end to allow for thermal expansion and contraction.

These guided supports often become loose and due to the action of the air stream, induced vibratory motion occurs generating noise and frequently fatigue failures. From the standpoint of qualitative noise control it is good practice to rigidly fasten, wherever feasible, all obstructions. One new tunnel at Langley Field has been designed with the turning vanes acting as structural members, aiding the elliptical corner rings in supporting the corner loading. Each end of the turning vanes is rigidly fastened to the corner ring so that the ring and vanes act as a structural unit. The vanes contribute materially to the rigidity of the unit so that the required cross section of the ring results in a plate instead of a large rolled or built-up member. The vanes are no longer structural parasites, for in addition to their function of changing the air stream direction, they contribute to over-all rigidity of the tunnel structure. A discussion of turning vanes, combined as an integral unit with elliptical corner rings, is included as appendix A.

Generally, the noise generated by a wind tunnel will most concern those auditors stationed outside the tunnel structure. Airborne noise will reach the auditors directly through openings in the tunnel structure if any exist such as air exchange towers, and by radiation from the tunnel structure. The direct airborne noise may be controlled

entirely or in part by acoustic baffles, as discussed in chapter II, by deflecting the noise away from the auditors, and by providing a tortuous passage for the noise to reach the auditors. High frequency noise has greater directional characteristics than low frequency noise so that the methods of deflection and provision of tortuous passages will have greater effect with high frequencies than with low. The noise radiating from the tunnel structure is caused by induced vibrations of the structure and consists principally of two parts; the vibrations induced by the dynamic air stream energy and the vibrations induced by solid or structure-borne energy. The structure-borne noise can be reduced by the inclusion, in the tunnel design, of vibration breaks which may be defined as a change in configuration and continuity of the structure of such form that the transference of solid borne vibrational energy past the change in continuity is eliminated or appreciably reduced. The most effective vibration break would be an air gap or the absence of solid contact which for most tunnels would be impractical. However, effective and practical vibration breaks can be designed for which the change in continuity is represented by an elastic medium such as a helical spring.

The major portion of the solid borne vibration is created in the vicinity of the tunnel drive motor and it is expedient to isolate this section, so far as is feasible,

from the remainder of the structure. Other vibration breaks may be incorporated as part of the expansion joints, several of which are generally required in the tunnel circuit to permit compensation for thermal expansion and contraction. Several wind tunnels at Langley Field have elastically supported expansion joints which also serve as vibration breaks. The helical springs, furnishing the elastic medium, are designed for both axial and lateral movement and permit thermal adjustment while contributing vertical support. A discussion of helical springs subjected to combined loading is included as appendix B.

In general, the noise radiating from the tunnel structure will be diminished or at least be capable of more effective control if the tunnel structure is stiff rather than flexible. This may not always be true but within the scope of the author's experience, and from the standpoint of qualitative noise control, increased stiffness has merit. Possibly, this arises from the fact that increased stiffness increases the natural frequencies of the tunnel structure and its component parts and that the frequencies of the major components of the impressed force for most wind tunnels are relatively low so that resonance tends to occur only at the higher frequencies where the amplitudes are small. The tendency for true resonant conditions to exist at high frequencies is small for there appears to be more structural

damping in a stiff structure than in a flexible one. Since the frequencies of the major components of the impressed forces are relatively low compared to the natural frequencies of the stiff structure, the major components will not be amplified and what amplification occurs will be at the higher frequencies which are more easily controlled by noise insulating blankets as indicated in chapter III. It follows therefore, that greater noise control success will generally be obtained from a stiff, sturdy structure than from a flexible structure. It should be pointed out that the feature of incorporating turning vanes as structural corner supports contributes materially to the stiffness of the wind tunnel. Usually, it is impractical to effect noise reduction by increasing the tunnel shell thickness, for from chapter III, it is seen that doubling the weight of the shell reduces the noise only 3 decibels. A noise insulating blanket will be much more effective for the same expenditure.

The two methods of quantitative noise control, acoustic baffles and noise insulating blankets, discussed in chapters II and III, respectively, are particularly effective at high frequencies but not at low frequencies. The low frequency components of noise are troublesome to control. Apparently, the only effective means of controlling low frequency noise generated by wind tunnels is by the inclusion, within the tunnel circuit, of resonating chambers

tuned to the predominating low frequencies. This method is comparatively new and will not be discussed in this thesis. One method, purely speculative, that may have qualitative merit for the control of low frequency noise is to design portions of the tunnel structure, and the supporting system for the acoustic baffles and turbulent damping screens so that their natural frequencies are resonant or nearly so with the predominant low frequency components of the generated noise. A portion of the noise energy would therefore be converted to heat due to the work done upon the structural system. A certain amount of damping would probably be necessary to prevent excessive vibrational amplitude.

The remainder of this chapter will be devoted to a general discussion of noise and vibration control measures that have been incorporated in the design and construction of several wind tunnels forming part of the physical plant of the National Advisory Committee for Aeronautics located at Langley Field, Va.

Figure 4 is an aerial photograph of the 16-foot transonic tunnel which, recently, has been repowered and modified. Before repowering, the noise level, while high, could be tolerated and vibration was never a serious problem so far as the tunnel structure was concerned. It was believed, however, that noise and vibration control measures would be necessary to compensate for the effects

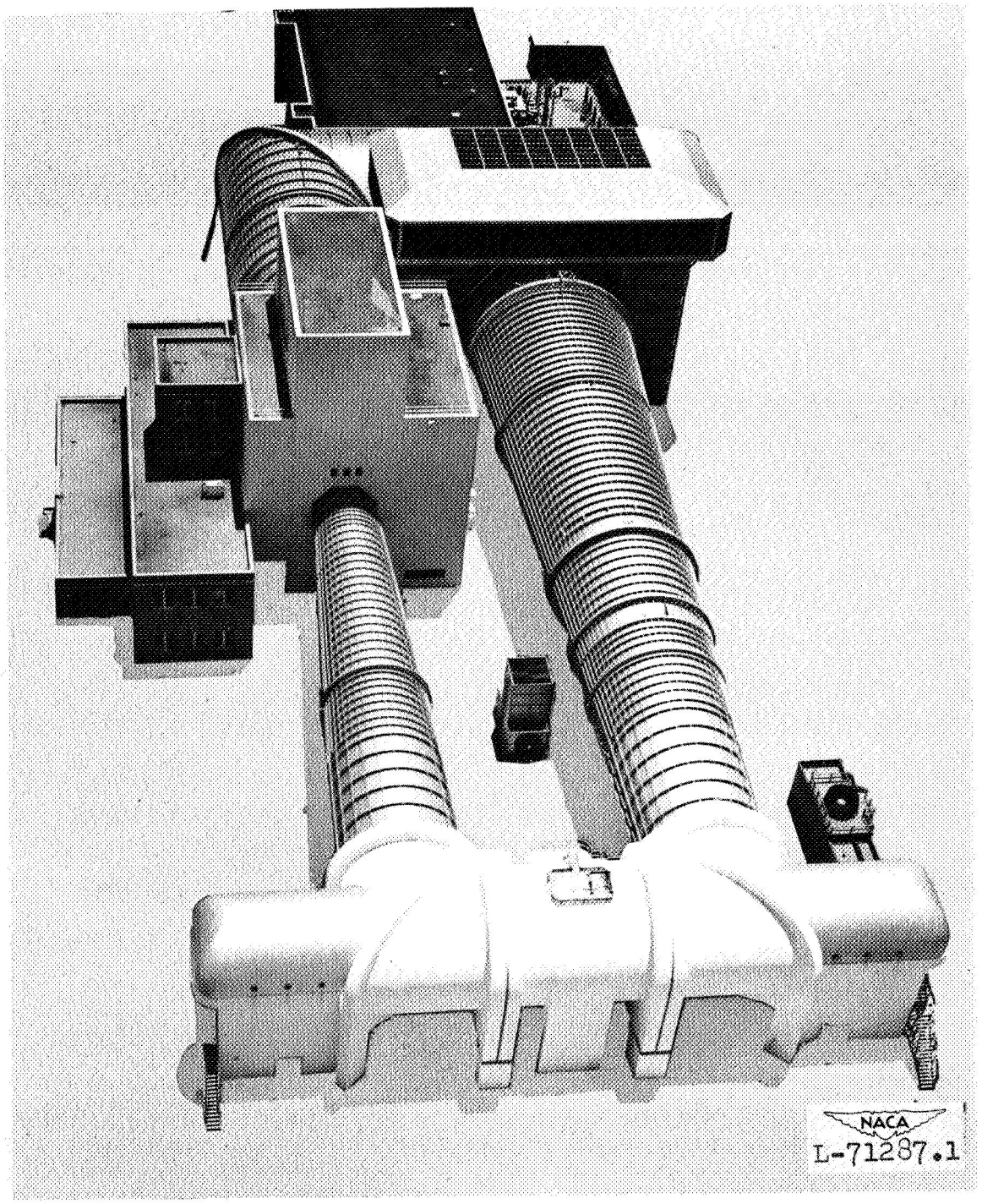

FIGURE 4

16-FOOT TRANSONIC TUNNEL

of the new power plant. The treatment, incorporated as part of the modifications, consisted of four parts:

(1) Enclosing the tunnel fans in a massive concrete housing

(2) Installing acoustic baffles in the air exchange tower

(3) Stiffening the tunnel shell

(4) Providing vibration breaks between the steel connecting shells and the concrete fan housing

It was anticipated that, at best, the above treatment would keep the noise level to about the same as that before modification and that vibration would be adequately controlled. If, after operation of the new power plant, the noise level could not be tolerated, further treatment in the form of an insulating blanket could be applied to the tunnel shell and the air exchange tower walls.

The function of part 1, the massive housing, shown in the lower portion of Figure 4, is to contain the noise generated by the fans so that the drive section will not be the major source of noise radiation. Furthermore, due to its massiveness, the amplitude of vibration in the vicinity of the drive section is minimized.

The function of part 2, the acoustic baffles, is to attenuate the airborne noise emitted from the louvers of the air exchange tower. In addition, the baffles attenuate,

somewhat, the noise radiating from the walls of the air exchange tower. Figure 5 is a photograph of a portion of the acoustic baffling system.

The function of part 3, tunnel shell stiffening, is to preclude the possibility of vibration and fatigue failures. The stiffening, in this case, contributes little or nothing to the reduction of the over-all noise level. Figure 6 is a photograph of the air exchange tower and adjacent portions of the tunnel shell clearly indicating the stiffening members.

The function of part 4, the vibration break, is to reduce the structure-borne noise and vibration transferred from the concrete fan and motor housing to the steel connecting shells. The connecting shells are supported by nests of helical springs which in turn are supported by concrete brackets integral with the housing. The shell and housing are separated by an air gap, their only contact being the springs. A neoprene seal prevents air and dirt from leaking into the air stream. Figure 7 is a construction photograph of the inside tunnel loop showing portions of the connecting shells, concrete housing, and spring nests. Supports for the connecting shells are as far removed from the drive housing as is practical in order to minimize the transmittance of vibration through the earth. Due to the length of connecting shells from the nearest anchor point,

FIGURE 5

ACOUSTIC BAFFLES IN AIR EXCHANGE TOWER
16-FOOT TRANSONIC TUNNEL

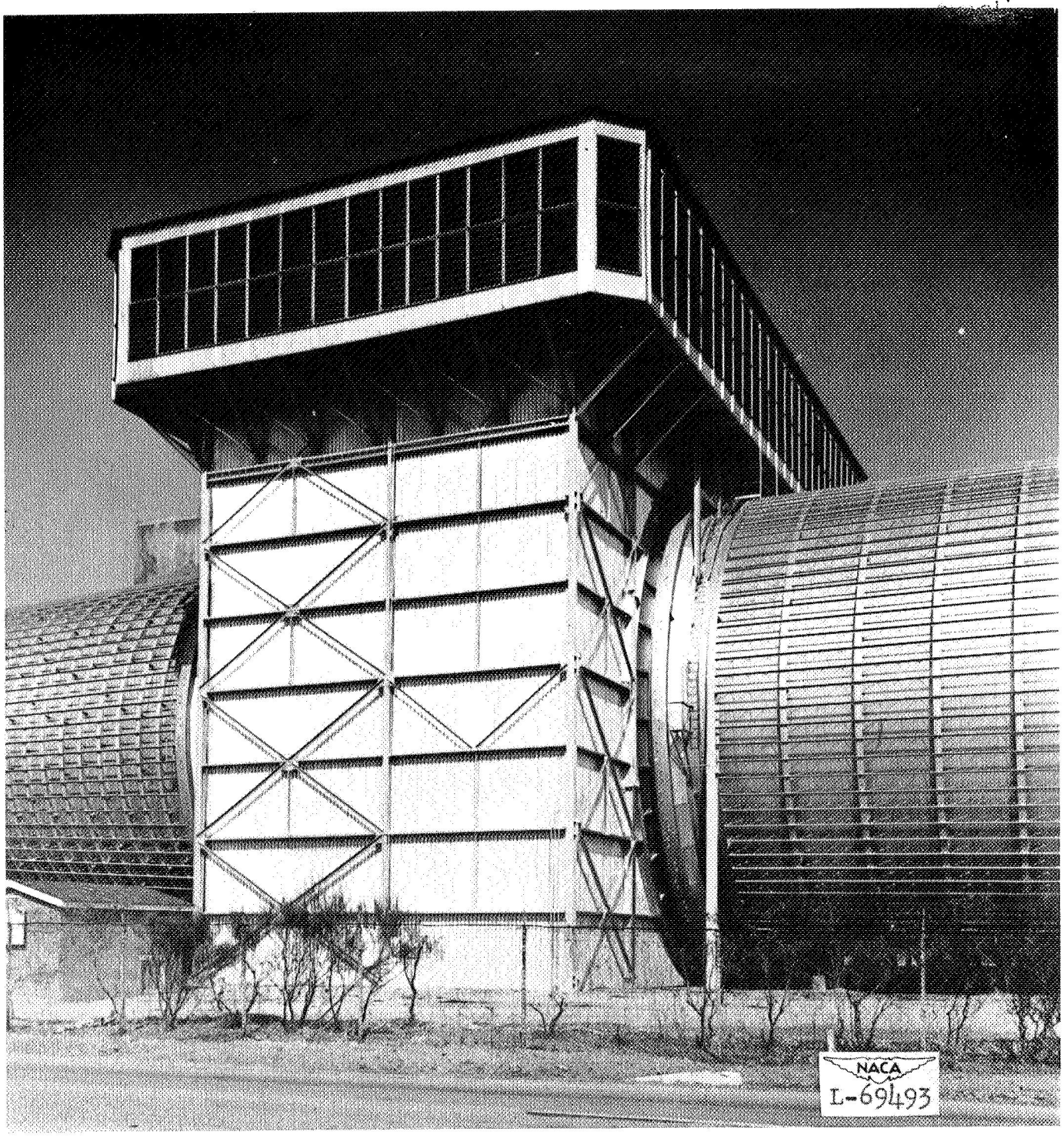

FIGURE 6

AIR EXCHANGE TOWER
16-FOOT TRANSONIC TUNNEL

FIGURE 7

DRIVE HOUSING AND CONNECTING SHELLS
16-FOOT TRANSONIC TUNNEL

the vibration break has the auxiliary function of expansion joint. The helical springs are subjected to both axial forces due to the dead load of the shells and lateral deflection due to thermal elongation and contraction of the shells. Figure 8 is a construction photograph of one of the four spring nests. Grouting of the base plate has not been completed.

The two 8-foot wind tunnels are shown in the aerial photograph, Figure 9. Both tunnels contain acoustic treatment. The upper tunnel, the 8-foot transonic pressure tunnel, contains a noise insulating blanket completely enclosing the shell except for several access doors and expansion joints. The blanket is rigid, consisting of two layers each of concrete and mastic supported by a framework of metal lath and angles which, in turn, is supported by the outer flanges of the support and stiffening rings. A typical detail of the noise insulating blanket is shown in Figure 10.

The lower tunnel of Figure 9, the 8-foot transonic tunnel, has a heavy concrete shell with an inside steel liner. The heavy walls, for this particular tunnel, effectively insulate the noise. The air exchange tower contains an acoustic baffling system, similar to that for the 16-foot transonic tunnel.

Figure 11 contains construction photographs of a typical mitered junction for the Unitary Plan 4- by 4-foot

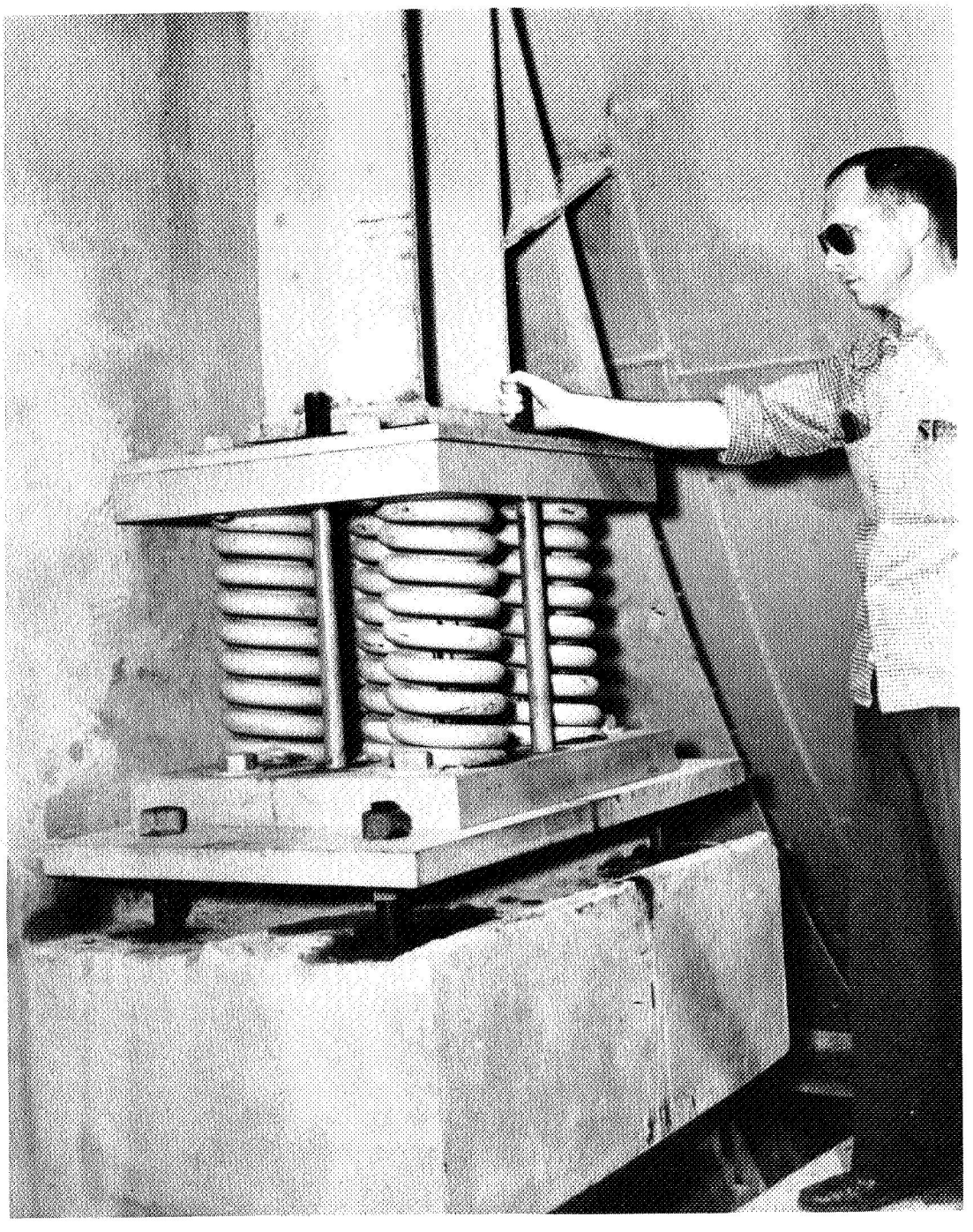

FIGURE 8

NACA L-62825

VIBRATION ABSORBING SUPPORTS FOR CONNECTING SHELLS
16-FOOT TRANSONIC TUNNEL

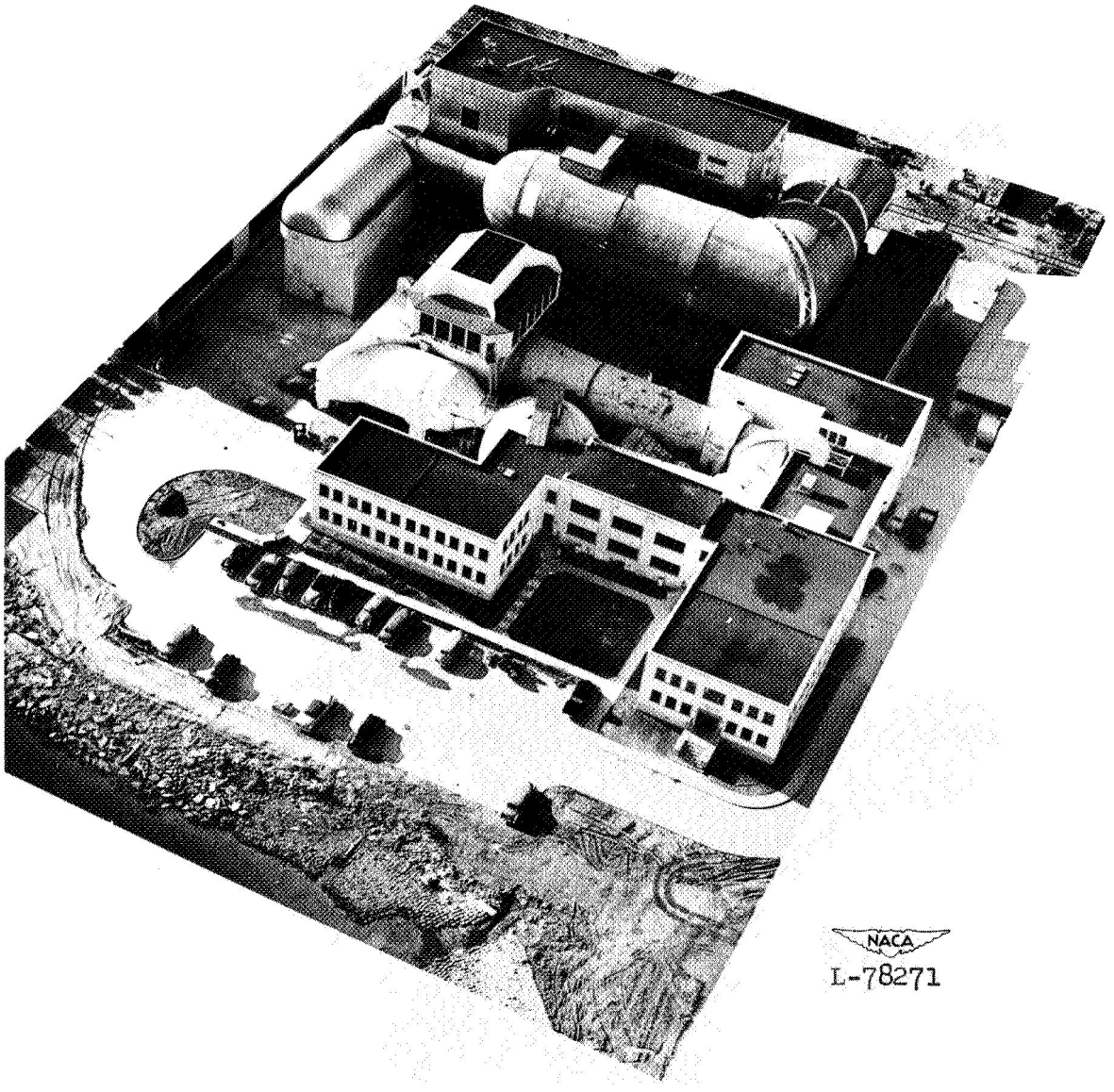

FIGURE 9

8-FOOT TRANSONIC PRESSURE TUNNEL
8-FOOT TRANSONIC TUNNEL AND LABORATORY

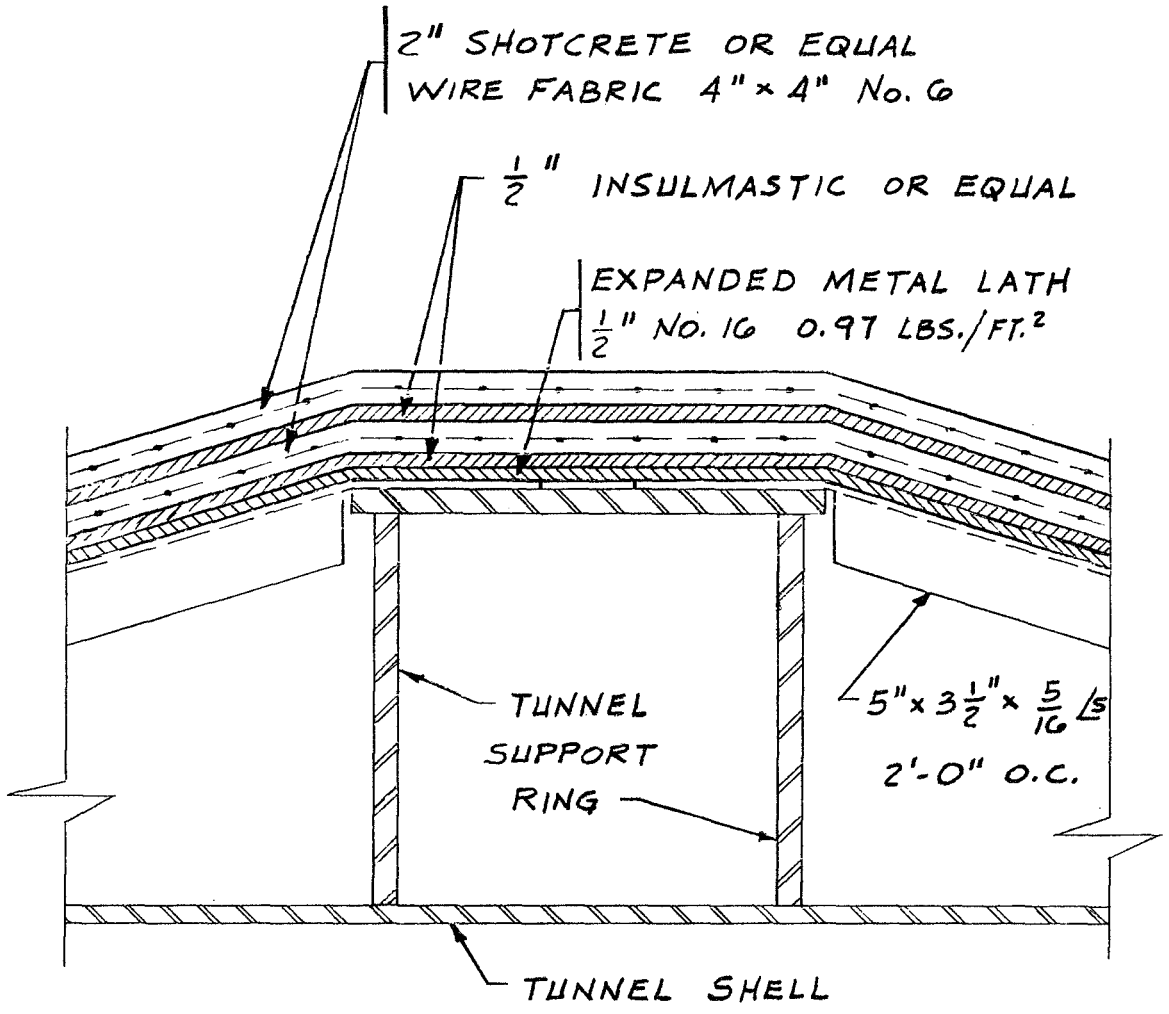

TYPICAL SHELL INSULATION

8-FOOT TRANSONIC PRESSURE TUNNEL

FIG. 10

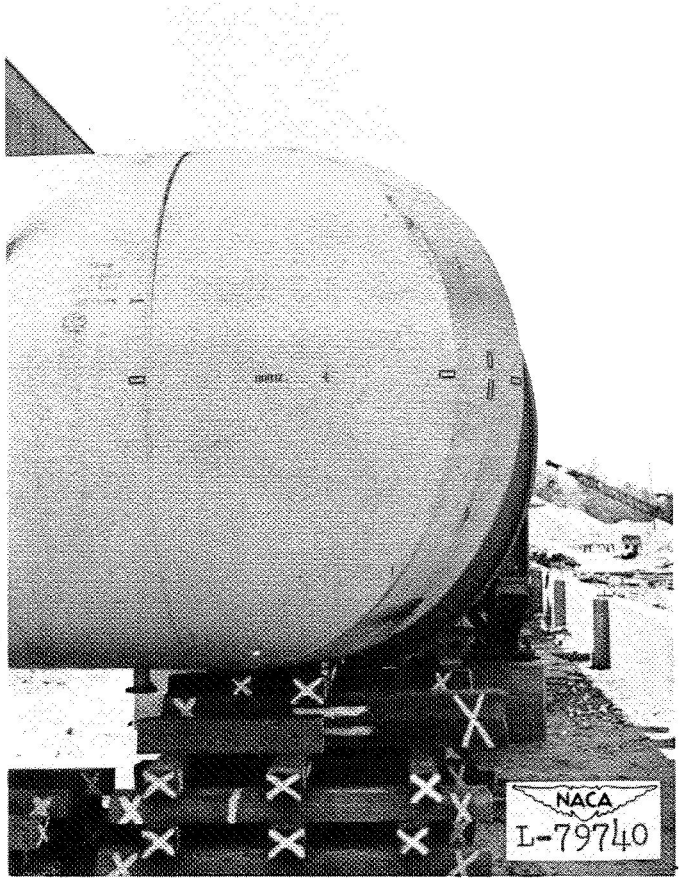

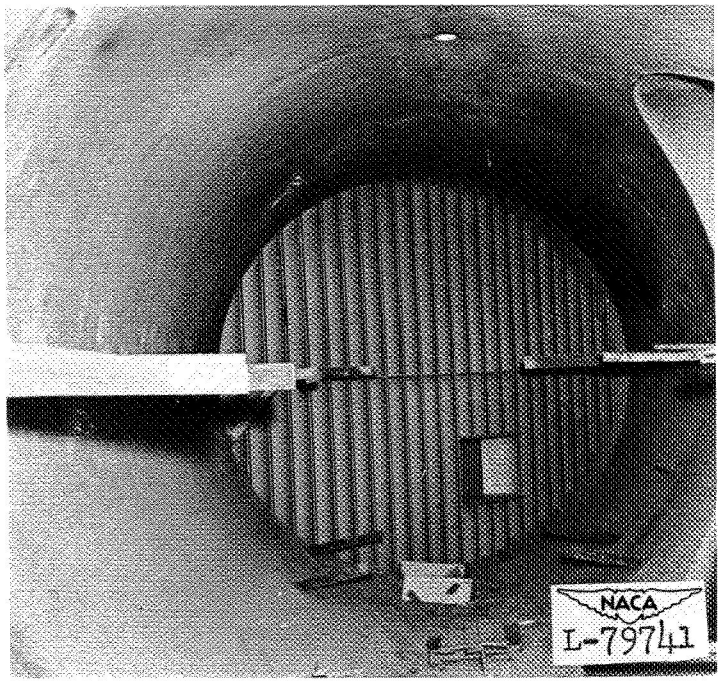

FIGURE 11

TURNING VANE SUPPORT FOR MITERED JUNCTION
UNITARY PLAN 4- BY 4-FOOT SUPERSONIC TUNNEL

supersonic tunnel. The turning vanes are welded to the inside surface of the elliptical plate reinforcing ring. Without the support obtained from the turning vanes, the reinforcing ring would, of necessity, be much heavier. In addition, the vanes contribute to a more rigid structural system without the detrimental effects of sliding connections.

Figures 12 and 13 are construction photographs of turbulence damping screens located in the 7- by 10-foot high-speed tunnel. The screens, four in number, are fine mesh, woven stainless steel wire elastically supported by helical springs.

Chapter IV, representing an example of noise and vibration control computations, includes further details and photographs of noise and vibration control treatment.

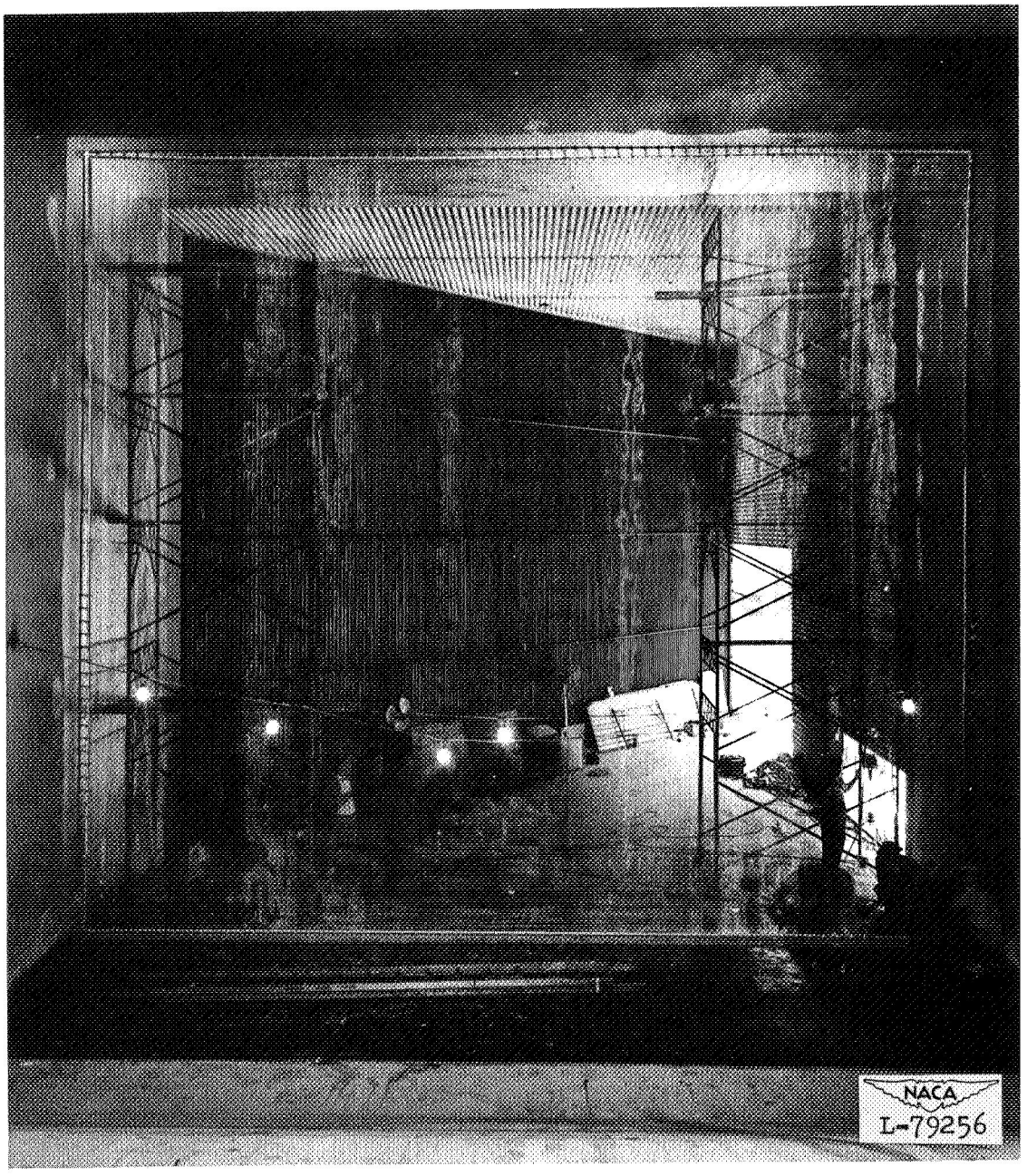

FIGURE 12

TURBULENCE DAMPING SCREENS
7- BY 10-FOOT HIGH-SPEED TUNNEL

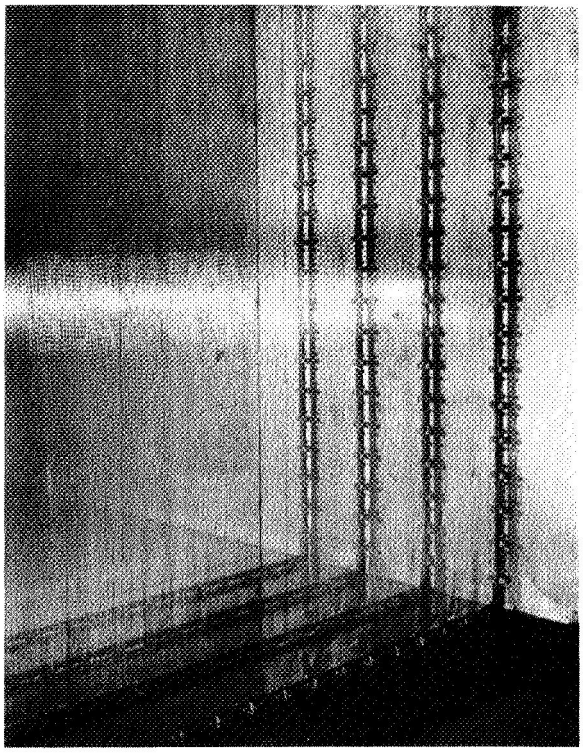

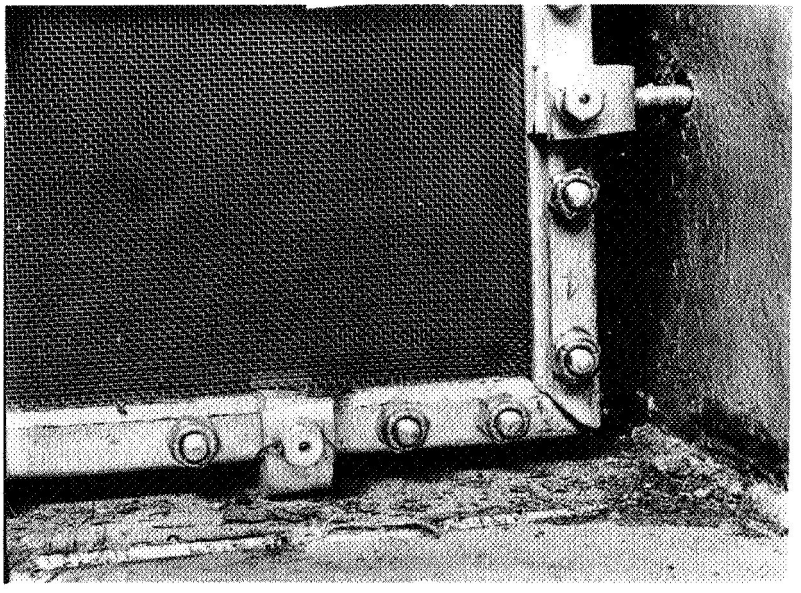

FIGURE 13

TURBULENCE DAMPING SCREEN DETAILS
7- BY 10-FOOT HIGH-SPEED TUNNEL

NACA L-79257

SYMBOLS

a	coefficient of sound absorption
A	cross-sectional area of duct (gross), ft^2
A_B	solid cross-sectional area of baffles, ft^2
A_o	cross-sectional open area of duct (net), ft^2
A_s	surface area of absorption material, ft^2
c	velocity of sound in air, ft/sec
C_f	friction coefficient
D	diameter of circular duct (gross), ft
D	noise pressure level of any frequency component, decibels
D_c	diameter of clear opening of circular duct (net), ft
D_D	difference in noise transmission loss between two different materials, decibels
D_L	difference in noise pressure level between any frequency component and the maximum frequency component, decibels
D_M	noise pressure level of maximum frequency component, decibels
D_o	reduction in effective noise transmission loss for insulation material due to the fact that the material contains k percent of material number two having greater acoustic transmittivity than material number one, decibels

D_R noise attenuation or reduction obtained by acoustic treatment, decibels

D_T total noise pressure level of all frequency components, decibels

E noise pressure energy of any frequency component, dynes/cm^2

E_M noise pressure energy of maximum frequency component, dynes/cm^2

E_o noise pressure energy of base, 0.0002 dynes/cm

E_T total noise pressure energy of all frequency components, dynes/cm^2

f frequency, cycles/sec

f friction factor

F_D friction drag force, lb

g acceleration of gravity, 32.2 ft/sec^2

H height of rectangular duct (gross), ft

H_c clear height of rectangular duct (net), ft

h_f friction loss, ft

I_R noise intensity reaching auditor within room, watts/cm^2

I_s noise intensity of noise source outside room, watts/cm^2

k relative amount of s_2 surface area of noise insulation material with respect to total area, percent

L length of acoustic baffles or absorption material, ft

m	hydraulic radius, ft
M	mass air flow, slugs/sec
n	number of acoustic baffle channels
p	static pressure (absolute), lb/ft^2
P_L	power loss, ft-lb/sec
q	dynamic pressure, lb/ft^2
Q	volume air flow, ft^3/sec
R	radius of circular duct (gross), ft
R	Reynolds number
R_c	clear radius of circular duct (net), ft
RF	noise reduction factor, decibels
s	surface area of noise insulation material
t	thickness of acoustic baffles or absorption material, ft
T	temperature, ^oF absolute
T	total transmittance of room walls, ft^2
U	total absorption of room walls, ft^2
V	velocity of air flow, ft/sec
W	width of rectangular duct (gross) or center to center spacing of acoustic baffles, ft
W_c	clear width of rectangular duct (net) or clear spacing between acoustic baffles, ft
%	ratio of the noise pressure energy of any frequency component to the noise pressure energy of the maximum frequency component, percent

$\sum\%$	summation of ratios defined above, percent
ϵ	roughness factor, ft
μ	coefficient of viscosity, slugs/ft sec
ν	kinematic viscosity, ft^2/sec
ρ	density, $slugs/ft^3$
τ	acoustic transmittivity
ω	angular frequency, radians/sec

CHAPTER II

ACOUSTIC BAFFLES

The type of acoustic baffling system considered here consists of panels, arranged as ribbon walls, parallel to each other and to the desired direction of air flow. Their purpose is to attenuate noise carried in the air stream flowing past their surfaces. Each panel unit is approximately 4 inches thick and consists of two perforated metal plates enclosing a sound absorbing material of mineral wool. Generally, it is important to provide a minimum of restriction to the air flow so, usually, each ribbon wall is provided with leading-edge and trailing-edge fairing. The baffle system considered here is similar in principle and purpose to the "splitters" commonly found in ventilating ducts.

From reference 1, the noise attenuation through a duct having interior wall surfaces lined with sound absorbent material equals

$$D_R = 1.05a^{1.4}\frac{A_s}{A_o} \qquad (2.1)$$

where D_R equals the noise attenuation in decibels; a equals the absorption coefficient; A_s equals the surface area of absorption material; and A_o equals the cross

sectional open area of the duct. The units for A_s and A_o must be the same.

Equation (2.1) applies to both rectangular and circular ducts with or without internal baffles or splitters. Five cases will be discussed, three for rectangular ducts and two for circular ducts, which cover the duct systems most commonly used. Two of the cases have particular application for wind tunnels.

Case 1

Figure 14 illustrates a rectangular duct with all interior surfaces lined with sound absorbent material having a uniform thickness equal to $\frac{t}{2}$, a length equal to L, and an absorption coefficient equal to a. The surface area of absorption material will equal

$$A_s = 2(W - t)L + 2(H - t)L \tag{2.2}$$

and the cross sectional open area will equal

$$A_o = (W - t)(H - t) \tag{2.3}$$

Let W_c and H_c represent the clear width and clear height, respectively, so that

$$\left.\begin{aligned} W_c &= W - t \\ H_c &= H - t \end{aligned}\right\} \tag{2.4}$$

then equations (2.2) and (2.3) may be written

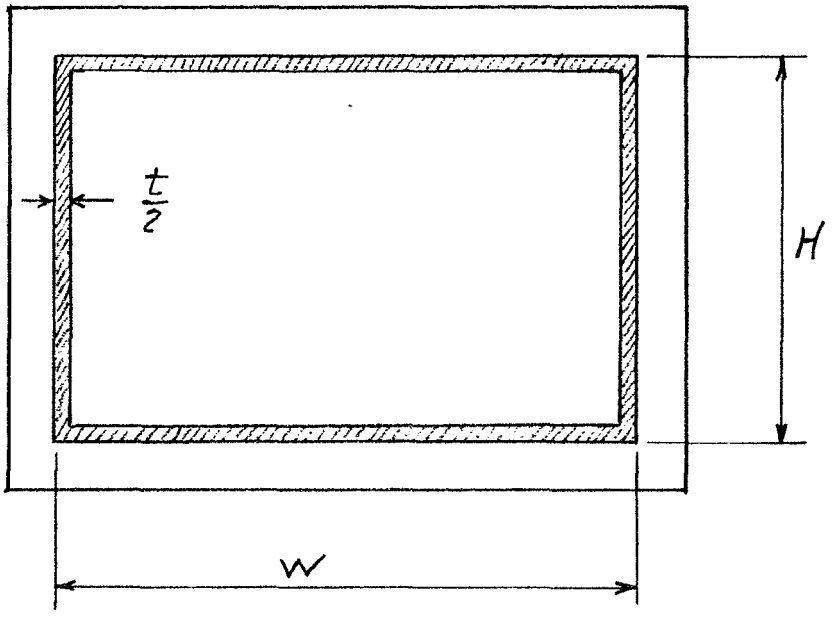

CASE 1

$$A_s = 2L(W_c + H_c)$$

$$A_o = W_c H_c$$

$$D_R = 2.1\, a^{1.4}\left(\frac{L}{W_c} + \frac{L}{H_c}\right)$$

FIG. 14

$$\left.\begin{aligned} A_s &= 2L(W_c + H_c) \\ A_o &= W_c H_c \end{aligned}\right\} \qquad (2.5)$$

Using equations (2.1) and (2.5), the noise attenuation through the duct will equal

$$D_R = 2.1a^{1.4}\left(\frac{L}{W_c} + \frac{L}{H_c}\right) \qquad (2.6)$$

Case 2

Figure 15 illustrates a rectangular duct with all interior surfaces lined with sound absorbent material having a uniform thickness equal to $\frac{t}{2}$ and length equal to L. The interior of the duct is divided into n equal cells by equal spaced ribbon wall baffles having uniform thickness t and length L. The absorption coefficient for the walls and baffles is assumed to equal a. The surface area of absorption material will equal

$$A_s = 2nL(W - t) + 2nL(H - t) \qquad (2.7)$$

and the cross sectional open area will equal

$$A_o = n(W - t)(H - t) \qquad (2.8)$$

Using equations (2.4), equations (2.7) and (2.8) become

$$\left.\begin{aligned} A_s &= 2nL(W_c + H_c) \\ A_o &= nW_c H_c \end{aligned}\right\} \qquad (2.9)$$

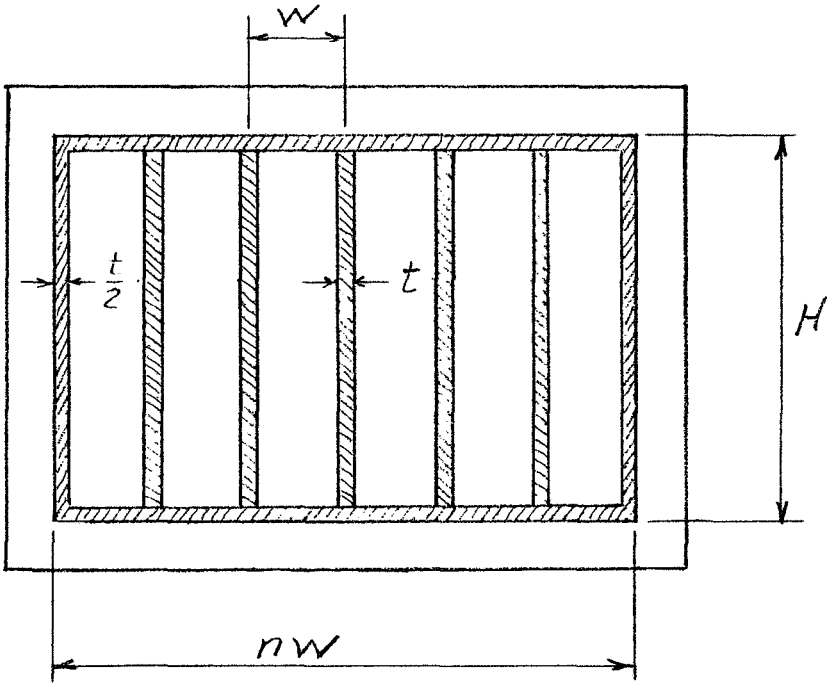

CASE 2

$$A_s = 2nL(W_c + H_c)$$

$$A_o = nW_c H_c$$

$$D_R = 2.1\, a^{1.4}\left(\frac{L}{W_c} + \frac{L}{H_c}\right)$$

FIG. 15

Combining equations (2.1) and (2.9), the noise attenuation through the duct will equal

$$D_R = 2.1a^{1.4}\left(\frac{L}{W_c} + \frac{L}{H_c}\right) \tag{2.10}$$

Case 3

Figure 16 illustrates a rectangular duct with the side surfaces lined with sound absorbent material having a uniform thickness equal to $\frac{t}{2}$ and a length equal to L. The top and bottom surfaces are unlined. The interior of the duct is divided into n equal cells by equal spaced ribbon wall baffles having uniform thickness t and length L. The absorption coefficient for the side walls and baffles is assumed to equal a and for the unlined top and bottom surfaces is assumed to equal zero. The surface area of absorption material will equal

$$A_s = 2nHL \tag{2.11}$$

and the cross sectional open area will equal

$$A_o = nH(W - t) \tag{2.12}$$

Using equation (2.4), equations (2.11) and (2.12) may be written

$$\left.\begin{aligned} A_s &= 2nLH \\ A_o &= nW_cH \end{aligned}\right\} \tag{2.13}$$

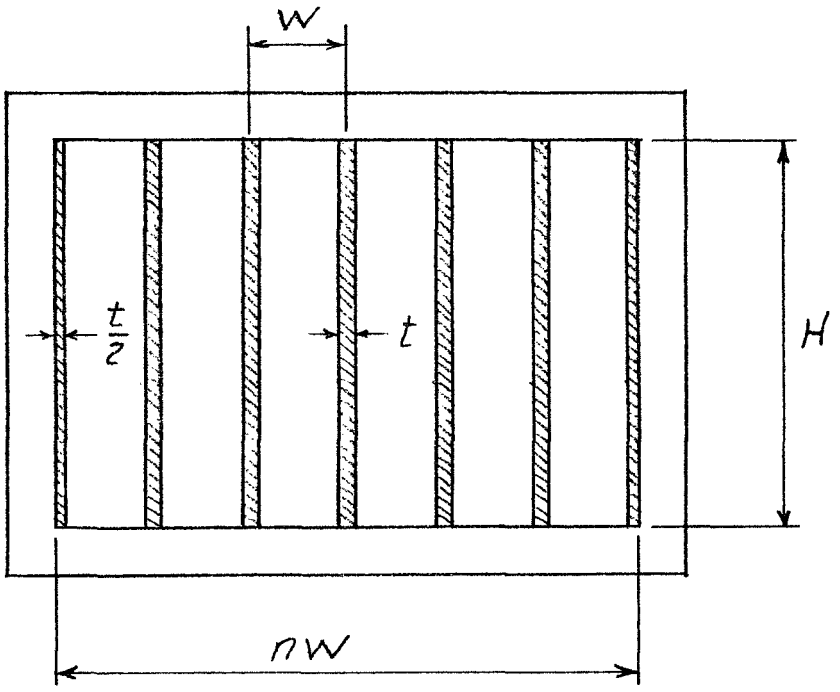

CASE 3

$$A_s = 2nLH$$

$$A_o = nW_cH$$

$$D_R = 2.1a^{1.4}\frac{L}{W_c}$$

FIG. 16

Combining equations (2.1) and (2.13), the noise attenuation through the duct will equal

$$D_R = 2.1a^{1.4}\frac{L}{W_c} \tag{2.14}$$

Case 4

Figure 17 illustrates a circular duct with the interior surface lined with sound absorbent material having a uniform thickness equal to $\frac{t}{2}$, a length equal to L, and an absorption coefficient equal to a. The surface area of absorption material will equal

$$A_s = \pi(D - t)L \tag{2.15}$$

and the cross sectional open area will equal

$$A_o = \frac{\pi}{4}(D - t)^2 \tag{2.16}$$

Let D_c and R_c represent the clear diameter and clear radius, respectively, so that

$$\left.\begin{aligned} D_c &= D - t \\ R_c &= \frac{D_c}{2} \end{aligned}\right\} \tag{2.17}$$

then equations (2.15) and (2.16) may be written

$$\left.\begin{aligned} A_s &= 2\pi LR_c \\ A_o &= \pi R_c^2 \end{aligned}\right\} \tag{2.18}$$

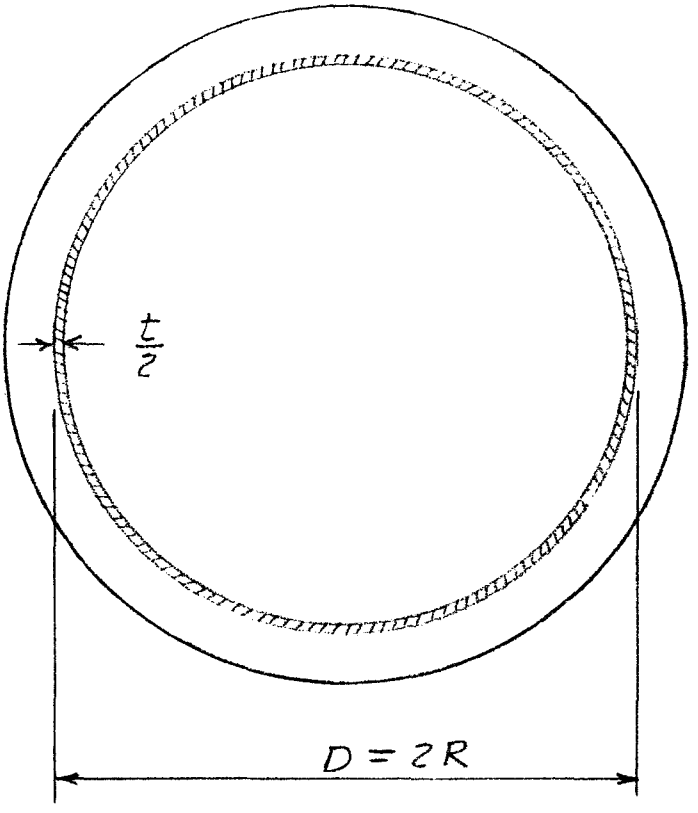

CASE 4

$$A_s = 2\pi L R_c$$

$$A_o = \pi R_c^2$$

$$D_R = 2.1\, a^{1.4}\, \frac{L}{R_c}$$

FIG. 17

Using equations (2.1) and (2.18), the noise attenuation through the duct will equal

$$D_R = 2.1a^{1.4}\frac{L}{R_c} \tag{2.19}$$

Case 5

Figure 18 illustrates a circular duct divided into n equal width cells by equal spaced ribbon wall baffles having uniform thickness t, length L, and absorption coefficient a. The absorption coefficient for the unlined perimeter of the duct is assumed to equal zero.

The equation of a circle with center at the origin of the Cartesian coordinates x and y may be expressed

$$y = R\left[1 - \left(\frac{x}{R}\right)^2\right]^{1/2} \tag{2.20}$$

If x varies in equal increments such that

$$\left.\begin{aligned} x_o &= 0 \\ x_1 &= W \\ x_2 &= 2W \\ x_k &= kW \\ x_{n/2} &= \frac{nW}{2} = R \end{aligned}\right\} \tag{2.21}$$

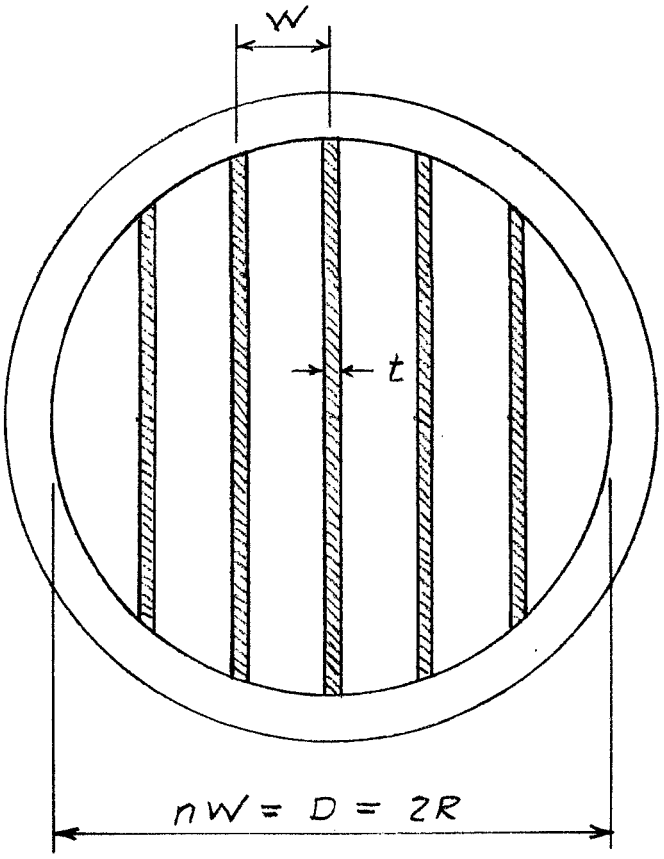

CASE 5

$$A_s = \frac{\pi}{2} n^2 WL$$

$$A_o = \frac{\pi}{4} n^2 W W_c$$

$$D_R = D_R = 2.1\, a^{1.4} \frac{L}{W_c}$$

FIG. 18

then

$$\left.\begin{aligned} y_o &= R = \frac{nW}{2} \\ y_1 &= \frac{nW}{2}\left[1 - \left(\frac{2}{n}\right)^2\right]^{1/2} \\ y_2 &= \frac{nW}{2}\left[1 - \left(\frac{4}{n}\right)^2\right]^{1/2} \\ y_k &= \frac{nW}{2}\left[1 - \left(\frac{2k}{n}\right)^2\right]^{1/2} \\ y_{n/2} &= 0 \end{aligned}\right\} \qquad (2.22)$$

Equations (2.22) represent the vertical height of any baffle in one quadrant of the duct. The total height of all baffles for all quadrants will then equal

$$Y = 4\left(\frac{y_o}{2} + y_1 + y_2 + \cdots y_k + \cdots y_{n/2}\right) \qquad (2.23)$$

Using equations (2.22), equation (2.23) becomes

$$Y = 2nW\left\{\frac{1}{2} + \sum_{k=1}^{k=\frac{n}{2}}\left[1 - \left(\frac{2k}{n}\right)^2\right]^{1/2}\right\} \qquad (2.24)$$

where the term under the summation sign is a function of n alone and may be written

$$f(n) = \frac{1}{2} + \sum_{k=1}^{k=\frac{n}{2}}\left[1 - \left(\frac{2k}{n}\right)^2\right]^{1/2} \qquad (2.25)$$

then equation (2.24) becomes

$$Y = 2nWf(n) \tag{2.26}$$

The total surface area of the baffles will equal

$$A_s = 2YL \tag{2.27}$$

The solid cross sectional area of the baffles will equal, approximately,

$$A_B = Yt \tag{2.28}$$

The cross sectional open area of the duct will equal, approximately,

$$A_o = \pi R^2 - A_B$$

and, since $R = \frac{nW}{2}$

$$A_o = \frac{\pi}{4}(nW)^2 - Yt \tag{2.29}$$

Using equation (2.26), equations (2.27) and (2.29) may be written

$$\left.\begin{aligned} A_s &= 4nWLf(n) \\ A_o &= 2nW\left[\frac{n\pi}{8}W - tf(n)\right] \end{aligned}\right\} \tag{2.30}$$

The term $f(n)$ is approximated very nearly by the equation

$$f(n) = \frac{n\pi}{8}\left(1 - \frac{0.728}{n}\right) \tag{2.31}$$

then

$$\left.\begin{aligned} A_s &= 4nWL\left(\frac{n\pi}{8}\right)\left(1 - \frac{0.728}{n}\right) \\ A_o &= 2nW\left(\frac{n\pi}{8}\right)\left[W - t\left(1 - \frac{0.728}{n}\right)\right] \end{aligned}\right\} \tag{2.32}$$

For all practical applications, n is sufficiently large so that the factor

$$\left(1 - \frac{0.728}{n}\right) \cong 1 \tag{2.33}$$

then, using equation (2.4), equations (2.32) become

$$\left.\begin{aligned} A_s &= \frac{\pi}{2}n^2WL \\ A_o &= \frac{\pi}{4}n^2WW_c \end{aligned}\right\} \tag{2.34}$$

Combining equations (2.1) and (2.34), the noise attenuation through the duct will equal

$$D_R = 2.1a^{1.4}\frac{L}{W_c} \tag{2.35}$$

Since the noise attenuation equations for all five cases have the same general form, it is convenient to describe all five cases by a single graph. Figure 19 is an alinement chart for equations (2.6) and (2.10) which also applies, with slight modification, for equations (2.14),

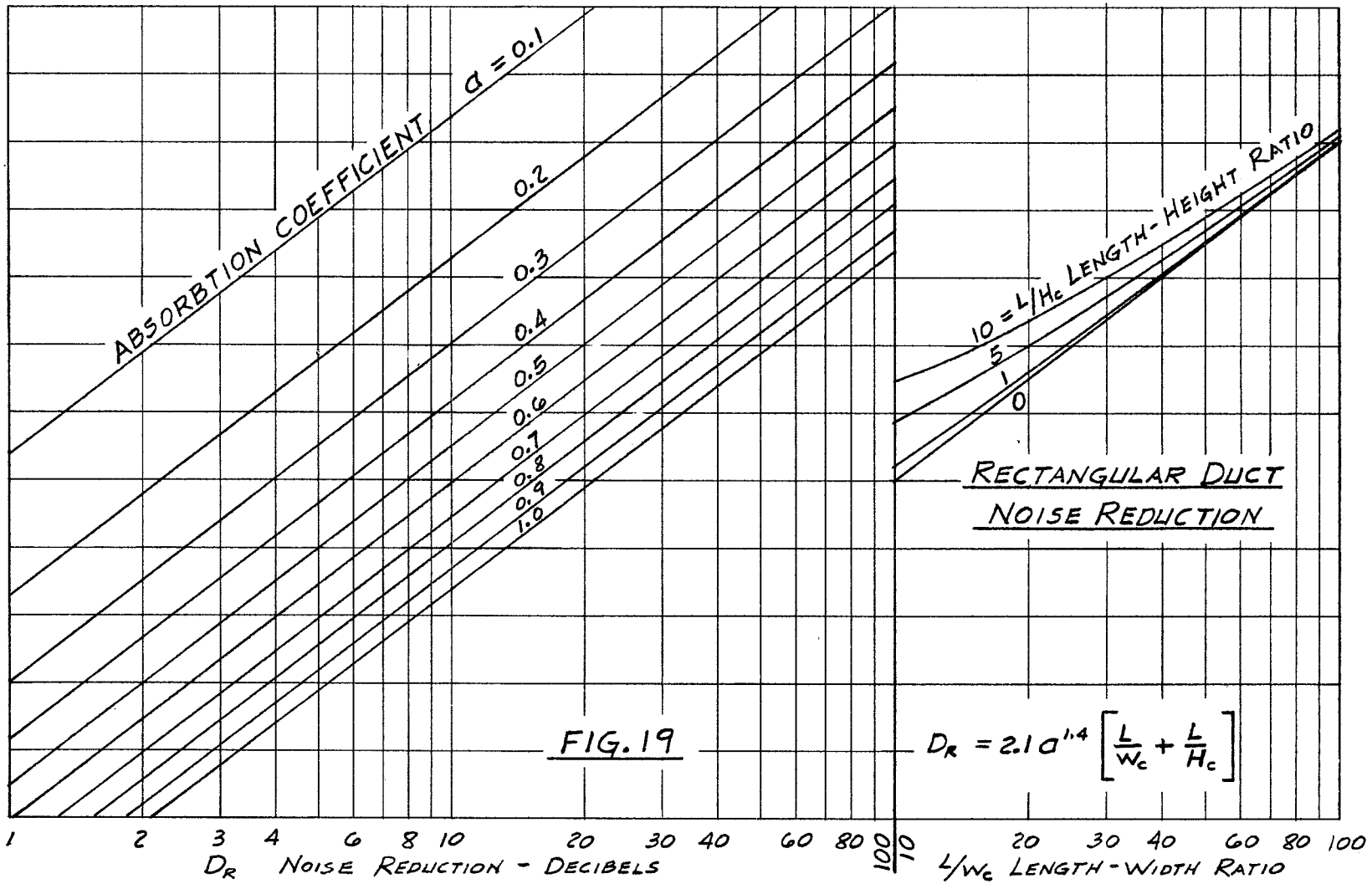
ABSORBTION COEFFICIENT, α = 0.1
0.2
0.3
0.4
0.5
0.6
0.7
0.8
0.9
1.0
10 = L/Hc LENGTH-HEIGHT RATIO
5
1
0
RECTANGULAR DUCT
NOISE REDUCTION
$D_R = 2.1\alpha^{1.4}\left[\frac{L}{W_c} + \frac{L}{H_c}\right]$
1 2 3 4 6 8 10 20 30 40 60 80 100
DR NOISE REDUCTION - DECIBELS
10 20 30 40 60 80 100
L/Wc LENGTH-WIDTH RATIO

FIG. 19

(2.19), and (2.35). Equations (2.14) and (2.35) are satisfied when $\frac{L}{H_c}$ equals zero and equation (2.19) is satisfied if $\frac{L}{R_c}$ is assumed to equal $\frac{L}{W_c}$ and when $\frac{L}{H_c}$ equals zero.

The critical factor in the formulas for noise attenuation is the absorption coefficient a. Many factors, apparently, influence this value including the method of measurement. The most common method of determining the sound absorption properties of various materials is the reverberation room method described in references 2, 3, and 4. References 2 and 5 tabulate many different materials and their absorption coefficients. However, the absorption coefficients, determined by the reverberation room method, do not seem to be compatable with the noise attenuation theory for ducts developed in reference 1 and represented by equation (2.1). Figure 20 is a graph of absorption coefficient against frequency for eight panels tabulated in reference 5 of the type used for acoustic baffles. This graph is included here only as an illustration of the results obtained from the reverberation room method and its use is not recommended.

Figure 21 illustrates the author's concept of the relationship between the absorption coefficient a of the acoustic baffles or absorption material and the frequency

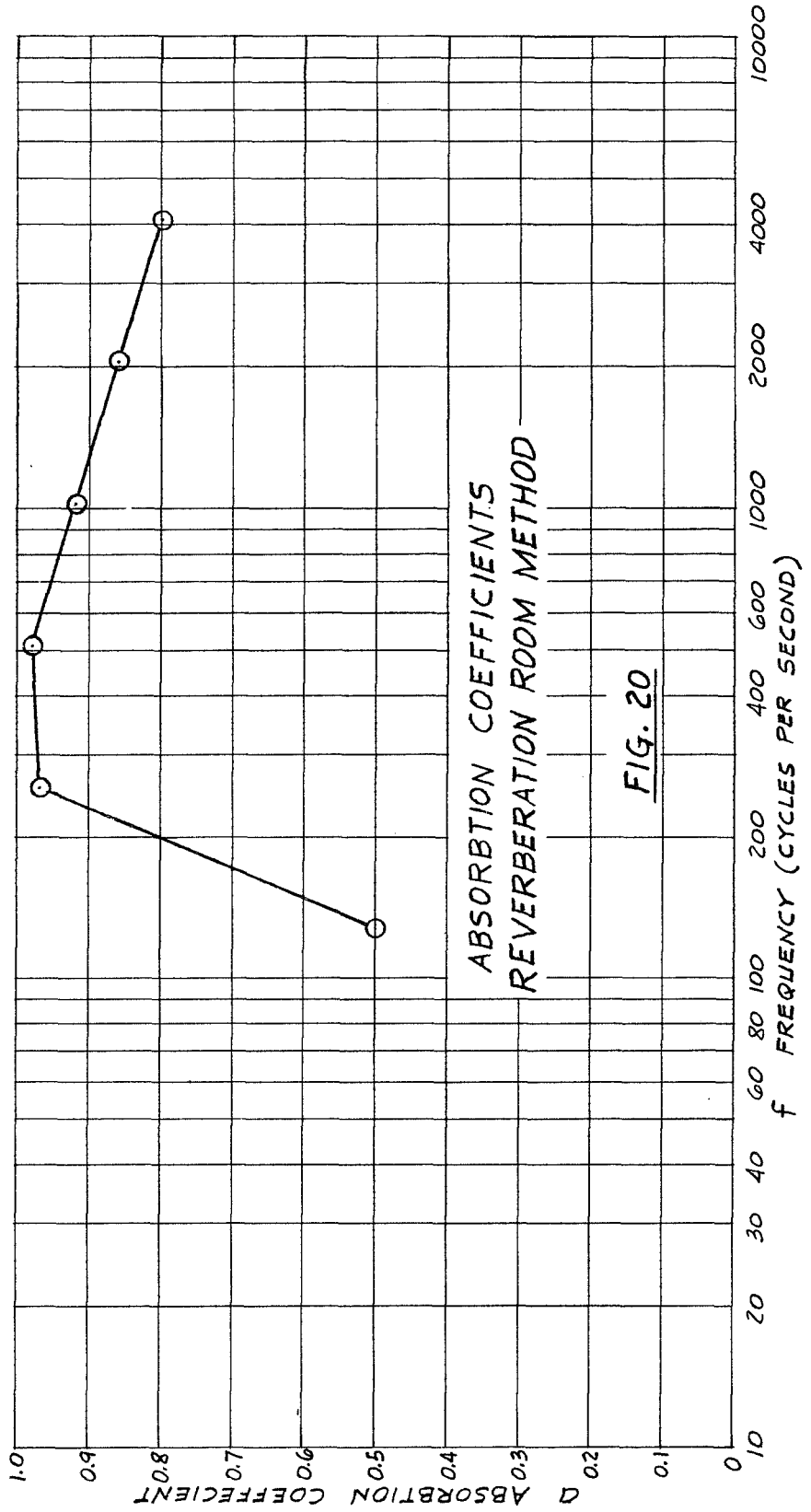
ABSORBTION COEFFICIENTS
REVERBERATION ROOM METHOD
α ABSORBTION COEFFICIENT
f FREQUENCY (CYCLES PER SECOND)
1.0
0.9
0.8
0.7
0.6
0.5
0.4
0.3
0.2
0.1
0
10
20
30
40
60
80
100
200
400
600
1000
2000
4000
10000

FIG. 20

Estimated Absorbtion Coefficient Curve For Perforated Metal Acoustic Baffles

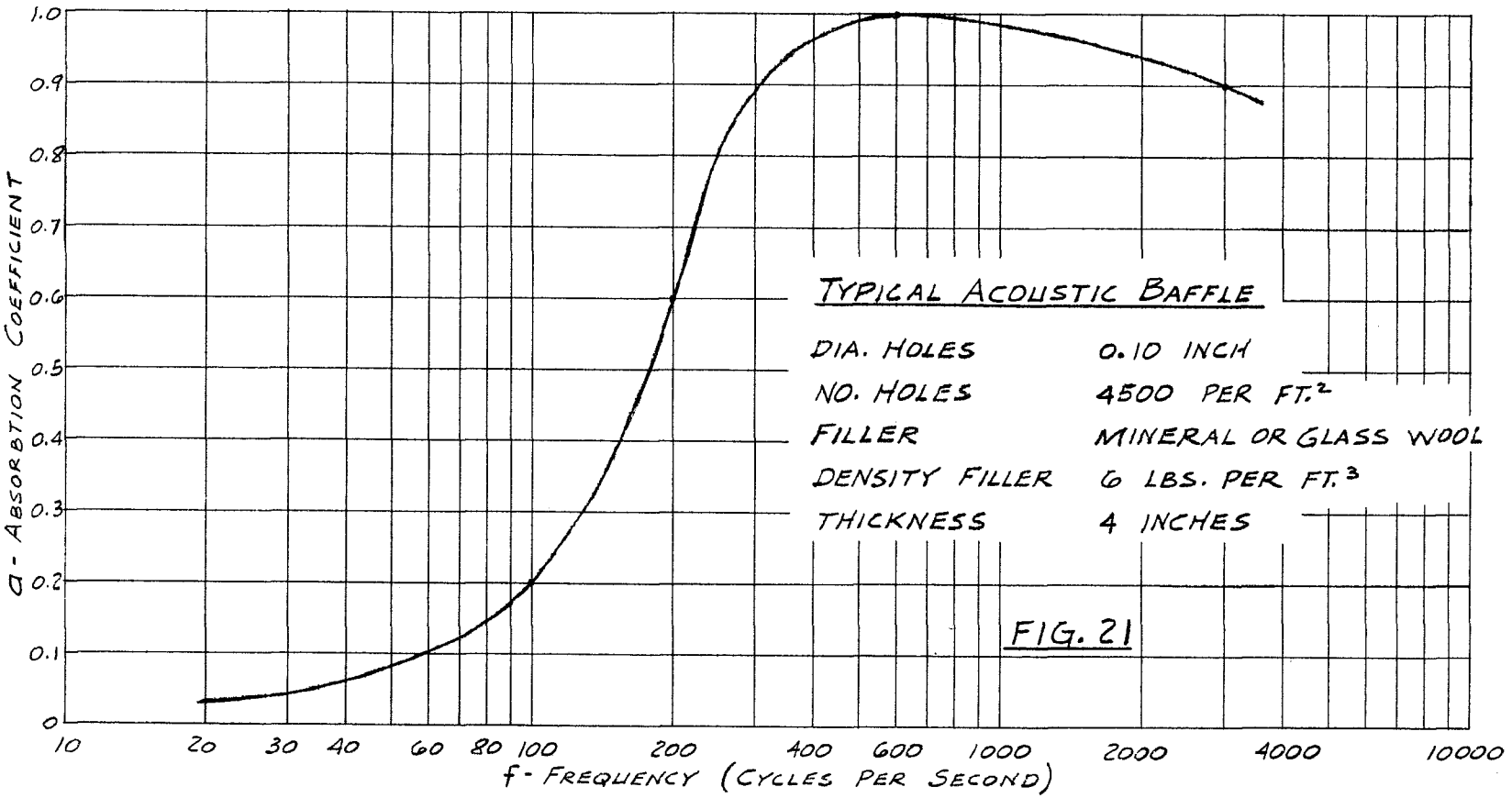

Fig. 21

f of the noise in the duct. This curve, to be used with the noise attenuation formulas represented by Figure 19, is based upon miscellaneous test data obtained from many sources and should be considered an approximation as there is considerable scatter of the various test points.

Factors that probably influence the absorption coefficient of any particular baffle are the per cent absorption area (the size and spacing of the perforations) and the density of the mineral wool sound absorbing material. The effect of these factors is not included here with the exception that Figure 21 lists information for a typical baffle and unless the deviations from the typical are large, Figure 21 should give reasonably good results. Another factor having influence upon the noise reduction through acoustic baffles is the natural frequencies of the ribbon walls as installed. No attempt is made here to evaluate this factor.

The structural design of the acoustic baffle plates, stiffening members, and fastening devices will depend upon the particular application and the forces exerted upon the system. Due to the dynamic nature of the loading, care should be taken to insure that fatigue stressing and stress concentrations are not critical. When the air stream, passing through the baffles, is moving at high velocities, particular consideration should be given to the possibility

that the air flow may not be uniform, especially when there is a sharp change in direction of the air stream before reaching the baffles. This effect may be manifested as high local velocities through portions of the baffles and lesser velocities through other portions resulting in increased loading and stresses upon the system. Also, if there is rapid change in temperature, such as occurs by discharge from pressure vessels, thermal loading must be considered.

In order for acoustic baffles, installed within the air stream of a wind tunnel, to have merit, the power or drag losses through the system must be able to be tolerated. In other words, the function of the source (the air stream) must not be inhibited by more than a predetermined acceptable amount.

Reference 6 discusses the flow of fluids in ducts with particular emphasis on hydraulic flow. However, the theory discussed there will prove useful in developing approximate methods for determining the drag and power losses of the air stream through acoustic baffles.

From reference 6, the head loss in friction in feet of the fluid equals

$$h_f = C_f \frac{L}{m} \frac{V^2}{2g} \qquad (2.36)$$

where

$$\frac{L}{m} = \frac{A_s}{A_o} \tag{2.37}$$

V is the mean velocity of fluid in feet per second, g is the acceleration of gravity, and C_f is the friction coefficient. The power loss due to friction will equal

$$P_L = h_f V A_o \rho g \tag{2.38}$$

where ρ is the density of the fluid in slugs per cubic foot. Using equations (2.36) and (2.37), equation (2.38) may be written

$$P_L = \frac{1}{2} C_f \rho A_s V^3 \tag{2.39}$$

or

$$P_L = F_D V \tag{2.39}$$

where

$$F_D = C_f A_s q \tag{2.40}$$

is the drag force in pounds and

$$q = \frac{1}{2}\rho V^2 \tag{2.41}$$

is the dynamic pressure in pounds per square foot.

From reference 6, the friction coefficient equals

$$C_f = \frac{f}{4} \tag{2.42}$$

where f is the friction factor. Both C_f and f are dimensionless. From reference 6, f may be determined by the expression

$$\frac{1}{\sqrt{f}} = 2 \log_{10}\left(\frac{2m}{\varepsilon}\right) + 1.74 \qquad (2.43)$$

where m equals the hydraulic radius in feet and ε is the roughness factor in feet. Using equation (2.43), equation (2.42) becomes

$$C_f = \frac{1}{16\left[\log_{10}\left(\frac{2m}{\varepsilon}\right) + 0.87\right]^2} \qquad (2.44)$$

which enables the friction coefficient to be determined for any particular duct if the roughness of the duct surfaces is known.

The hydraulic radius m may be expressed

$$m = \frac{A_o L}{A_s} \qquad (2.45)$$

and for cases 3 and 5, generally applicable to wind tunnels, using equations (2.13) and (2.34),

$$m = \frac{W_c}{2} \qquad (2.46)$$

Equation (2.44) may then be written

$$C_f = \frac{1}{16\left[\log_{10}\left(\frac{7.413 W_c}{\varepsilon}\right)\right]^2} \qquad (2.47)$$

Reference 7 tabulates roughness factors for gases corresponding to various kinds of duct surfaces. These factors written as equations (2.48)

$$\left.\begin{aligned}
&\varepsilon = 0.0000015 \text{ foot - very smooth} \\
&\quad \text{corresponding to drawn tubing} \\
&\varepsilon = 0.00015 \text{ foot - medium smooth} \\
&\quad \text{corresponding to new steel or wrought} \\
&\quad \text{iron pipe} \\
&\varepsilon = 0.0005 \text{ foot - average} \\
&\quad \text{corresponding to galvanized iron} \\
&\varepsilon = 0.003 \text{ foot - medium rough} \\
&\quad \text{corresponding to average concrete} \\
&\varepsilon = 0.01 \text{ foot - very rough} \\
&\quad \text{corresponding to average riveted steel}
\end{aligned}\right\} \qquad (2.48)$$

are presented for comparative purposes. The particular value of roughness factor ε, that would most nearly apply

to acoustic baffles is unknown for experimental data are lacking. The very rough condition is probably conservative.

Figure 22 is a graph of equation (2.47) using factors (2.48) and represents the friction factor C_f for air flow through acoustic baffles for the condition of turbulent flow where

$$R = \frac{VL}{\nu} \geqslant 5 \times 10^6 \qquad (2.49)$$

where R is the Reynolds number and ν is the kinematic viscosity in square feet per second.

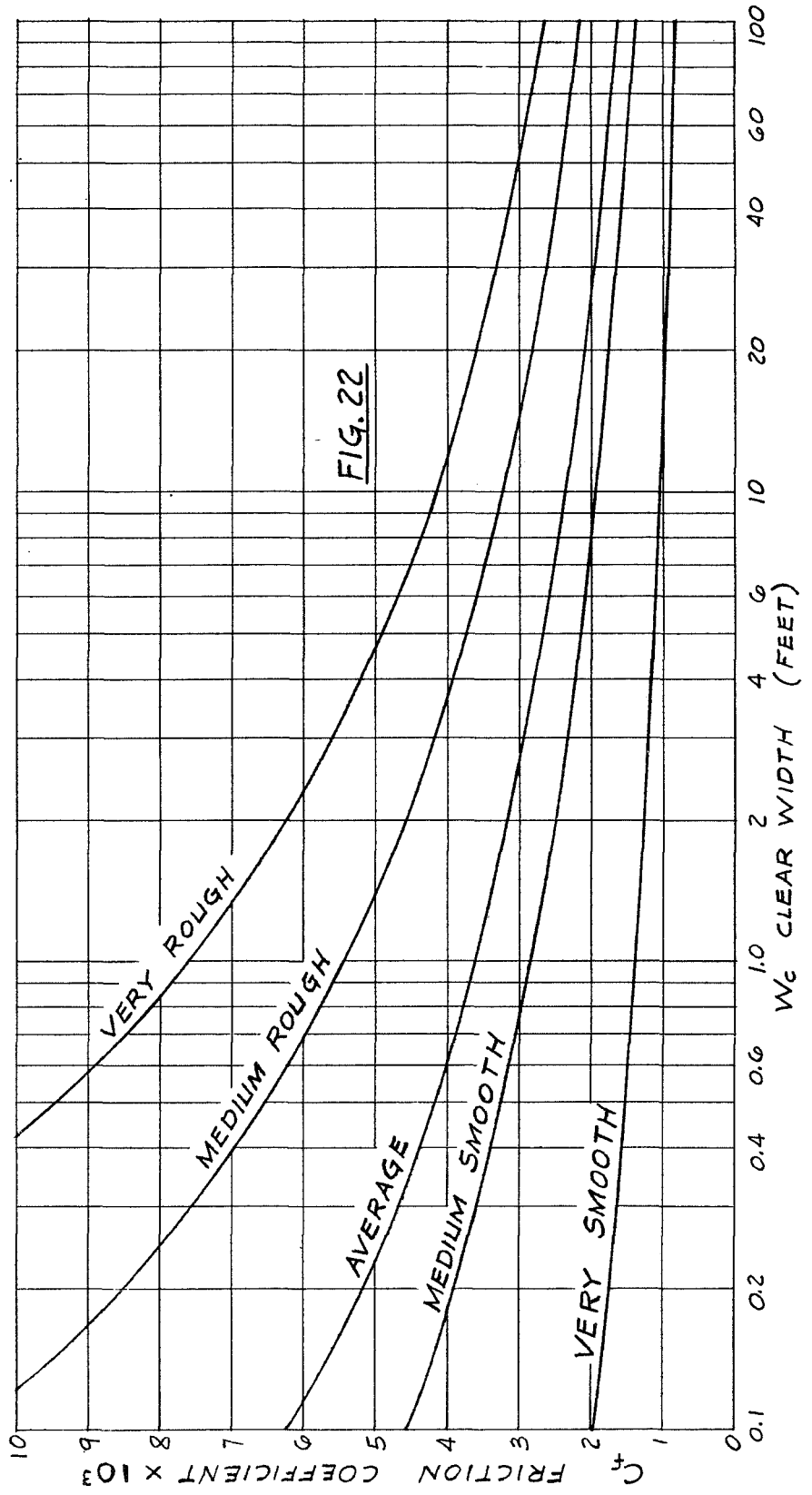
FIG. 22
VERY ROUGH
MEDIUM ROUGH
AVERAGE
MEDIUM SMOOTH
VERY SMOOTH
C_f FRICTION COEFFICIENT x 10^3
10 9 8 7 6 5 4 3 2 1 0
W_c CLEAR WIDTH (FEET)
0.1 0.2 0.4 0.6 1.0 2 4 6 10 20 40 60 100

CHAPTER III

NOISE INSULATION

Noise attenuation, by insulation, is the reduction of noise by the placement of a barrier between the noise source and the auditor. The barrier may be pervious or impervious, flexible or rigid and its function is to eliminate the transmission of direct air stream energy from the source to the auditor. A vast amount of test data has been compiled by many sources concerning noise transmission loss for practically every conceivable building material. References 8 and 9 tabulate much of this data.

In the past, it was generally believed that, in order for insulation material to be effective, the material had to be both rigid and dense. Several authorities had developed various mass or weight laws for which substantiating test data appeared to be compatible. Since each mass law satisfies one particular set of test data and not another, it appears that the method of testing influences the results. Within the past 15 years much more information has been produced concerning the standardization of test procedures and the investigation of lightweight flexible blankets. Reference 10 presents the basic theoretical information necessary for the design of noise attenuating lightweight, flexible blankets but since the subject is vast, still

relatively undeveloped, and lacking in test data it will not be considered here.

Reference 11 presents a discussion of noise attenuation through single walls from the mass law standpoint, taking into account the flexibility of the system. From reference 11

$$D_R = 10 \log_{10} b^2 - 10 \log_{10}\left[\log_e(1 + b^2)\right] \qquad (3.1)$$

where

$$b = \frac{\omega\sigma}{2\rho c} \qquad (3.2)$$

and ω is the angular frequency, σ is the surface density of the wall, ρ is the air density, and c is the velocity of sound in air. For the condition of 20° centigrade air temperature, equation (3.2) may be written

$$b = \frac{f\sigma}{27} \qquad (3.3)$$

where f is the circular frequency in cycles per second and σ is the surface density of the wall in pounds per square foot. Figure 23 is a graph of equations (3.1) and (3.3) and applies principally to homogeneous single walls. However, Figure 23 has application for nonhomogeneous lightweight blankets if used with care.

NOISE TRANSMISSION LOSS VS SURFACE DENSITY

RANDOM INCIDENCE MASS LAW

$$D_R = 10 \log_{10} b^2 - 10 \log_{10} \left[\log_e (1 + b^2) \right]$$

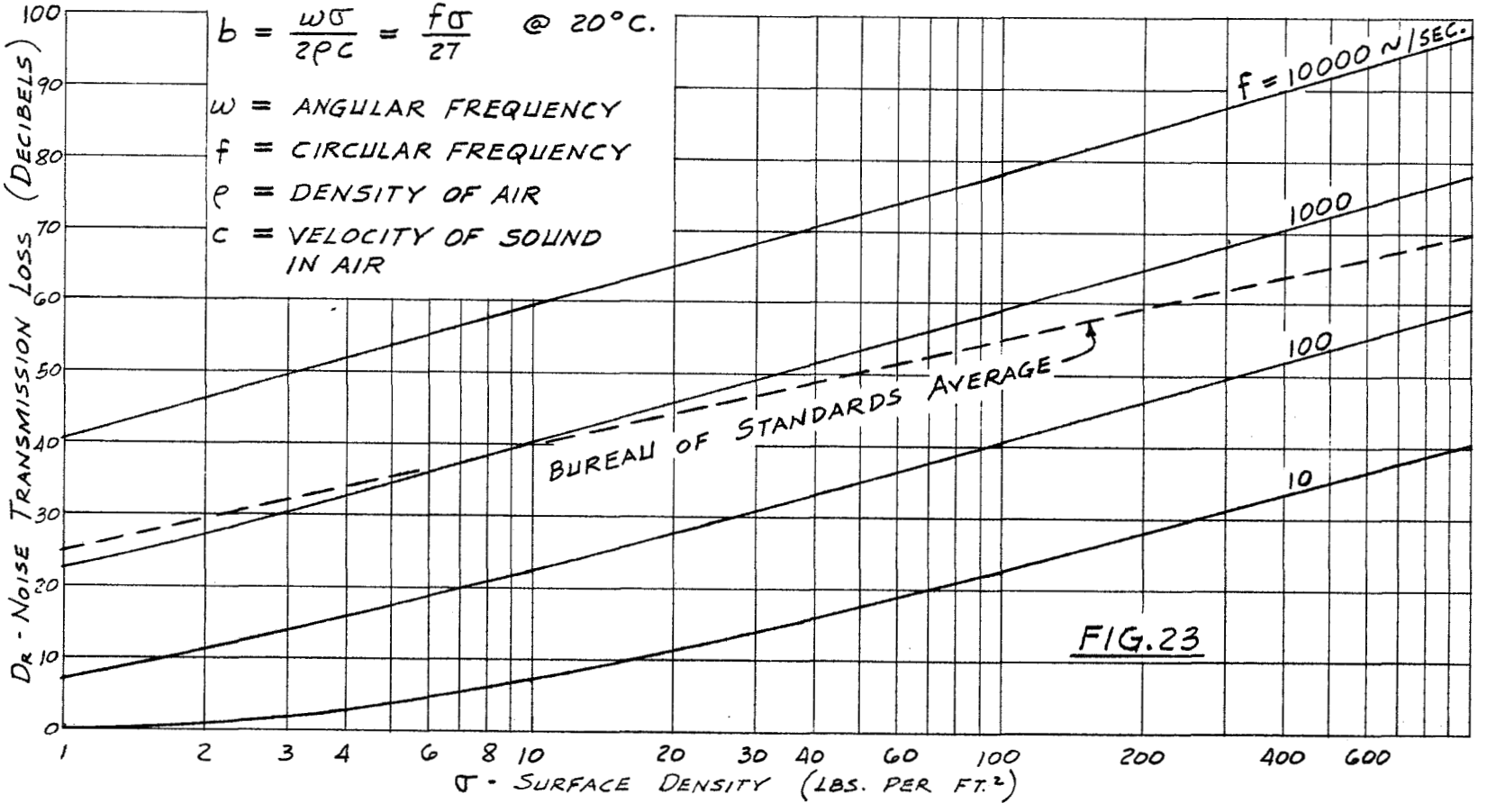

FIG. 23

For noise control of wind tunnels, the purpose of a noise insulating blanket, whether rigid or flexible, is to attenuate the noise radiating from the tunnel shell. It may, depending upon the particular application, have an auxiliary function as thermal insulation. The blanket must be durable and if exposed to the elements should have a weather resistant protective cover. Frequently a pleasing external appearance is important. All of these requirements can be accomplished with commercially available materials.

The basic principles for designing a noise insulating blanket are very important. Most important is to provide an air space of at least several inches between the duct shell and the inside blanket surface. If the blanket is to consist of porous lightweight material, such as mineral wool, one or more impervious septa are required. Usually, one impervious septum is sufficient and can also serve as a weather resistant protective cover on the outside face of the blanket. The weight of the septum per square foot of surface area should not be less than 25 per cent of the weight of the mineral wool. Any reasonably dense material may serve as a septum. Suggested materials are steel, wood, concrete, plaster, aluminum alloy, and preformed or sprayed on asphaltic or vinyl base compounds.

Lightweight blankets of mineral wool with an impervious septum of asphaltic or vinyl base compounds have

a wide range of usefulness. They are light in weight and do not require an extensive supporting structure. They are flexible and pliable and will withstand considerable thermal movement of the duct shell without damage. They are relatively easy to install over irregularly shaped contours. Portions of the blanket can be easily removed and replaced for access to the duct shell.

Design data for noise insulating blankets are contained on the graph Figure 23. This is a weight law graph and will give excellent results when used discriminately. Comments for the use of this graph are included below:

(a) The attached graph Figure 23 is a plot of noise attenuation against surface density with a parameter of noise frequency. This graph applies to damped, single layer impervious panels. If the panels are undamped, considerable discrepancy will occur between actual results and theory for the condition of imposed noise frequency being at or near the natural frequency of the panel.

(b) For the condition of multilayered impervious panels, lightweight blankets, or a combination of both, the noise attenuation may be considerably greater than indicated on the graph, using the total surface density of the individual layers.

(c) In summary, impervious, single layered panels will have a noise attenuation in close agreement with the weight law formula except for the condition of resonance; multilayered panels will have a noise attenuation at least as great as indicated by the weight law formula. The resonance restriction applies to multilayered panels as well as to single layered panels but is much less likely to occur.

(d) Superimposed upon the graph is a Bureau of Standards average curve for frequencies from 100 cycles per second to 2000 cycles per second. This average curve may be used when there is no knowledge of the imposed frequency.

(e) Considerable effort should be made to predict the first harmonic of the imposed frequency as it is apparent from the graph that there is considerable variation in noise attenuation depending upon the parameter noise frequency. For the case of a wind-tunnel fan, the first harmonic is relatively simple to obtain as it is the revolutions per second times the number of blades.

As mentioned in chapter I, the acoustic treatment for noise control may neglect the noise sources, and instead, be applied to the auditors in such form as soundproof rooms, etc. References 8, 9, 12, and 13 discuss the attenuation of noise through partitions, with particular emphasis upon the architectural acoustics of rooms. It is, however,

convenient to include an analysis of noise insulation for rooms, based upon the theory discussed in references 8, 9, 12, and 13, but developed in such manner that it can be readily extended to the use of insulating blankets for wind tunnels.

Noise control for auditors, in the form of acoustic treatment for rooms, must take in consideration the fact that most rooms will have certain portions of wall, floor, and ceiling areas different in construction and material from the remainder. For instance, doors and windows are generally different in material and construction from the remainder of the surface areas and will have coefficients of sound transmission or acoustic transmittivity different from the other portions. Furthermore, openings such as cracks between the door and frame, key holes, and open windows transmit noise disproportionately in excess of the opening size. In addition, the absorption characteristics of the interior surfaces of the room will affect the intensity of noise reaching the auditor.

From references 8 and 9

$$\frac{I_s}{I_R} = \frac{U}{T} \tag{3.4}$$

where I_s is the intensity of the noise source outside of the room, I_R is the intensity of the noise reaching the

auditor within the room, U is the total absorption units of the room walls, and T is the total transmittance of the room walls. The assumption is made that a diffuse sound field exists for both the source and the room interior and that a noise of intensity I_s exists for all boundaries of the room. When the outside intensity is different for different parts of the boundary, as is often the case, each part of the boundary must be considered separately.

The total absorption units will equal

$$U = a_1 s_1 + a_2 s_2 + a_3 s_3 + \ldots \tag{3.5}$$

and the total transmittance will equal

$$T = \tau_1 s_1 + \tau_2 s_2 + \tau_3 s_3 + \ldots \tag{3.6}$$

where a_1, a_2, a_3, etc., are the absorption coefficients for various portions of wall surfaces s_1, s_2, s_3, etc., and τ_1, τ_2, τ_3, etc., are the corresponding coefficients of sound transmission or acoustic transmittivity for the wall surfaces.

The noise reduction factor, in decibels, will equal

$$RF = 10 \log_{10} \frac{I_s}{I_R} = 10 \log_{10} \frac{U}{T} \tag{3.7}$$

where U and T are defined by equations (3.5) and (3.6), respectively. For the particular condition of one portion

of the room (for instance, a partition) being subjected to external noise while the remainder of the room boundaries are not then

$$T = \tau s \tag{3.8}$$

and

$$RF = 10 \log_{10} \frac{U}{\tau s} \tag{3.9}$$

which may be written

$$RF = 10 \log_{10} \frac{1}{\tau} + 10 \log_{10} \frac{U}{s} \tag{3.10}$$

where U is the total absorption units of the room walls and s is the area of the partition or panel. The term

$$10 \log_{10} \frac{1}{\tau} = D_R \tag{3.11}$$

is defined as the transmission loss of the panel. Values for D_R may be obtained from the tabulated data contained in references 8 and 9 and from the graph of Figure 23. Therefore, for the condition of one panel transmission, using equations (3.10) and (3.11), equation (3.7) becomes

$$RF = D_R + 10 \log_{10} \frac{U}{s} \tag{3.12}$$

When equation (3.12) is rewritten as

$$D_R = RF - 10 \log_{10} \frac{U}{s} \tag{3.13}$$

it is in the form used for the experimental determination of noise transmission loss. Two rooms are used, the source room and the receiving room. Both rooms are highly reverberant and heavily insulated so that external noise entering the room is negligible. The rooms are separated by an opening where test panels can be mounted. Generally, the opening is sufficiently large to preclude the possibility that the method of supporting or clamping the boundaries of the test specimen will affect the transmission loss measurements significantly. Once the panel is mounted in the opening, measurements are made in the receiving room to determine the number of absorption units U. Noise is generated in the source room, usually a warble tone, and measurements made to determine the level in both the source and receiving rooms. The difference in noise levels, of the source and receiving rooms, is the noise reduction factor RF. Knowing RF, U, and s, the area of the test panel, the transmission loss D_R is determined from equation (3.13).

Consider the condition of a room whose walls consist of only two different materials, each having a noise transmission loss different from the other. Then

$$T = \tau_1 s_1 + \tau_2 s_2 \qquad (3.14)$$

Let

$$s_2 = \frac{k}{100} s \tag{3.15}$$

where s is the total wall area and k is the per cent of s_2 area to the total area. Then

$$s = s_1 + \frac{k}{100} s \tag{3.16}$$

and

$$s_1 = \left(1 - \frac{k}{100}\right) s \tag{3.17}$$

Using equation (3.11), the acoustic transmittivity for material number 1 will equal

$$\tau_1 = 10^{-D_{R1}/10} \tag{3.18}$$

and for material number 2

$$\tau_2 = 10^{-D_{R2}/10} \tag{3.19}$$

Combining equations (3.7), (3.14), (3.15), (3.17), (3.18), and (3.19), there results

$$RF = 10 \log_{10} \left[\frac{\frac{U}{s}}{\left(1 - \frac{k}{100}\right) 10^{-D_{R1}/10} + \frac{k}{100}\, 10^{-D_{R2}/10}} \right] \tag{3.20}$$

which may be written

$$RF = D_{R1} + D_{R2} - 10 \log_{10}\left[10^{D_{R2}/10} + \frac{k}{100}\left(10^{D_{R1}/10} - 10^{D_{R2}/10}\right)\right] + 10 \log_{10} \frac{U}{s} \qquad (3.21)$$

Let

$$D_{R1} - D_{R2} = D_D \qquad (3.22)$$

be the difference in noise transmission loss between material number 1 and material number 2. And let

$$D_{R1} - RF = D_o \qquad (3.23)$$

be the reduction in effective noise transmission loss for the entire room due to the fact that the walls contain k per cent of material number 2 having greater transmittivity than material number 1. Using equations (3.22) and (3.23), equation (3.21) becomes

$$D_o = 10 \log_{10}\left[1 + \frac{k}{100}\left(10^{D_D/10} - 1\right)\right] - 10 \log_{10} \frac{U}{s} \qquad (3.24)$$

If the absorption coefficient for the wall surfaces is uniform, or nearly so, then

$$U = as \qquad (3.25)$$

and

$$D_o = 10 \log_{10}\left[1 + \frac{k}{100}\left(10^{D_D/10} - 1\right)\right] - 10 \log_{10} a \quad (3.26)$$

Equation (3.26) can be extended, approximately, to the case of a blanket enclosing a wind-tunnel shell. Frequently, the insulating blanket will contain discontinuities such as access doors which are necessary for operation and maintenance. These discontinuities generally represent a small percentage of the surface area but may have considerably greater acoustic transmittivity than the blanket and therefore allowing disproportionate transmission of noise. For the case of a wind tunnel outdoors, the absorption coefficient a may be taken equal to unity. Then equation (3.26) becomes

$$D_o = 10 \log_{10}\left[1 + \frac{k}{100}\left(10^{D_D/10} - 1\right)\right] \quad (3.27)$$

Figure 24 is a graph of equation (3.27) which is verified by reference 14. Figure 24 clearly illustrates the disproportionate increase in transmittivity that an insulating blanket would have for a relatively small percentage of open area. For instance, if a blanket having a 40-decibel noise transmission loss has only 1 per cent open area, the insulative properties would be diminished

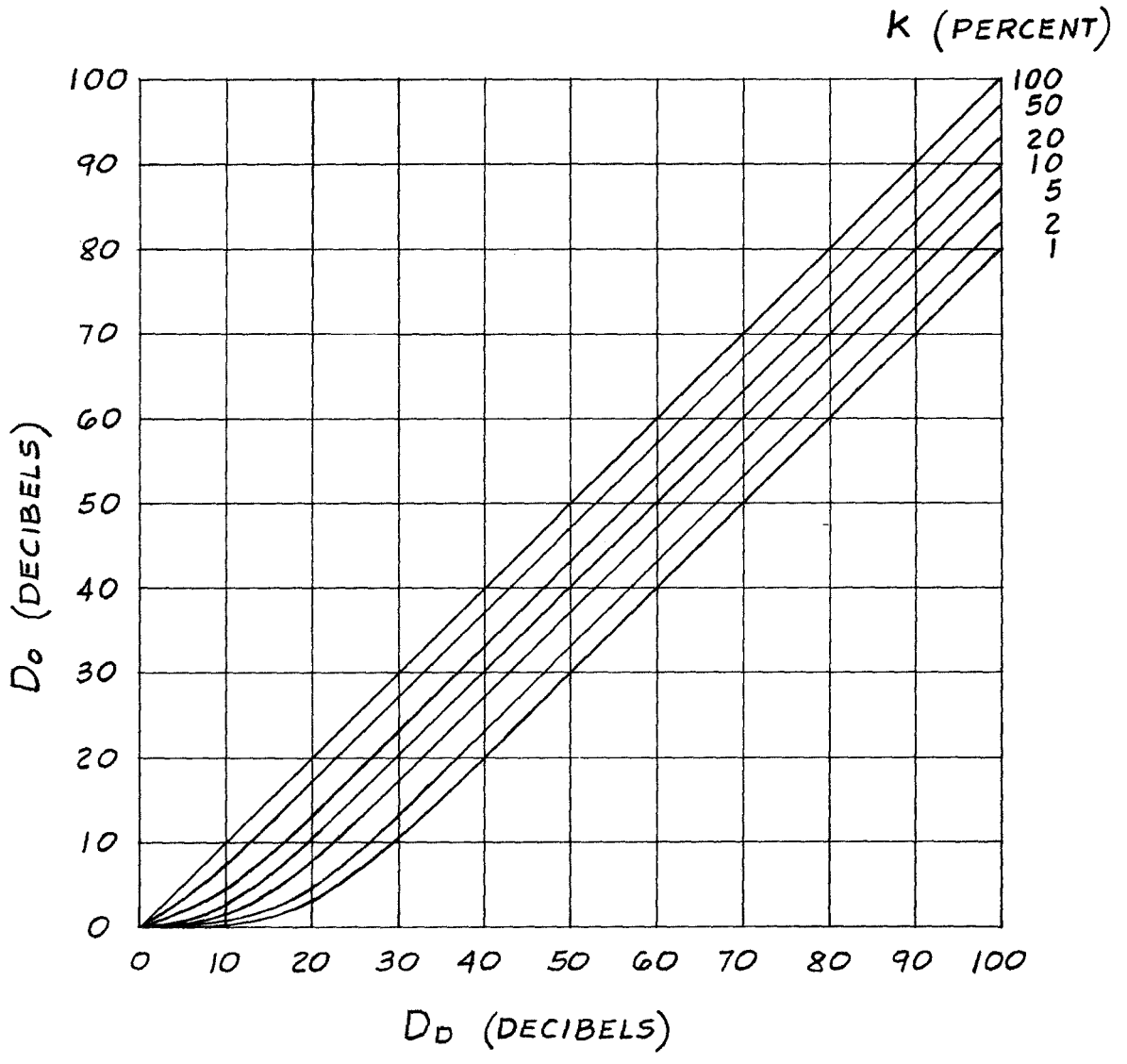
K (PERCENT)
100
50
20
10
5
2
1
100
90
80
70
60
50
40
30
20
10
0
D_o (DECIBELS)
0
10
20
30
40
50
60
70
80
90
100
D_D (DECIBELS)

FIG. 24

20 decibels. In other words, the 1 per cent open area results in a 50 per cent decibel loss. It is apparent, therefore, that, so far as is possible, noise leaks should be eliminated or diminished.

For the case of a wind-tunnel shell containing a noise insulating blanket, all of the noise leaks may not affect the auditor. A rough rule of thumb is that the majority of noise reaching the auditor radiates from those surfaces visible to a human auditor and only those leaks contained in the visible surface are important. This rule is more nearly accurate for the higher frequencies than the lower because high frequencies have greater directional properties than low frequencies.

CHAPTER IV

EXAMPLE - 7- BY 10-FOOT HIGH-SPEED TUNNEL

The 7- by 10-foot high-speed tunnel located in the West Area of Langley Field has recently been modified for noise and vibration control. Before modifications to this tunnel, two critical faults requiring immediate attention were observed. Many fatigue cracks involving the structural supporting and stiffening members were noted about points of stress concentration such as welds and coped sections. The noise level of the tunnel at top speed operation was sufficiently high that complaints of inefficiency, discomfort, and interference were received from nearby research facilities.

In order to eliminate these faults, five corrective measures were decided upon; these modifications were as follows:

1. All fatigue cracks were repaired and the tunnel shell stiffened.

2. The sliding base plates for the support legs were adjusted to carry more vertical loading.

3. The metal expansion joint nearest the fan was removed and replaced with a neoprene expansion joint.

4. Acoustic baffles were placed in the air stream, both upstream and downstream from the fan.

5. A lightweight noise insulating blanket was installed, enclosing the fan section between the expansion joint and the exhaust tower.

The first three modifications were primarily for vibration and fatigue control and have very little effect upon noise control. Modifications 4 and 5 were primarily for noise control and will be discussed in detail.

An acoustic survey was made for the tunnel circuit by both NACA and a private consultant. Both surveys agreed in general but not always in detail. This paper is based upon the NACA results. The acoustic survey indicated that more noise emanated from the vicinity of the fan than elsewhere and that acoustic treatment should be applied there. Furthermore, in the vicinity of the fan, the noise seemed to radiate about equally from the tunnel shell and the exhaust tower louvers. Other portions of the tunnel such as the test section, turning vanes, and intake tower contributed to the over-all noise level but the relative noise level proportions of each source with respect to the over-all would have been difficult if not impossible to determine. However, both the NACA and the consultant believed that the noise level from the vicinity of the fan was sufficiently higher than the total from the remainder of the sources that

properly designed acoustic treatment applied in the fan vicinity would provide a satisfactory noise reduction. This meant that a noise level difference of 10 or more decibels existed; otherwise acoustic treatment of the fan vicinity alone would not be adequate. Modifications for the fan vicinity were then planned in the belief that further treatment would be unnecessary and that an over-all noise reduction of 10 or more decibels could be obtained. Subsequent developments verified this as an over-all noise reduction of 12 decibels was obtained after the acoustic treatment.

Acoustic baffles seemed to be the most practical form of treatment to control the noise radiating from the exhaust tower louvers. Two locations for the baffles were considered; the exhaust tower and the air stream. Baffles placed in the exhaust tower would attenuate the noise radiating from the louvers only, while baffles placed in the air stream would attenuate the noise radiating from the louvers and from the remainder of the tunnel circuit. The principal objection to placing the baffles in the air stream was the loss of power anticipated due to air flow drag. The power loss, computed in accordance with the theory included in chapter II, for baffles placed fore and aft of the tunnel fan was about 200 horsepower. This loss could be tolerated and the baffles were installed in the air stream.

Furthermore, it was estimated that a portion of the power lost through drag would be regained through partial elimination of turbulence. This factor has not been verified as yet.

The tunnel shell from the expansion joint to the exhaust tower was insulated with a flexible lightweight blanket. The insulating blanket consisted of the following:

1. Structural framework serving the dual purpose of stiffening the tunnel shell and supporting the insulating blanket.
2. Road mesh tack welded to the structural framework
3. Seven inches of preformed bonded Fiberglas wired to the road mesh
4. Expanded metal lath wired through the Fiberglas to the road mesh
5. Insulmastic vinyl coat (6 gallons per 100 square feet) sprayed on the expanded lath
6. Insulmastic gilsonite coat (8 gallons per 100 square feet) sprayed on the vinyl
7. Aluminum colored slate granules sprayed on the gilsonite, while still soft, to provide an aluminum colored appearance

Figure 25 represents a typical frequency spectrum made of the noise generated by the 7- by 10-foot high-speed tunnel before the noise and vibration control measures were

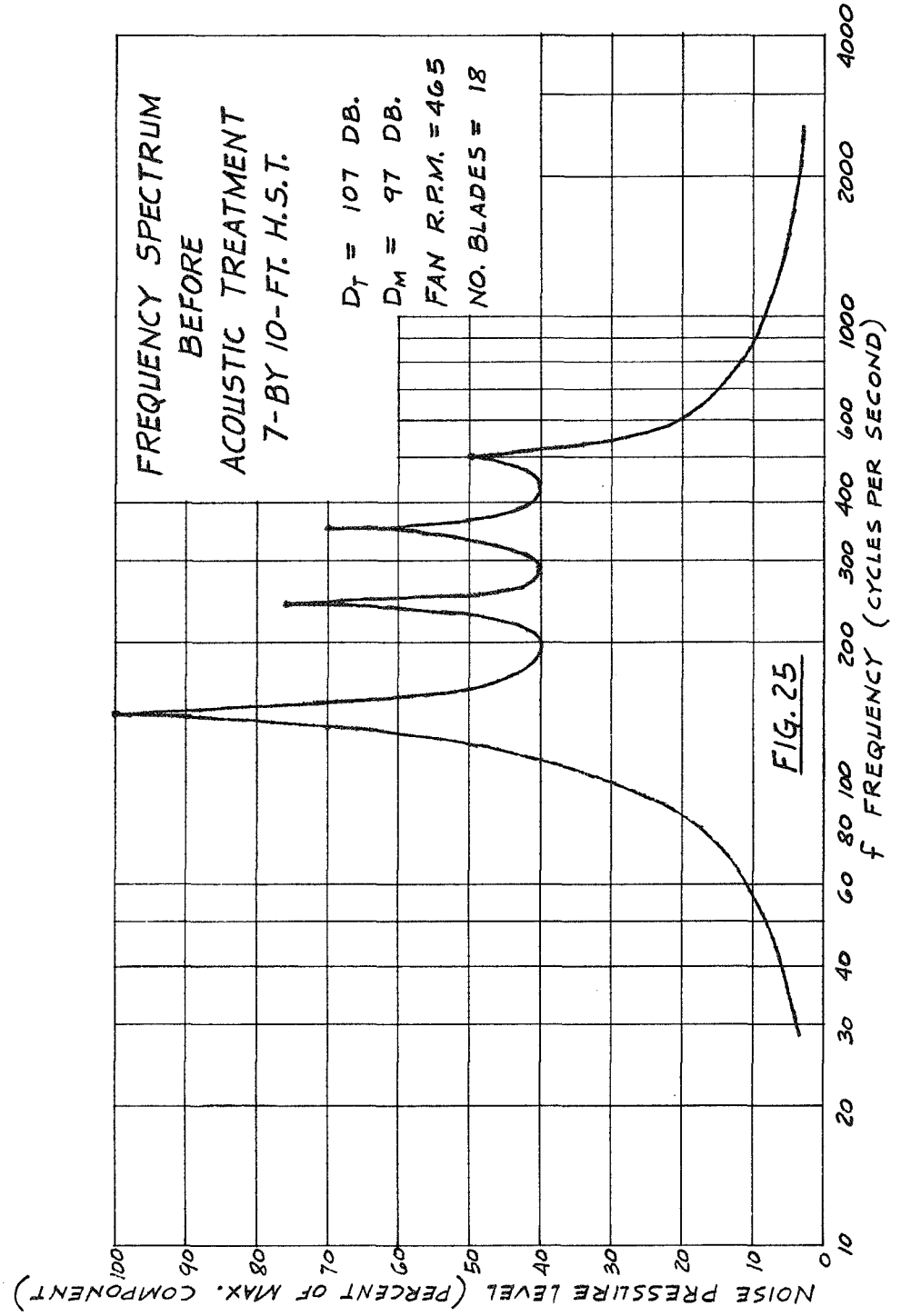
FREQUENCY SPECTRUM
BEFORE
ACOUSTIC TREATMENT
7-BY 10-FT. H.S.T.
D_T = 107 DB.
D_M = 97 DB.
FAN R.P.M. = 465
NO. BLADES = 18
NOISE PRESSURE LEVEL (PERCENT OF MAX. COMPONENT)
f FREQUENCY (CYCLES PER SECOND)
0
10
20
30
40
50
60
70
80
90
100
10
20
30
40
60
80
100
200
300
400
600
1000
2000
4000

FIG. 25

applied. Four predominant frequency components are apparent. The first and strongest component corresponds almost exactly to the first harmonic of the fan but the other components are not in such good agreement with the higher fan harmonics. The total noise, resulting almost entirely from the four predominant components, equaled 107 decibels. The location of the measurement was on the ground, about 100 feet directly opposite the fan and motor section where two sides of the exhaust tower louvers could be plainly seen. This site was chosen because it was far enough away to avoid reflection interference but in a position to receive direct radiation from two sides of the exhaust tower and from the tunnel shell opposite the fan.

Figure 26 shows schematic sections through the tunnel at the vicinity of the fan and exhaust tower illustrating the acoustic treatment. The contour of the tunnel shell has been simplified in order to simplify the computations.

Before proceeding with the computations for the 7- by 10-foot high-speed tunnel, it will be convenient to discuss a method of noise analysis. The total noise pressure level equals

$$D_T = 20 \log_{10} \frac{E_T}{E_o} \qquad (4.1)$$

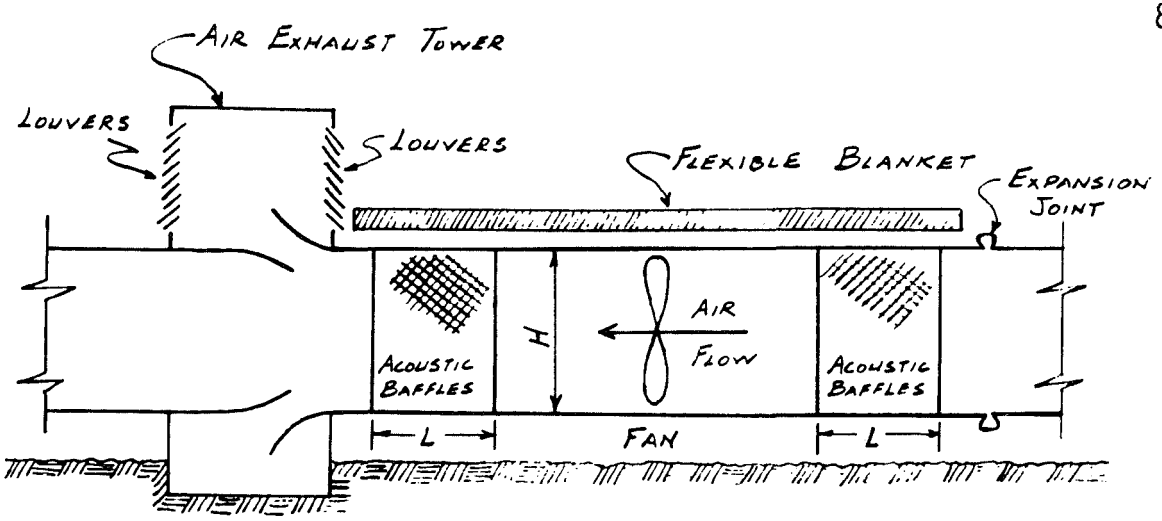

SCHEMATIC SECTION THRU FAN & EXHAUST TOWER

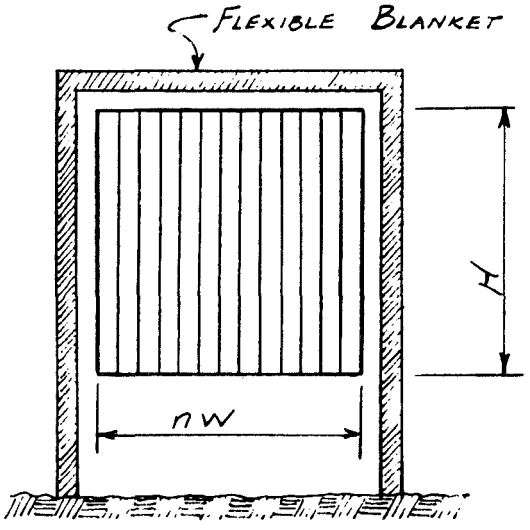

SCHEMATIC SECTION THRU ACOUSTIC BAFFLES

FIG. 26

where

$$E_o = 0.0002 \text{ dynes per cm}^2 \tag{4.2}$$

is the base noise pressure energy and

$$E_T = E_1 + E_2 + E_3 + \ldots = \Sigma E \tag{4.3}$$

is the total noise pressure energy. Let

$$E_1 = E_M \tag{4.4}$$

where E_M equals the noise pressure energy of the maximum component. Then

$$100 \frac{E_T}{E_M} = 100 + 100 \frac{E_2}{E_M} + 100 \frac{E_3}{E_M} + \ldots = \Sigma\% \tag{4.5}$$

where $\Sigma\%$ represents the summation of the percentages of all of the components. The maximum noise pressure level equals

$$D_M = 20 \log_{10} \frac{E_M}{E_o} \tag{4.6}$$

Combining equations (4.1) and (4.6)

$$D_T - D_M = 20 \log_{10} \frac{E_T}{E_M} \tag{4.7}$$

and using equation (4.5)

$$D_T = D_M + 20 \log_{10} \left(\frac{\Sigma\%}{100} \right) \tag{4.8}$$

The difference in decibels of any component from the maximum component will equal

$$D_L = D_M - D \tag{4.9}$$

where

$$D = 20 \log_{10} \frac{E}{E_o} \tag{4.10}$$

then

$$D_L = - 20 \log_{10}\left(\frac{E}{E_M}\right) \tag{4.11}$$

or

$$D_L = 40 - 20 \log_{10}\left(100 \frac{E}{E_M}\right) \tag{4.12}$$

Let

$$\% = 100 \frac{E}{E_M} \tag{4.13}$$

represent the percentage of any component to the maximum component, then

$$D_L = 40 - 20 \log_{10}(\%) \tag{4.14}$$

If a noise frequency spectrum is plotted with the frequency components expressed as percentages of the maximum component, equations (4.8) and (4.14) will prove useful in analyzing the noise. Figure 27 contains a plot of equation (4.14).

DECIBEL TO PERCENT RELATIONSHIP

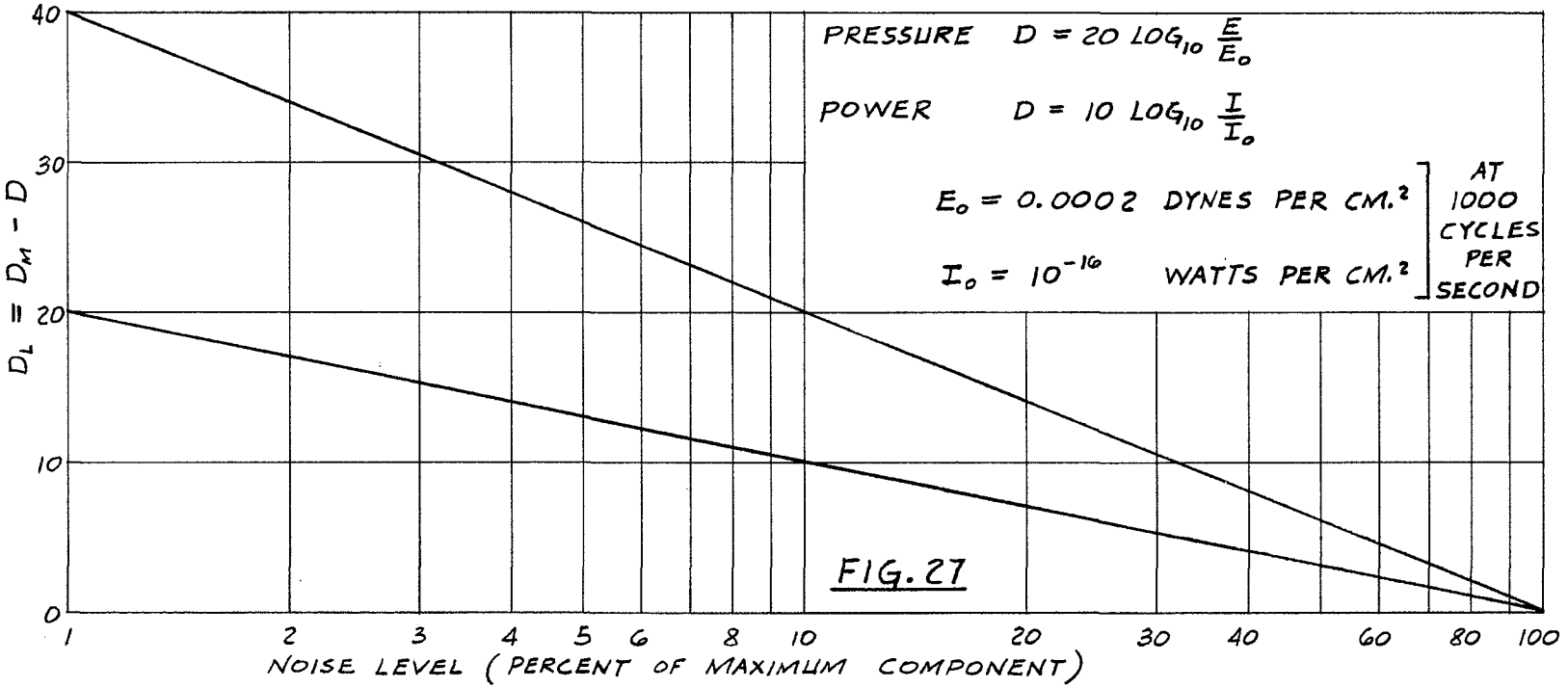

FIG. 27

The following pages contain, without comment, the successive steps in analyzing the acoustic treatment applied to the 7- by 10-foot high-speed tunnel.

Acoustic Baffle and Tunnel Properties

$L = 18$ feet

$H = 26$ feet

$W = 2$ feet

$t = 0.33$ feet

$n = 14$

$A = 730$ square feet

$V = 72$ ft/sec (before baffle installation)

$\rho = 0.00206$ slugs/ft^3

$T = 140^\circ$ F + 460 = 600° F absolute

$M = 106.3$ slugs/sec

$p = 2116 - 7 = 2109$ lb/ft^2

Standard Conditions

$\rho_o = 0.002378$ slugs/ft^3

$p_o = 2116$ lb/ft^2

$T_o = 60^\circ$ F + 460 = 520° F absolute

$\mu_o = 3.73 \times 10^{-7}$ slugs/ft sec

ACOUSTIC BAFFLE ANALYSIS

$$\frac{L}{W_c} = \frac{18}{1.67} = 10.78$$

Before baffles				After baffles				
Frequency f	Per cent strongest component %	Decibels lower D_L	Decibels absolute D	Absorption coefficient a	Noise reduction D_R	Decibels absolute D	Decibels lower D_L	Per cent strongest component %
140	100	0	97.0	0.34	5.0	92.0	0	100.0
240	76	2.5	94.5	0.77	15.0	79.5	12.5	23.5
350	70	3.2	93.8	0.94	21.0	72.8	19.2	11.0
500	50	6.0	91.0	0.99	22.0	69.0	23.0	7.2
	296							141.7

$\frac{\sum\%}{100} = 2.96$

$20 \log_{10} 2.96 = 20 \times 0.471 = 9.44$

$D_T = D_M + 20 \log_{10}\left(\frac{\sum\%}{100}\right)$

$= 97 + 9.44 = 106.44$ decibels

$\frac{\sum\%}{100} = 1.417$

$20 \log_{10} 1.417 = 20 \times 0.151 = 3.02$

$D_T = D_M + 20 \log_{10}\left(\frac{\sum\%}{100}\right)$

$= 92 + 3.02 = 95.02$ decibels

Density

$$\rho = \rho_o \times \frac{p}{p_o} \times \frac{T_o}{T}$$

$$= 0.002378 \times \frac{2109}{2116} \times \frac{520}{600} = 0.00206 \text{ slugs/ft}^3$$

Coefficient of Viscosity

$$\mu = \mu_o \left[\frac{T}{T_o}\right]^{3/4}$$

$$= 3.73 \times 10^{-7} \left[\frac{600}{520}\right]^{3/4} = 3.73 \times 10^{-7} \times 1.118$$

$$= 4.16 \times 10^{-7} \text{ slugs/ft-sec}$$

Kinematic Viscosity

$$\nu = \frac{\mu}{\rho}$$

$$= \frac{4.16 \times 10^{-7}}{2.06 \times 10^{-3}} = 2.02 \times 10^{-4} \text{ ft}^2/\text{sec}$$

Air Flow Quantity

$$Q = \frac{M}{\rho}$$

$$= \frac{106.3}{0.00206} = 51{,}600 \text{ ft}^3/\text{sec}$$

Cross-Sectional Open Area through Baffles

$$A_o = nHW_c$$

$$= 14 \times 26 \times 1.67 = 606 \text{ sq ft}$$

Velocity through Baffles

$$V = \frac{Q}{A_o}$$

$$= \frac{51,600}{600} = 85.1 \text{ ft/sec}$$

Reynolds Number

$$R = \frac{VL}{\nu}$$

$$= \frac{85.1 \times 18}{2.02 \times 10^{-4}} = 7.58 \times 10^6 > 5 \times 10^6$$

Turbulent flow

Surface Area of Baffles

$$A_s = 2nHL$$

$$= 2 \times 14 \times 26 \times 18 = 13,110 \text{ ft}^2$$

Dynamic Pressure

$$q = \frac{1}{2}\rho V^2$$

$$= \frac{1}{2} \times 2.06 \times 10^{-3}(85.1)^2 = 7.46 \text{ lb/ft}^2$$

Friction Coefficient

$$W_c = 1.67 \text{ ft}$$

$$\varepsilon = \text{Very rough}$$

$$C_f = 6.6 \times 10^{-3}$$

Drag Force

$$F_D = C_f A_s q$$

$$= 6.6 \times 10^{-3} \times 13{,}110 \times 7.46 = 646 \text{ lb}$$

Power Loss

$$P_L = F_D V$$

$$= 646 \times 85.1 = 55{,}000 \text{ ft-lb/sec}$$

$$\div 550$$

$$= 100 \text{ horsepower each set of baffles}$$

$$\text{Total } P_L = 2 \times 100 = 200 \text{ horsepower}$$

Flexible Blanket

2.00 lb/ft^2	=	structural framework
0.44	=	8 gage 4" x 4" mesh
6.13	=	7 in. - 10-1/2 lb/ft^2 P.F. bonded Fiberglas
1.47	=	13 gage expanded metal lath
1.75	=	Insulmastic Vinyl coat 6 gal/100 sq ft Insulmastic Gilsonite coat 8 gal/100 sq ft aluminum colored slate granules
11.79 lb/ft^2		

From Mass Law Graph for frequencies between 100 ~/sec and 1000 ~/sec

$$D_R \tilde{=} 30 \text{ decibels}$$

The value of 30 decibels for the noise transmission loss through the flexible lightweight blanket is only a very rough approximation. Actually, the blanket is probably more effective. However, in this case, refinement is unnecessary because the acoustic baffles reduce the noise only 12 decibels proving to be the weak point in the noise control system. Since the preliminary analysis indicated that the noise intensities radiating from the exhaust tower and the tunnel shell were approximately equal, and since the baffles principally affected the tower and the blanket principally affected the shell, then the excess in effectiveness of the blanket over the baffles would have little influence upon the total noise reduction.

The following construction photographs show the noise control measures applied to the 7- by 10-foot high-speed tunnel. Figure 28 shows the upstream acoustic baffles. The downstream baffles are identical with the upstream as to material and construction but, since the tunnel size increases downstream, the height H and number of channels n are greater. Average values were used in the example. Figures 29, 30, and 31 show successive steps in the erection of the insulating blanket. The aluminum colored slate granules had not been applied at the time of Figure 31.

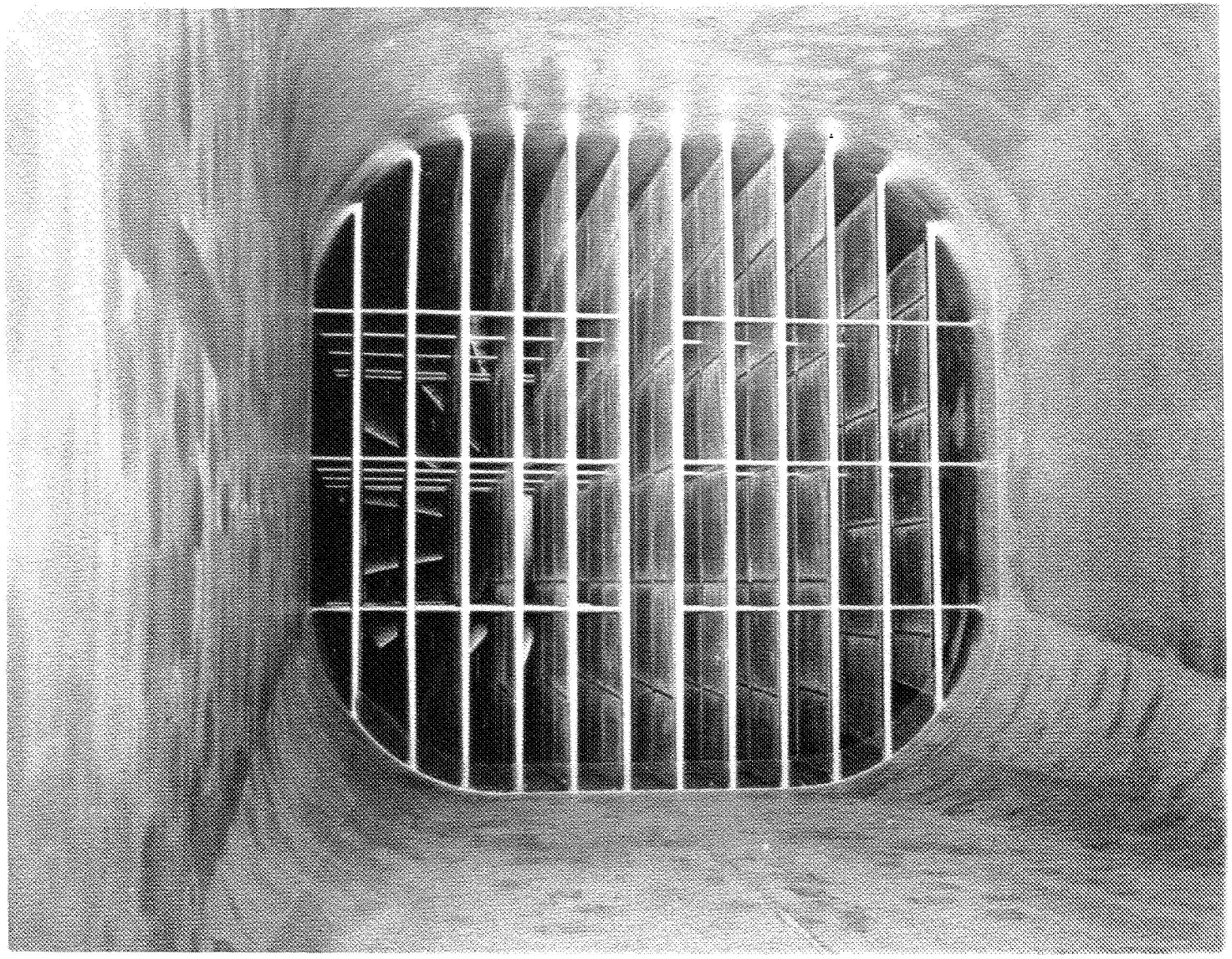

FIGURE 28

UPSTREAM ACOUSTIC BAFFLES
7- BY 10-FOOT HIGH-SPEED TUNNEL

NACA L-68722

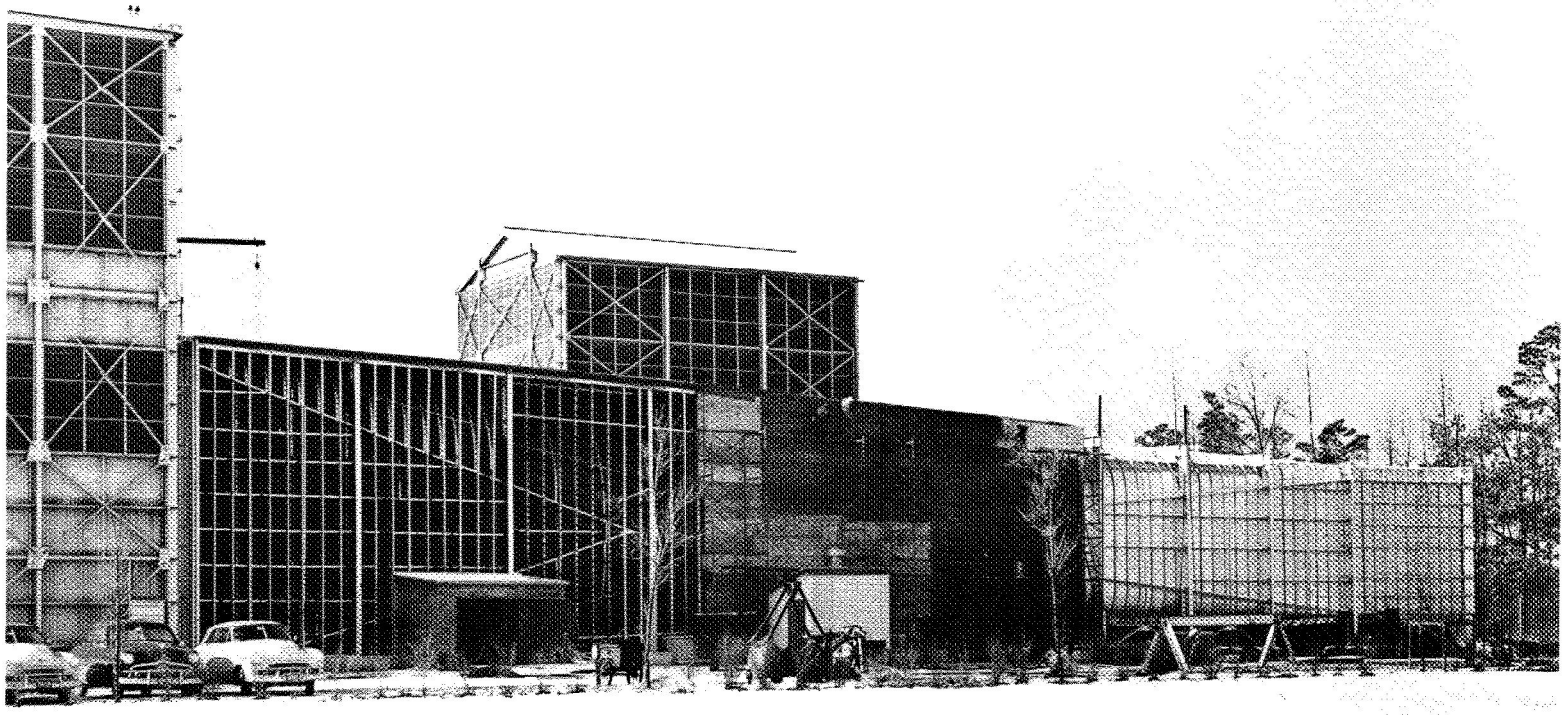

NACA
L-69286

FIGURE 29

INSTALLATION OF FIBERGLAS
NOISE INSULATING BLANKET
7- BY 10-FOOT HIGH-SPEED TUNNEL

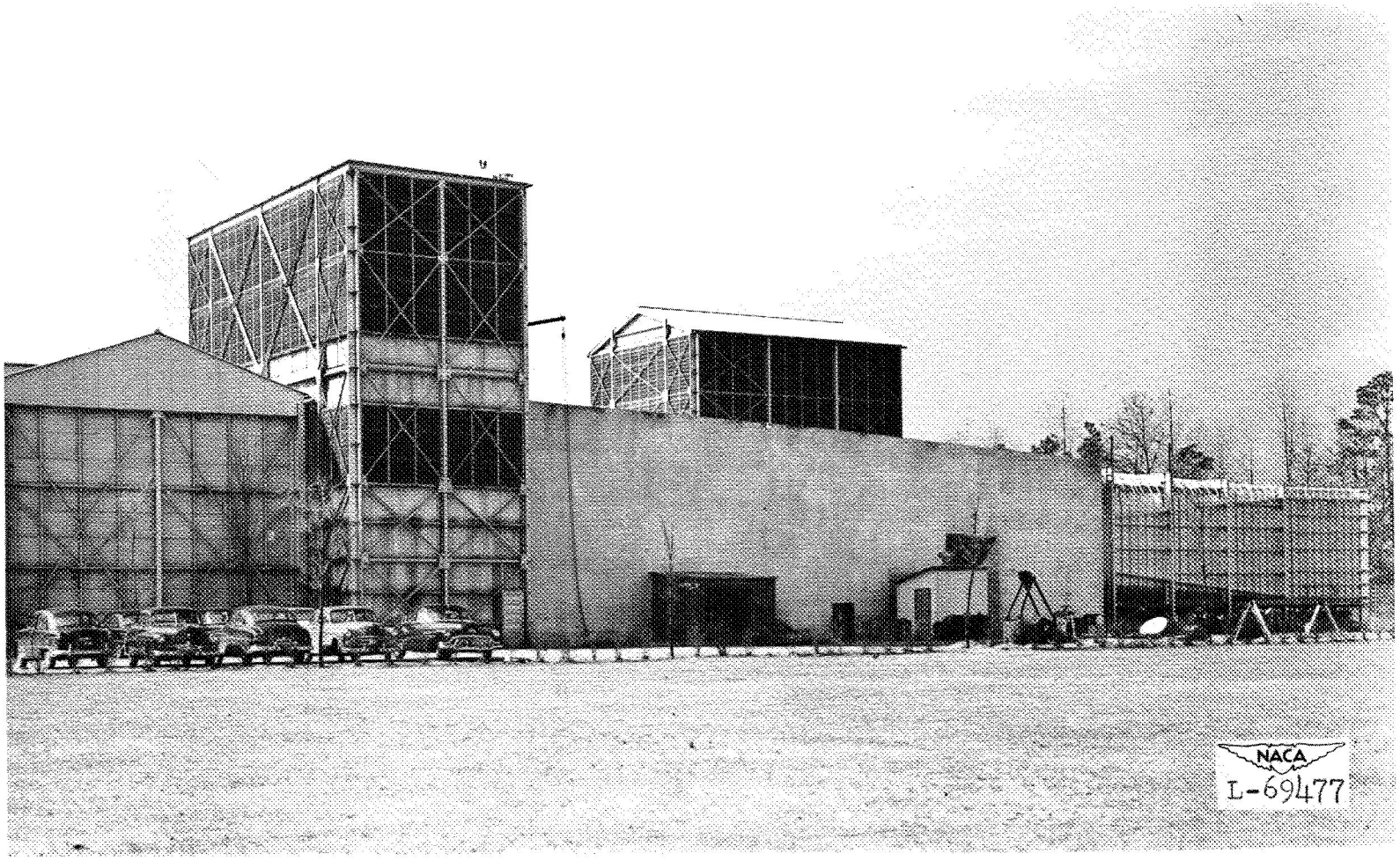

FIGURE 30

VINYL COAT
NOISE INSULATING BLANKET
7- BY 10-FOOT HIGH-SPEED TUNNEL

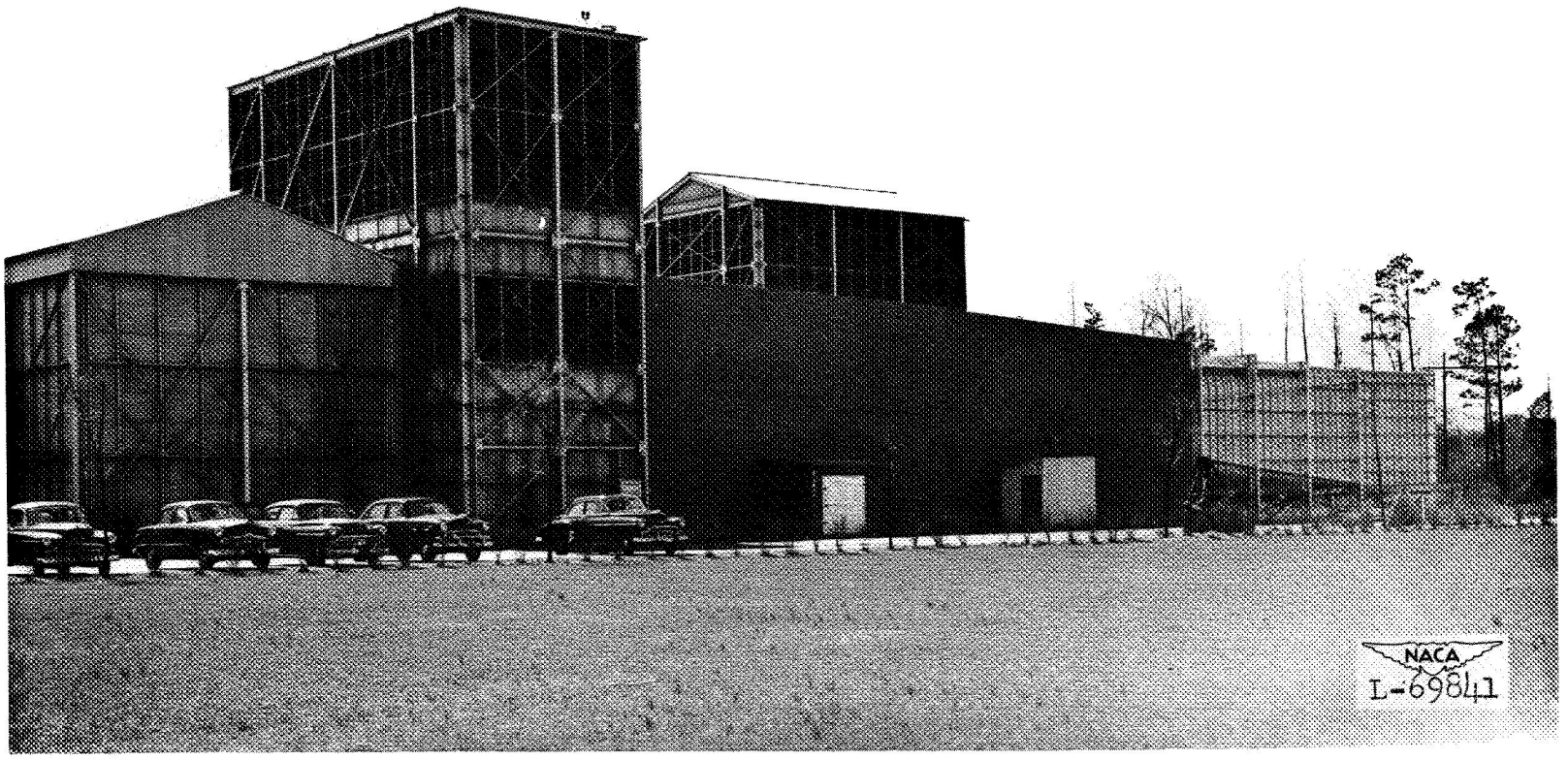

FIGURE 31

GILSONITE COAT
NOISE INSULATING BLANKET
7- BY 10-FOOT HIGH-SPEED TUNNEL

CHAPTER V

CONCLUDING REMARKS

Four methods have been discussed in detail for controlling the noise and vibration generated by a wind tunnel. Two of the methods, acoustic baffles and noise insulation, discussed in chapter II and chapter III, respectively, have been classed as quantitative noise control measures for which a measurable, and generally predictable, noise attenuation results. The other two methods, turning vane support and helical springs, discussed in appendix A and appendix B, respectively, are classed as qualitative noise and vibration control measures for which the attenuation may be measurable but unpredictable.

The qualitative control measures, helical springs and turning vane support, have been arranged as independent units in the appendix with their own symbols, figures, and references. This has been done both for convenience and because they have wide application in the field of structural design other than noise and vibration control.

Chapter IV considers an example, the 7- by 10-foot high-speed tunnel, for which quantitative noise control measures were applied. The example illustrates that, with the aid of a preliminary noise survey, reasonable

predictions can be made using the methods discussed in chapter II and chapter III.

Noise and vibration control is relatively undeveloped and for the case of wind tunnels is still in its infancy. Much more theoretical work and substantiating test data are necessary before it becomes a reliable medium in the hands of the structural designer.

REFERENCES

1. Sabine, Hale J., "The Absorption of Noise in Ventilating Ducts." Journal of the Acoustical Society of America, Vol. 12, July 1940, p. 53.

2. Knudsen, Vern O., "The Absorption of Sound - Measurements, Coefficients of Absorption, and Other Properties of Acoustical Materials." Architectural Acoustics. John Wiley and Sons, N. Y., 1932. Chapter VIII, pp. 187-251.

3. Heyl, Paul R., and Chrisler, V. L., "Architectural Acoustics." Nat. Bur. of Stds., Circular C418, issued January 10, 1938.

4. Chrisler, V. L., "Dependence of Sound Absorption upon the Area and Distribution of the Absorbent Material." Nat. Bur. of Stds. Research Paper RP 700. (Part of Jour. of Research of Nat. Bur. of Stds., Vol. 13, Aug. 1934).

5. "Sound Absorption Coefficients of the More Common Acoustic Material." Nat. Bur. of Stds. Letter Circular LC 870, dated August 1, 1947.

6. Daugherty, R. L., Hydraulics. McGraw-Hill Book Company, Inc., N. Y. and London 1937, chapter VIII, pp. 187-228.

7. Madison, Richard D., and Elliot, Walter R., Friction Charts for Gases Including Correction for Temperature, Viscosity, and Pipe Roughness. Heating, Piping, and Air Conditioning, October 1946 ASHVE Journal Section, pp. 107-112.

8. Knudsen, Vern O., "Architectural Acoustics." John Wiley and Sons, N. Y., 1932, chapters XII and XIII, pp. 299-330.

9. Chrisler, V. L., Sound Insulation of Wall and Floor Constructions. Building Materials and Structures. Report BM517, March 28, 1939, also supplement issued December 20, 1940.

10. Beranck, Leo L., and Work, George A., Sound Transmission thru Multiple Structures Containing Flexible Blankets. Journal of the Acoustical Society of America, Vol. 21, July 1949, p. 419.

11. London, Albert, Transmission of Reverberant Sound Through Single Walls. U. S. Department of Commerce, National Bureau of Standards, Research Paper RP 1998, Vol. 42, June 1949.

12. Beranck, Leo L., "Acoustic Measurements." John Wiley and Sons, N. Y., 1949, chapter 19, pp. 836-887.

13. Olson, Harry F., "Elements of Acoustical Engineering." D. Van Nostrand Co., Inc., N. Y., 1949, chapter XI, pp. 397-456.

14. Sabine, Hale J., "Less Noise - Better Hearing." The Celotex Corporation, Chicago, 1941, Figure 7.4, p. 81.

APPENDIX A

TURNING VANE SUPPORT FOR ELLIPTICAL CORNER RINGS

Discussion

When fluid under pressure is contained in a cylindrical duct system, the shell of the duct may be stressed in several ways. The simplest case occurs when the duct is uniform, without discontinuity and unrestrained by stiffening rings. Then the maximum stress is the hoop stress. When discontinuities or restraint exist, the stress distribution is more complicated.

A particular type of discontinuity that is common to many duct systems is the mitered junction resulting from the necessity for changing the direction of air flow. The mitered junction of two cylinders is elliptical in form. Usually the stress distribution at the junction is severe resulting in the need for reinforcement. Usually, the reinforcement is a stiffening ring, elliptical in shape, designed to support at least two conditions of loading: the pressure loading due to the effect of the pressure acting directly on the exposed surface of the ring, and the pressure plating loading due to the effect of the longitudinal and circumferential stresses in the cylinders.

Reference 1 discusses the stress distribution acting upon elliptical corner rings due to pressure and pressure plating loading. The bending moments, tension forces, and shear forces in the stiffening ring are determined and presented in the form of coefficients. No account is taken of restraints imposed on the ring by any internal structure such as turning vanes, or by external structure such as supports, but the ring alone is considered and is assumed to be in equilibrium under the applied pressure and pressure plating forces. The fact that the shells will not normally be connected to the ring at its center line is also ignored.

Most wind tunnels utilize turning vanes, at the mitered junctions, to change the direction of air flow. Usually, one end of the turning vanes is rigidly fastened to the elliptical corner ring while the opposite end is secured by a slotted connection to permit differences in thermal movement between vanes and ring. Consequently, the vanes are structural parasites contributing nothing to structural rigidity.

The following material presents a method by which the turning vanes and ring can be analyzed as an integral structural unit. Each end of the vanes is assumed to be rigidly attached to the inner surface of the ring. It will be shown that, generally, the contribution of the vanes to the support of the mitered junction is sufficiently large

that the requirements for the stiffening ring can be satisfied by a plate instead of the usual rolled or built-up sections. Although the vanes, designed as integral components with the ring, will be loaded more than otherwise, the vane requirements are little greater, if any, than dictated by good design practice.

The theory presented herein is based upon the following assumptions:

1. The elliptical ring is flexible and will not contribute bending resistance.

2. The vanes are uniformly spaced and so numerous that the distance between vanes may be considered small with respect to the major axis of the ellipse so that the reaction of the vanes upon the ring approximates continuous loading.

3. External restraints, such as supporting legs, are not considered.

4. Restraint of shell displacement by the reinforcing ring is not considered.

5. The shell is connected to the ring at the ring center line.

The loading considered herein, acting upon the mitered junction, is due entirely to pressure. The pressure may be positive, if internal, or negative (a partial vacuum) if

external. The restraint, offered by the turning vanes, is that necessary to keep the flexible ring in an elliptical configuration.

SYMBOLS

a	one-half major axis of ellipse
b	one-half minor axis of ellipse and radius of cylindrical shell
c	length measured along the circumference of shell
D	uniform spacing of turning vanes
F_φ	axial force on turning vanes (tensile force positive)
L	length measured along the cylinder
p	pressure on shell (internal pressure positive)
s	length measured along the perimeter of ellipse
t	thickness of cylindrical shell
T_φ	tangential force on elliptical ring (tension force positive)
V_φ	restraining force per unit of perimeter, parallel to Y-axis, acting on reinforcing ring
w	width of reinforcing ring exposed to pressure
x, y	Cartesian coordinates of a point on the ellipse
X_φ, Y_φ, Z_φ	applied forces per unit of perimeter, parallel to the Cartesian coordinate axes, acting on reinforcing ring
θ	one-half stream deflection angle
σ_c	intensity of circumferential stress in cylinder
σ_L	intensity of longitudinal stress in cylinder

φ angular coordinate of a point on ellipse

ψ inclination of normal to the major axis of a point on ellipse

REFERENCE

1. Appleyard, W., Bending Moment, Tension, and Shear at a Mitered Junction of Two Cylindrical Pressure Vessels. Royal Aircraft Establishment, Farnborough, England. Technical Note No. Aero 1906, July 1947.

1. GEOMETRY

Figures 1 and 2 illustrate the geometrical properties of the mitered junction. From Figure 2(a), it is seen that the relationship between the stream deflection angle and the ellipse axes equals

$$\cos \theta = \frac{b}{a} \tag{1.1}$$

The equation of the ellipse, in Cartesian coordinates, equals

$$\frac{x^2}{a^2} + \frac{y^2}{b^2} = 1 \tag{1.2}$$

and in polar coordinates

$$\left.\begin{aligned} x &= a \cos \varphi \\ y &= b \sin \varphi \end{aligned}\right\} \tag{1.3}$$

A differential element of ellipse perimeter equals

$$ds = \left[(dx)^2 + (dy)^2\right]^{1/2} \tag{1.4}$$

and using equations (1.3) becomes

$$ds = b(1 + \tan^2\theta \sin^2\varphi)^{1/2} d\varphi \tag{1.5}$$

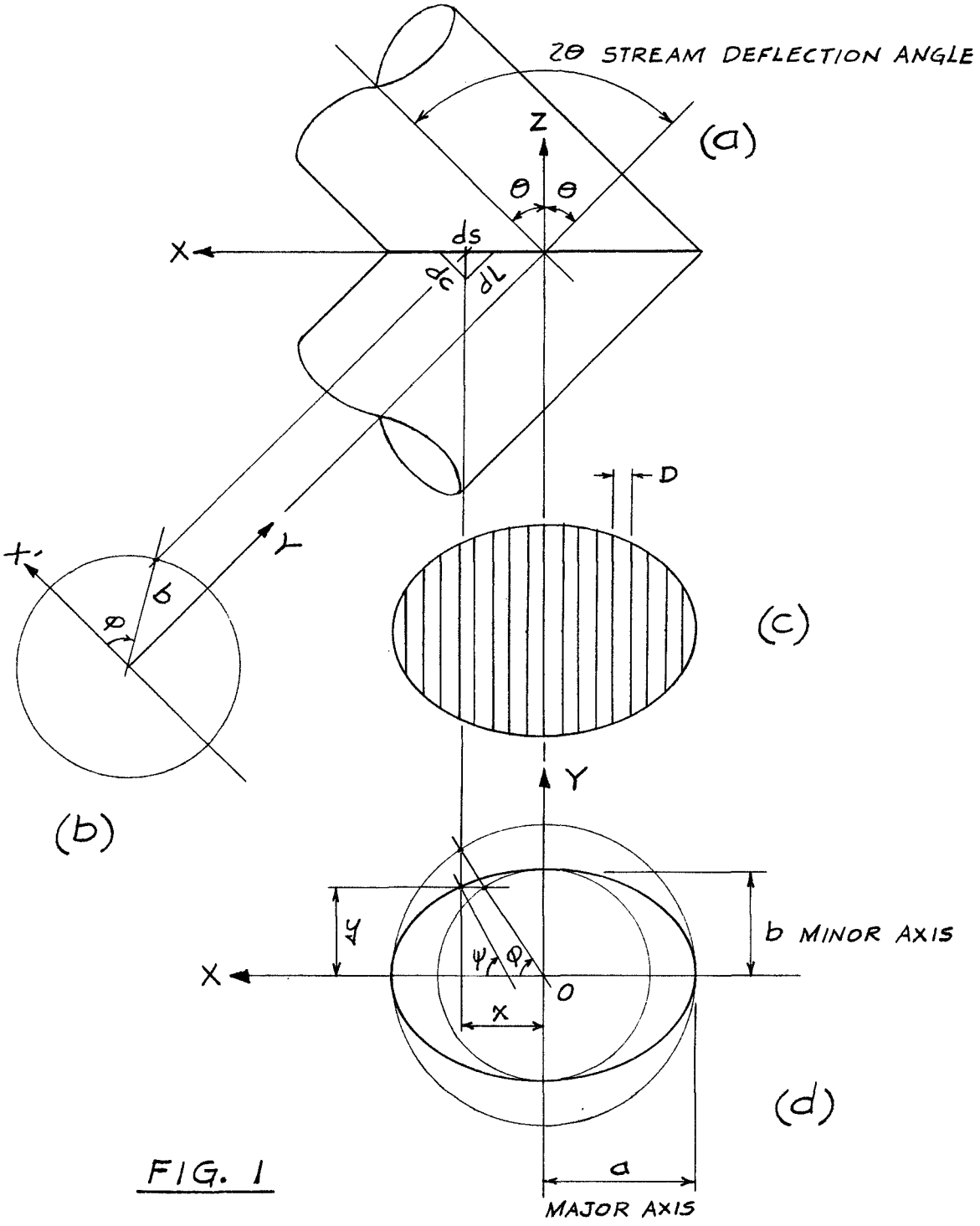
2θ STREAM DEFLECTION ANGLE
(a)
Z
θ
θ
X
ds
dc
dL
D
(c)
Y
(b)
φ
b
y
ψ
φ
X
O
x
b MINOR AXIS
(d)
a
MAJOR AXIS

FIG. 1

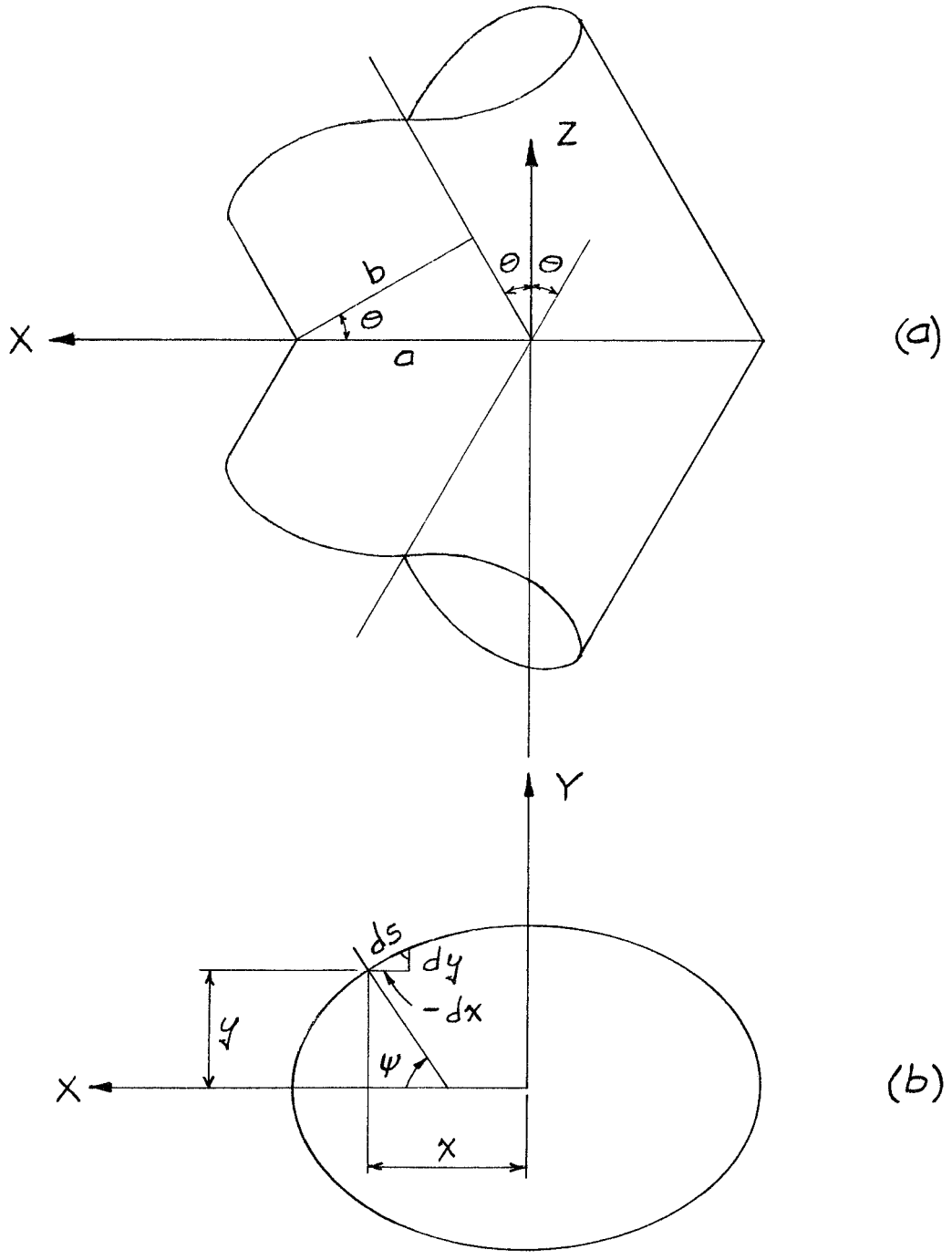

FIG. 2

From Figure 1, it is seen that a differential element of shell circumference will equal

$$dc = b\, d\varphi \tag{1.6}$$

and then a differential element of shell length will equal

$$dL = \left[(ds)^2 - (b\, d\varphi)^2\right]^{1/2} \tag{1.7}$$

or

$$dL = \left[\left(\frac{ds}{b\, d\varphi}\right)^2 - 1\right]^{1/2} b\, d\varphi \tag{1.8}$$

Using equation (1.5), equation (1.8) becomes

$$dL = b \tan\theta \sin\varphi\, d\varphi \tag{1.9}$$

Let ψ represent the angular coordinate, with respect to the major axis, of any normal point on the ellipse. Then, from Figure 2(b),

$$\left.\begin{aligned} \tan\psi &= -\frac{dx}{dy} \\ \sin\psi &= -\frac{dx}{ds} \\ \cos\psi &= \frac{dy}{ds} \end{aligned}\right\} \tag{1.10}$$

and using equations (1.3)

$$\left.\begin{aligned} \tan\psi &= \frac{a}{b}\tan\varphi \\ \sin\psi &= a\sin\varphi\,\frac{d\varphi}{ds} \\ \cos\psi &= b\cos\varphi\,\frac{d\varphi}{ds} \end{aligned}\right\} \tag{1.11}$$

Using equations (1.11)

$$d\psi = \frac{a}{b}\,\frac{\sec^2\varphi\,d\varphi}{\sec^2\psi} = \frac{a}{b}\,\frac{\cos^2\psi\,d\varphi}{\cos^2\varphi} \tag{1.12}$$

$$\cos^2\varphi = \frac{\cos^2\psi}{b^2\left(\frac{d\varphi}{ds}\right)^2} \tag{1.13}$$

$$\sin^2\varphi = \frac{\tan^2\varphi}{1+\tan^2\varphi} = \left(\frac{b}{a}\right)^2 \frac{\tan^2\psi}{1+\left(\frac{b}{a}\right)^2\tan^2\psi} \tag{1.14}$$

Using equations (1.1), (1.5), and (1.14)

$$\left(\frac{d\varphi}{ds}\right)^2 = \frac{1}{b^2}\left(1-\sin^2\theta\,\sin^2\psi\right) \tag{1.15}$$

then

$$\cos^2\varphi = \frac{\cos^2\psi}{1-\sin^2\theta\,\sin^2\psi} \tag{1.16}$$

and

$$d\psi = \frac{1 - \sin^2\theta \sin^2\psi}{\cos \theta} d\varphi \tag{1.17}$$

or

$$d\varphi = \frac{\cos \theta \, d\psi}{1 - \sin^2\theta \sin^2\psi} \tag{1.18}$$

Using equations (1.1), (1.5), (1.14), and (1.18)

$$ds = \frac{b \cos \theta \, d\psi}{(1 - \sin^2\theta \sin^2\psi)^{3/2}} \tag{1.19}$$

Equation (1.14) may be written

$$\sin^2\varphi = \frac{\cos^2\theta \sin^2\psi}{1 - \sin^2\theta \sin^2\psi} \tag{1.20}$$

Also, using equations (1.5), (1.18), and (1.19), the quantity

$$(1 + \tan^2\theta \sin^2\varphi)^{1/2} = \frac{ds}{b \, d\varphi} = \frac{1}{(1 - \sin^2\theta \sin^2\psi)^{1/2}} \tag{1.21}$$

2. GENERAL LOADING

Figure 3(b) shows the assumed loading acting upon any small length, Δs, of the elliptical ring perimeter. The ring is assumed to be a flexible cord held in an elliptical shape by the load distribution shown. The summation of the horizontal forces must equal zero or

$$T_\varphi \sin \psi + X_\varphi \Delta s - \left(T_\varphi + \Delta T_\varphi\right) \sin(\psi + \Delta\psi) = 0 \qquad (2.1)$$

or

$$\left(T_\varphi + \Delta T_\varphi\right) \sin(\psi + \Delta\psi) - T_\varphi \sin \psi = X_\varphi \Delta s \qquad (2.2)$$

which may be written

$$\Delta\left(T_\varphi \sin \psi\right) = X_\varphi \Delta s \qquad (2.3)$$

As Δs approaches zero, equation (2.3) becomes the total differential

$$d\left(T_\varphi \sin \psi\right) = X_\varphi \, ds \qquad (2.4)$$

which equals

$$\sin \psi \, dT_\varphi + T_\varphi \cos \psi \, d\psi = X_\varphi \, ds \qquad (2.5)$$

The summation of the vertical forces must equal zero or

$$\left(T_\varphi + \Delta T_\varphi\right)\cos(\psi + \Delta\psi) + Y_\varphi \Delta s - V_\varphi \Delta s - T_\varphi \cos \psi = 0 \qquad (2.6)$$

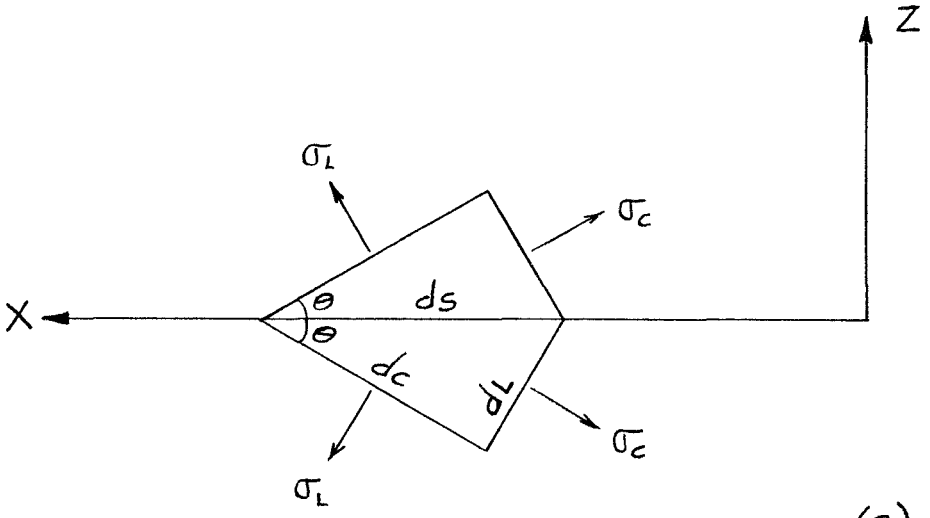
Z
X
σ_L
σ_c
θ
θ
ds
d_c
d_L
σ_c
σ_L

(a)

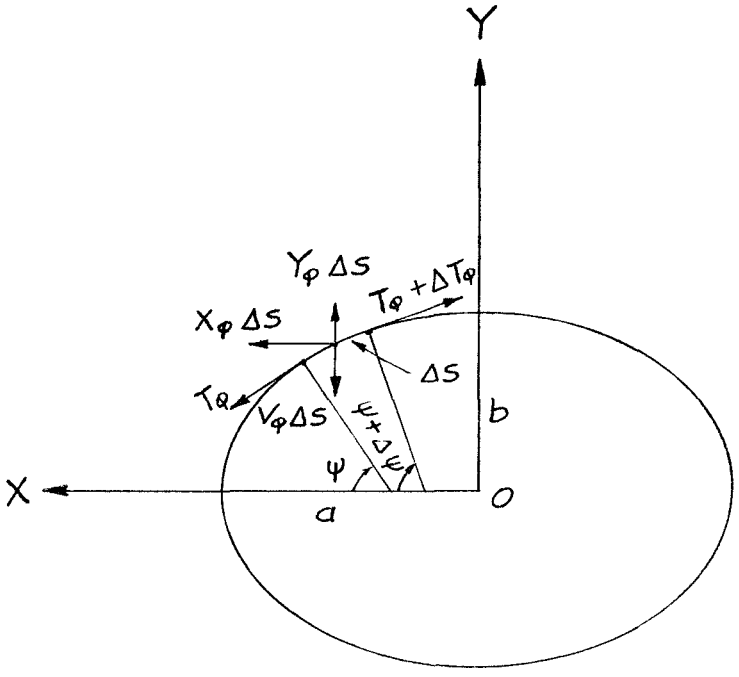
Y
X
$Y_\varphi \Delta s$
$T_\varphi + \Delta T_\varphi$
$X_\varphi \Delta s$
Δs
T_φ
$V_\varphi \Delta s$
$\varepsilon + \Delta\varepsilon$
ψ
b
a
0

(b)

FIG. 3

or

$$\left(T_\varphi + \Delta T_\varphi\right)\cos(\psi + \Delta\psi) - T_\varphi \cos\psi = \left(V_\varphi - Y_\varphi\right)\Delta s \qquad (2.7)$$

which may be written

$$\Delta\left(T_\varphi \cos\psi\right) = \left(V_\varphi - Y_\varphi\right)\Delta s \qquad (2.8)$$

As Δs approaches zero, equation (2.8) becomes the total differential

$$d\left(T_\varphi \cos\psi\right) = \left(V_\varphi - Y_\varphi\right)ds \qquad (2.9)$$

which equals

$$\cos\psi\, dT_\varphi - T_\varphi \sin\psi\, d\psi = \left(V_\varphi - Y_\varphi\right)ds \qquad (2.10)$$

Using equations (1.19) and (2.5), there results

$$\sin\psi\, dT_\varphi + T_\varphi \cos\psi\, d\psi = \frac{b \cos\theta\, X_\varphi\, d\psi}{\left(1 - \sin^2\theta \sin^2\psi\right)^{3/2}} \qquad (2.11)$$

Dividing each side of the equation by $\sin\psi\, d\psi$, then

$$\frac{dT_\varphi}{d\psi} + \cot\psi T_\varphi = \frac{b \cos\theta\, X_\varphi}{\sin\psi\left(1 - \sin^2\theta \sin^2\psi\right)^{3/2}} \qquad (2.12)$$

which may be written

$$\frac{dT_\varphi}{d\psi} + f_1(\psi)T_\varphi = f_2(\psi) \qquad (2.13)$$

which is a first order linear differential equation and where

$$\left.\begin{aligned} f_1(\psi) &= \cot \psi \\ f_2(\psi) &= \frac{b \cos \theta \, X_\varphi}{\sin \psi \left(1 - \sin^2\theta \sin^2\psi\right)^{3/2}} \end{aligned}\right\} \qquad (2.14)$$

Let

$$T_\varphi = uv \qquad (2.15)$$

and when substituted in equation (2.12)

$$u = \frac{1}{\sin \psi} \qquad (2.16)$$

and

$$v = b \cos \theta \int \frac{X_\varphi \, d\psi}{\left(1 - \sin^2\theta \sin^2\psi\right)^{3/2}} + C \qquad (2.17)$$

where C is a constant of integration that must be adjusted for the boundary conditions.

Rewrite equations (2.5) and (2.10) as follows:

$$\sin \psi \, dT_\varphi = X_\varphi \, ds - T_\varphi \cos \psi \, d\psi \qquad (2.18)$$

$$\cos \psi \, dT_\varphi = \left(V_\varphi - Y_\varphi\right) ds - T_\varphi \sin \psi \, d\psi \qquad (2.19)$$

Dividing equation (2.18) by (2.19), there results

$$\tan \psi = \frac{X_\varphi \, ds - T_\varphi \cos \psi \, d\psi}{(V_\varphi - Y_\varphi) ds + T_\varphi \sin \psi \, d\psi} \tag{2.20}$$

and using equation (1.19)

$$V_\varphi = \frac{\cos \psi}{\sin \psi} X_\varphi + Y_\varphi - \frac{(1 - \sin^2\theta \sin^2\psi)^{3/2}}{b \cos \theta \sin \psi} T_\varphi \tag{2.21}$$

3. PRESSURE LOADING

The pressure loading, due to the effect of the pressure acting directly on the exposed surface of the reinforcing ring, is the same as for a pressure vessel of elliptical cross section. The pressure loading components, at any point on the junction defined by the Cartesian coordinates x and y or the angular coordinate φ, will equal

$$\left.\begin{aligned} X_\varphi \, ds &= pw \, dy \\ Y_\varphi \, ds &= -pw \, dx \end{aligned}\right\} \qquad (3.1)$$

where p is the pressure acting on the ring and w is the width of ring exposed to pressure. Using equations (1.3)

$$\left.\begin{aligned} X_\varphi \, ds &= pwb \cos \varphi \, d\varphi \\ Y_\varphi \, ds &= pwa \sin \varphi \, d\varphi \end{aligned}\right\} \qquad (3.2)$$

and using equation (1.5)

$$\left.\begin{aligned} X_\varphi &= \frac{pw \cos \varphi}{\left(1 + \tan^2\theta \sin^2\varphi\right)^{1/2}} \\ Y_\varphi &= \frac{pw \sin \varphi}{\cos \theta \left(1 + \tan^2\theta \sin^2\varphi\right)^{1/2}} \end{aligned}\right\} \qquad (3.3)$$

Figures 4 and 5 are graphs of equations (3.3).

With the aid of equations (1.16), (1.20), and (1.21), equations (3.3) may be written

$$\left.\begin{aligned} X_\varphi &= pw \cos \psi \\ Y_\varphi &= pw \sin \psi \end{aligned}\right\} \qquad (3.4)$$

Substituting equations (3.4) in equation (2.17)

$$v = pwb \cos \theta \int \frac{\cos \psi \, d\psi}{\left(1 - \sin^2\theta \sin^2\psi\right)^{3/2}} + C \qquad (3.5)$$

which after integration equals

$$v = \frac{pwb \cos \theta \sin \psi}{\left(1 - \sin^2\theta \sin^2 \psi\right)^{1/2}} + C \qquad (3.6)$$

From equations (2.15), (2.16), and (3.5)

$$T_\varphi = \frac{pwb \cos \theta}{\left(1 - \sin^2\theta \sin^2\psi\right)^{1/2}} + \frac{C}{\cos \psi} \qquad (3.7)$$

If the stream deflection angle, 2θ, equals zero, the tensile force in the ring will be constant, with respect to φ, and will equal the hoop stress, or

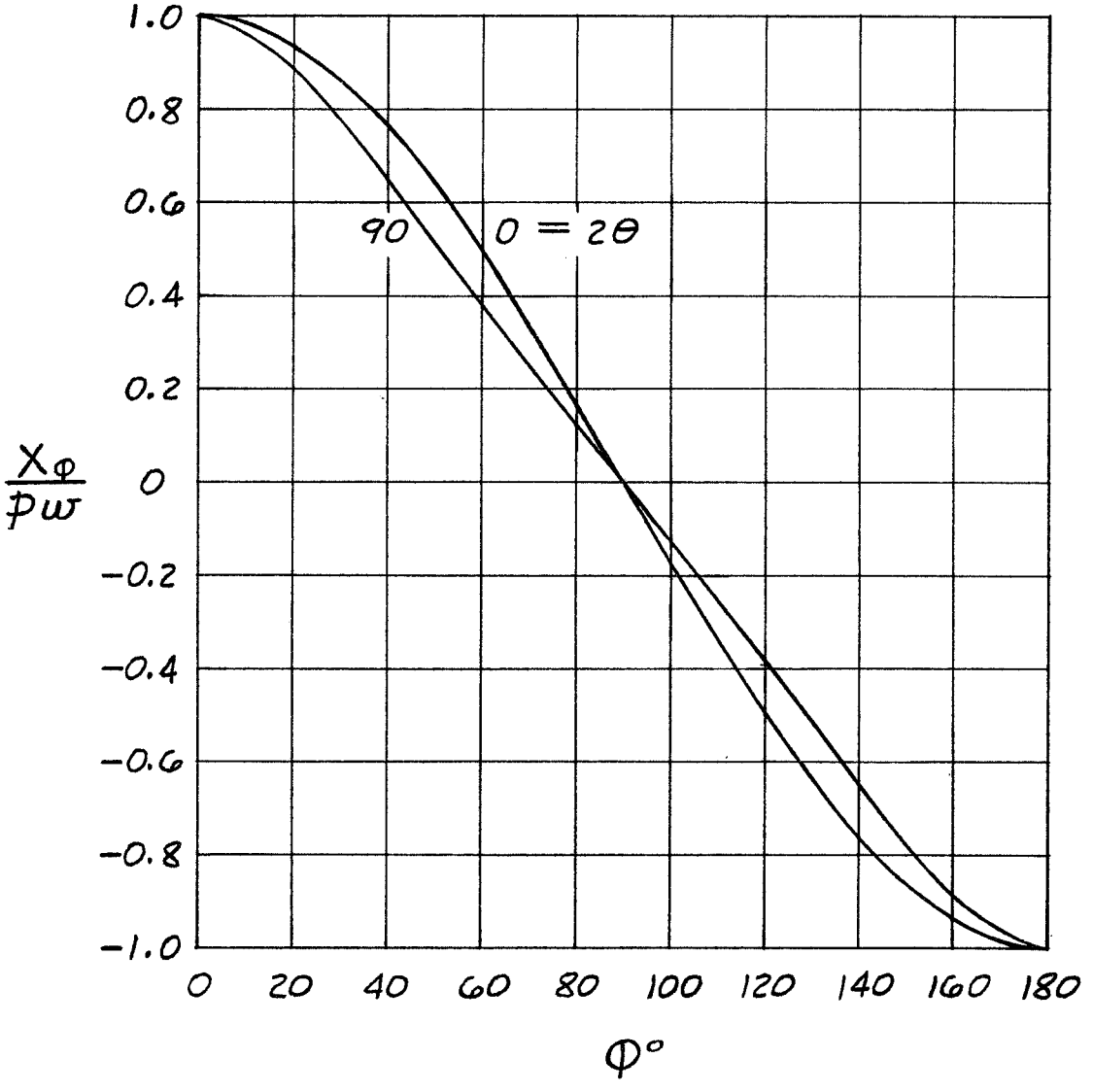

PRESSURE LOADING

FIG. 4

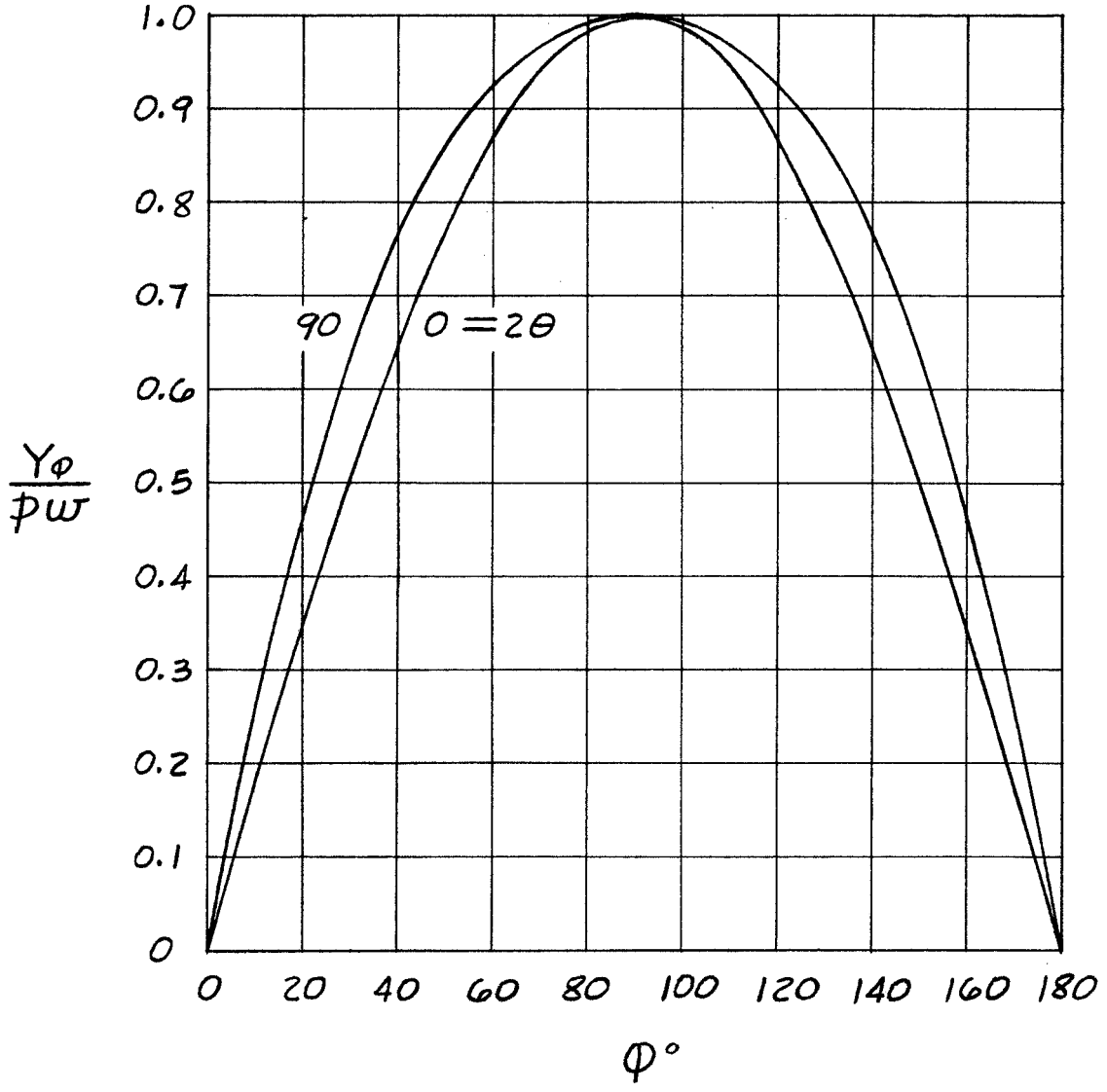

PRESSURE LOADING

FIG. 5

$$\left(T_\phi\right)_{2\theta=0} = pwb \tag{3.8}$$

and

$$C = 0 \tag{3.9}$$

Equation (3.7) then becomes

$$T_\phi = \frac{pwb \cos\theta}{\left(1 - \sin^2\theta \sin^2\psi\right)^{1/2}} \tag{3.10}$$

Using equation (1.21)

$$T_\phi = pwb \cos\theta\left(1 + \tan^2\theta \sin^2\phi\right)^{1/2} \tag{3.11}$$

Figure 6 is a graph of equation (3.11).

Combining equations (2.21), (3.4), and (3.10), there results

$$V_\phi = pw \sin^2\theta \sin\psi \tag{3.12}$$

From equation (1.10) and, by definition, V_ϕ ds is positive when acting inward on the ring, equation (3.12) may be written

$$V_\phi = pw \sin^2\theta \frac{dx}{ds} \tag{3.13}$$

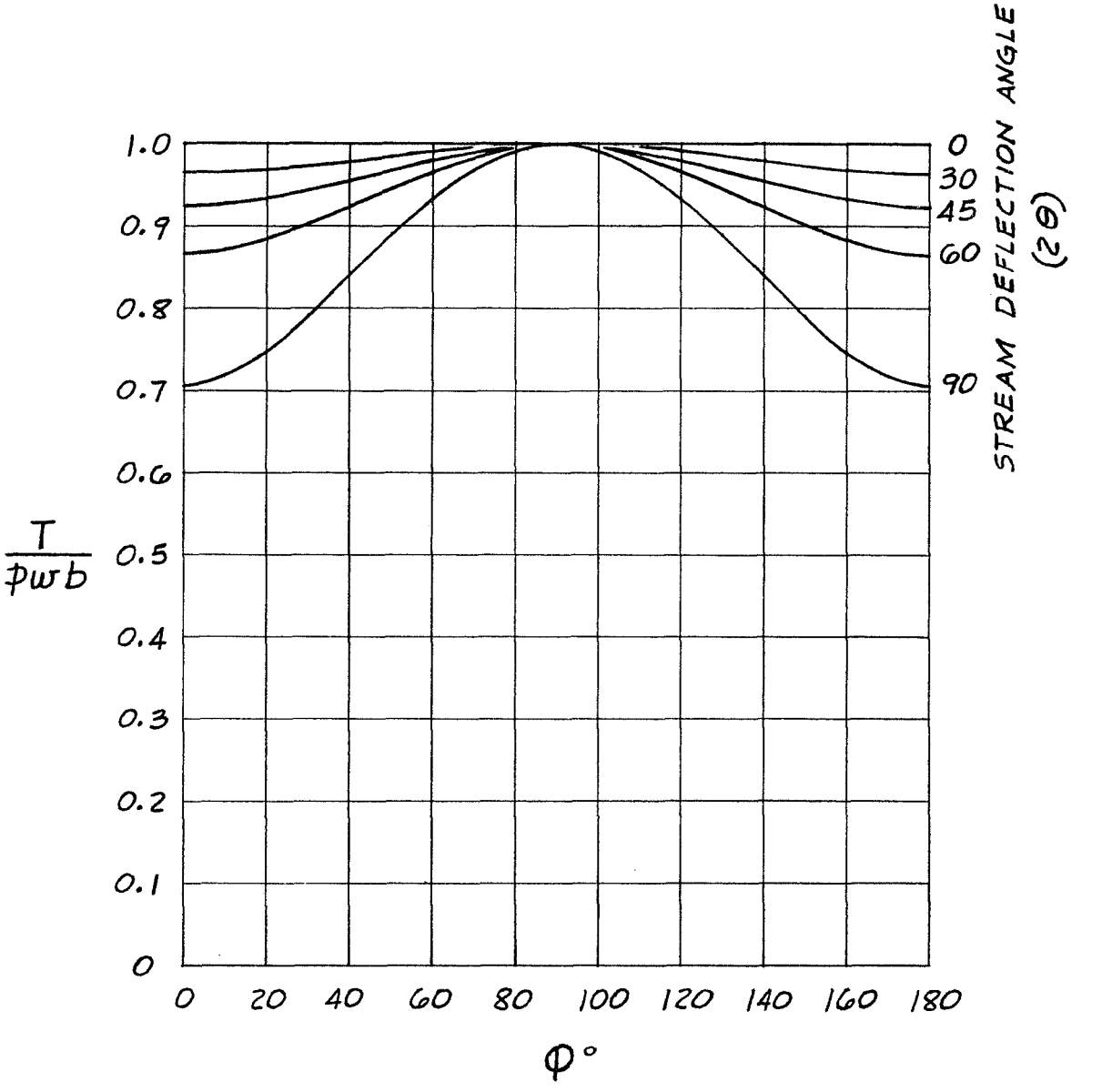

PRESSURE LOADING

FIG. 6

or

$$V_\varphi \, ds = pw \sin^2\theta \, dx \tag{3.14}$$

Let

$$F_\varphi = \int_{x_1}^{x_2} V \, ds = pw \sin^2\theta (x_2 - x_1) \tag{3.15}$$

represent the force, necessary to maintain the flexible ring in an elliptical configuration, that acts upon a small section of ring defined by the boundary $(x_2 - x_1)$. If

$$x_2 - x_1 = D \tag{3.16}$$

is the uniform spacing of the turning vanes, small with respect to the major axis 2a, then

$$F_\varphi = pwD \sin^2\theta \tag{3.17}$$

represents the forces, exerted by the turning vanes, which keep the flexible ring in an elliptical shape when subjected to pressure acting directly upon the exposed surface of the ring. For this particular case, all of the vanes are equally loaded, the forces being independent of the angle φ. Figure 7 is a graph of equation (3.17).

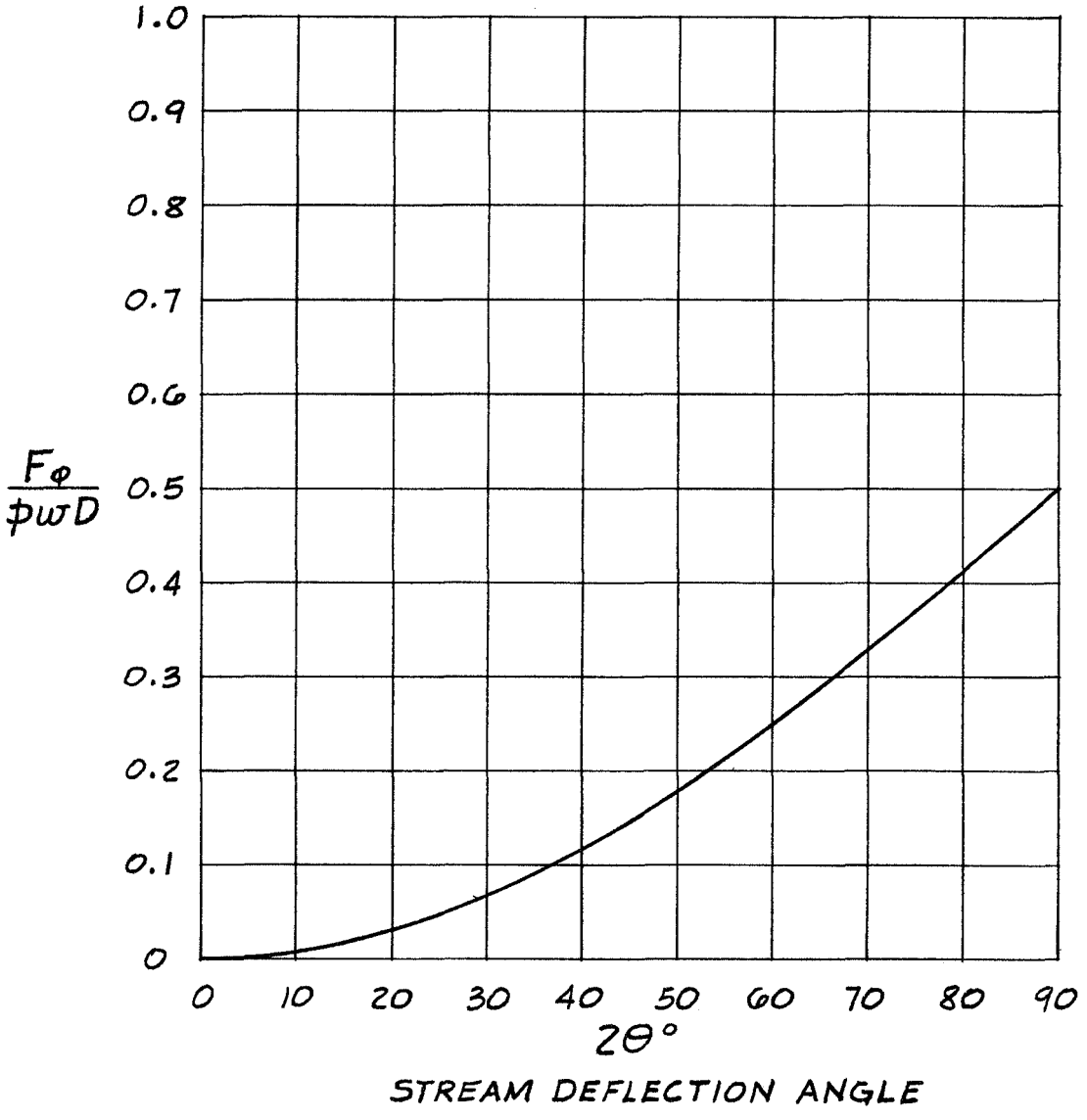

PRESSURE LOADING

FIG. 7

4. PRESSURE PLATING LOADING

Figure 1(a) shows a differential element of shell surface bounded by a circumferential length of shell dc, a longitudinal length of shell dL, and a length of mitered joint perimeter ds. Figure 3(a) shows an enlarged view of this differential element and its counterpart on the opposite side of the junction.

The state of stress in the shell at the mitered junction will include: longitudinal and circumferential stresses due to pressure, and shearing and bending stresses due to restraint of the shell displacements by the reinforcing ring. Figure 3(a) shows the longitudinal and circumferential stresses, which are those normally encountered in cylindrical pressure vessels, and which equal

$$\left.\begin{aligned} \sigma_L &= \frac{pb}{2t} \\ \sigma_c &= \frac{pb}{t} \end{aligned}\right\} \qquad (4.1)$$

where p is the pressure acting on the shell, b is the radius of the shell and one-half of the minor axis of the ellipse, and t is the shell thickness.

The pressure plating stresses, due to the longitudinal and circumferential stresses in the shell, produce loading

components, at any point on the junction defined by the angular coordinate φ, in the X-direction, equal to

$$X_\varphi \, ds = 2(\sigma_L t \, dc \sin\theta - \sigma_c t \, dL \cos\theta \sin\varphi) \qquad (4.2)$$

and in the Y-direction, equal to

$$Y_\varphi \, ds = 2(\sigma_c t \, dL \cos\varphi) \qquad (4.3)$$

Due to symmetry, the loading components in the Z-direction are equal and opposite, acting perpendicular to the plane of the ring, or

$$Z_\varphi \, ds = \sigma_L t \, dc \cos\theta + \sigma_c t \, dL \sin\theta \sin\varphi \qquad (4.4)$$

Substituting for σ_L, σ_c, dL, dc, and simplifying, equations (4.2), (4.3), and (4.4) become

$$\left.\begin{aligned} X_\varphi \, ds &= pb^2 \sin\theta \cos 2\varphi \, d\varphi \\ Y_\varphi \, ds &= pb^2 \tan\theta \sin 2\varphi \, d\varphi \\ Z_\varphi \, ds &= \frac{pb^2}{2} \cos\theta(1 + 2\tan^2\theta \sin^2\varphi)d\varphi \end{aligned}\right\} \qquad (4.5)$$

and, using equation (1.5),

$$\left.\begin{aligned} X_\varphi &= \frac{pb \sin\theta \cos 2\varphi}{\left(1 + \tan^2\theta \sin^2\varphi\right)^{1/2}} \\ Y_\varphi &= \frac{pb \tan\theta \sin 2\varphi}{\left(1 + \tan^2\theta \sin^2\varphi\right)^{1/2}} \\ Z_\varphi &= \frac{pb}{2} \frac{\left(1 + 2\tan^2\theta \sin^2\varphi\right)}{\left(1 + \tan^2\theta \sin^2\varphi\right)^{1/2}} \cos\theta \end{aligned}\right\} \qquad (4.6)$$

Equations (4.5) and (4.6) are verified by reference 1. Figures 8, 9, and 10 are graphs of equations (4.6).

Using equation (1.19), equation (2.17) becomes

$$v = \int X_\varphi \, ds + C \qquad (4.7)$$

and from the first of equations (4.5)

$$v = pb^2 \sin\theta \int \cos 2\varphi \, d\varphi + C \qquad (4.8)$$

which, after integration, equals

$$v = pb^2 \sin\theta \sin\varphi \cos\varphi + C \qquad (4.9)$$

Combining equations (2.15), (2.16), and (4.9), and using equations (1.5) and (1.11)

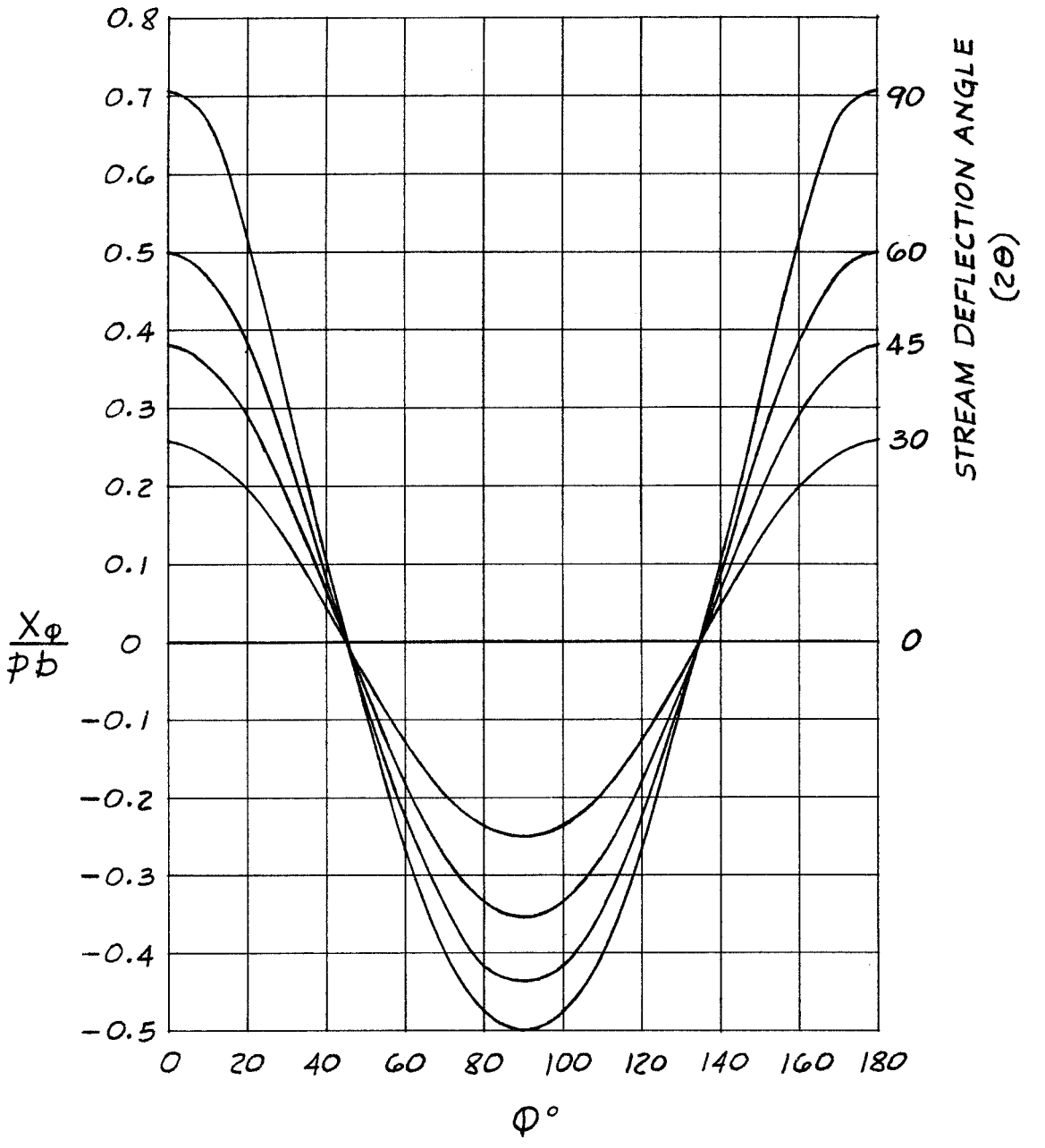

PRESSURE PLATING LOADING

FIG. 8

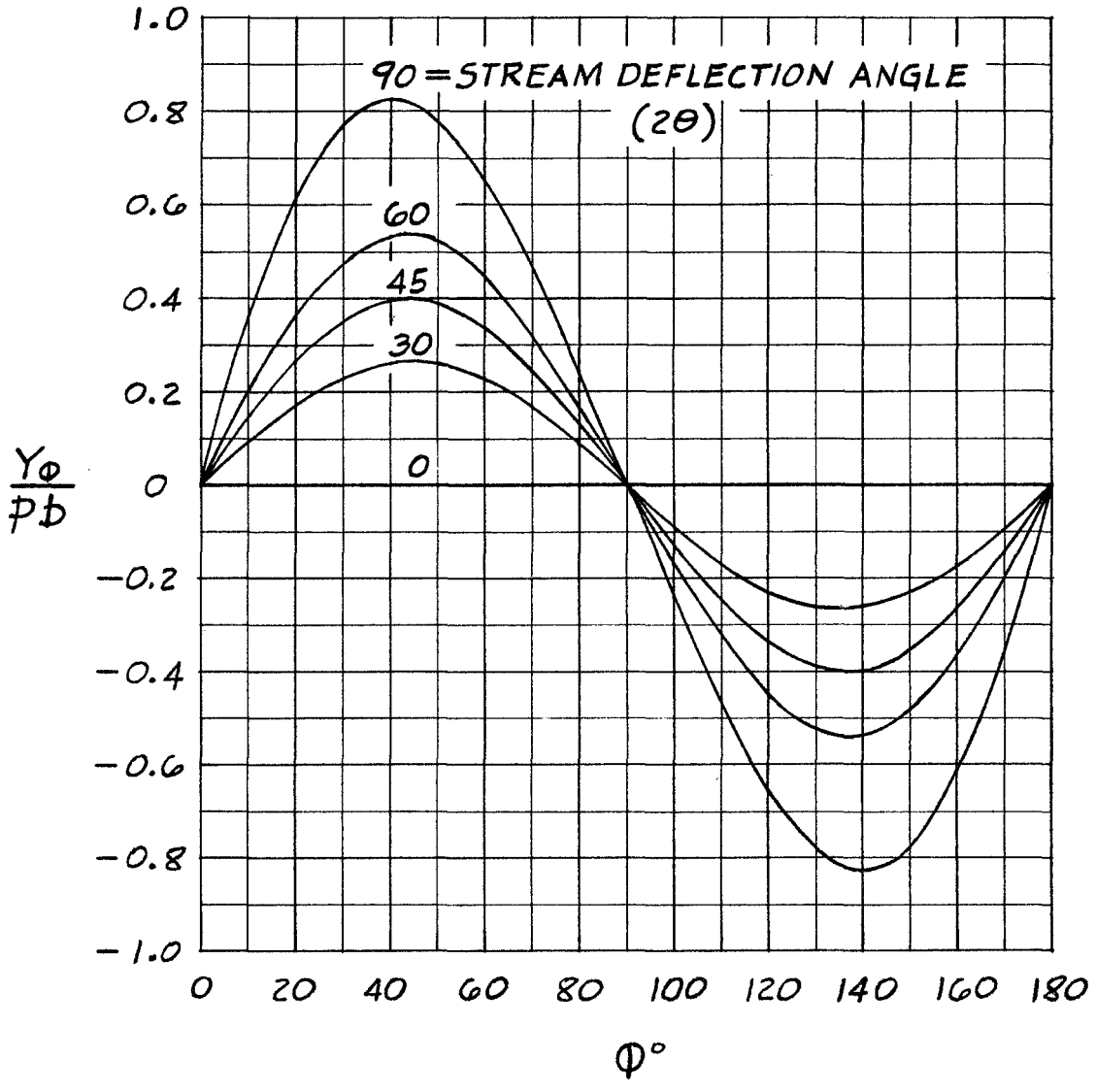

PRESSURE PLATING LOADING

FIG. 9

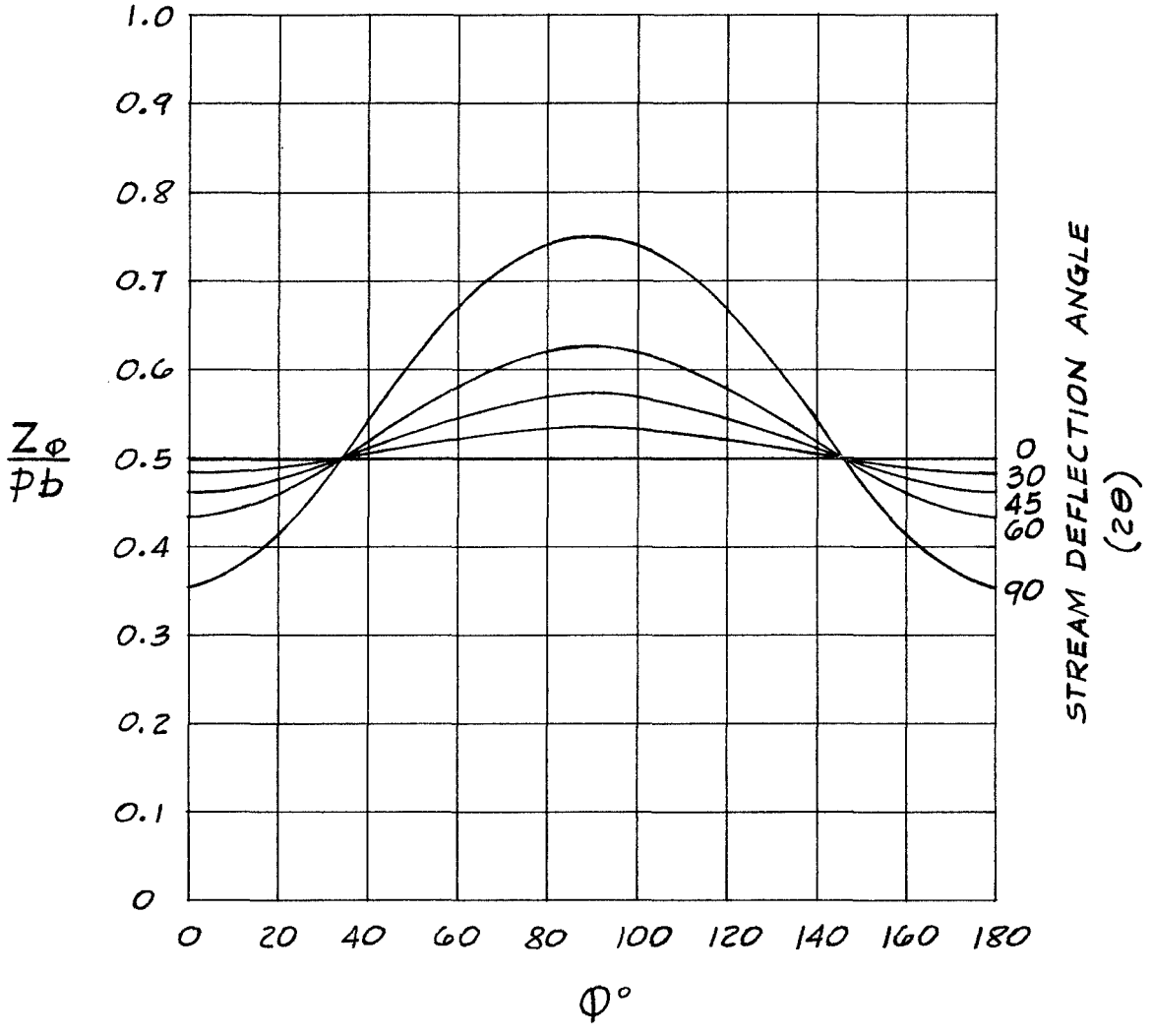

PRESSURE PLATING LOADING

FIG. 10

$$T_\varphi = pb^2 \sin\theta \cos\theta \cos\varphi \left(1 + \tan^2\theta \sin^2\varphi\right)^{1/2} + \frac{\cos\theta \left(1 + \tan^2\theta \sin^2\varphi\right)^{1/2}}{\sin\varphi} C \qquad (4.10)$$

If the stream deflection angle, 2θ, equals zero, the tensile force in the ring due to the pressure plating loading will vanish. Therefore

$$\left(T_\varphi\right)_{2\theta=0} = 0 \qquad (4.11)$$

and

$$C = 0 \qquad (4.12)$$

Equation (4.10) then becomes

$$T_\varphi = pb^2 \sin\theta \cos\theta \cos\varphi \left(1 + \tan^2\theta \sin^2\varphi\right)^{1/2} \qquad (4.13)$$

Figure 11 is a graph of equation (4.13).

Combining equations (2.21), (4.6), and (4.13), and using equations (1.5), (1.11), and (1.21) there results

$$V_\varphi = 2pb \sin^2\theta \tan\theta \frac{\sin\varphi \cos\varphi}{\left(1 + \tan^2\theta \sin^2\varphi\right)^{1/2}} \qquad (4.14)$$

From equations (1.3) and (1.5) and, by definition, V_φ ds is positive when acting inward on the ring, equation (4.14) may be written

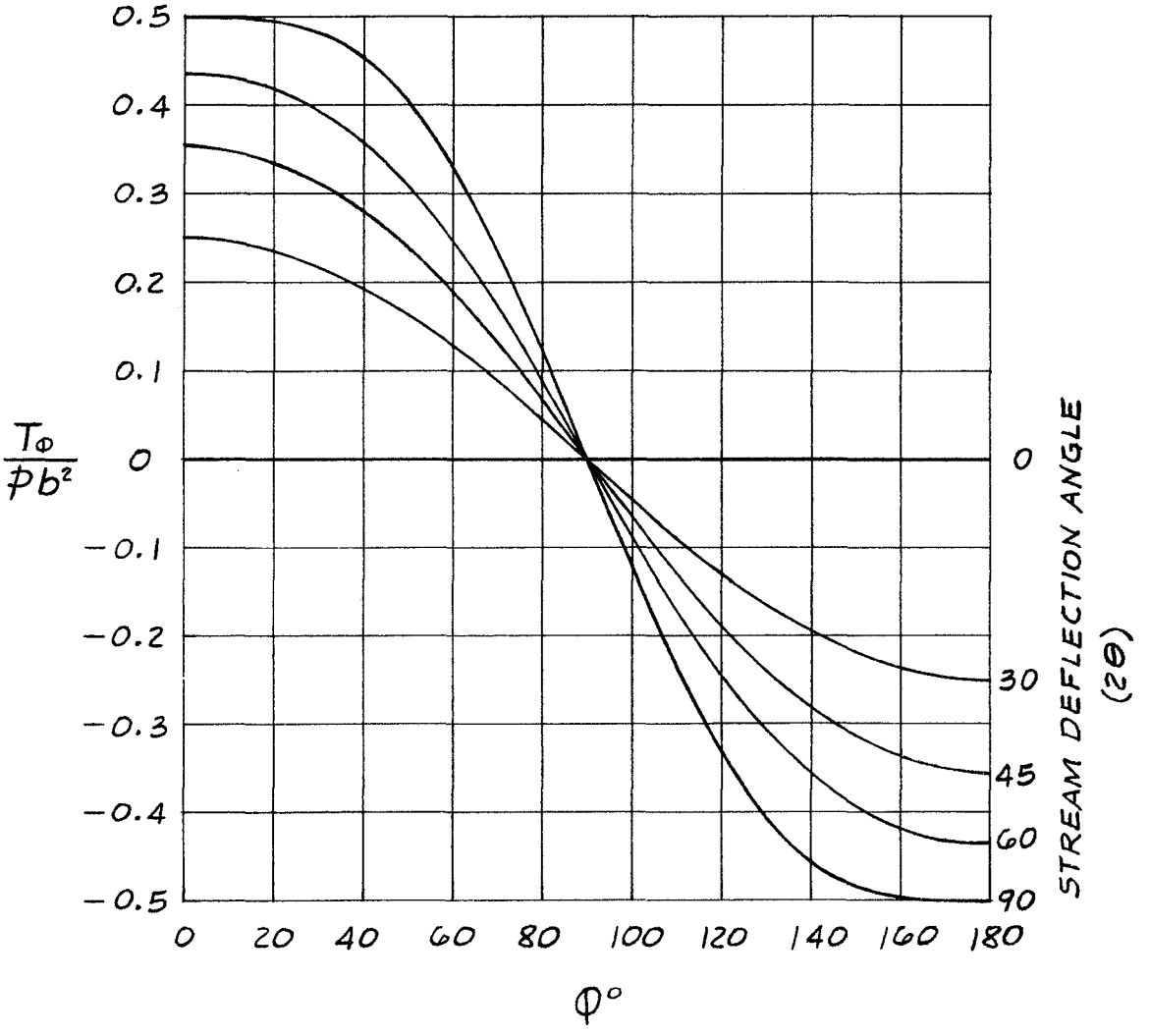

PRESSURE PLATING LOADING

FIG. 11

$$V_\varphi \, ds = \frac{2pb}{a} \sin^3\theta x \, dx \tag{4.15}$$

Let

$$F_\varphi = \int_{x_1}^{x_2} V_\varphi \, ds = \frac{2pb}{a} \sin^3\theta (x_2 - x_1) \frac{(x_2 + x_1)}{2} \tag{4.16}$$

represent the force, necessary to maintain the flexible ring in an elliptical configuration, that acts upon a small section of the ring defined by the boundary $(x_1 - x_2)$. If

$$x_2 - x_1 = D \tag{4.17}$$

is the uniform spacing of the turning vanes, small with respect to the major axis 2a, and

$$\frac{x_2 + x_1}{2} \cong x = a \cos \varphi \tag{4.18}$$

then

$$F_\varphi = 2pbD \sin^3\theta \cos \varphi \tag{4.19}$$

represents the forces, exerted by the turning vanes, which keep the flexible ring in an elliptical shape when subjected to pressure plating loading. Figure 12 is a graph of equation (4.19).

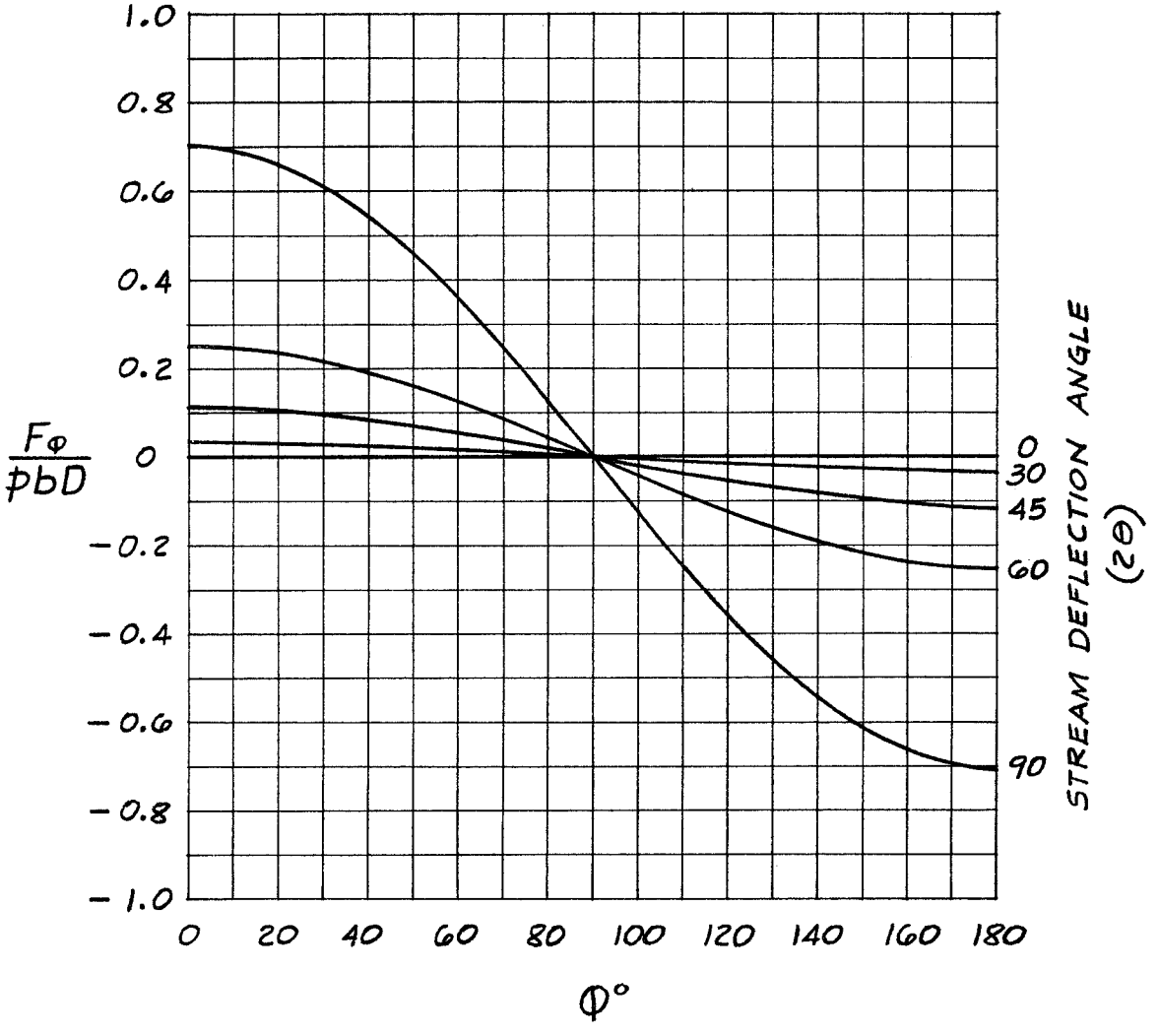

PRESSURE PLATING LOADING

FIG. 12

APPENDIX B

HELICAL COMPRESSION SPRINGS SUBJECTED TO COMBINED LOADING

Discussion

It is the purpose of this section to develop formulas for the engineering design of helical compression springs subjected to combined loading. The following material is restricted to helical coil springs with uniform coil diameter, uniform pitch, and round wire. The combined loading consists of an axial compressive force, a lateral force perpendicular to the coil axis, and a bending moment. In addition to formulas, graphs and alinement charts are included in order to simplify design procedure.

Under certain conditions, the use of helical compression springs for the support of portions of large structures such as wind tunnels will prove extremely advantageous. If the structure to be supported is subjected to dynamic loading, the spring supports, if properly designed, will provide specific controlled natural frequencies for the system allowing a minimum of dynamic forces to be transmitted through the supports into adjacent portions of the structure. The springs, therefore, act as

a vibration break, reducing to a minimum the transfer of dynamic forces from one portion of the structure to another.

If the structure to be supported requires many supporting points, a spring supporting system will have the advantage of providing an elastic foundation which will compensate for small deflections acting in the axial direction of the coil springs caused by temperature changes in the structure. This effect results from the relatively small spring constant of a spring or nest of springs as compared with that of a rigid support. A small deflection imposed upon a coil spring results in only a small change in reaction while the same deflection imposed upon a rigid support results in a relatively large change in reaction.

The need for elastic supports for a particular structure will, of course, depend upon the requirements, function, and predicted behavior of the structure. Assuming an elastic supporting system is advantageous, the formulas and graphs included herein should prove useful to the designer in providing the proper elastic system. Helical coil springs subjected to axial forces only are in general use throughout the engineering profession and formulas for designing them are readily available. However, when helical coil springs are used to support large structures, the springs may be subjected to forces

perpendicular to the coil axis and to bending moments as well as to axial forces. The lateral forces and bending moments may be due to the thermal movement of the structure. The following theory includes stress analysis of coil springs subjected to axial and lateral forces and to bending moments resulting in formulas simplified for use by the designer. The results are not exact but are on the safe side. Graphs are included which apply to the special case of high strength alloy steel springs subjected to an axial force, and a lateral deflection with the ends of the spring remaining parallel. This is the most general case and will find the widest usage. Sufficient theory is presented so that other cases can be developed.

As mentioned earlier, the following theory is restricted to helical springs with uniform coil diameter, uniform pitch, and round wire. This type is most easily manufactured, most generally used, and results in less complicated stress analysis. Additional study leading to the development of theory for springs having variable coil diameter, variable pitch, with wire cross section other than round may be desirable but would definitely be classified as "special" insofar as practical applications are concerned. A further restriction in the following theory is that the axial force applied to the spring is compressive. The stress analysis part of the theory is valid for tension

springs as well as for compression springs, but the simplifications made for ease of the structural designer would not be on the safe side. Furthermore, it is the opinion of the author, that for the support of large structures, a compression spring is generally more practical than a tension spring. A tension spring, if overloaded, may rupture. A properly designed compression spring, if overloaded, will at worst compress to solid height without rupture and from then on behave as a solid bar. An important consideration for compression springs is stability or resistance against buckling. The following theory includes stability considerations so that a compression spring can be designed with a specified lateral deflection and can be compressed to solid height without buckling or rupture. Due to the stability considerations, the lateral deflection imposed upon a compression spring will be more limited than that for a comparable tension spring. However, for most practical applications, compression springs can be designed with a satisfactory allowable lateral deflection. For special applications, where the lateral deflections are prohibitively large for the following theory, a system may be devised where the structure is "hung" from compression springs thus avoiding the undesirable features of tension springs.

It is the author's considered opinion that there are many applications where a structure subjected to thermal movement may be more advantageously supported by springs than by rollers or sliding base plates. A spring system would act essentially the same as a compound roller system in that movement could occur in any direction lateral to the coil axis. The springs have the added advantage of compensating for small movements parallel to the coil axis.

Most of the data is arranged more conveniently for analysis than for design. In order to design a spring with the included formulas and graphs, physical characteristics should be assumed, where necessary, and the procedure conducted in an analytical manner. This design procedure is in no way unusual as most structural design is performed in this manner.

SYMBOLS

aL	dimensionless factor
A	cross-sectional area of spring wire, $in.^2$
A_1, A_2	dimensional factors usually constant
C	axial force on spring wire, lb
CR	subscript denoting "critical"
d	diameter of spring wire, in.
D	mean coil diameter of helical spring, in.
e	eccentricity of axial force on spring end faces, in.
E	modulus of elasticity in tension and compression, $lb/in.^2$
$(EA)_s$	equivalent compressive rigidity for a helical spring, lb
$(EI)_s$	equivalent flexural rigidity for a helical spring, $lb\text{-}in.^2$
F	dimensionless stress amplification factor
F	subscript denoting "free length"
F_M, F_P	dimensionless factors, usually constant
G	modulus of elasticity in shear, $lb/in.^2$
$(GA)_s$	equivalent shearing rigidity for a helical spring, lb
H	lateral force applied to spring ends, lb

I	diameter moment of inertia of spring wire, $in.^4$
I_P	polar moment of inertia of spring wire, $in.^4$
J	dimensionless factor
k	spring constant, lb/in.
K_B	curvature correction factor for bending stress
K_S	curvature correction factor for shearing stress
K_W	correction factor for curvature and fatigue
L	axial length of active coils for any loading, in.
L_{CR}	critical axial length of active coils, in.
L_F	axial free length of active coils, in.
L_P	axial length of active coils for applied force P, in.
L_S	axial solid length of active coils, in.
L_T	total axial free length of all coils, in.
M	bending moment applied to spring ends, in.-lb
M_m	bending moment about m-m axis of spring wire cross section, in.-lb
M_R	bending moment about R-axis of spring wire cross section, in.-lb
n	number of active coils
N	cross-sectional form factor
p	coil pitch for any loading, in.
p_F	coil pitch at free length, in.
p_S	coil pitch at solid length, in.

P	axial force, lb
P_E	Euler axial force, lb
P_{CR}	critical axial force, lb
r	radius of spring wire, in.
R	radius of helix, in.
s	length of spring wire or helix, in.
s	subscript denoting "spring"
s	subscript denoting "solid"
S	subscript denoting "shear"
T	torque on spring wire, in.-lb
U	strain energy, in.-lb
U_T	total strain energy, in.-lb
V_m	shearing force parallel to m-m axis of spring wire cross section, lb
V_R	shearing force parallel to R-axis of spring wire cross section, lb
x, y, z	Cartesian coordinates
Z	dimensionless deflection factor
α	coil pitch angle for any loading, radians
α_F	coil pitch angle at free length, radians
α_s	coil pitch angle at solid length
β	curvature correction factor
γ_M	angle of rotation of applied moment M, radians

δ	axial deflection for any loading, in.
δ_C	axial deflection due to curvature, in.
δ_{CCR}	axial deflection due to curvature for critical loading, in.
δ_P	axial deflection for axial loading, in.
δ_{PCR}	axial deflection for critical axial load, in.
δ_s	axial solid deflection, in.
Δ	lateral deflection of spring ends, in.
ν	Poisson's ratio
σ	normal stress on spring wire cross section, $lb/in.^2$
σ_C	compressive normal stress on spring wire cross section, $lb/in.^2$
σ_B	bending normal stress on spring wire cross section, $lb/in.^2$
τ	shearing stress on spring wire cross section, $lb/in.^2$
τ_T	torque shearing stress on spring wire cross section, $lb/in.^2$
τ_S	direct shearing stress on spring wire cross section, $lb/in.^2$
φ	angular coordinate of a point on helix, radians

REFERENCES

1. Timoshenko, S., Strength of Materials, Part II. Van Nostrand Co., Inc., N. Y., 1941. Section 56, pp. 304-311, "Open Coiled Helical Spring."

2. Roark, Raymond, Formulas for Stress and Strain. McGraw-Hill Book Co., Inc., N. Y., 1943. Section 35, pp. 117-119, "Beams of Relatively Great Depth."

3. Timoshenko, S., Theory of Elastic Stability. McGraw-Hill Book Co., Inc., N. Y., 1936. Section 30, pp. 165-167, "Lateral Buckling of Compressed Helical Springs."

4. "The Effect of Shearing Force on the Critical Load." Ibid. Section 26, pp. 139-141.

5. Ibid. p. 27

6. Timoshenko, S., Strength of Materials, Part I. Van Nostrand Co., Inc., N. Y., 1940, p. 272.

7. Roark, Raymond J., Formulas for Stress and Strain. McGraw-Hill Book Co., Inc., N. Y., 1943, p. 144. Table VII, Case 2.

8. Timoshenko, S., Theory of Elasticity. McGraw-Hill Book Co., Inc., N. Y., 1934, p. 10.

9. Mechanical Springs, Their Engineering and Design. Wallace Barnes Co., Bristol, Conn., 1948.

1. SPRING GEOMETRY

Before discussing the theory for loaded helical springs, it will be convenient to develop formulas, to be used later, showing the relationship between the basic geometric properties of a helix. The following theory is valid only for a helix with uniform pitch and uniform coil diameter.

Figure 1(a) shows a typical open coiled helix. Let any point along the coil axis be the origin of a rectangular system of coordinate axes, as indicated in Figure 1(b), with the Z-axis coincident with the coil axis. The pitch angle α represents the angle between any differential length ds of the helix and the projection of ds upon the X-Y plane perpendicular to the coil axis. With the aid of Figure 1(b), the following differential relationships are obtained.

$$\sin \alpha = \frac{dz}{ds} \qquad (a)$$

$$\cos \alpha = \frac{R\, d\varphi}{ds} \qquad (b)$$

$$\tan \alpha = \frac{dz}{R\, d\varphi} \qquad (c)$$

From equations (a), (b), and (c), the basic geometric relationships are derived. Using equation (a), we write

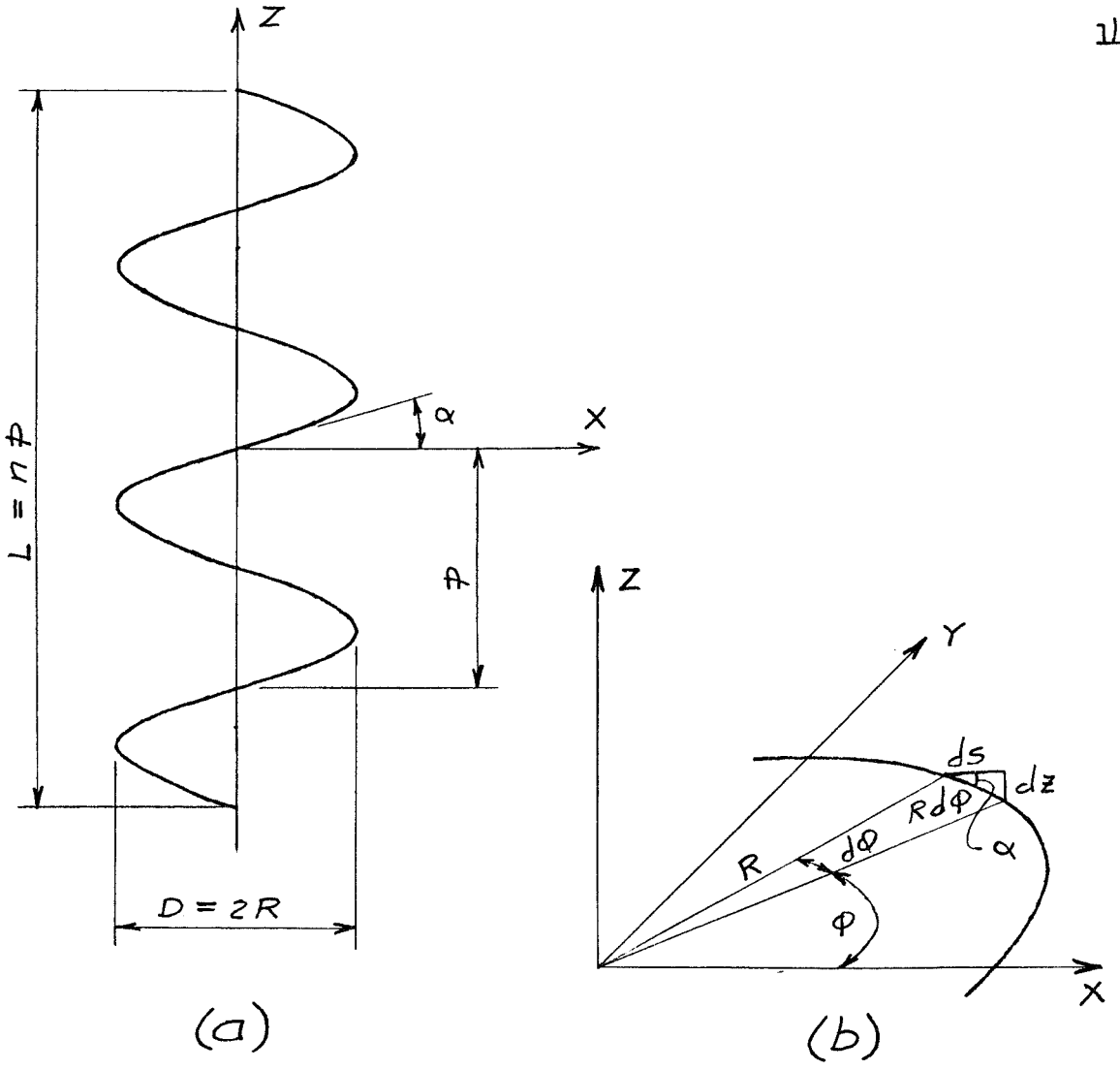

FIG. 1

$$dz = ds \sin \alpha$$

$$\int_0^L dz = \sin \alpha \int_0^s ds$$

from which

$$L = s \sin \alpha$$

or

$$s = \frac{L}{\sin \alpha} \tag{1-1}$$

Using equation (b), we write

$$ds = \frac{R\, d\varphi}{\cos \alpha} \tag{1-2}$$

$$\int_0^s ds = \frac{R}{\cos \alpha} \int_0^{2\pi n} d\varphi$$

from which

$$s = \frac{2n\pi R}{\cos \alpha} = \frac{n\pi D}{\cos \alpha} \tag{1-3}$$

Using equation (c), we write

$$dz = R\, d\varphi \tan \alpha$$

$$\int_0^z dz = R \tan \alpha \int_0^{\varphi} d\varphi$$

from which

$$z = R\varphi \tan \alpha \tag{1-4}$$

Also

$$\int_0^p dz = R \tan \alpha \int_0^{2\pi} d\varphi$$

from which

$$p = 2\pi R \tan \alpha = \pi D \tan \alpha \qquad (1\text{-}5)$$

or, rearranging

$$\tan \alpha = \frac{p}{\pi D} \qquad (1\text{-}6)$$

Also

$$\int_0^L dz = R \tan \alpha \int_0^{2n\pi} d\varphi$$

$$L = 2n\pi R \tan \alpha = n\pi D \tan \alpha = np \qquad (1\text{-}7)$$

The above equations containing only the basic geometric properties of a helix (p, D, α, L, s) will be used later in deriving the stress analysis and deflection equations of a loaded spring. The helix represents the center line of the spring wire and the equations derived for the helix will in turn apply to the coil spring except for the condition of solid compression. Due to the fact that the spring wire has finite dimensions, the pitch angle, unlike that of a dimensionless helix, can never equal zero. It will be convenient at this time to discuss the geometric characteristics of a coil spring when the spring has been compressed solid.

Figure 1(c) shows one cycle of a helix representing the center line of the wire for one complete coil of a helical spring compressed solid. Since the coils are in

contact, the distance between any two adjacent coils perpendicular to the wire center line (helix) will be equal to d, the wire diameter. Let α_s and p_s be the pitch angle and pitch, respectively, of the spring at solid compression. Figure 1(d) shows the geometric relationship between p_s, α_s, and d. From the figure

$$\frac{d}{p_s} = \cos \alpha_s$$

from which

$$p_s = \frac{d}{\cos \alpha_s} \qquad (d)$$

Also, from equation (1-5) for the condition of solid compression

$$p_s = \pi D \tan \alpha_s$$

Then

$$\frac{d}{\cos \alpha_s} = \pi D \tan \alpha_s$$

and

$$\sin \alpha_s = \frac{d}{\pi D} \qquad (e)$$

Also

$$\cos \alpha_s = \left(1 - \sin^2 \alpha_s\right)^{1/2} = \left[1 - \left(\frac{d}{\pi D}\right)^2\right]^{1/2} \qquad (f)$$

Combining equations (d) and (f),

$$p_s = \frac{d}{\left[1 - \left(\frac{d}{\pi D}\right)^2\right]^{1/2}}$$

or

$$\frac{p_s}{d} = \frac{1}{\left[1 - \left(\frac{d}{\pi D}\right)^2\right]^{1/2}} \qquad (1\text{-}8)$$

Equation (1-8) shows the relationship between p_s, d, and D for the condition of solid compression. It is advantageous to investigate the limiting values for the ratio p_s/d. The ratio D/d can vary from a minimum of 1 to an unlimited maximum. So for $\frac{D}{d} = 1$

$$\frac{p_s}{d} = \frac{1}{\left[1 - \left(\frac{1}{\pi}\right)^2\right]^{1/2}} \cong 1.055$$

and for $\frac{D}{d} = \infty$

$$\frac{p_s}{d} = 1$$

However, for manufacturing reasons, it is difficult and impractical to coil a spring with a D/d ratio less than 4. Consequently, for $\frac{D}{d} = 4$

$$\frac{p_s}{d} = \frac{1}{\left[1 - \left(\frac{1}{4\pi}\right)^2\right]^{1/2}} \cong 1.002$$

The above discussion of a helical spring at solid length indicates that the ratio p_s/d is dependent upon the ratio D/d only and is very nearly equal to a constant

for all practical values of D/d. Therefore, there will be little appreciable error if the following assumption is made:

$$\frac{p_s}{d} = 1 \quad \text{or} \quad p_s = d \tag{1-9}$$

Consequently, from equation (1-7), the axial length of active coils for the condition of solid length becomes

$$L_s = np_s = nd \tag{1-10}$$

and from equation (1-6) and equation (e)

$$\tan \alpha_s = \frac{p_s}{\pi D} = \sin \alpha_s = \frac{d}{\pi D} \tag{1-11}$$

It is evident, therefore, that, for the condition of solid length, the pitch angle α_s is sufficiently small that the following assumptions are reasonable:

$$\sin^2 \alpha_s = \tan^2 \alpha_s = 0 \quad \text{and} \quad \cos \alpha_s = 1 \tag{1-12}$$

Due to the action of a combined system of forces and bending moments, a helical spring will undergo distortion. The distortion can be divided into three components, axial deflection, lateral deflection, and curvature which can be independently related to the applied forces and bending moments. The axial deflection, furthermore, can be related to the geometric properties of the helix and will be considered in this section under spring geometry. Let α, p,

L, and δ be respectively the pitch angle, pitch, axial length of active coils, and axial deflection when the spring is subjected to combined loading. Let α_s, p_s, L_s, and δ_s represent the above quantities for the condition of solid length and let α_F, p_F, L_F, and δ_F represent the above quantities for the free length or unloaded condition. The assumption is made that, under a reasonable loading system, where the distortions are not permanent, the coil and wire diameters D and d are constant. The following relationships between the above quantities are apparent.

For the unloaded condition

$$\delta_F = 0$$

For the loaded condition

$$\delta = L_F - np$$

and from equations (1-7) and (1-5)

$$L_F = np_F \quad \text{and} \quad p = \pi D \tan \alpha$$

then

$$\delta = n(p_F - \pi D \tan \alpha) \tag{1-13}$$

or

$$\tan \alpha = \frac{1}{\pi D}\left(p_F - \frac{\delta}{n}\right) \tag{1-14}$$

For the solid length condition

$$\delta_s = L_F - np_s$$

or

$$\delta_s = n(p_F - d) \tag{1-15}$$

In order to be reasonably certain that the combined loading system acts upon the spring in the predicted manner, the spring end conditions and the method of loading must be properly designed. Figure 2(a) shows an unloaded helical compression spring, typical of the type under consideration in this paper. Each end of the spring has two inactive closed coils with the end faces ground perpendicular to the coil axis. The spring is designed to be mounted between two loading plates which are rigidly attached to the two structures requiring elastic separation and which transfer the combined system of forces and bending moments to the spring. The ground end faces of the spring provide square contact between the spring ends and loading plate and contribute toward uniform axial loading of the coils and transfer of bending moment. Figure 2(b) illustrates the mounting of the spring to the loading plate. The plug transfers the lateral force and aids in transferring the bending moment. The inactive coils at each end of the spring permit the plug to project into the core of the spring without clashing with the active coils.

The total length of the spring for the unloaded condition shall be designated by L_T as shown in Figure 2(a) and shall equal the total axial length of active and inactive coils. If the number of inactive coils at each end of the spring is two, then

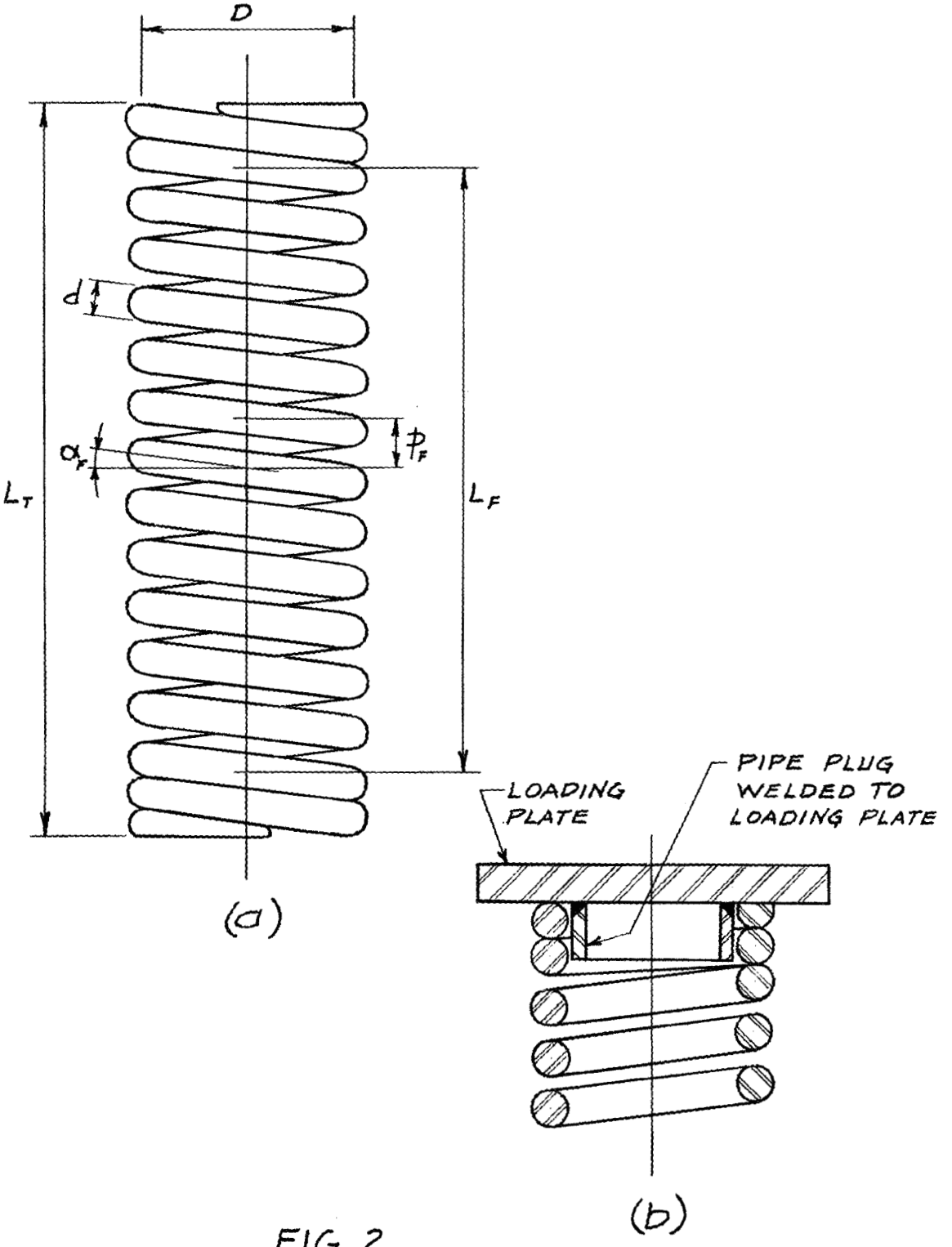
D
d
α_F
p_F
L_T
L_F
(a)
LOADING PLATE
PIPE PLUG WELDED TO LOADING PLATE
(b)

FIG. 2

$$L_T = L_F + 4p_s$$

and since

$$L_F = np_F \quad \text{and} \quad p_s = d$$

then

$$L_T = np_F + 4d \tag{1-16}$$

2. GENERAL LOADING

The helical springs shall be subjected to a combined loading consisting of an axial force P, a lateral force H, and a bending moment M. General stress analysis formulas will be developed for this loading which will be used to analyze the special symmetrical case of the spring subjected to a lateral deflection with the spring ends remaining parallel to the original coil axis.

Figure 3(a) shows a helical compression spring, represented by its axis line OA coincident with the Z-axis before distortion. The combined loading is shown but is not assumed to be acting in Figure 3(a). When the loading is applied, the spring will undergo distortion consisting of an axial deflection δ, a lateral deflection Δ, and curvature. The distortions and spring wire stresses will be functions of any known system of loading.

Figure 3(b) shows the special symmetrical case. A lateral deflection curve will be determined as functions of Δ, L, and P with a configuration such that the spring end faces remain perpendicular to the Z-axis. With these restrictions, the spring wire stresses and axial deflection δ will become functions of only the axial load P, the lateral deflection Δ, and the basic geometric properties of the spring.

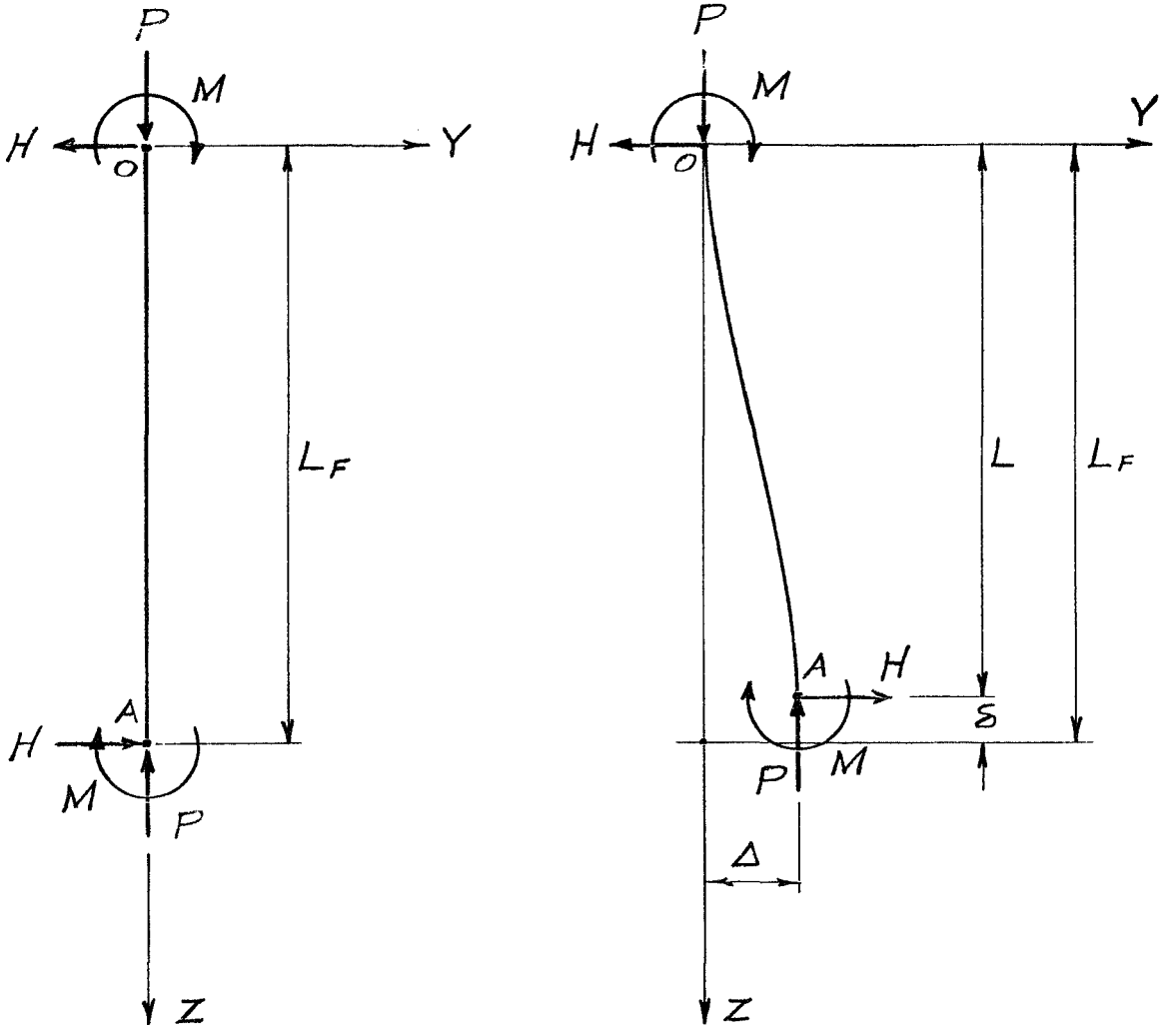

FIG. 3

The spring distortion and the combined loading acting upon the cross section of any differential length ds of the spring wire is shown in Figure 4. The lateral distortion is represented by the length y and the axial distortion is included in the length z. The curved line FEG, lying on the X'-Y' plane, represents a projected arc of the spring helix of radius R and center O'. The center of the wire cross section E coincides with the intersection of the radial axis R, lying on the X'-Y' plane, and arc FEG. The tangential axis T, lying on the X'-Y' plane, is tangent to the arc FEG at point E. Axes m-m and R are perpendicular to each other, intersect at point E, and lie on the face ABCD of the wire cross section. Axis n is perpendicular to axes R and m-m and intersects face ABCD at point E. Axes n and m-m deviate from axes T and Z", respectively, by the pitch angle α.

Figure 4(b) shows the moments and forces acting upon the cross section of the spring wire. The sign convention will be chosen such that the moments and forces shown are positive. The effect upon the cross section of each component of the combined loading, P, H, and M, will be determined separately and then combined for the total or general loading condition.

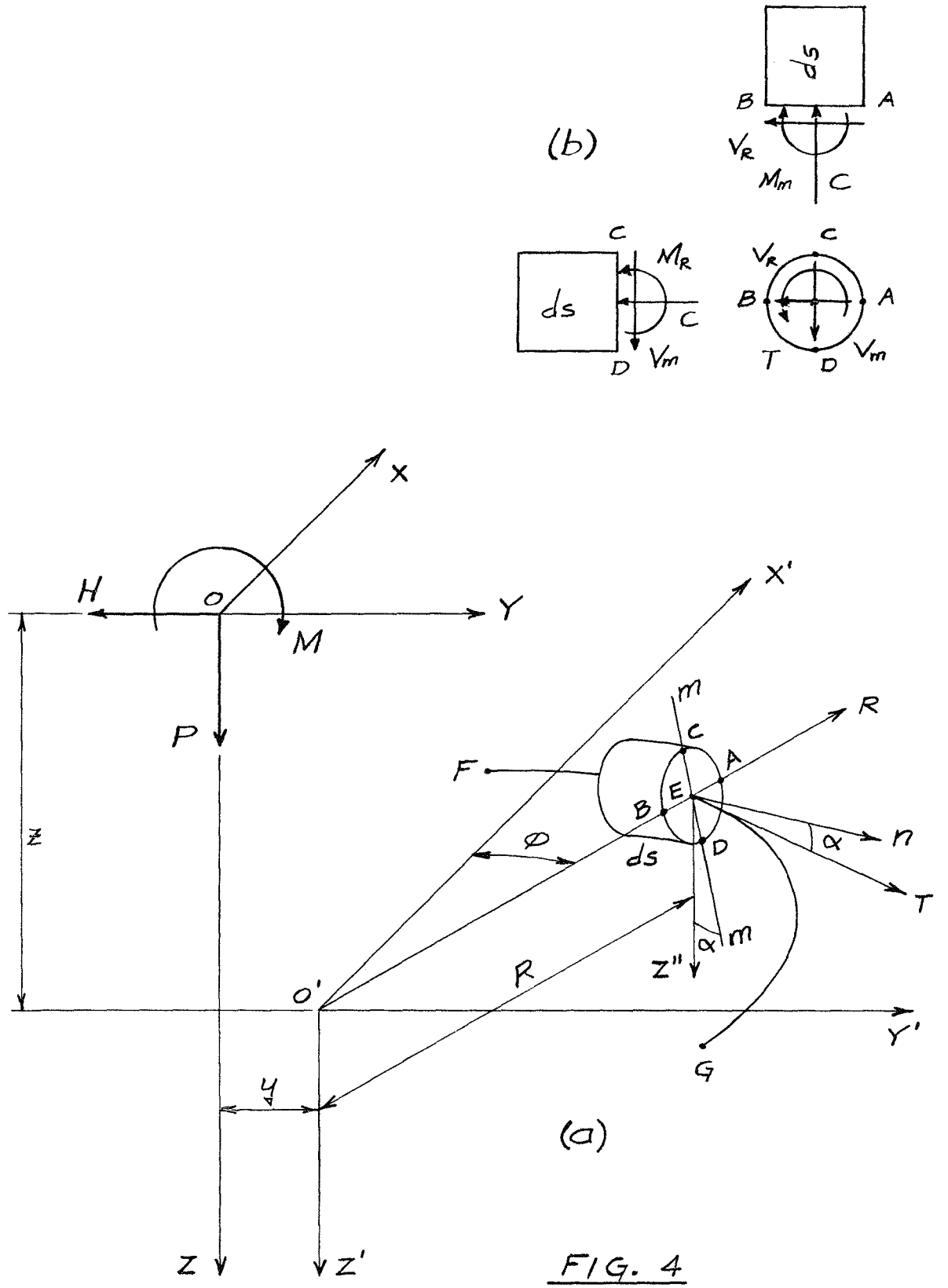
(b)
ds
B
A
V_R
M_m
C
ds
C
M_R
C
D
V_m
V_R
C
B
A
T
D
V_m
X
H
O
Y
M
P
Z
X'
m
R
C
A
F
E
B
D
ds
φ
α
n
T
m
α
Z''
R
O'
Y'
G
y
(a)
Z
Z'

FIG. 4

3. AXIAL LOADING

The effect of the axial force alone upon the distorted spring is shown in Figures 5, 6, 7, and 8. The applied axial force P, acting at point O, coincident with the Z-axis, produces a moment and a force at point O' as shown in Figure 5. The force is coincident with the Z'-axis and the moment, indicated by the double arrowhead vector, acts about the X'-axis. The double arrowhead vector follows the right-hand screw convention.

The effect at point E due to the force P acting at point O' is a force parallel to the Z"-axis and a moment about the tangential axis T. However, the force P at point O' can be resolved into components, as shown in Figure 6(a), parallel to the m-m and n axes. These components produce at point E a shearing force parallel to the m-m axis, a compressive force parallel to the n-axis, a torque about the n-axis, and a moment about the m-m axis. The direction of these forces and moments acting upon the wire cross section ABCD is shown in Figure 6(b). With the aid of Figure 6, the following expressions are obtained.

$$C = P \sin \alpha \qquad (a)$$

$$M_m = PR \sin \alpha \qquad (b)$$

$$T = PR \cos \alpha \qquad (c)$$

$$V_m = P \cos \alpha \qquad (d)$$

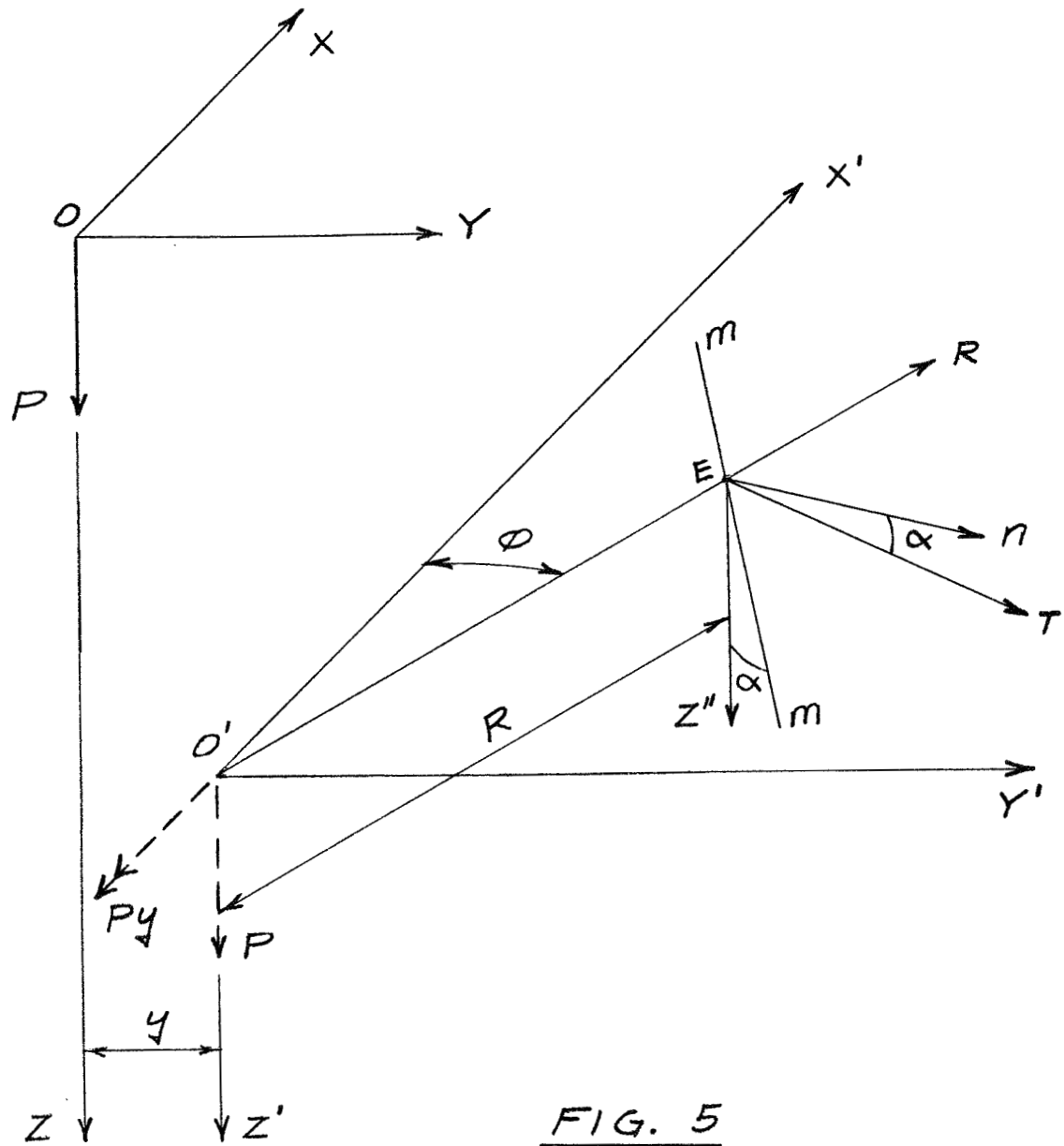

FIG. 5

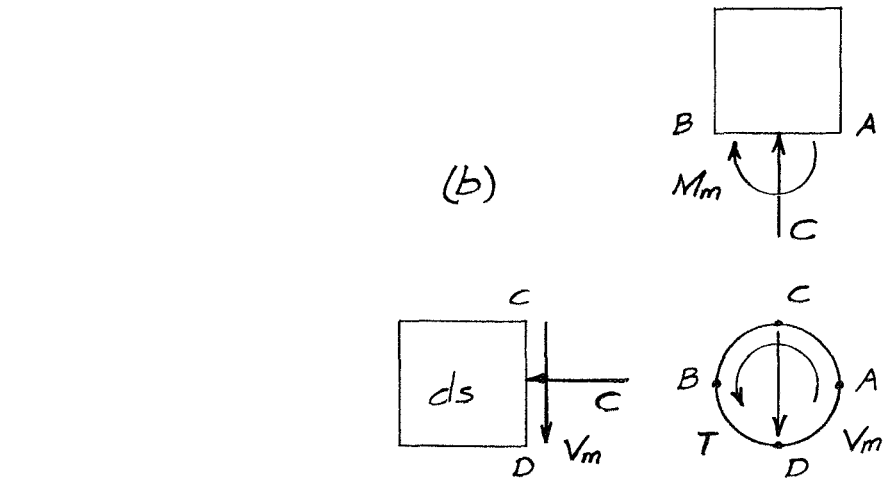

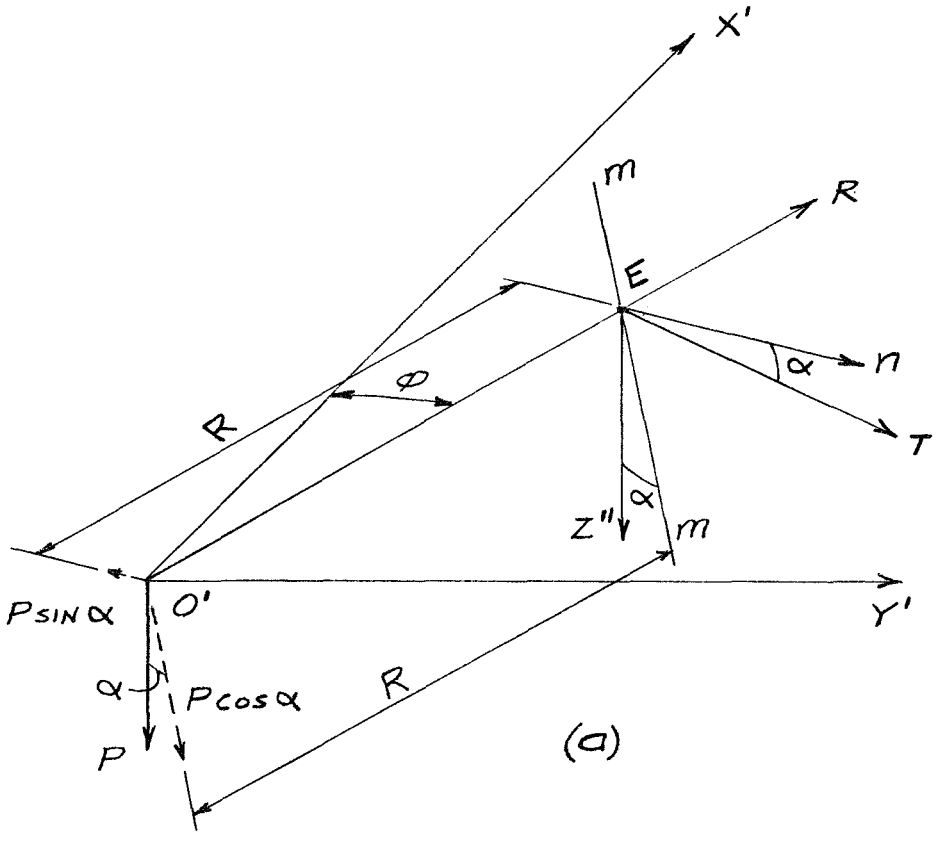

FIG. 6

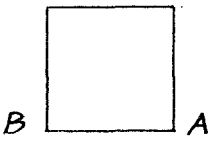
B
A

(b)

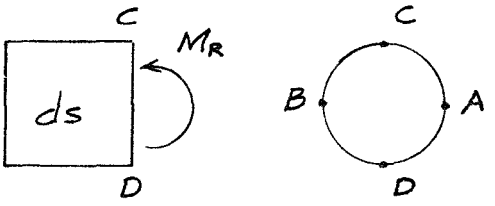
C
M_R
ds
D
C
B
A
D

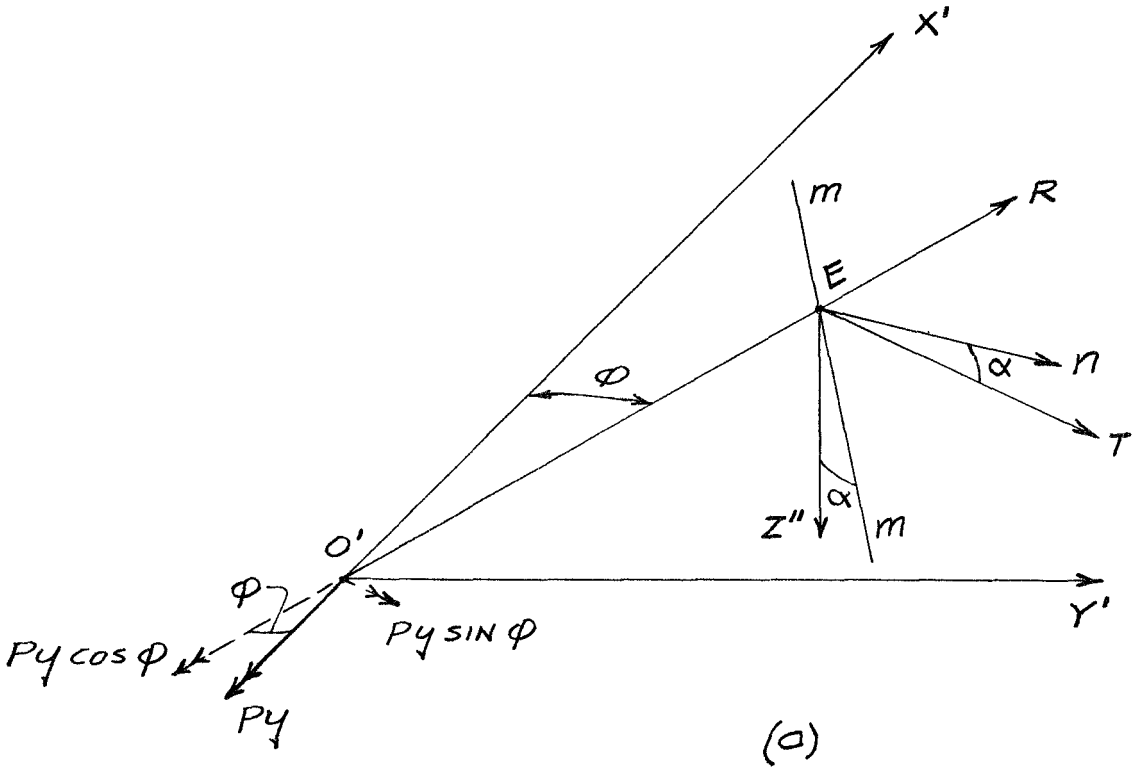
X'
m
R
E
α
n
T
φ
α
Z''
m
O'
φ
Y'
$P_y \cos\varphi$
$P_y \sin\varphi$
P_y

(a)

FIG. 7

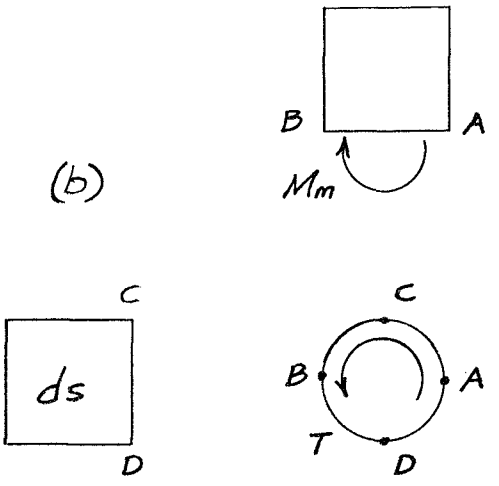
B
A
Mm
(b)
C
ds
D
C
B
A
T
D

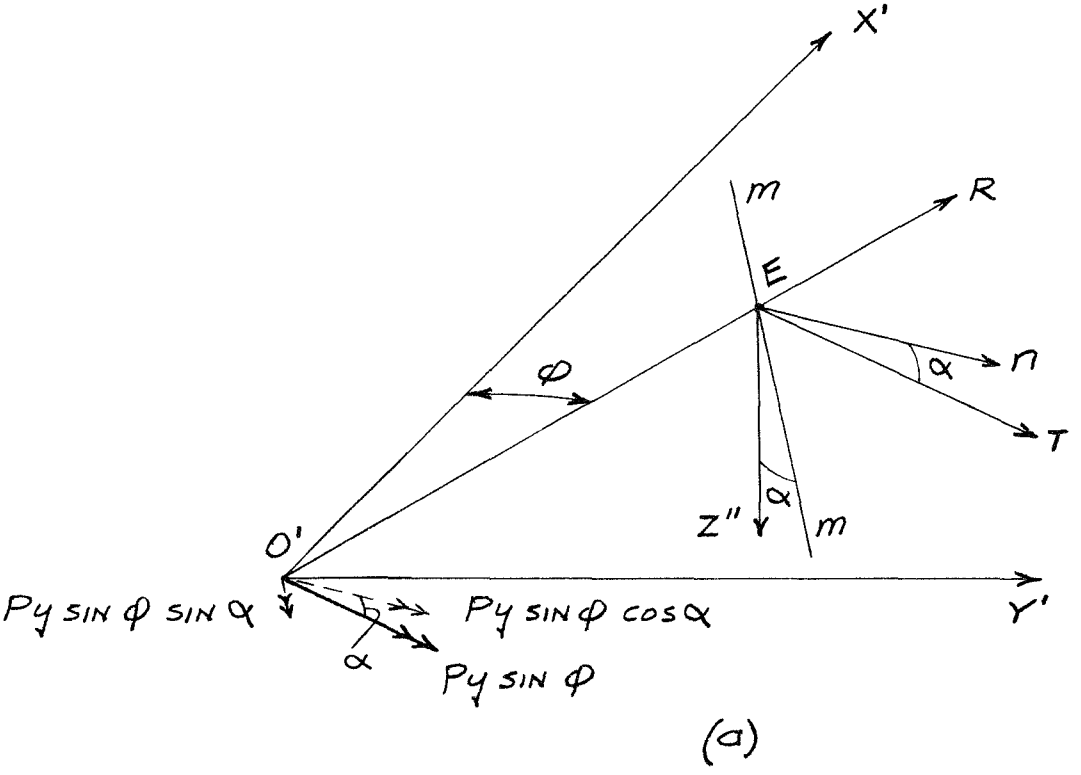
X'
m
R
E
φ
α
n
T
α
Z''
m
O'
Py SIN φ SIN α
Py SIN φ COS α
Y'
α
Py SIN φ
(a)

FIG. 8

The moment Py, acting about the X'-axis, can be resolved into components about the R and T axes as shown in Figure 7. The effect at point E due to the moment Py cos φ results in the expression

$$M_R = Py \cos \varphi \qquad (e)$$

The moment Py sin φ acting about the T-axis can be resolved into components about the m-m and n axes as shown in Figure 8. The effect at point E, due to these components, results in the following expressions.

$$M_m = Py \sin \varphi \sin \alpha \qquad (f)$$

$$T = Py \sin \varphi \cos \alpha \qquad (g)$$

The total effect of the axial force alone upon the distorted spring can be obtained by combining, in the proper manner, the above equations (a) through (g). Using the subscript A to designate forces and moments acting upon the wire cross section due to the axial force P, we obtain

$$
\left.
\begin{aligned}
C_A &= P \sin \alpha \\
M_{mA} &= PR \sin \alpha + Py \sin \alpha \sin \varphi \\
M_{RA} &= Py \cos \alpha \\
T_A &= PR \cos \alpha + Py \cos \alpha \sin \varphi \\
V_{mA} &= P \cos \alpha \\
V_{RA} &= 0
\end{aligned}
\right\} \qquad (3\text{-}1)
$$

4. LATERAL LOADING

The effect of the lateral force alone upon the distorted spring is shown in Figures 9, 10, 11, 12, and 13. The applied lateral force H, acting at point O, coincident with the Y-axis, produces a moment and a force at point O' as shown in Figure 9. The force is coincident with the Y'-axis and the moment, indicated by the double arrowhead vector, acts about the X'-axis.

The force H, acting at point O', can be resolved into components parallel to the R and T axes as shown in Figure 10. The effect at point E due to the force H sin φ results in the expression

$$V_R = H \sin \varphi \qquad (a)$$

The force H cos φ, parallel to the T-axis, can be resolved into components parallel to the m-m and n axes as shown in Figure 11. The effect at point E of these components is a shearing force parallel to the m-m axis, a compressive force parallel to the n-axis, a torque about the n-axis, and a moment about the m-m axis. The direction of these forces and moments acting upon the wire cross section ABCD is shown in Figure 11(b). With the aid of Figure 11, the following expressions are obtained.

$$C = H \cos \varphi \cos \alpha \qquad (b)$$

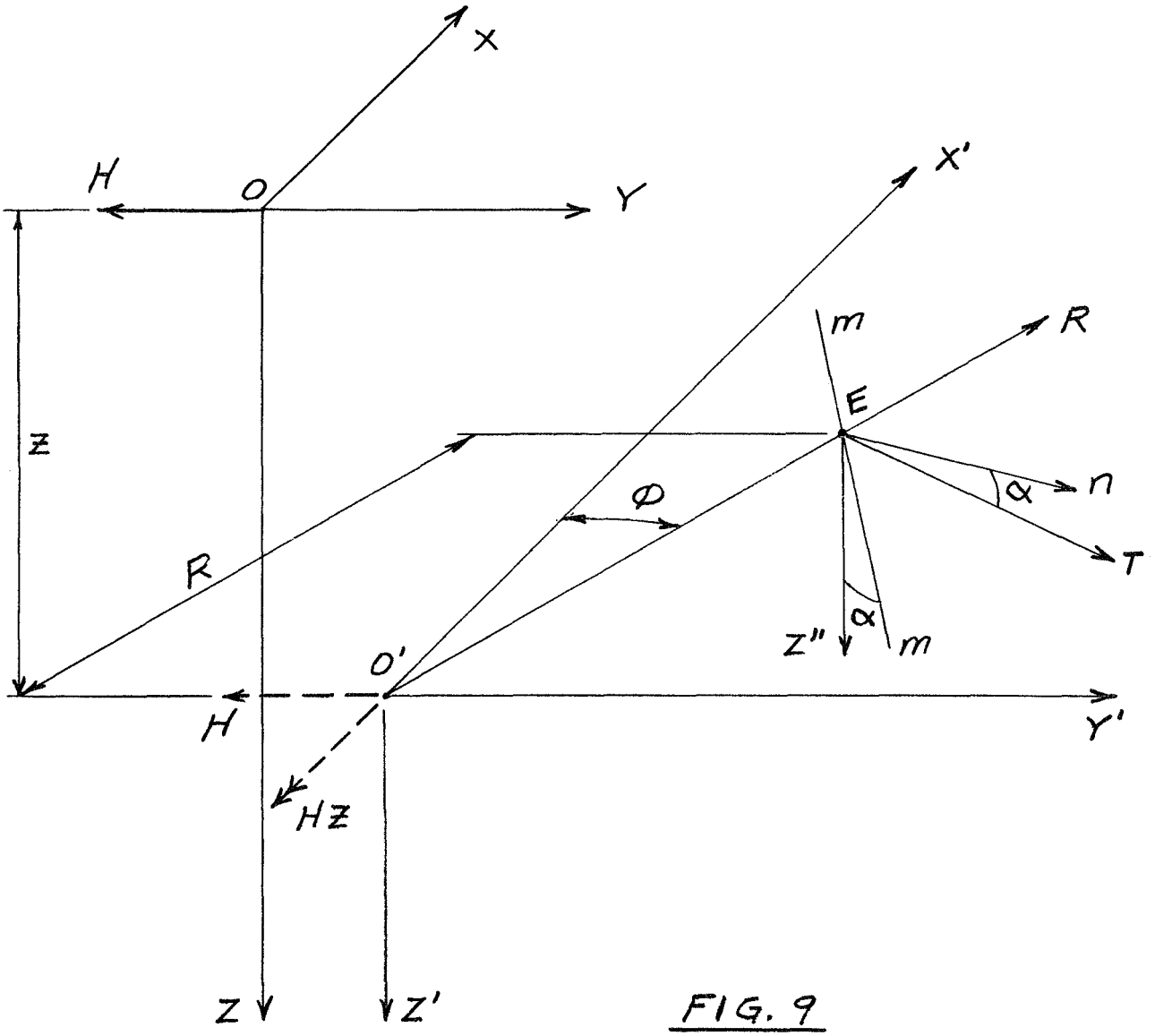

FIG. 9

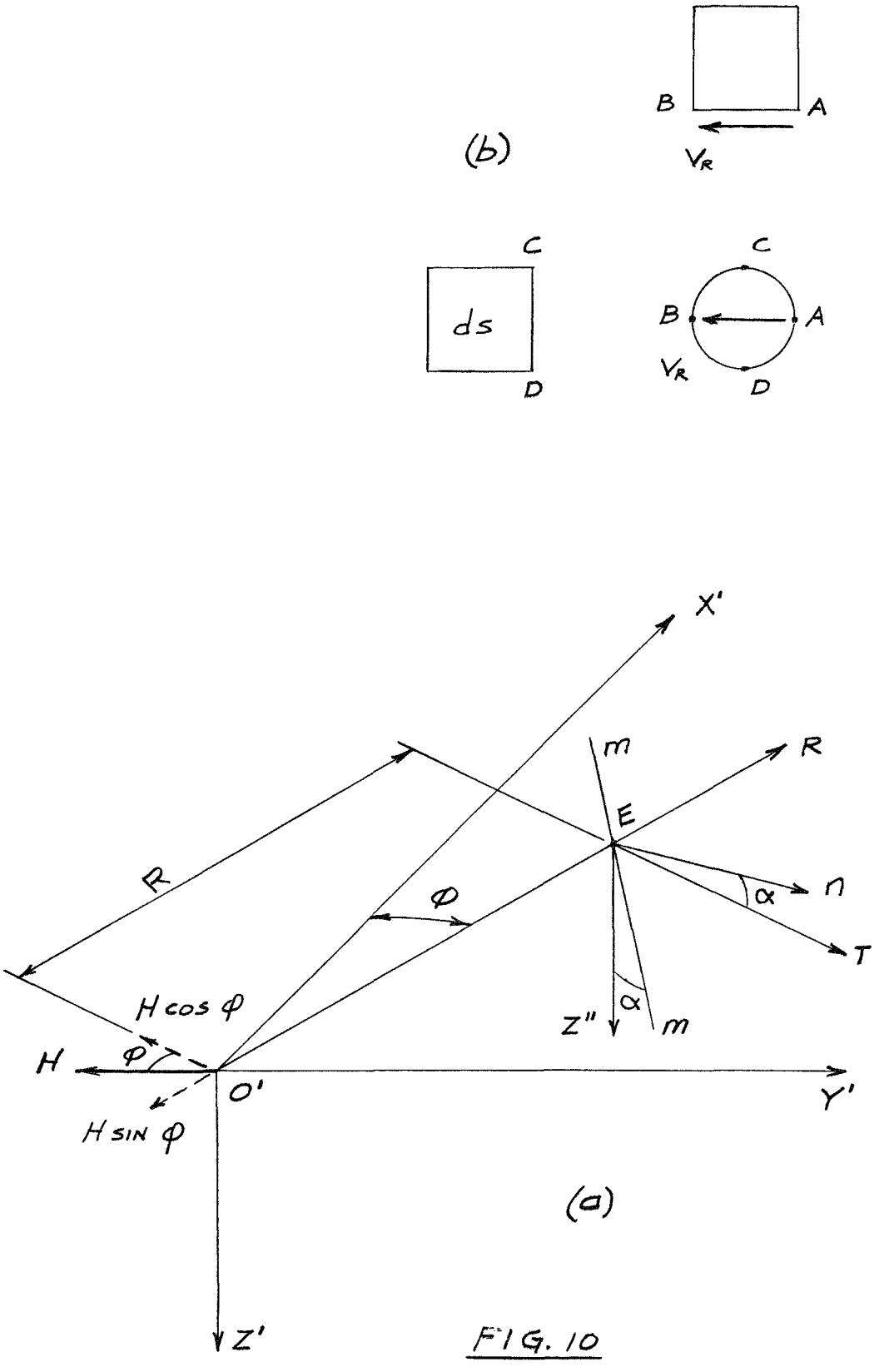

FIG. 10

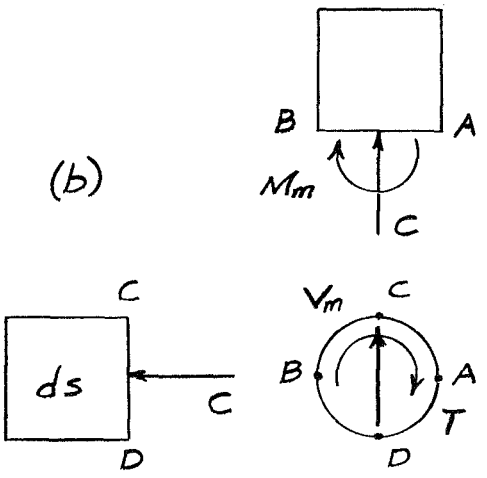
(b)
B
A
M_m
C
C
ds
C
D
V_m
C
B
A
T
D

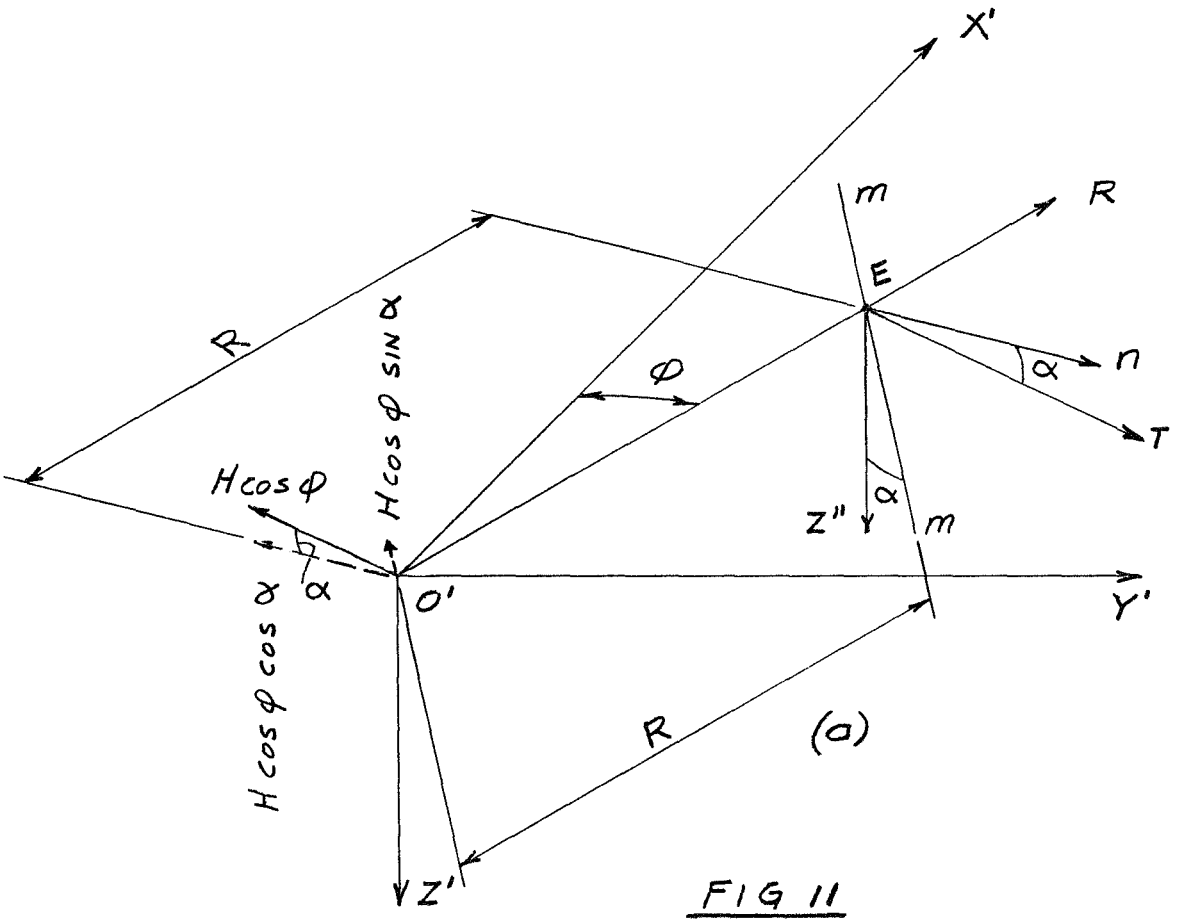
X'
m
R
E
R
$H\cos\phi\sin\alpha$
ϕ
n
α
T
$H\cos\phi$
$H\cos\phi\cos\alpha$
α
α
Z"
m
O'
Y'
R
(a)
Z'

FIG 11

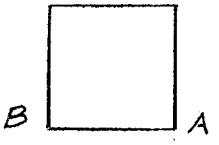

(b)

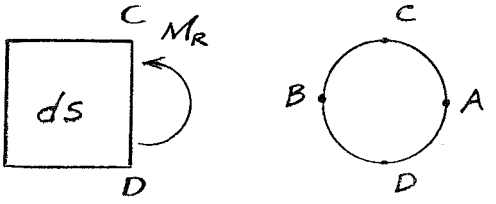

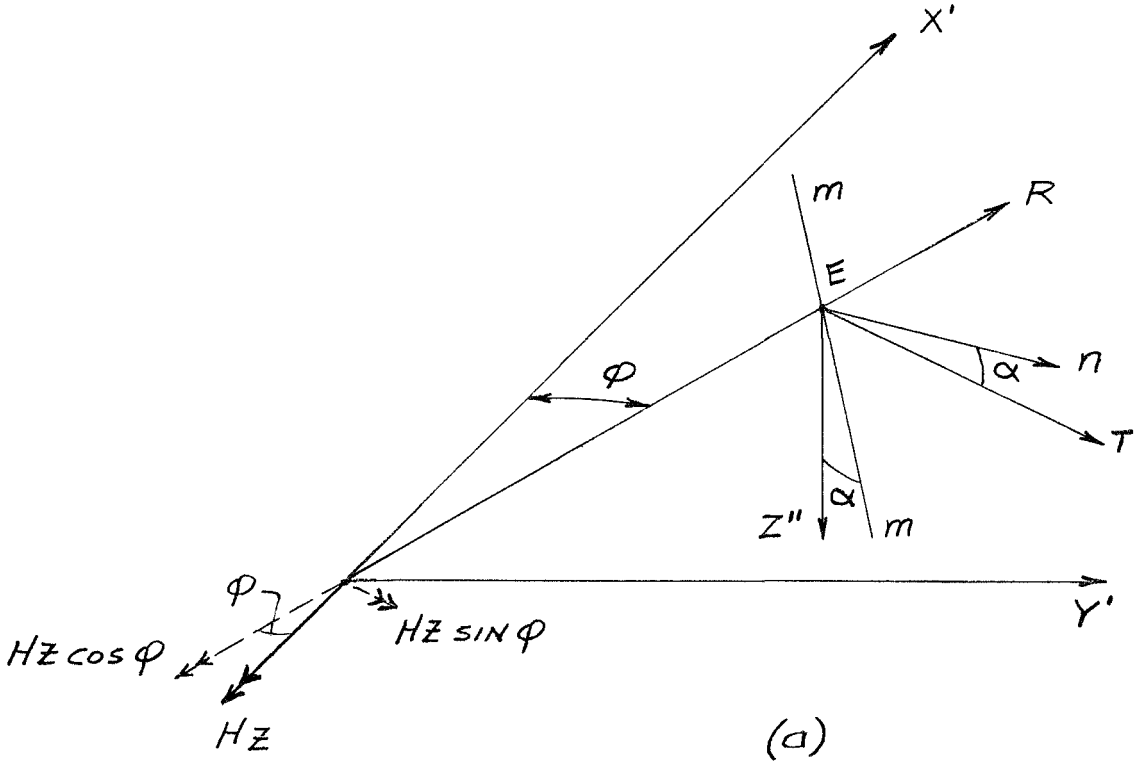

(a)

FIG. 12

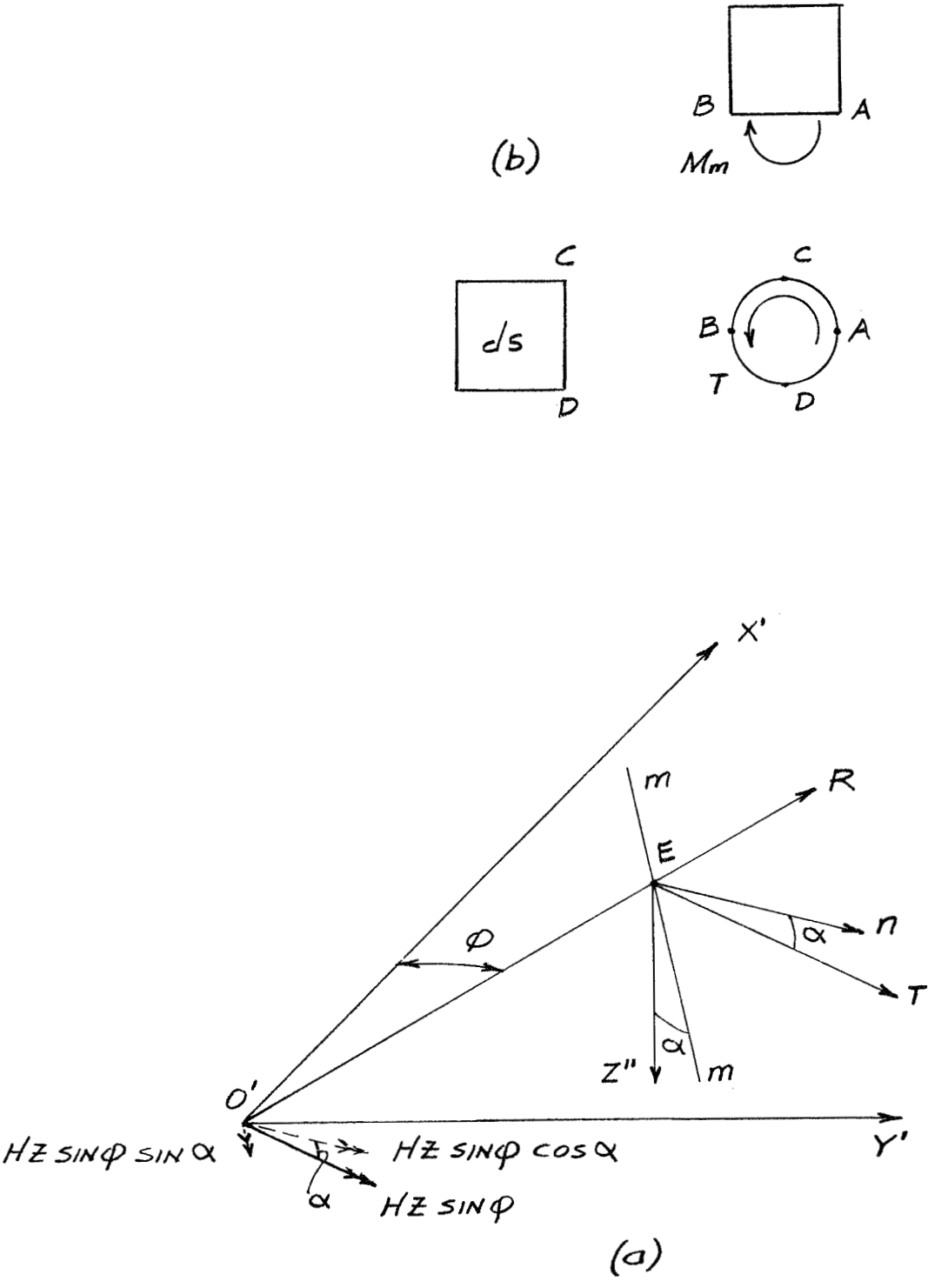
B
A
Mm
(b)
C
ds
D
C
B
A
T
D
X'
m
R
E
n
α
T
Φ
α
Z"
m
O'
HZ SINΦ SIN α
HZ SINΦ COS α
Y'
α
HZ SINΦ
(a)

FIG. 13

$$M_m = HR \cos \varphi \cos \alpha \qquad (c)$$

$$T = -HR \cos \varphi \sin \alpha \qquad (d)$$

$$V_m = -H \cos \varphi \sin \alpha \qquad (e)$$

The moment Hz, acting about the X'-axis, can be resolved into components about the R and T axes as shown in Figure 12. The effect at point E due to the moment Hz cos φ results in the expression

$$M_R = Hz \cos \varphi \qquad (f)$$

The moment Hz sin φ acting about the T-axis can be resolved into components about the m-m and n axes as shown in Figure 13. The effect at point E, due to these components, results in the following expressions.

$$M_m = Hz \sin \varphi \sin \alpha \qquad (g)$$

$$T = Hz \sin \varphi \cos \alpha \qquad (h)$$

The total effect of the lateral force alone upon the distorted spring can be obtained by combining, in the proper manner, the above equations (a) through (h). Using the subscript L to designate forces and moments acting upon the wire cross section due to the lateral force H, we obtain

$$
\left.
\begin{aligned}
C_L &= H \cos \alpha \cos \theta \\
M_{mL} &= Hz \sin \alpha \sin \varphi + HR \cos \alpha \cos \varphi \\
M_{RL} &= Hz \cos \varphi \\
T_L &= Hz \cos \alpha \sin \varphi - HR \sin \alpha \cos \varphi \\
V_{mL} &= -H \cos \varphi \sin \alpha \\
V_{RL} &= H \sin \varphi
\end{aligned}
\right\} \qquad (4\text{-}1)
$$

5. BENDING MOMENT

The effect of the bending moment alone upon the distorted spring is shown in Figures 14, 15, and 16. The applied bending moment M, acting at point O about the X-axis, produces a moment about the X'-axis as indicated in Figure 14 by the double arrowhead vector.

The moment M, acting about the X'-axis, can be resolved into components about the R and T axes as shown in Figure 15. The effect at point E due to the moment $M \cos \varphi$ results in the expression

$$M_R = -M \cos \varphi \qquad (a)$$

The moment $M \sin \varphi$ acting about the T-axis can be resolved into components about the m-m and n axes as shown in Figure 16. The effect at point E, due to these components, results in the following expressions.

$$M_m = -M \sin \varphi \sin \alpha \qquad (b)$$

$$T = -M \sin \varphi \cos \alpha \qquad (c)$$

Using the subscript M to designate forces and moments acting upon the wire cross section due to the bending moment M, we obtain

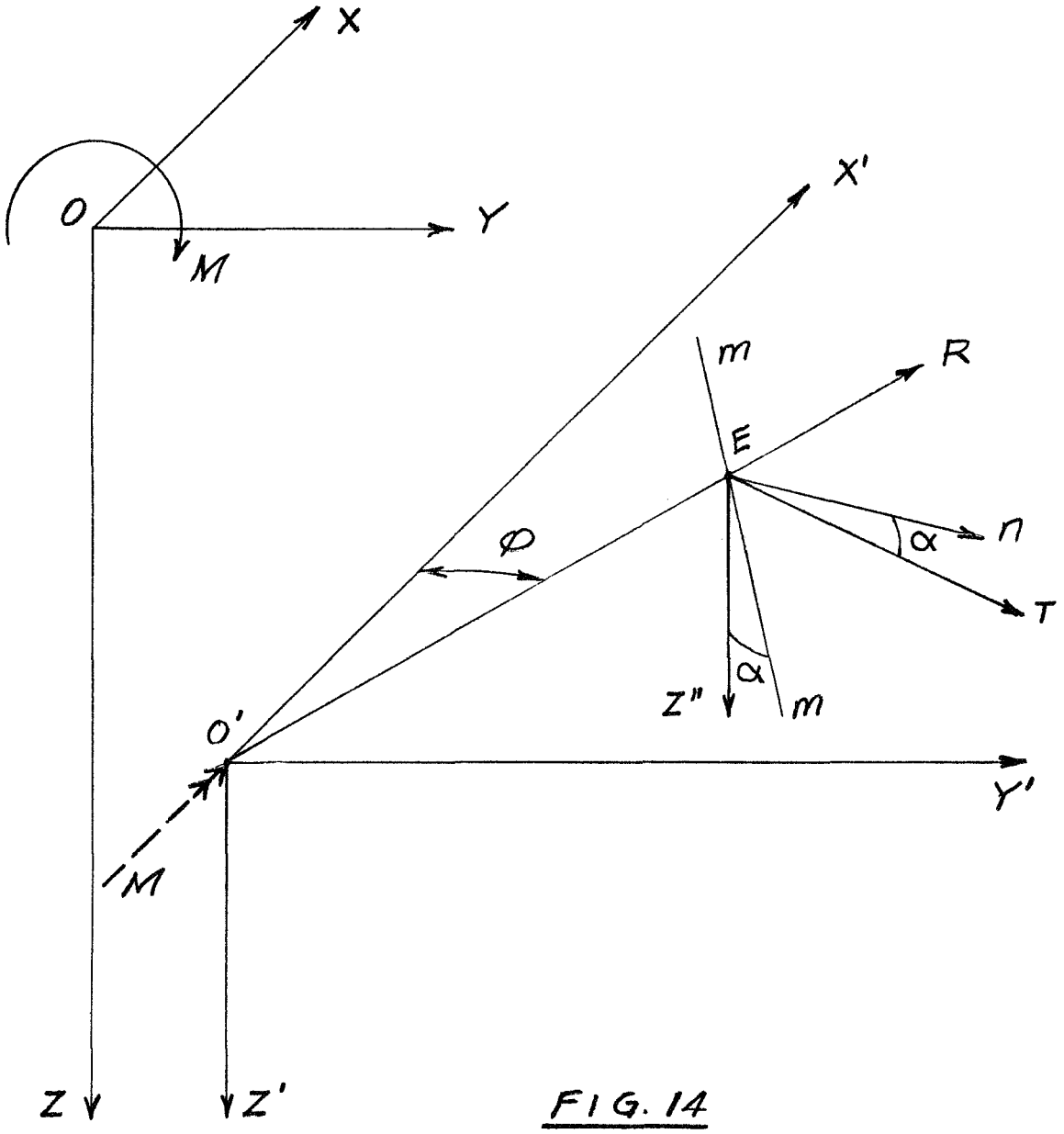

FIG. 14

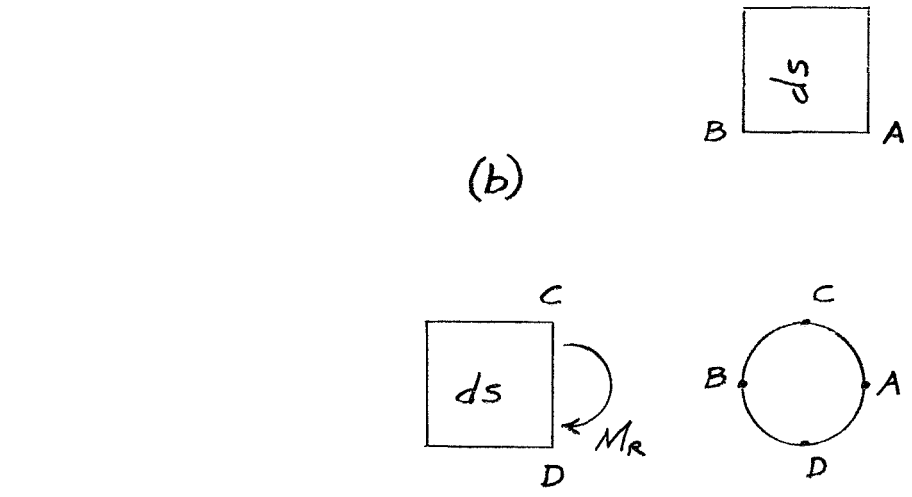
ds
B
A
(b)
C
ds
M_R
D
C
B
A
D

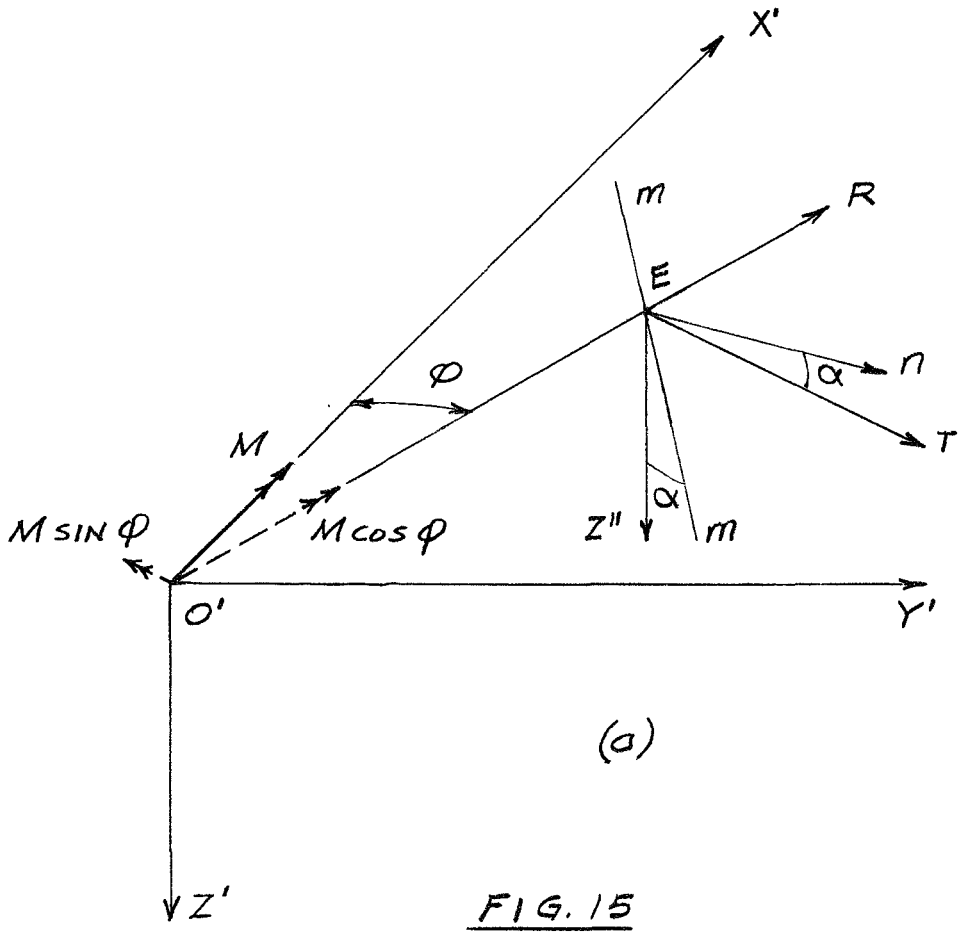
X'
m
R
E
φ
α
n
T
M
α
$M \sin \varphi$
$M \cos \varphi$
Z''
m
O'
Y'
(a)
Z'

FIG. 15

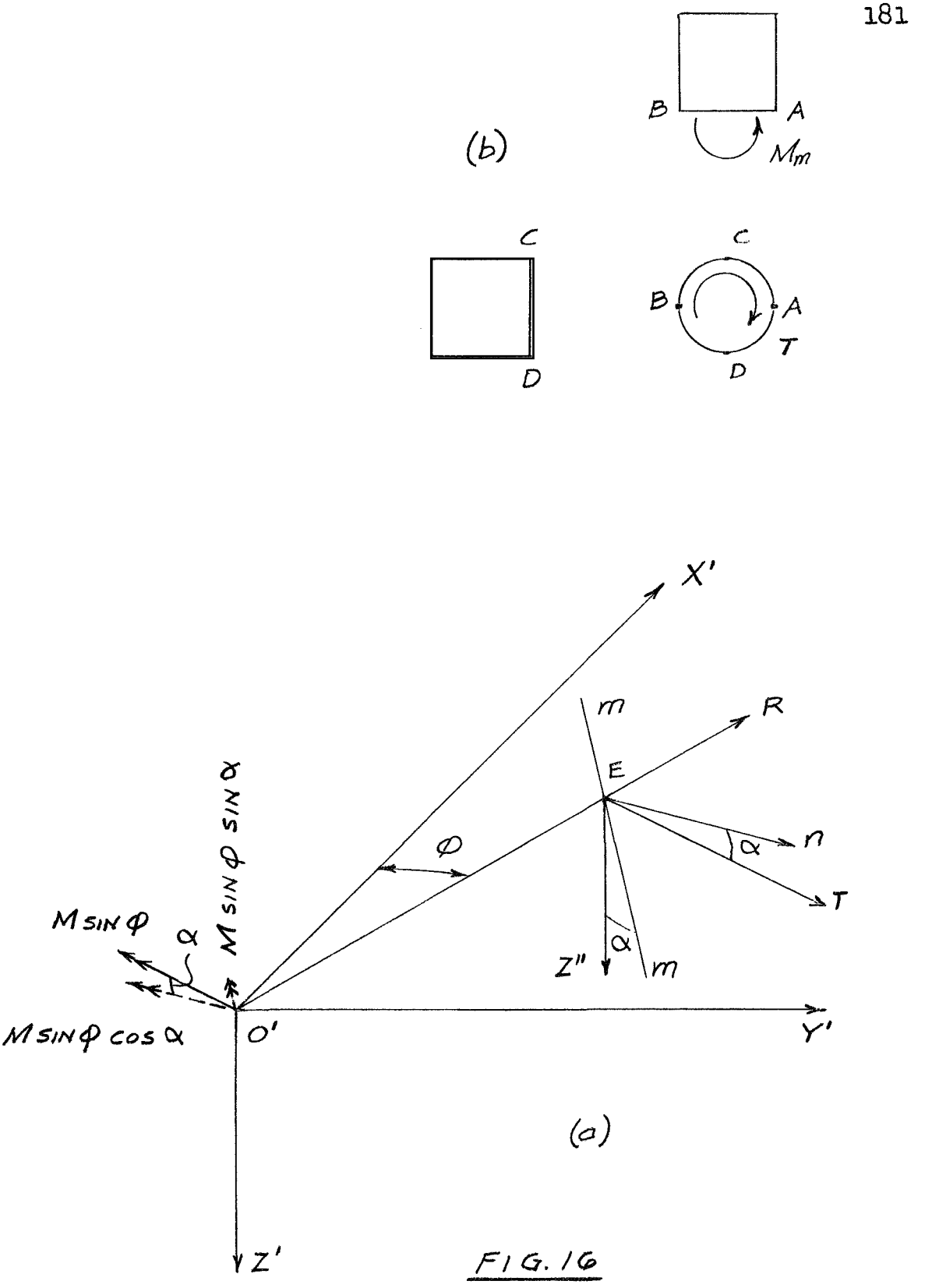
(b)
B
A
M_m
C
D
C
B
A
T
D
X'
m
R
E
n
T
α
φ
M SIN φ
α
M SIN φ SIN α
M SIN φ COS α
O'
Z''
α
m
Y'
(a)
Z'

FIG. 16

$$
\left.
\begin{aligned}
C_M &= 0 \\
M_{mM} &= -M \sin \alpha \sin \varphi \\
M_{RM} &= -M \cos \varphi \\
T_M &= -M \cos \alpha \sin \varphi \\
V_{mM} &= 0 \\
V_{RM} &= 0
\end{aligned}
\right\} \qquad (5\text{-}1)
$$

6. COMBINED LOADING

The forces and moments acting upon the cross section of the spring wire due to the combined loading system shown in Figure 4 will be obtained by superposing the forces and moments on the cross section due to each of the loading components (P, H, and M) separately. Considering the three sets of equations (3-1), (4-1), and (5-1), by superposition the following relationships are obtained:

$$\left.\begin{aligned} C &= P \sin\alpha + H \cos\alpha \cos\varphi \\ M_m &= PR \sin\alpha + (Hz + Py - M)\sin\alpha \sin\varphi + \\ &\quad HR \cos\alpha \cos\varphi \\ M_R &= (Hz + Py - M)\cos\varphi \\ T &= PR \cos\alpha + (Hz + Py - M)\cos\alpha \sin\varphi - \\ &\quad HR \sin\alpha \cos\varphi \\ V_m &= P \cos\alpha - H \sin\alpha \cos\varphi \\ V_R &= H \sin\varphi \end{aligned}\right\} \quad (6\text{-}1)$$

Equations (6-1) give expressions for the forces and moments acting upon any cross section of the spring wire due to the combined loading shown in Figure 4. Each expression for force or moment may be considered to be equivalent to that force or moment due to the axial force P acting alone when multiplied by a dimensionless amplification factor, or

$$\left.\begin{aligned} C &= P \sin \alpha F_1 \\ M_m &= PR \sin \alpha F_2 \\ M_R &= PRF_3 \\ T &= PR \cos \alpha F_4 \\ V_m &= P \cos \alpha F_5 \\ V_R &= PF_6 \end{aligned}\right\} \qquad (6\text{-}2)$$

where

$$\left.\begin{aligned} F_1 &= 1 + \frac{H}{P} \frac{\cos \varphi}{\tan \alpha} \\ F_2 &= 1 + \left(\frac{Hz}{PR} + \frac{y}{R} - \frac{M}{PR}\right)\sin \varphi + \frac{H}{P} \frac{\cos \varphi}{\tan \alpha} \\ F_3 &= \left(\frac{Hz}{PR} + \frac{y}{R} - \frac{M}{PR}\right)\cos \varphi \\ F_4 &= 1 + \left(\frac{Hz}{PR} + \frac{y}{R} - \frac{M}{PR}\right)\sin \varphi - \frac{H}{P} \tan \alpha \cos \varphi \\ F_5 &= 1 - \frac{H}{P} \tan \alpha \cos \varphi \\ F_6 &= \frac{H}{P} \sin \varphi \end{aligned}\right\} \qquad (6\text{-}3)$$

7. DEFLECTIONS

The loading (P, H, and M), shown in Figure 4, either combined or acting separately, produces forces and moments which act upon and deform the spring wire cross section. The deformations of the cross section result in axial and lateral movement of the spring ends and distortion of the coil axis.

The method of determining the deflections and distortion of the helical spring for the symmetrical loading case of an axial force and a lateral deflection with the spring ends remaining parallel to the original coil axis will be analogous to the solution for a structural member with a solid circular cross section. The main difference in concept in the solution for the helical spring from that for a solid structural member is that shearing distortion of the spring is appreciable and must be included while it is generally neglected for the case of the solid structural member.

The use of the analogy between the helical spring and a solid structural member is convenient but not necessary. Sufficient data have been developed in the preceding sections so that a specific expression or a more accurate trigonometric series could be assumed for the deflection shape and the solution obtained by energy methods. However,

this would provide no more accuracy and would be much more cumbersome.

Before considering the distortion of the spring under the action of the combined loading shown in Figure 3(b), the distortions produced by each of the combined loads P, H, and M acting separately will be determined by energy methods. In using energy methods, all deformations are assumed to be elastic and wire curvature effects are neglected. When the loading acts separately, the principle of superposition is valid and expressions equating the total work done to the total energy stored can be easily written. For the condition of either P, H, or M acting alone, equations (6-1) may be used in deriving the strain energy expressions if only those terms involving the particular load under consideration are used.

The differential strain energy in any element, ds, of the wire cross section will consist of the following components:

$$
\left.
\begin{aligned}
dU_1 &= \frac{C^2 ds}{2EA} && \text{compression} \\
dU_2 &= \frac{M_m{}^2 ds}{2EI} && \text{bending in plane of curvature} \\
dU_3 &= \frac{M_R{}^2 ds}{2EI} && \text{bending out of plane of curvature} \\
dU_4 &= \frac{T^2 ds}{2GI_P} && \text{torsion} \\
dU_5 &= N \frac{V_m{}^2 ds}{2GA} && \text{shear out of plane of curvature} \\
dU_6 &= N \frac{V_R{}^2 ds}{2GA} && \text{shear in plane of curvature}
\end{aligned}
\right\} \quad (a)
$$

where, from reference 2, N is a factor dependent upon the form of the cross section, which for circular solid

$$N = \frac{10}{9}$$

The total differential energy is equal to the sum of the component differential energies or

$$dU_T = \sum dU = dU_1 + dU_2 + dU_3 + dU_4 + dU_5 + dU_6$$

and the total energy stored in the spring is equal to the energy stored in all of the differential lengths or

$$U_T = \int_0^s \sum dU$$

and, using equations (a)

$$U_T = \frac{1}{2}\int_0^s \left[\frac{C^2}{EA} + \frac{M_m^2}{EI} + \frac{M_R^2}{EI} + \frac{T^2}{GI_P} + N\frac{V_m^2}{GA} + N\frac{V_R^2}{GA}\right] ds$$

From equation (1-2)

$$ds = \frac{R\, d\varphi}{\cos \alpha}$$

then

$$U_T = \frac{R}{2\cos\alpha}\int_0^{2n\pi}\left[\frac{C^2}{EA} + \frac{M_m^2}{EI} + \frac{M_R^2}{EI} + \frac{T^2}{GI_P} + N\frac{V_m^2}{GA} + N\frac{V_R^2}{GA}\right] d\varphi \qquad (b)$$

where

$$\left.\begin{aligned} &E = \text{modulus of elasticity in tension and compression}\\ &G = \text{modulus of elasticity in shear}\\ &A = \frac{\pi d^2}{4} \quad \text{cross-sectional area of wire}\\ &I = \frac{\pi d^4}{64} \quad \text{diameter moment of inertia of wire}\\ &I_P = \frac{\pi d^4}{32} \quad \text{polar moment of inertia of wire} \end{aligned}\right\} \qquad (c)$$

For the condition of P acting alone, equations (6-1) will be valid if H, M, and y are put equal to zero. Then

$$\left.\begin{aligned} C &= P \sin \alpha \\ M_m &= PR \sin \alpha \\ M_R &= 0 \\ T &= PR \cos \alpha \\ V_m &= P \cos \alpha \\ V_R &= 0 \end{aligned}\right\} \qquad (d)$$

and equation (b) will become

$$U_T = \frac{R}{2 \cos \alpha} \int_0^{2n\pi} \left[\frac{P^2 \sin^2 \alpha}{EA} + \frac{P^2 R^2 \sin^2 \alpha}{EI} + \frac{P^2 R^2 \cos^2 \alpha}{GI_P} + N \frac{P^2 \cos^2 \alpha}{GA} \right] d\varphi$$

or

$$U_T = \frac{n\pi D}{2} \frac{P^2}{GA} \left[\cos \alpha \left(N + \frac{AR^2}{I_P} \right) + \frac{G}{E} \sin \alpha \tan \alpha \left(1 + \frac{AR^2}{I} \right) \right] \qquad (e)$$

From equations (c)

$$\left.\begin{aligned} \frac{AR^2}{I} &= 4\left(\frac{D}{d}\right)^2 \\ \frac{AR^2}{I_P} &= 2\left(\frac{D}{d}\right)^2 \end{aligned}\right\} \qquad (f)$$

and substituting in equation (e)

$$U_T = \frac{2nDP^2}{Gd^2} \left\{ \cos \alpha \left[N + 2\left(\frac{D}{d}\right)^2 \right] + \frac{G}{E} \sin \alpha \tan \alpha \left[1 + 4\left(\frac{D}{d}\right)^2 \right] \right\} \qquad (g)$$

Since, for practical reasons, the ratio $\frac{D}{d}$ will not be less than 4, there will be little appreciable error if equation (g) is written

$$U_T = \frac{4nP^2}{Gd}\left(\frac{D}{d}\right)^3\left(\cos\alpha + \frac{2G}{E}\sin\alpha\tan\alpha\right) \qquad (h)$$

The total work done by the external force P will equal the total stored energy of strain or

$$\frac{P\delta_P}{2} = U_T$$

and

$$\delta_P = \frac{8nP}{Gd}\left(\frac{D}{d}\right)^3 F_P \qquad (7\text{-}1)$$

where

$$F_P = \cos\alpha + \frac{2G}{E}\sin\alpha\tan\alpha \qquad (7\text{-}2)$$

Equations (7-1) and (7-2) are verified by reference 1 with the exception that equation (7-2) is written

$$F_P = \frac{\cos\alpha}{\beta} + \frac{2G}{E}\sin\alpha\tan\alpha$$

where

$$\beta = 1 + \frac{3}{16\left[\left(\frac{D}{d}\right)^2 - 1\right]}$$

which is defined as a curvature correction factor. Figure 17 contains a plot of β against $\frac{D}{d}$ and indicates that the curvature correction has very little significance if $\frac{D}{d}$ is greater than 4.

For the condition of H acting alone, equations (6-1) will be valid if

$$P = 0$$

$$M = HL$$

then

$$\left.\begin{aligned} C &= H \cos \alpha \cos \varphi \\ M_m &= H\left[-(L - z)\sin \alpha \sin \varphi + R \cos \alpha \cos \varphi\right] \\ M_R &= -H(L - z)\cos \varphi \\ T &= -H\left[(L - z)\cos \alpha \sin \varphi + R \sin \alpha \cos \varphi\right] \\ V_m &= -H \sin \alpha \cos \varphi \\ V_R &= H \sin \varphi \end{aligned}\right\} \quad (i)$$

Using equation (1-4)

$$z = R\varphi \tan \alpha$$

and equation (b), after integrating and simplifying there results

$$U_T = \frac{4nH^2}{Gd}\left(\frac{D}{d}\right)^3\left[\frac{2}{3}\left(\frac{L}{D}\right)^2\left(\cos \alpha + \frac{2G}{E} \sin \alpha \tan \alpha + \frac{2G}{E \cos \alpha}\right) + \frac{G \cos \alpha}{E}\right] \quad (j)$$

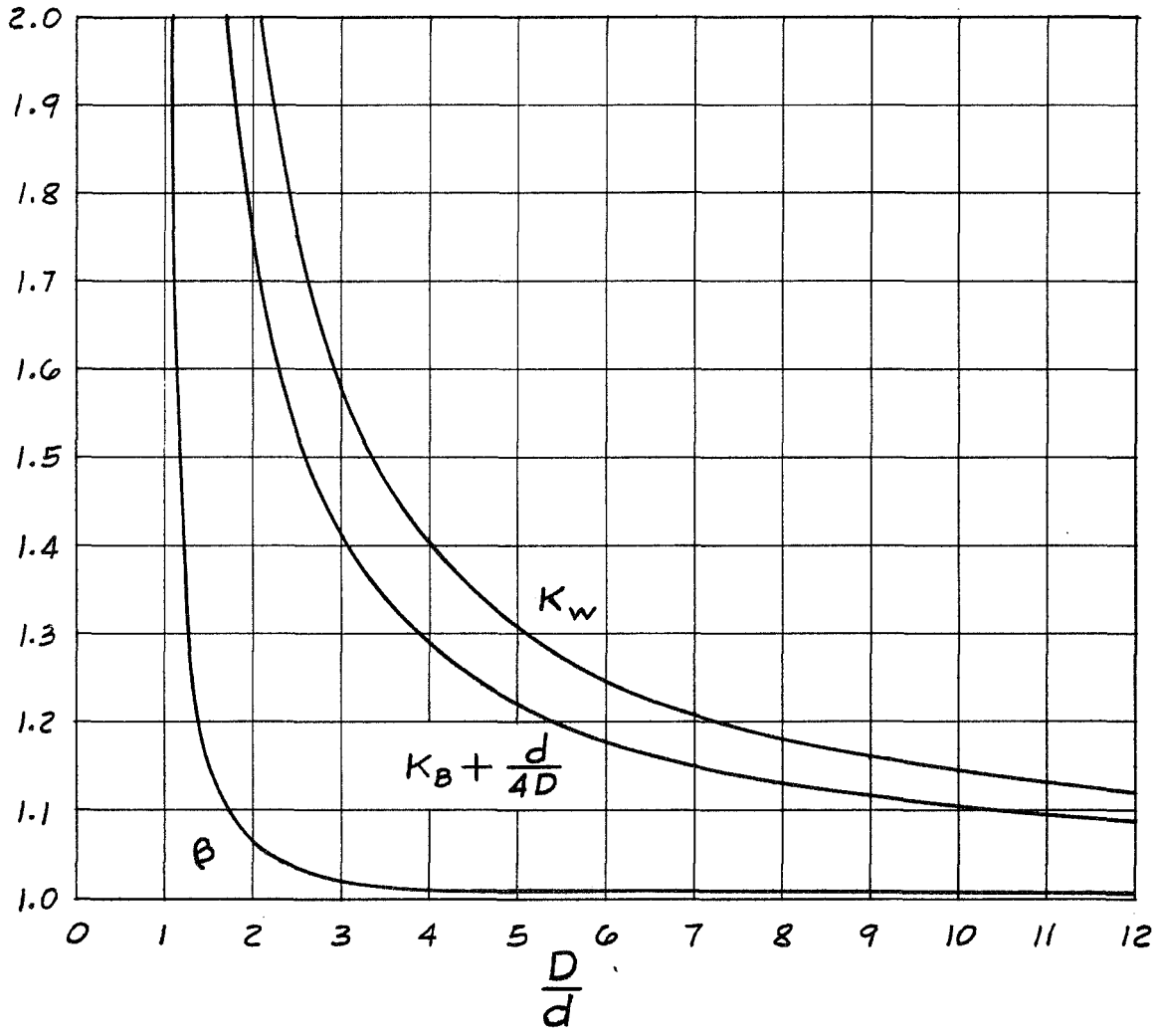
2.0
1.9
1.8
1.7
1.6
1.5
1.4
1.3
1.2
1.1
1.0
0
1
2
3
4
5
6
7
8
9
10
11
12
K_w
$K_B + \frac{d}{4D}$
β
$\frac{D}{d}$

FIG. 17

The total work done by the external force H will equal the total stored energy of strain or

$$\frac{H\,\Delta_H}{2} = U_T$$

and

$$\Delta_H = \frac{8nH}{Gd}\left(\frac{D}{d}\right)^3 F_H \qquad (7\text{-}3)$$

where

$$F_H = \frac{2}{3}\left(\frac{L}{D}\right)^2\left(\cos\alpha + \frac{2G}{E}\sin\alpha\tan\alpha + \frac{2G}{E\cos\alpha}\right) + \frac{G\cos\alpha}{E} \qquad (7\text{-}4)$$

Equations (7-3) and (7-4) are verified by reference 1 for the condition of α being very small.

For the condition of M acting alone, equations (6-1) will be valid if P and H are put equal to zero. Then

$$\left.\begin{aligned} C &= 0 \\ M_m &= -M\sin\alpha\sin\varphi \\ M_R &= -M\cos\varphi \\ T &= -M\cos\alpha\sin\varphi \\ V_m &= 0 \\ V_R &= 0 \end{aligned}\right\} \qquad (k)$$

and equation (b) will become

$$U_T = \frac{R}{2\cos\alpha}\int_0^{2n\pi}\left[\frac{M^2\sin^2\alpha\,\sin^2\varphi}{EI} + \frac{M^2\cos^2\varphi}{EI} + \frac{M^2\cos^2\alpha\,\sin^2\varphi}{GI_P}\right]d\varphi$$

and, after integrating and collecting terms,

$$U_T = \frac{8nM^2}{Gd^3}\left(\frac{D}{d}\right)\left(\cos \alpha + \frac{2G}{E} \sin \alpha \tan \alpha + \frac{2G}{E \cos \alpha}\right) \qquad (l)$$

The total work done by the external moment M will equal the total stored energy of strain, or

$$\frac{M\gamma_M}{2} = U_T$$

where γ_M equals the angle of rotation of the applied moment M and then

$$\gamma_M = \frac{16nM}{Gd^3}\left(\frac{D}{d}\right)F_M \qquad (7\text{-}5)$$

where

$$F_M = \cos \alpha + \frac{2G}{E} \sin \alpha \tan \alpha + \frac{2G}{E \cos \alpha} \qquad (7\text{-}6)$$

Equation (l) is verified by reference 1.

Now that the axial deflection, lateral deflection, and rotation have been determined for the condition of an axial force, a lateral force, and a bending moment each acting separately upon the spring, it will be convenient to develop equivalent rigidity factors. The term, equivalent rigidity factor, is used rather loosely but, for the purpose of this paper, shall apply to helical compression springs

and shall correspond to the rigidity factors for a structural member of solid circular cross section. For instance, Figure 18(a) represents a structural member rigidly fixed at one end. The cross section is assumed solid and circular with a radius equal to R. The loading P, H, and M, each acting alone upon the member, produces distortions measured by δ_P, Δ_H, and γ_M, respectively. Let E and G represent the moduli of elasticity and rigidity as defined previously and let A and I represent the cross-sectional area and moment of inertia of the cross section about the axis of bending. From basic mechanics of materials theory, the following relationships for the structural member shown in Figure 18 can be verified. The deflection under axial load P, Figure 18(b), will equal

$$\delta_P = \frac{PL}{EA}$$

and the compressive rigidity will equal

$$(AE) = \frac{PL}{\delta_P} \qquad (m)$$

The rotation of one end with respect to the other end under pure bending M, Figure 18(c), will equal

$$\gamma_M = \frac{L}{\rho}$$

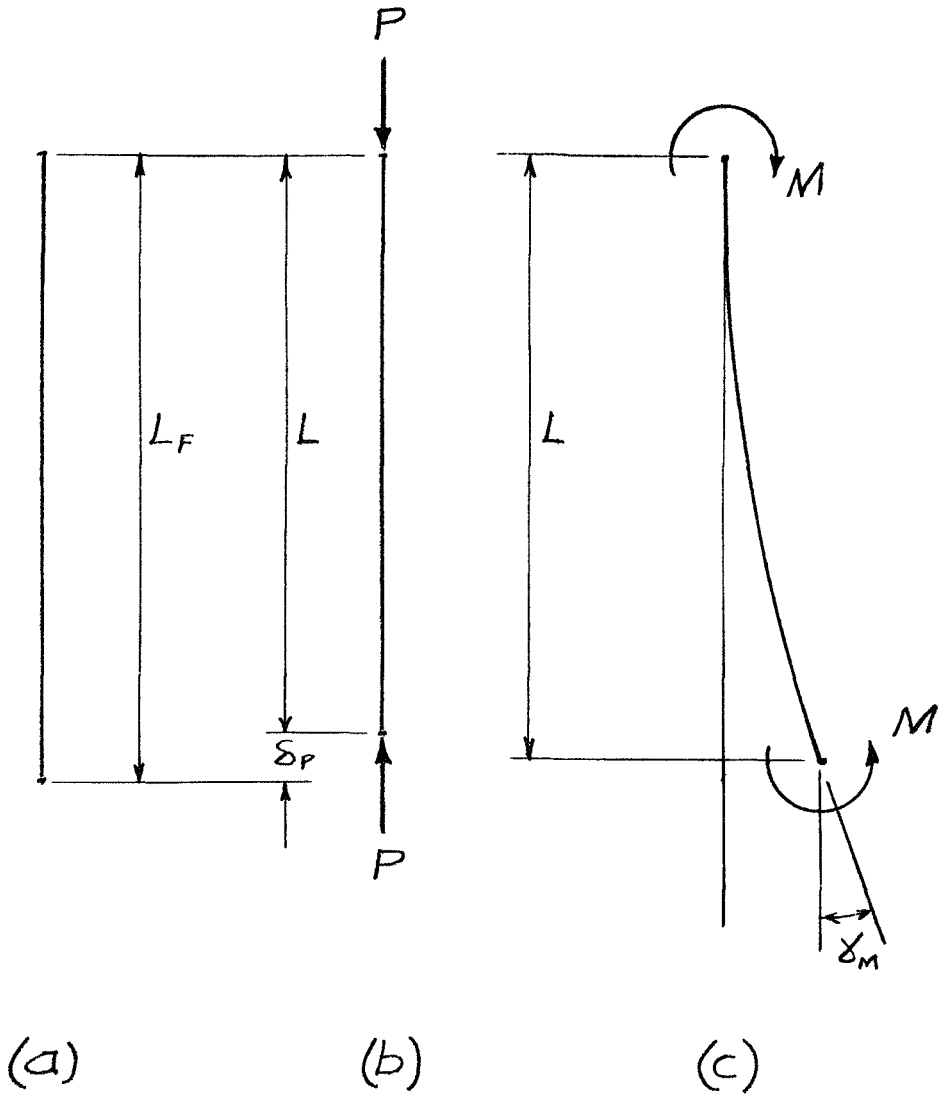

FIG. 18

where ρ equals the radius of curvature of the elastic axis. Furthermore,

$$\rho = \frac{EI}{M}$$

so that

$$\gamma_M = \frac{ML}{EI}$$

and then the flexural rigidity will equal

$$(EI) = \frac{ML}{\gamma_M} \qquad (n)$$

The maximum lateral deflection, Δ_H, due to the application of lateral forces H, Figure 19(a), results from both shearing and bending deformations of the cross section. For most structural members, the shearing deformations are small compared to the bending deformations and usually are neglected. However, since this example is being developed as an analogy for helical springs, the shearing distortion will be included. Figure 19(a) represents the distorted structural member, rigidly fixed at one end, and subjected to lateral forces H and a bending moment

$$M = HL$$

Figure 19(b) represents any differential element, ds, of the member center line subjected to the lateral force H which can be resolved into components parallel and perpendicular

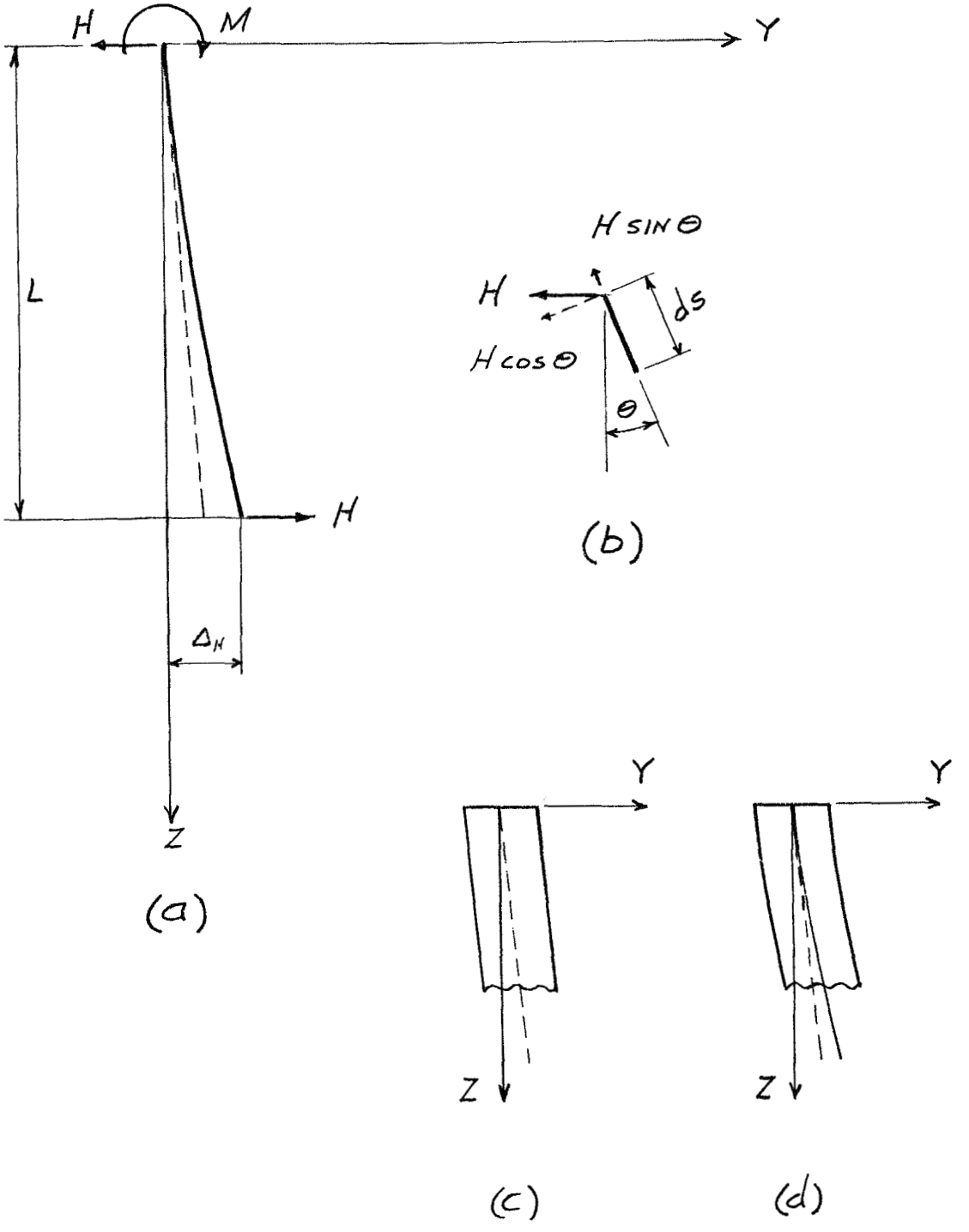

FIG. 19

to the center line. The angle of curvature θ will be assumed small so that

$$H \sin \theta \cong 0$$

and

$$H \cos \theta \cong H$$

The shearing force on any cross section will be

$$V = H$$

which will produce distortion resulting in a deflected shape having a constant slope equal to

$$\frac{V}{GA} = \frac{NH}{GA} \qquad (o)$$

The curvature of the deflected shape due to shearing distortions will then equal

$$\frac{d}{dz}\left(\frac{V}{GA}\right) = 0 \qquad (p)$$

The broken line in Figure 19(a) represents the constant slope distortion of the elastic axis due to shearing deformations of the cross sections. The solid line represents the total distortion of the elastic axis due to the sum of the shearing and bending deformations of the cross sections. From basic mechanics of materials, the curvature of the elastic axis can be expressed

$$\frac{d^2y}{dz^2} = \frac{M - Hz}{EI} = \frac{HL}{EI} - \frac{Hz}{EI} \qquad (q)$$

which is due to bending only, since from equation (p), the shearing curvature equals zero. Integrating equation (q)

$$\left.\begin{aligned} \frac{dy}{dz} &= \frac{HLz}{EI} - \frac{Hz^2}{2EI} + C_1 \\ y &= \frac{HLz^2}{2EI} - \frac{Hz^3}{6EI} + C_1 z + C_2 \end{aligned}\right\} \qquad (r)$$

where C_1 and C_2 are constants of integration which must be adjusted to satisfy the boundary conditions.

Figure 19(c) represents the fixed end of the member under the action of shearing deformation alone. The broken line represents the distorted elastic axis and has a constant slope given by equation (o). Since the end is fixed or clamped, the end cross section will remain perpendicular to the Z-axis. Figure 19(d) represents the fixed end of the member under the action of both shearing and bending deformations. The solid line represents the distorted elastic axis. It is seen, therefore, that at the fixed end, if shearing deformations exist, the distorted elastic axis will coincide with and be parallel to the distorted axis caused by shearing deformations alone and will not be parallel to the original or Z-axis.

At the origin of the coordinate axis, the boundary conditions require that the deflection and slope of the distorted elastic axis, represented by equations (r), must coincide with the deflection and slope of the elastic curve caused by shearing deformations, or

$$(y)_{z=0} = 0$$

$$\left(\frac{dy}{dz}\right)_{z=0} = \frac{NH}{GA}$$

from which

$$C_1 = \frac{NH}{GA}$$

$$C_2 = 0$$

resulting in

$$y = \frac{HLz^2}{2EI} - \frac{Hz^3}{6EI} + \frac{NHz}{GA} \qquad (s)$$

Using the expression for the distorted elastic axis, equation (s), and the limiting condition

$$(y)_{z=L} = \Delta_H$$

the lateral deflection under lateral loading will equal

$$\Delta_H = \frac{HL^3}{3EI} + \frac{NHL}{GA}$$

and the shearing rigidity will equal

$$(GA) = \frac{NHL}{\Delta_H - \frac{HL^3}{3(EI)}} \qquad (t)$$

Equations (m), (n), and (t) are the rigidity factors corresponding to compression, flexure, and shear, respectively, for a structural member with a solid circular cross section. Using equations (7-1) and (m), the equivalent compressive rigidity for a helical spring will equal

$$(EA)_s = \frac{Gd^2}{8\left(\frac{D}{d}\right)^3 F_P}\left(\frac{L}{nd}\right) \qquad (7\text{-}7)$$

Using equations (7-5) and (n), the equivalent flexural rigidity for a helical spring will equal

$$(EI)_s = \frac{Gd^4}{16\left(\frac{D}{d}\right) F_M}\left(\frac{L}{nd}\right) \qquad (7\text{-}8)$$

Using equations (7-3), (7-4), (7-6), (t), and (7-8), the equivalent shearing rigidity for a helical spring will equal

$$(GA)_s = \frac{NGd^2}{8\left(\frac{D}{d}\right)^3 \frac{G \cos \alpha}{E}}\left(\frac{L}{nd}\right) \qquad (7\text{-}9)$$

Equivalent rigidity factors are discussed and derived in references 1 and 3 for close coiled springs and equations (7-7), (7-8), and (7-9) are verified for the condition of the coil pitch angle α being very small.

Let Figure 20(a) represent a structural member with a solid circular cross section subjected to an axial force and a lateral deflection with the ends remaining nominally parallel to the original axis. The term "nominally parallel" is used since it was determined previously that, only for the condition of shearing deformations being negligible, is it reasonable to assume the ends of the distorted elastic axis parallel to the original axis. Figure 20(b) represents any differential element, ds, of the distorted elastic axis subjected to the lateral force H which can be resolved into components parallel and perpendicular to the axis. The angle of curvature θ will be assumed small so that

$$H \sin \theta \cong 0$$

and

$$H \cos \theta \cong H$$

The shearing force on any cross section due to the lateral forces H will be

$$V = H$$

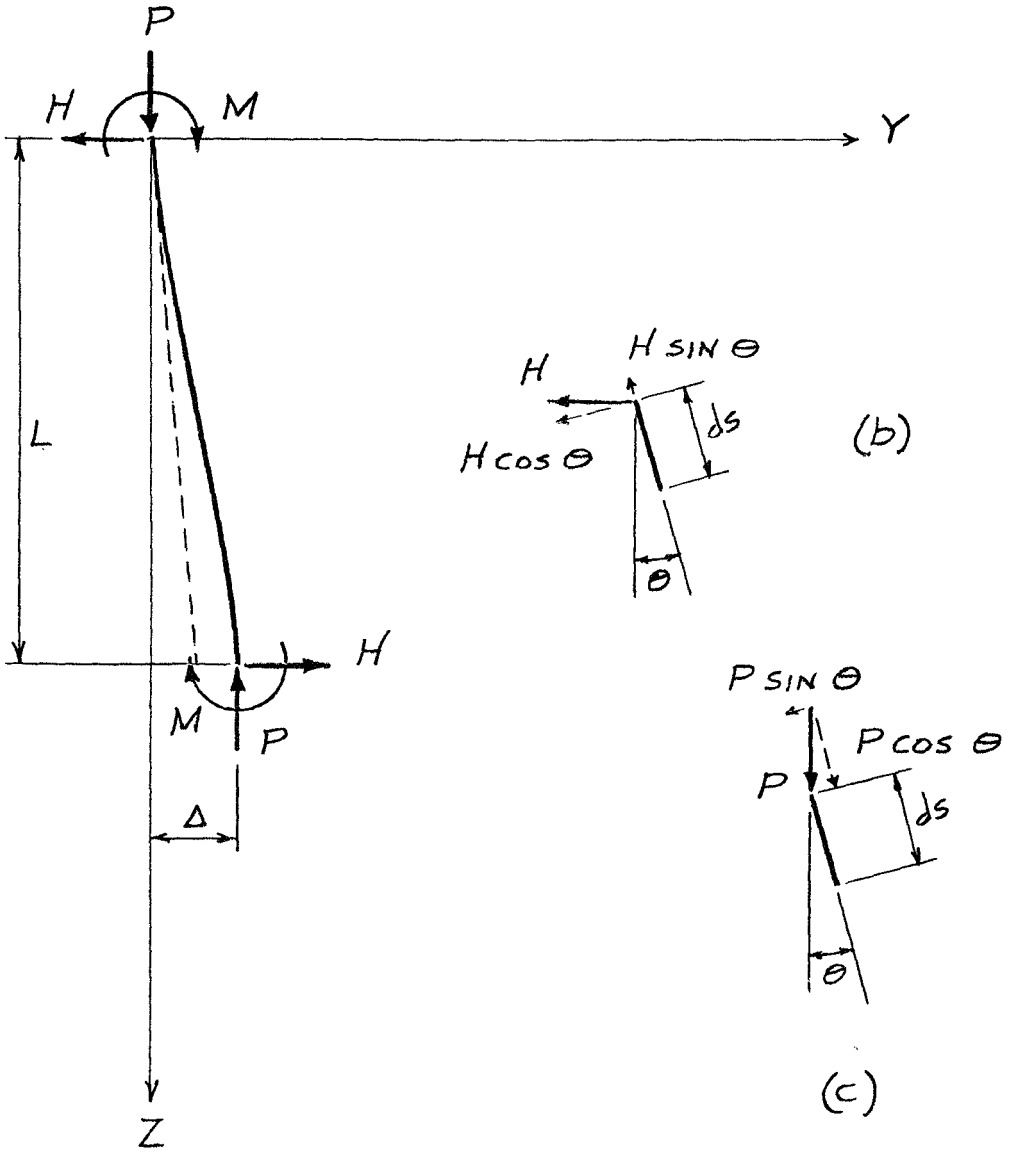

FIG. 20

which will produce distortion resulting in a deflected shape having a constant slope equal to

$$\frac{V}{GA} = \frac{NH}{GA} \qquad (u)$$

The curvature of the deflected shape due to shearing deformation produced by the lateral forces H will then equal

$$\frac{d}{dz}\left(\frac{V}{GA}\right) = 0$$

Figure 20(c) represents any differential element, ds, of the distorted elastic axis subjected to the axial force P which can be resolved into components parallel and perpendicular to the axis. The angle of curvature θ will be assumed small so that

$$P \sin \theta \cong P \tan \theta = P \frac{dy}{dz}$$

and

$$P \cos \theta \cong P$$

The shearing force on any cross section due to the axial forces P will be

$$V = P \frac{dy}{dz}$$

which will produce distortion resulting in a deflected shape having a slope equal to

$$\frac{V}{GA} = \frac{NP}{GA}\frac{dy}{dz}$$

The curvature of the deflected shape due to shearing deformation produced by the axial forces P will then equal

$$\frac{d}{dz}\left(\frac{V}{GA}\right) = \frac{NP}{GA}\frac{d^2y}{dz^2} \qquad (v)$$

Equation (v) is verified by reference 4.

The broken line in Figure 20(a) represents the distortion of the elastic axis due to the shearing deformations of the cross sections caused by the lateral forces H and having the constant slope expressed by equation (u). The solid line represents the total distortion of the elastic axis due to the sum of the shearing and bending deformations of the cross sections.

The curvature of the distorted elastic axis will equal the sum of the bending and shearing curvatures and will equal

$$\frac{d^2y}{dz^2} = \frac{M - Py - Hz}{EI} + \frac{NP}{GA}\frac{d^2y}{dz^2} \qquad (w)$$

Integrating equation (w)

$$\left.\begin{aligned} \frac{dy}{dz} &= -aC_1 \sin az + aC_2 \cos az - \frac{H}{P} \\ y &= C_1 \cos az + C_2 \sin az + \frac{M}{P} - \frac{H}{P}z \end{aligned}\right\} \qquad (x)$$

where

$$a^2 = \frac{P}{EI\left(1 - \frac{NP}{GA}\right)} \tag{7-10}$$

and C_1 and C_2 are constants of integration which must be adjusted to satisfy the boundary conditions. Using the same reasoning that led to the derivation of equation (s), at the origin of the coordinate axis, the boundary conditions will be

$$(y)_{z=0} = 0$$

$$\left(\frac{dy}{dz}\right)_{z=0} = \frac{NH}{GA}$$

from which

$$C_1 = -\frac{M}{P}$$

$$C_2 = \frac{H}{aP}\left(1 + \frac{NP}{GA}\right)$$

and then equations (x) become

$$\left.\begin{aligned} \frac{dy}{dz} &= \frac{Ma}{P} \sin az + \frac{H}{P}\left(1 + \frac{NP}{GA}\right)\cos az - \frac{H}{P} \\ y &= -\frac{M}{P} \cos az + \frac{H}{aP}\left(1 + \frac{NP}{GA}\right)\sin az + \frac{M}{P} - \frac{H}{P} z \end{aligned}\right\} \tag{7-11}$$

Using the limiting condition

$$(y)_{z=L} = \Delta$$

and equation (7-11), the lateral deflection will equal

$$\Delta = \frac{M}{P}(1 - \cos aL) + \frac{HL}{P}\left[\frac{\sin aL}{aL}\left(1 + \frac{NP}{GA}\right) - 1\right] \quad (7\text{-}12)$$

From statics and symmetry

$$2M = P\Delta + HL \quad (7\text{-}13)$$

then

$$\Delta = \frac{2M}{P}\left[\frac{\frac{2 \sin aL}{aL}(1 + J) - (1 + \cos aL)}{\frac{2 \sin aL}{aL}(1 + J)}\right] \quad (7\text{-}14)$$

$$H = \frac{P\Delta}{L}\left[\frac{1 + \cos aL}{\frac{2 \sin aL}{aL}(1 + J) - (1 + \cos aL)}\right] \quad (7\text{-}15)$$

$$M = \frac{P\Delta}{2}\left[\frac{\frac{2 \sin aL}{aL}(1 + J)}{\frac{2 \sin aL}{aL}(1 + J) - (1 + \cos aL)}\right] \quad (7\text{-}16)$$

where

$$aL = \left[\frac{\frac{P}{P_E}}{1 - J}\right]^{1/2} \pi \quad (7\text{-}17)$$

$$J = \frac{NP}{GA} = \frac{NP_E}{GA}\left(\frac{P}{P_E}\right) \quad (7\text{-}18)$$

$$P_E = \frac{\pi^2 EI}{L^2} \quad (7\text{-}19)$$

The total axial deflection of the member subjected to the combined loading shown in Figure 20 will consist of compressive and curvature deformations. From basic mechanics of materials, the compressive deflection will equal

$$\delta_P = \frac{PL}{EA} \tag{7-20}$$

The curvature deflection is equal to approximately the difference between the length of the deformed elastic axis and the length of the chord L, which from reference 5, equals

$$\delta_C = \frac{1}{2}\int_0^L \left(\frac{dy}{dz}\right)^2 dz$$

and using equations (7-11), (7-13), (7-15), and (7-16)

$$\delta_C = \frac{\Delta^2}{L}\frac{1}{4}\left\{\left(\frac{2M}{P\Delta}\right)^2\left(\frac{aL}{2}\right)^2\left[1 - \frac{\sin aL}{aL}\cos aL\right] + \left(\frac{HL}{P\Delta}\right)^2\left[\left(1 + \frac{\sin aL}{aL}\cos aL\right)(1 + J)^2 - 4\frac{\sin aL}{aL}(1 + J) + 2\right] + \left(\frac{2M}{P\Delta}\right)\left(\frac{HL}{P\Delta}\right)\left[\sin^2 aL(1 + J) - 2(1 - \cos aL)\right]\right\} \tag{7-21}$$

The total axial deflection will equal the sum of the compressive and curvature deflections or

$$\delta = \delta_P + \delta_C \tag{7-22}$$

where δ_P and δ_C are expressed by equations (7-20) and (7-21), respectively.

Equations (7-15) through (7-22) determine the lateral force and axial deflection for a structural member, with solid circular cross section, subjected to an axial compressive force and a lateral deflection with the end cross sections remaining perpendicular to the original elastic axis. In order for these equations to be applicable to a helical compression spring, the rigidity factors (EA), (EI), and (GA) for the solid circular member need only be replaced by the corresponding rigidity factors $(EA)_s$, $(EI)_s$, and $(GA)_s$ for a helical spring, expressed by equations (7-7), (7-8), and (7-9), respectively.

The member of Figure 20(a), subjected to an axial force alone, will now be investigated for stability. Let Figure 21 represent a structural member with a solid circular cross section subjected to axial forces P, a bending moment M, and a lateral deflection Δ. This condition is discussed in reference 4 but will be carried out in some detail here as an aid in clarifying the analogy between the solid structural member and the helical spring. The curvature of the distorted elastic axis will equal the sum of the bending and shearing curvatures, and will equal

$$\frac{d^2y}{dz^2} = \frac{M - Py}{EI} + \frac{NP}{GA}\frac{d^2y}{dz^2} \qquad (y)$$

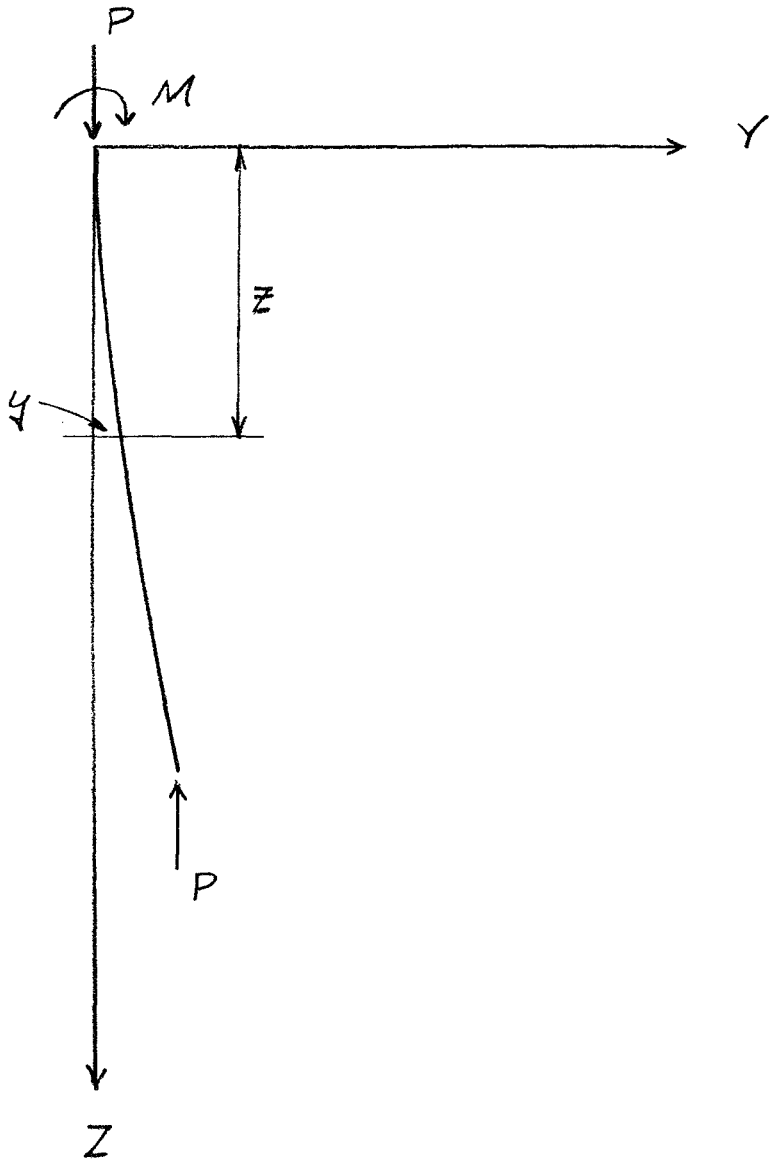

FIG. 21

Integrating equation (y)

$$\left.\begin{aligned} \frac{dy}{dz} &= -aC_1 \sin az + aC_2 \cos az \\ y &= C_1 \cos az + C_2 \sin az + \frac{M}{P} \end{aligned}\right\} \qquad (z)$$

where a is defined by equation (7-10), and C_1 and C_2 are constants of integration which must be adjusted to satisfy the boundary conditions. At the origin of the coordinate axis

$$(y)_{z=0} = 0$$

$$\left(\frac{dy}{dz}\right)_{z=0} = 0$$

from which

$$C_1 = -\frac{M}{P}$$

$$C_2 = 0$$

and then equations (z) become

$$\left.\begin{aligned} \frac{dy}{dz} &= \frac{Ma}{P} \sin az \\ y &= -\frac{M}{P} \cos az + \frac{M}{P} \end{aligned}\right\} \qquad (7\text{-}23)$$

Using the limiting condition

$$(y)_{z=L} = \Delta$$

and equations (7-23), the lateral deflection will equal

$$\Delta = \frac{M}{P}(1 - \cos aL) \qquad (7\text{-}24)$$

From statics

$$\frac{M}{P} = \Delta \qquad (7\text{-}25)$$

then

$$\cos aL = 0$$

and

$$aL = \frac{\pi}{2}, \frac{3\pi}{2}, \frac{5\pi}{2}, \text{ etc.}$$

The critical load is obtained by using the smallest value of aL; therefore, using $\frac{\pi}{2}$ and equation (7-10)

$$\left[\frac{P_{CR}L^2}{EI\left(1 - \frac{NP_{CR}}{GA}\right)}\right]^{1/2} = \frac{\pi}{2}$$

or

$$P_{CR} = \frac{\frac{P_E}{4}}{1 + \frac{NP_E}{4GA}} \qquad (7\text{-}26)$$

where P_E is expressed by equation (7-19).

For the case of a structural member with hinged ends, it is evident from symmetry that each half of the bar is in the same condition as the entire bar of Figure 21 and for the case of fixed ends, each quarter of the bar may be represented by Figure 21. Hence for hinged ends

$$P_{CR} = \frac{P_E}{1 + \frac{NP_E}{GA}} \qquad (7\text{-}27)$$

and for fixed ends

$$P_{CR} = \frac{4P_E}{1 + \frac{4NP_E}{GA}} \qquad (7\text{-}28)$$

Owing to the effect of shearing forces, the critical loads for hinged and fixed end bars are diminished by the ratios

$$\frac{1}{1 + \frac{NP_E}{GA}}$$

and

$$\frac{4}{1 + \frac{4NP_E}{GA}}$$

respectively. Generally, for the case of solid bars, these ratios differ very little from unity so that the shearing effect may be neglected. However, for the case of helical springs, the shearing effect should be considered and, in order for equations (7-27) and (7-28) to be applicable to helical compression springs, the rigidity factors EA, EI, and GA for the solid circular member need only be replaced by the corresponding rigidity factors $(EA)_s$, $(EI)_s$, and $(GA)_s$ for a helical spring expressed by equations (7-7), (7-8), and (7-9), respectively.

The structural member, represented by Figure 20(a), subjected to axial forces P and a lateral deflection Δ with the ends remaining nominally parallel to the original elastic axis Z is faced with the same instability problem as if only the axial forces were acting. For the straight bar subjected to axial forces, the critical load, expressed by equation (7-27) or (7-28),may be defined as the axial load which is sufficient to keep the bar in a slightly bent form. In other words, the critical load will hold the bar in a slightly different configuration from the original. For the initially distorted bar of Figure 20(a), the critical load may also be defined as that axial load which will hold the bar in a slightly different configuration.

Assume, before axial forces are applied, the bar represented by Figure 20 is subjected to a lateral deflection Δ with the bar ends remaining nominally parallel to its original axis Z. At each end of the bar, there will be the reactions H and M and the distorted elastic axis will appear as shown in Figure 22(a). The application of the axial forces P decreases the reactions H and M. As P increases, M approaches zero while H passes through zero becoming negative as indicated in Figures 22(b) and 22(c). The distorted elastic axis will maintain the same general configuration until M equals zero, at which point, the loading and shape become unstable

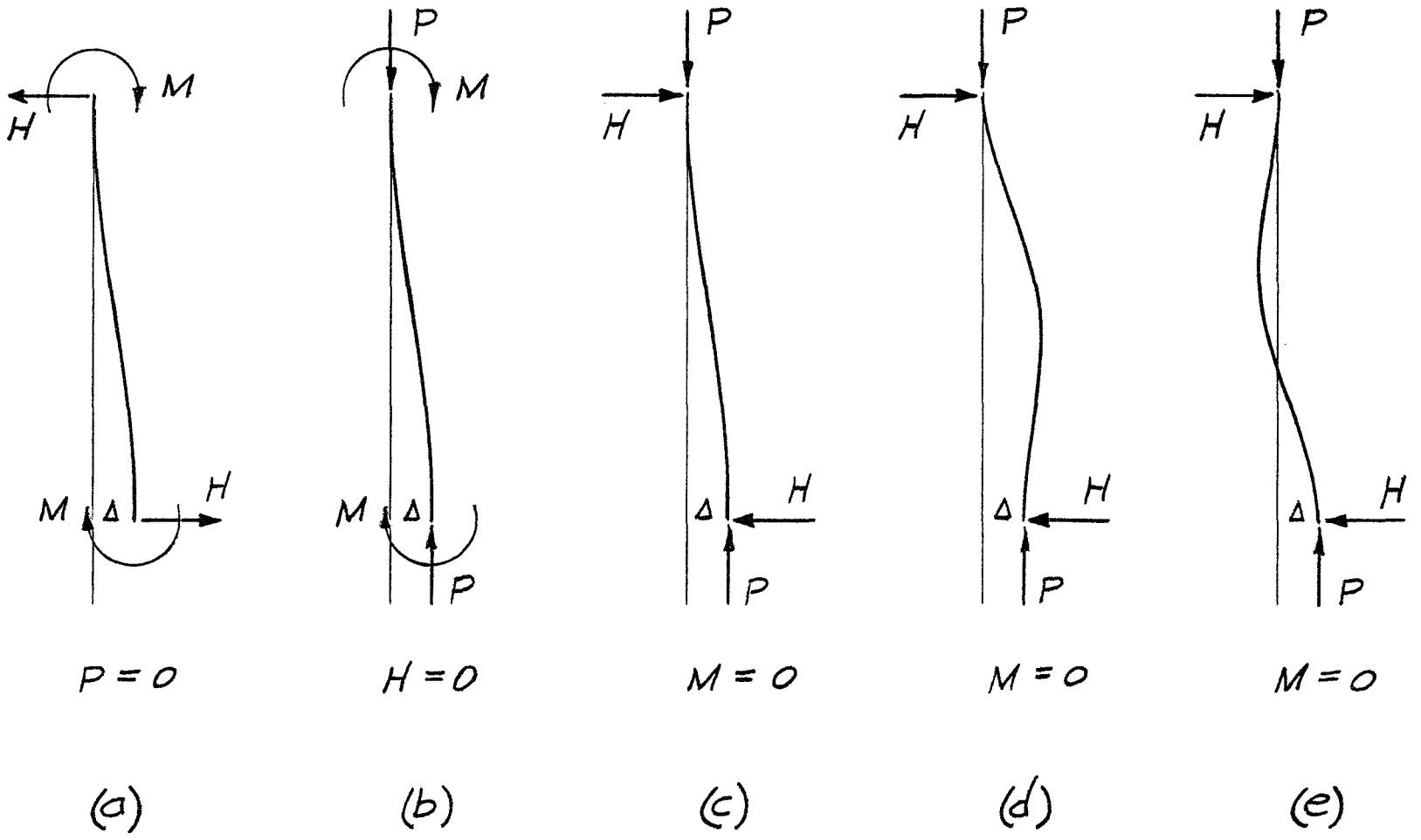

FIG. 22

and either of the two forms shown in Figures 22(d) and 22(e) may prevail. The critical axial load will then be that load for which M equals zero.

For convenience, rewrite equations (7-15), (7-16), and (7-21) as follows:

$$\frac{HL}{P_E\Delta} = \frac{P}{P_E}\left[\frac{1 + \cos aL}{\frac{2 \sin aL}{aL}(1 + J) - (1 + \cos aL)}\right] \qquad (7\text{-}29)$$

$$\frac{2M}{P_E\Delta} = \frac{P}{P_E}\left[\frac{\frac{2 \sin aL}{aL}(1 + J)}{\frac{2 \sin aL}{aL}(1 + J) - (1 + \cos aL)}\right] \qquad (7\text{-}30)$$

$$\frac{\delta_C}{L} = \left(\frac{\Delta}{L}\right)^2 Z \qquad (7\text{-}31)$$

where

$$Z = \frac{1}{4}\left\{\frac{\left(\frac{2M}{P_E\Delta}\right)^2}{\left(\frac{P}{P_E}\right)^2}\left(\frac{aL}{2}\right)^2\left[1 - \frac{\sin aL}{aL}\cos aL\right] + \right.$$

$$\frac{\left(\frac{HL}{P_E\Delta}\right)^2}{\left(\frac{P}{P_E}\right)^2}\left[\left(1 + \frac{\sin aL}{aL}\cos aL\right)(1+J)^2 - 4\frac{\sin aL}{aL}(1 + J) + 2\right] +$$

$$\left.\frac{\left(\frac{2M}{P_E\Delta}\right)\left(\frac{HL}{P_E\Delta}\right)}{\left(\frac{P}{P_E}\right)^2}\left[\sin^2 aL(1 + J) - 2(1 - \cos aL)\right]\right\} \qquad (7\text{-}32)$$

By combining equations (7-29) and (7-30), there results

$$\frac{P}{P_E} = \frac{2M}{P_E\Delta} - \frac{HL}{P_E\Delta} \tag{7-33}$$

As $\frac{P}{P_E}$ increases, the following conditions are obtained:

$$\left.\begin{aligned} &\frac{P}{P_E} = 0 \\ &aL = 0 \\ &\frac{HL}{P_E\Delta} = \frac{2M}{P_E\Delta} = \frac{\frac{12}{\pi^2}}{1 + \frac{12}{\pi^2}\left(\frac{NP_E}{GA}\right)} \\ &Z = \frac{1}{4}\left[\frac{\pi^4}{360}\left(\frac{2M}{P_E\Delta}\right)^2 + 2\right] \end{aligned}\right\} \tag{7-34}$$

$$\left.\begin{aligned} &\frac{HL}{P_E\Delta} = 0 \\ &aL = \pi \\ &\frac{P}{P_E} = \frac{2M}{P_E\Delta} = \frac{1}{1 + \frac{NP_E}{GA}} \\ &Z = \frac{1}{4}\left(\frac{\pi}{2}\right)^2 \end{aligned}\right\} \tag{7-35}$$

$$\left.\begin{aligned} \frac{2M}{P_E\Delta} &= 0 \\ aL &= 2\pi \\ \frac{P}{P_E} = \frac{HL}{P_E\Delta} &= \frac{4}{1 + 4\left(\frac{NP_E}{GA}\right)} \\ Z &= \frac{1}{4}\left[2 + (1 + J)^2\right] \end{aligned}\right\} \qquad (7\text{-}36)$$

It is seen that the third of equations (7-35) is apparently the same as equation (7-27) and the third of equations (7-36) is apparently the same as equation (7-28). However, the equations are not truly equivalent for the reason that the terms P_E and GA are functions of the length L which in turn is a function of both the axial force P and lateral deflection Δ. Therefore, equations (7-27) and (7-28) will be identical with equations (7-35) and (7-36), respectively, only for the particular case when Δ equals zero. For the condition of a solid structural member with circular cross section composed of carbon or alloy steel, the difference between the free length and the loaded length will generally be so slight that the use of the free or original length L_F for all values of L will sacrifice very little accuracy. However, for helical springs, the loaded length must be taken into consideration and will be done so in section 9, Design.

Equations (7-36) represent the unstable or critical condition for which the distorted elastic axis may change form and may be defined as the limiting condition of instability. Figure 23 is a graph of equation (7-29) which includes conditions (7-34) through (7-36). The broken line represents the limiting condition of instability or change in configuration.

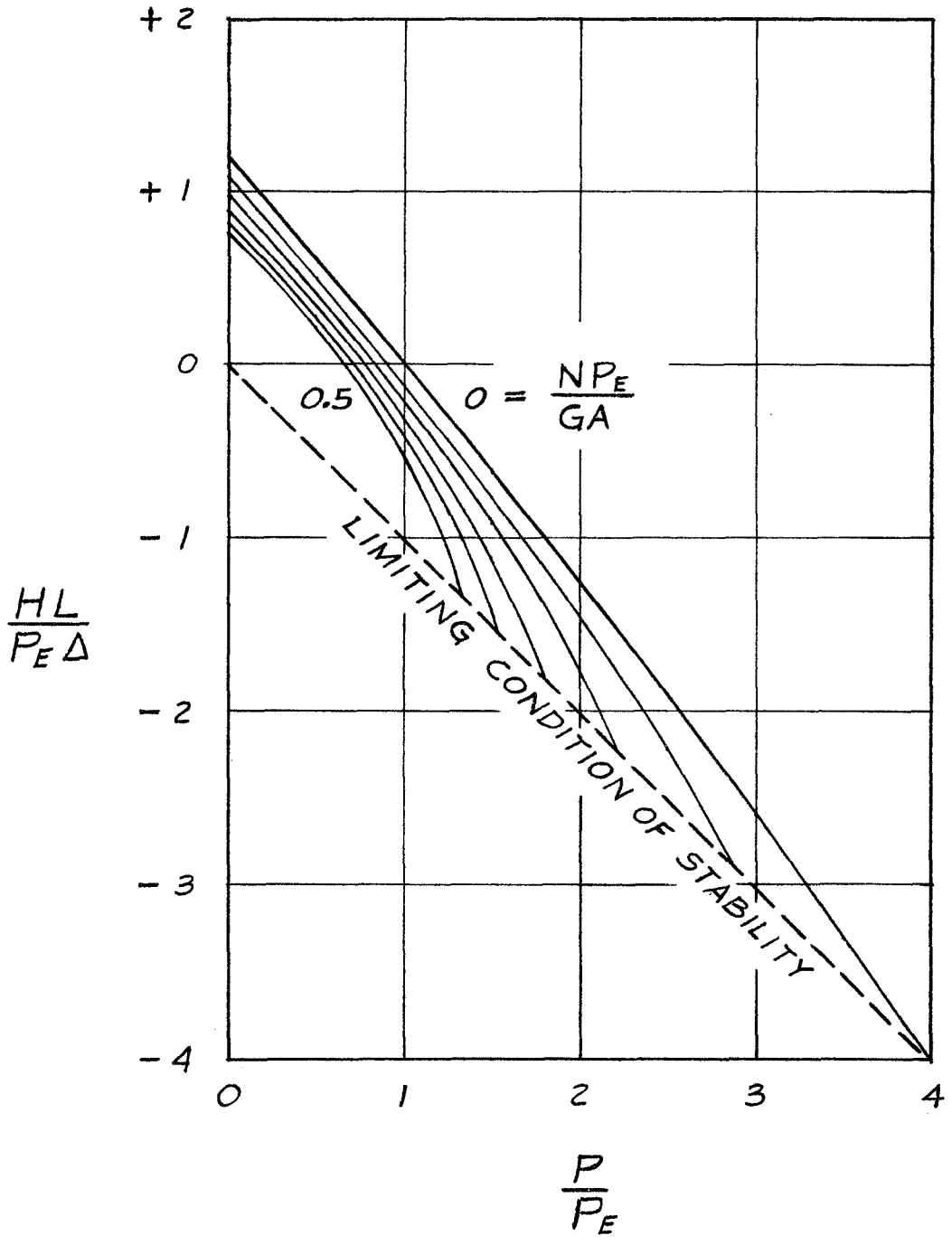
+2
+1
0
-1
-2
-3
-4
0
1
2
3
4
0.5
$0 = \frac{NP_E}{GA}$
LIMITING CONDITION OF STABILITY
$\frac{HL}{P_E \Delta}$
$\frac{P}{P_E}$

FIG. 23

8. UNIT STRESSES

The forces and moments acting upon the wire cross section ABCD due to the combined loading P, H, and M shown in Figure 4 will produce shearing and normal stresses on the face of the cross section. With the aid of equations (6-1), the stresses at the points A, B, C, and D can be determined and combined into principal stresses.

The principal stresses on the cross section, due to an axial force P only, will be maximum at point B as discussed in reference 6. Furthermore, the helical compression springs are designed primarily to support an axial force and while additional loading such as H and M increase the stresses they are generally not of primary importance. Therefore, the principal stresses will be determined for point B of the wire cross section and used for the design of springs subjected to an axial force and a lateral deflection with the spring ends remaining nominally parallel to the original coil axis. It is conceivable, of course, that a loading system could be chosen so that some point other than point B would have maximum principal stresses. That situation will not be considered here, however, as it will be shown later that the maximum lateral

deflection will be a function of the axial force P so that P will always remain the primary load.

At point B, Figure 4, there are four force and moment components (C, M_m, T, and V_m) that contribute to principal stresses. The compression force C produces uniform normal stress over the cross section which equals

$$\sigma_C = \frac{C}{A}$$

where

$$A = \frac{\pi d^2}{4} \quad \text{cross-sectional area}$$

Using equations (6-2), the uniform normal stress becomes

$$\sigma_C = \frac{4P}{\pi d^2} F_1 \sin \alpha \qquad (a)$$

The bending moment M_m produces maximum normal stress at point B which equals

$$\sigma_B = \frac{M_m}{I} \frac{d}{2} K_B$$

where

$$I = \frac{\pi d^4}{64} \quad \text{diameter moment of inertia}$$

and K_B is the curvature correction factor for bending stresses. Using equations (6-2), the bending normal stress becomes

$$\sigma_B = \frac{32PR}{\pi d^3} K_B F_2 \sin \alpha \qquad (b)$$

The torque T produces shearing stresses which are normal to and maximum on the perimeter of the cross section and which equal

$$\tau_T = \frac{T}{I_P} \frac{d}{2} K_S$$

where

$$I_P = \frac{\pi d^4}{32} \quad \text{polar moment of inertia}$$

and K_S is the curvature correction factor for shearing stresses. Using equations (6-2), the torque shearing stress becomes

$$\tau_T = \frac{16PR}{\pi d^3} K_S F_4 \cos \alpha \qquad (c)$$

The shearing force V_m produces shearing stresses which are maximum along the diameter BA. Assuming the distribution is uniform, the stress equals

$$\tau_S = \frac{V_m}{A} K_S$$

where

$$A = \frac{\pi d^2}{4} \quad \text{cross-sectional area}$$

and K_S is the curvature correction factor for shearing stresses. Using equations (6-2), the shearing stress becomes

$$\tau_S = \frac{4P}{\pi d^2} K_S F_5 \cos \alpha \qquad (d)$$

The total normal stress acting at point B equals the sum of the compressive and bending stresses.

$$\sigma = \sigma_C + \sigma_B$$

or

$$\sigma = \frac{32PR}{\pi d^3} \sin \alpha \left(K_B F_2 + \frac{d}{8R} F_1 \right) \qquad (e)$$

The total shearing stress acting at point B equals the sum of the torque and direct shearing stresses.

$$\tau = \tau_T + \tau_S$$

or

$$\tau = \frac{16PR}{\pi d^3} K_S \cos \alpha \left(F_4 + \frac{d}{4R} F_5 \right) \qquad (f)$$

With reference to equations (6-3), it is apparent that

$$F_2 = F_1 + F_7$$

where

$$F_7 = \left(\frac{Hz}{PR} + \frac{Y}{R} - \frac{M}{PR} \right) \sin \varphi \qquad (g)$$

Then equation (e) may be written

$$\sigma = \frac{32PR}{\pi d^3} \sin \alpha \left(K_B F_1 + K_B F_7 + \frac{d}{4D} F_1 \right)$$

or

$$\sigma = \frac{32PR}{\pi d^3} \sin \alpha \left[\left(K_B + \frac{d}{4D} \right) F_1 + K_B F_7 \right] \qquad (h)$$

The term $\frac{d}{4D}$ will be small compared to K_B (for practical reasons never greater than $\frac{1}{16}$). Therefore, it will be conservative, with little appreciable error, to write equation (h)

$$\sigma = \frac{32PR}{\pi d^3} \left(K_B + \frac{d}{4D} \right) \sin \alpha \left(F_1 + F_7 \right) \qquad (i)$$

The curvature correction factor for bending, K_B, is given in reference 7 as

$$K_B = 1 + 0.4125 \left[\frac{1}{\left(\frac{D}{d} \right) - 1} + \frac{1}{\frac{D}{d}} \right] \qquad (j)$$

Figure 17 contains a plot of $\left(K_B + \frac{d}{4D} \right)$ against $\frac{D}{d}$.

With reference to equations (6-3), it is apparent that

$$F_4 = F_5 + F_7$$

Then equation (f) may be written

$$\tau = \frac{16PR}{\pi d^3} K_S \cos \alpha \left(F_5 + F_7 + \frac{d}{2D} F_5\right)$$

or

$$\tau = \frac{16PR}{\pi d^3} K_S \cos \alpha \left[\left(1 + \frac{d}{2D}\right)F_5 + F_7\right] \qquad (k)$$

Since the term $\frac{d}{2D}$ will be small compared to 1 (never greater than $\frac{1}{8}$), it will be conservative with little appreciable error to write equation (k)

$$\tau = \frac{16PR}{\pi d^3} K_S \left(1 + \frac{d}{2D}\right) \cos \alpha \left(F_5 + F_7\right) \qquad (l)$$

From reference 6, it is seen that the term

$$K_S \left(1 + \frac{d}{2D}\right) = K_W \qquad \text{Wahl factor}$$

where

$$K_W = \frac{4\left(\frac{D}{d}\right) - 1}{4\left(\frac{D}{d}\right) - 4} + \frac{0.615}{\frac{D}{d}} \qquad (8\text{-}1)$$

The Wahl factor K_W is the correction factor for curvature and fatigue developed by A. M. Wahl for helical springs subjected to an axial force. Figure 17 contains a plot of K_W against $\frac{D}{d}$.

A comparison of the two quantities $\left(K_B + \frac{d}{4D}\right)$ and K_W shown in Figure 17 shows that it will be a safe assumption to write equation (i)

$$\sigma = \frac{32PR}{\pi d^3} K_W F_2 \sin \alpha \qquad (8\text{-}2)$$

Also, equation (l) can be written

$$\tau = \frac{16PR}{\pi d^3} K_W F_4 \cos \alpha \qquad (8\text{-}3)$$

Equations (8-2) and (8-3) give the resultant normal and shearing stresses, respectively, at point B of the wire cross section. Each equation for resultant stress contains the same correction factor for curvature and fatigue K_W defined by equation (8-1).

The resultant normal and shearing stresses are related to principal stresses by the following relationships.

$$\sigma_{\substack{max \\ min}} = \frac{\sigma}{2} \pm \left[\left(\frac{\sigma}{2}\right)^2 + \tau^2\right]^{1/2} \qquad (m)$$

and

$$\tau_{max} = \frac{\sigma_{max} - \sigma_{min}}{2} \qquad (n)$$

Substituting equations (8-2) and (8-3) in equations (m) and (n), there results

$$\sigma_{\substack{max \\ min}} = \frac{16PR}{\pi d^3} K_W \left[F_2 \sin \alpha \pm \left(F_2^2 \sin^2 \alpha + F_4^2 \cos^2 \alpha \right)^{1/2} \right] \qquad (o)$$

$$\tau_{max} = \frac{16PR}{\pi d^3} K_W \left(F_2^2 \sin^2 \alpha + F_4^2 \cos^2 \alpha \right)^{1/2} \qquad (p)$$

With the use of equations (6-3), expanding and collecting terms, equations (o) and (p) become

$$\sigma_{max} = \frac{8PD}{\pi d^3} K_W \left[F_2 \sin \alpha + F \right] \qquad (8-4)$$

$$\tau_{max} = \frac{8PD}{\pi d^3} K_W F \qquad (8-5)$$

where

$$F = \left\{ \left[1 + \left(\frac{Hz}{PR} + \frac{y}{R} - \frac{M}{PR} \right) \sin \varphi \right]^2 + \left(\frac{H}{P} \right)^2 \cos^2 \varphi \right\}^{1/2} \qquad (8-6)$$

For the symmetrical loading condition expressed by equation (7-13) where

$$M = \frac{P\Delta}{2} + \frac{HL}{2}$$

equation (8-6) becomes

$$F = \left\{ \left[1 + \left(\frac{2Hz}{PD} + \frac{2y}{D} - \frac{\Delta}{D} - \frac{HL}{PD} \right) \sin \varphi \right]^2 + \left(\frac{H}{P} \right)^2 \cos^2 \varphi \right\}^{1/2} \qquad (q)$$

An inspection of equation (q) shows that it is maximum when

$$y = z = 0 \quad \text{and} \quad \varphi = -\frac{\pi}{2}$$

or

$$y = \Delta, \quad z = L, \quad \text{and} \quad \varphi = \frac{\pi}{2}$$

and will equal

$$F = 1 + \frac{\Delta}{D} + \frac{HL}{PD} \tag{8-7}$$

Also, when F is maximum, F_2 is maximum and equals F. Therefore, equations (8-4) and (8-5) become

$$\sigma_{max} = \frac{8PD}{\pi d^3} K_W(1 + \sin \alpha)\left(1 + \frac{\Delta}{D} + \frac{HL}{PD}\right) \tag{8-8}$$

$$\tau_{max} = \frac{8PD}{\pi d^3} K_W\left(1 + \frac{\Delta}{D} + \frac{HL}{PD}\right) \tag{8-9}$$

which determine the principal stresses at point B of the spring wire cross section, Figure 4. It is seen that equations (8-8) and (8-9) are equivalent to the principal stresses at point B due to an axial force P, acting alone, when multiplied by an amplification factor F defined by equation (8-7). The subscript max, associated with σ and τ, refer to the maximum principal stresses at point B near each end of the spring helix. Henceforth, when stresses in the spring are considered, the maximum stresses defined by equations (8-8) and (8-9) shall govern. Therefore,

the subscript max may be dropped and the stress equations written

$$\sigma = \frac{8PD}{\pi d^3} K_W(1 + \sin \alpha)F \qquad (8\text{-}10)$$

$$\tau = \frac{8PD}{\pi d^3} K_W F \qquad (8\text{-}11)$$

where F is defined by equation (8-7).

9. DESIGN

The previous sections have led to the development of deflection and stress equations for helical springs loaded in a specific manner. The maximum stresses result from the stresses due to axial loads combined with the stresses caused by lateral deflection with the spring ends remaining nominally parallel to the original coil axis. Although this is a special condition, the deflection and stress equations, in their present form, are too general for convenient design usage. In order to provide convenient design formulas and graphs, certain basic assumptions are necessary.

The axial load will be assumed to be the most important component of the combined loading so that the helical spring will be designed primarily to support the axial loading. The total stress, resulting from the secondary stress, due to the lateral deflection, combined with the primary stress, must be less than a predetermined allowable. Furthermore, in order to satisfy stability considerations, the lateral deflection will be governed by the axial load. Before considering the effect of the secondary loading, formulas and graphs for the design and analysis of the primary loading will be developed. Many handbooks and trade publications give formulas, tables, and graphs for the analysis and design of helical springs

subjected to axial load. However, they are not conveniently arranged for combining with the secondary loading considered in this paper.

From equations (7-7) and (7-20)

$$\delta_P = \frac{8nP}{Gd}\left(\frac{D}{d}\right)^3 F_P \tag{9-1}$$

or

$$P = \frac{G\delta_P d}{8n\left(\frac{D}{d}\right)^3 F_P} \tag{9-2}$$

and from equations (8-7) and (8-11), for the condition of an axial force only,

$$\tau_P = \frac{8PD}{\pi d^3} K_W \tag{9-3}$$

Combining equations (9-2) and (9-3)

$$\tau_P = \frac{G\delta_P K_W}{n\pi d\left(\frac{D}{d}\right)^2 F_P} \tag{9-4}$$

For the condition of solid length

$$\tau_s = \frac{G\delta_s K_W}{n\pi d\left(\frac{D}{d}\right)^2 F_{Ps}} \tag{9-5}$$

where, from equation (1-15)

$$\delta_s = n(p_F - d) \tag{a}$$

and from equation (7-2)

$$F_{Ps} = \cos \alpha_s + \frac{2G}{E} \sin \alpha_s \tan \alpha_s \qquad (b)$$

but since α_s is small, and from equation (1-12)

$$F_{Ps} = 1 \qquad (c)$$

Using equations (a) and (c), equation (9-5) becomes

$$\tau_s = \frac{GK_W}{\pi\left(\frac{D}{d}\right)^2}\left(\frac{p_F}{d} - 1\right) \qquad (9\text{-}6)$$

which is plotted as a nomograph for Figure 24.

The usefulness of a helical spring as an elastic medium depends upon its axial deflection range which is the difference between the free and solid lengths. Generally, the spring will be designed to support a loading system with an axial deflection somewhat less than the solid deflection, for when the spring is compressed solid, its usefulness as an elastic medium is ended. However, it is conservative, and good design practice, to design the spring so that the maximum allowable stress occurs at solid compression and not before. Figure 24 will enable the designer to determine readily the relationship between the ratios $\frac{D}{d}$ and $\frac{p_F}{d}$ for a given wire material, represented by G, and an allowable shearing stress at solid compression, represented by τ_s.

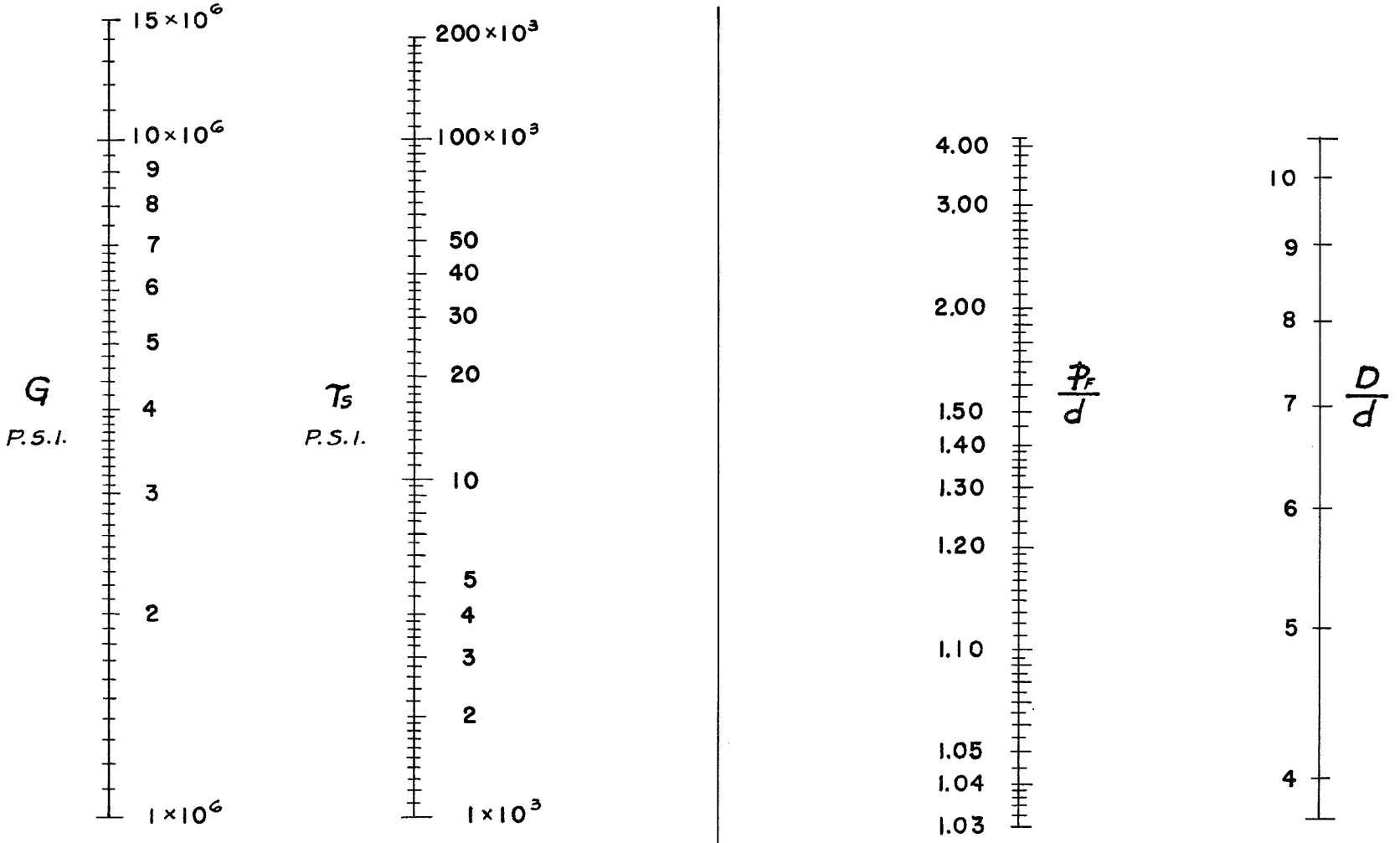
G
P.S.I.
15×10^6
10×10^6
9
8
7
6
5
4
3
2
1×10^6
τs
P.S.I.
200×10^3
100×10^3
50
40
30
20
10
5
4
3
2
1×10^3
Pf/d
4.00
3.00
2.00
1.50
1.40
1.30
1.20
1.10
1.05
1.04
1.03
D/d
10
9
8
7
6
5
4

FIG. 24

It will be convenient at this point to discuss basic properties for the more common applications of helical springs used as elastic structural medium. The spring wire material will be assumed to be carbon or alloy steel with a Poisson's ratio

$$\nu = 0.3 \tag{d}$$

From reference 8

$$\frac{G}{E} = \frac{1}{2(1 + \nu)} \tag{e}$$

and using (d)

$$\frac{G}{E} = 0.385 \tag{f}$$

The design stress will be assumed to be the shearing principal stress since the elastic limit in shear, for spring steel, is lower than that for tension and compression. The maximum allowable shearing unit stress will be assumed to occur when the spring is compressed solid under the action of an axial force alone.

Reference 9 tabulates the shearing modulus of elasticity G and the shearing elastic limit with respect to various spring wire materials. For carbon or alloy steel

$$10{,}000{,}000 \text{ psi} \leq G \leq 11{,}500{,}000 \text{ psi} \tag{g}$$

Furthermore, reference 9 provides, graphically, values for the maximum allowable shearing stress at solid compression

with respect to spring wire material and spring wire diameter. For carbon or alloy steels, helical springs with wire diameters in excess of 0.5 inch are generally hot-wound from hot-rolled bars. The torsional elastic limit for hot-rolled bars is less than that for cold-rolled wire of the same material and may be within the relatively low range of 75,000 to 110,000 psi. Consequently, the allowable shearing stress at solid compression will be less for hot-rolled bars than for cold-rolled wire of the same material. Figure 25 gives the relationship between the allowable shearing stress at solid compression and wire diameter for several different spring steels. A value of

$$\tau_s = 80{,}000 \text{ psi} \qquad (h)$$

is conservative for small wire diameters but reasonable for large wire diameters.

Figure 26 is a plot of equation (9-6) for conditions (g) and (h) and gives the relationship between the ratios $\frac{D}{d}$ and $\frac{p_F}{d}$ which maintains a shearing stress at solid compression equal to 80,000 psi. It is seen that the range or bandwidth governed by condition (g) is relatively small so that a mean value of

$$G = 10{,}750{,}000 \text{ psi} \qquad (i)$$

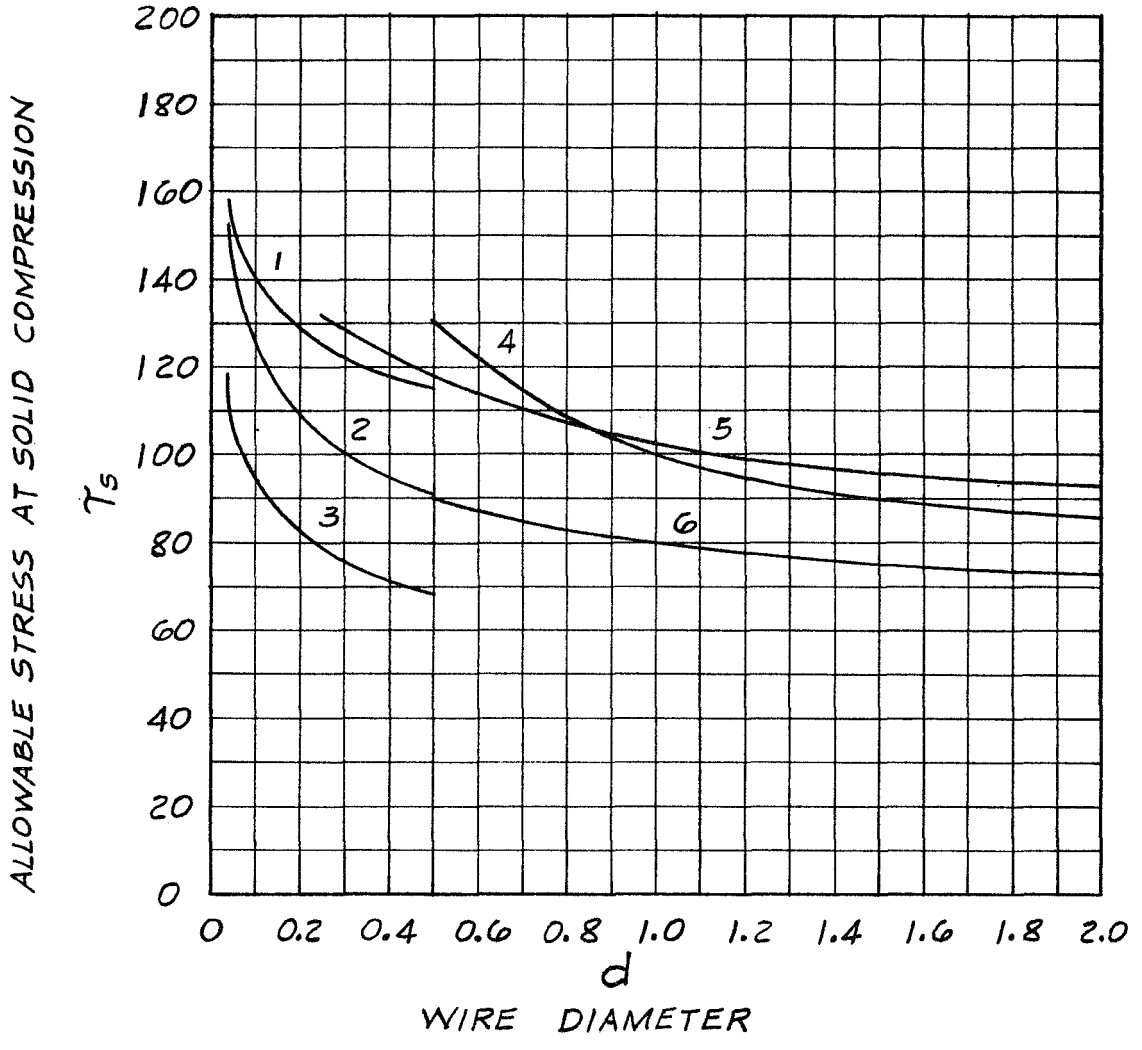

1 PRETEMPERED ALLOY STEEL WIRE
2 PRETEMPERED CARBON STEEL WIRE
3 HARD DRAWN CARBON STEEL WIRE
4 ALLOY STEEL BAR SAE 6150 OR SAE 9260
5 ALLOY STEEL WIRE OR BAR A151 8655
6 CARBON STEEL BAR SAE 1095

FIG. 25

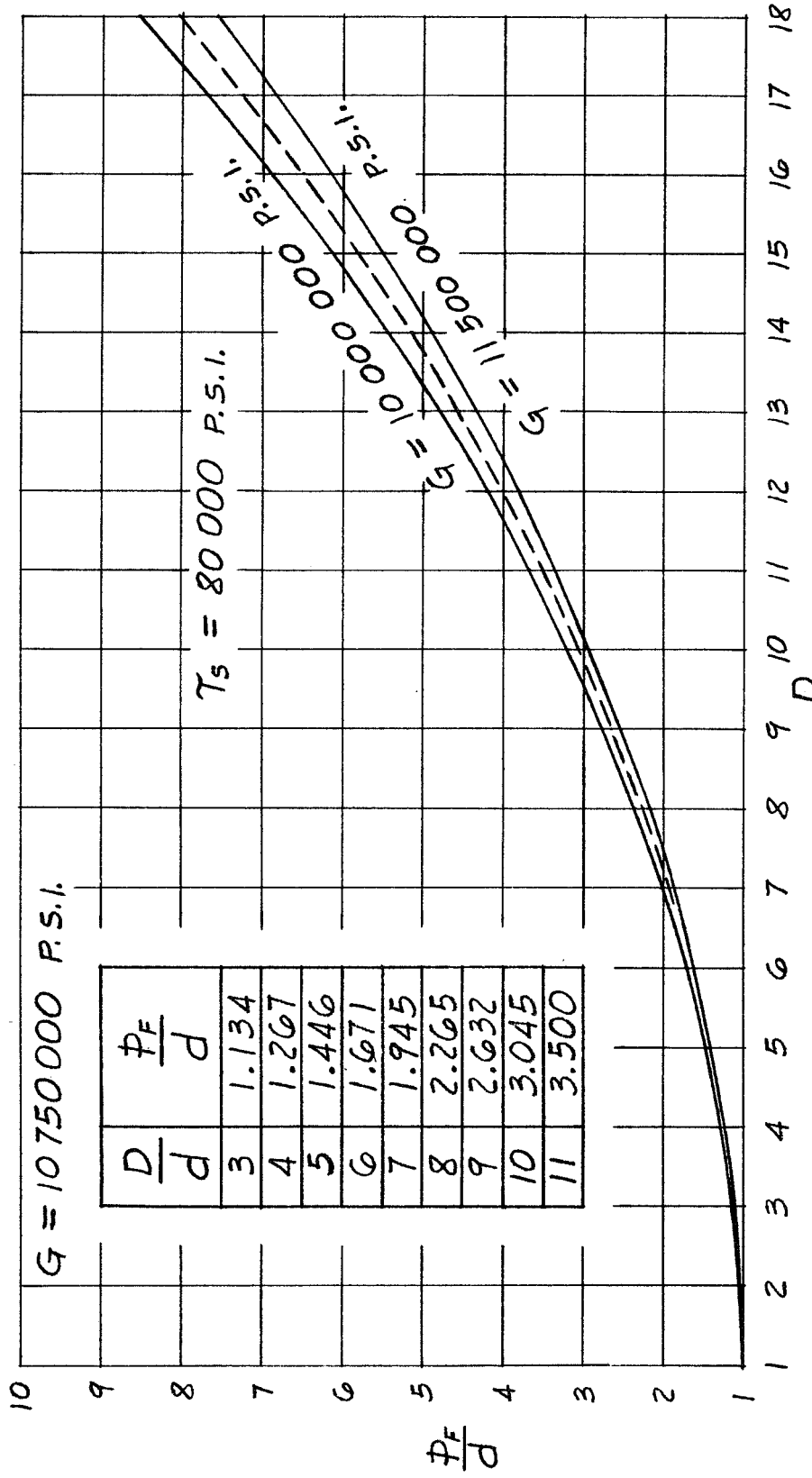
$\frac{F_F}{d}$
$\frac{D}{d}$
T_s = 80 000 P.S.I.
G = 10 750 000 P.S.I.
G = 10 000 000 P.S.I.
G = 11 500 000 P.S.I.
D/d | Ff/d
3 | 1.134
4 | 1.267
5 | 1.446
6 | 1.671
7 | 1.945
8 | 2.265
9 | 2.632
10 | 3.045
11 | 3.500

FIG. 26

represented by the broken line will reasonably approximate all practical applications. Furthermore, for the purpose of this paper, the limits of the ratio $\frac{D}{d}$ shall be taken as

$$4 \leq \frac{D}{d} \leq 10 \qquad (j)$$

which include all practical application of heavy duty springs.

Included with Figure 26 is a table listing the corresponding values of the ratios $\frac{D}{d}$ and $\frac{p_F}{d}$ corresponding to conditions (h) and (i). The graph and table of Figure 26 are included in this paper as a convenience to the designer for there will be many applications where a shearing stress at solid compression of 80,000 psi is convenient, especially for large diameter wire. However, the theory is in no way restricted to its use and applications for higher stresses may be easily determined. It should be pointed out that equation (9-6) and the graph and table of Figure 26 include the stress concentration and fatigue factor K_W.

With the aid of Figure 26, a good indication of the magnitude of the pitch angle α and the factors F_P and F_M used in equations (7-7), (7-8), and (7-9) may be obtained. For any given compression spring, the pitch angle α will be greatest at free length and smallest at solid length. From equation (1-6)

$$\tan \alpha_F = \frac{\frac{p_F}{d}}{\frac{D}{d}} \frac{1}{\pi} \qquad (k)$$

Using the values from Figure 26, for the range defined by condition (j), it is seen that $\tan \alpha_F$ will be small. Therefore, using condition (f) and equations (7-2) and (7-6), for all practical purposes,

$$\left.\begin{aligned} \cos \alpha &= 1 \\ F_P &= 1 \\ F_M &= 1.77 \end{aligned}\right\} \qquad (9\text{-}7)$$

since for any applied compressive force, α will be smaller than α_F. For the case of a tension spring, α will be smallest at the free length condition and largest under the applied loading so that the pitch angle may not be able to be considered small. Consequently, equations (9-7) may not be valid for a tension spring.

With the aid of conditions (9-7) and equation (a), equation (9-2) may be written

$$P = \frac{\left(\frac{\delta_P}{\delta_s}\right)\left(\frac{p_F}{d} - 1\right)}{8\left(\frac{D}{d}\right)^3} Gd^2 \qquad (9\text{-}8)$$

which is plotted as two nomographs, Figure 27 and Figure 28. Since, from conditions (9-7), F_P equals unity, the axial force per unit deflection will be constant, dependent upon only the physical properties of the spring. This value is termed the "spring constant" and from equation (9-2) will equal

$$k = \frac{P}{\delta_P} = \frac{Gd}{8n\left(\frac{D}{d}\right)^3} \qquad (9\text{-}9)$$

which is plotted as two nomographs, Figure 29 and Figure 30.

The usual procedure in designing helical springs is to determine by trial the physical properties which will satisfy given loading and deflection requirements and assumed material characteristics. Generally, the axial load P, the spring constant k, and the lateral deflection Δ will be the given loading and deflection requirements. The assumed material characteristics will be the wire material, the torsional modulus of elasticity G, and the allowable shearing stress at solid compression τ_s. As mentioned previously, the effect of the lateral deflection will be assumed to be secondary so that the initial design of the spring will be for axial load only.

The three equations, (9-6), (9-8), and (9-9) rewritten as equation (9-10)

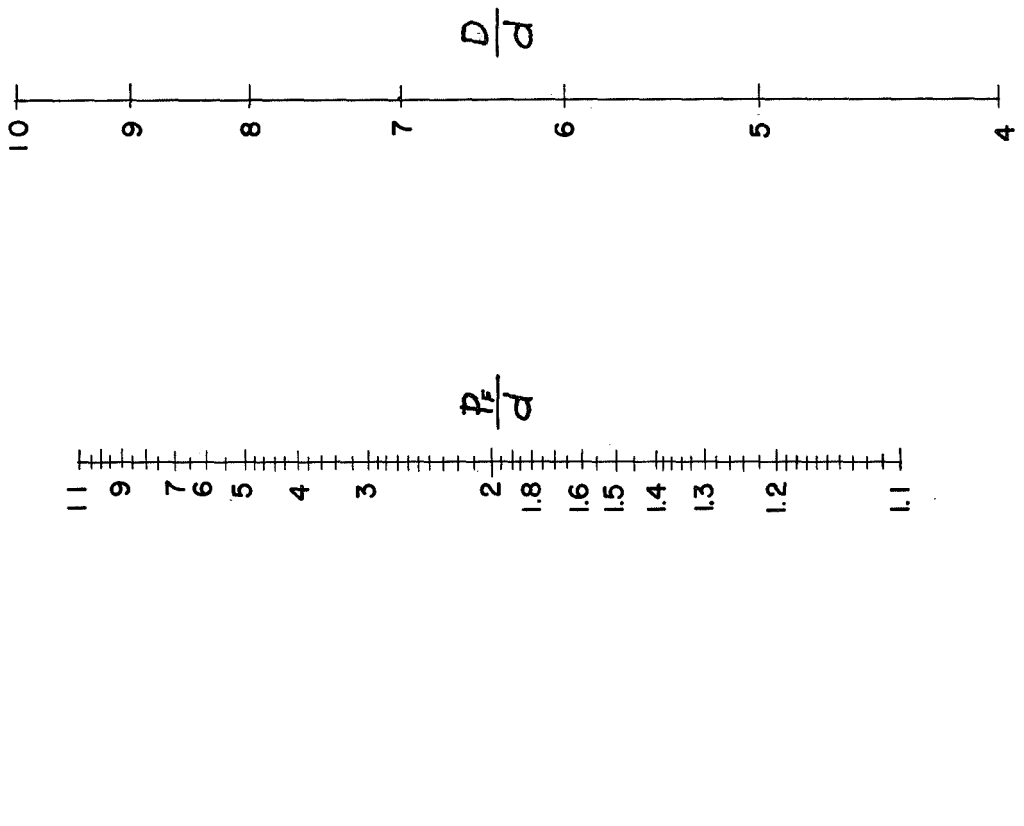
D/d
10 9 8 7 6 5 4
Pf/d
11 9 7 6 5 4 3 2 1.8 1.6 1.5 1.4 1.3 1.2 1.1
P/Gd²
1.0 ×10⁻³ .8 .6 .5 .4 .3 .2 .1 ×10⁻³ .08 .06 .05 .04 .03 .02 .01 ×10⁻³
δp/δs
1.0 .9 .8 .7 .6 .5 .4 .3 .2 .1

FIG. 27

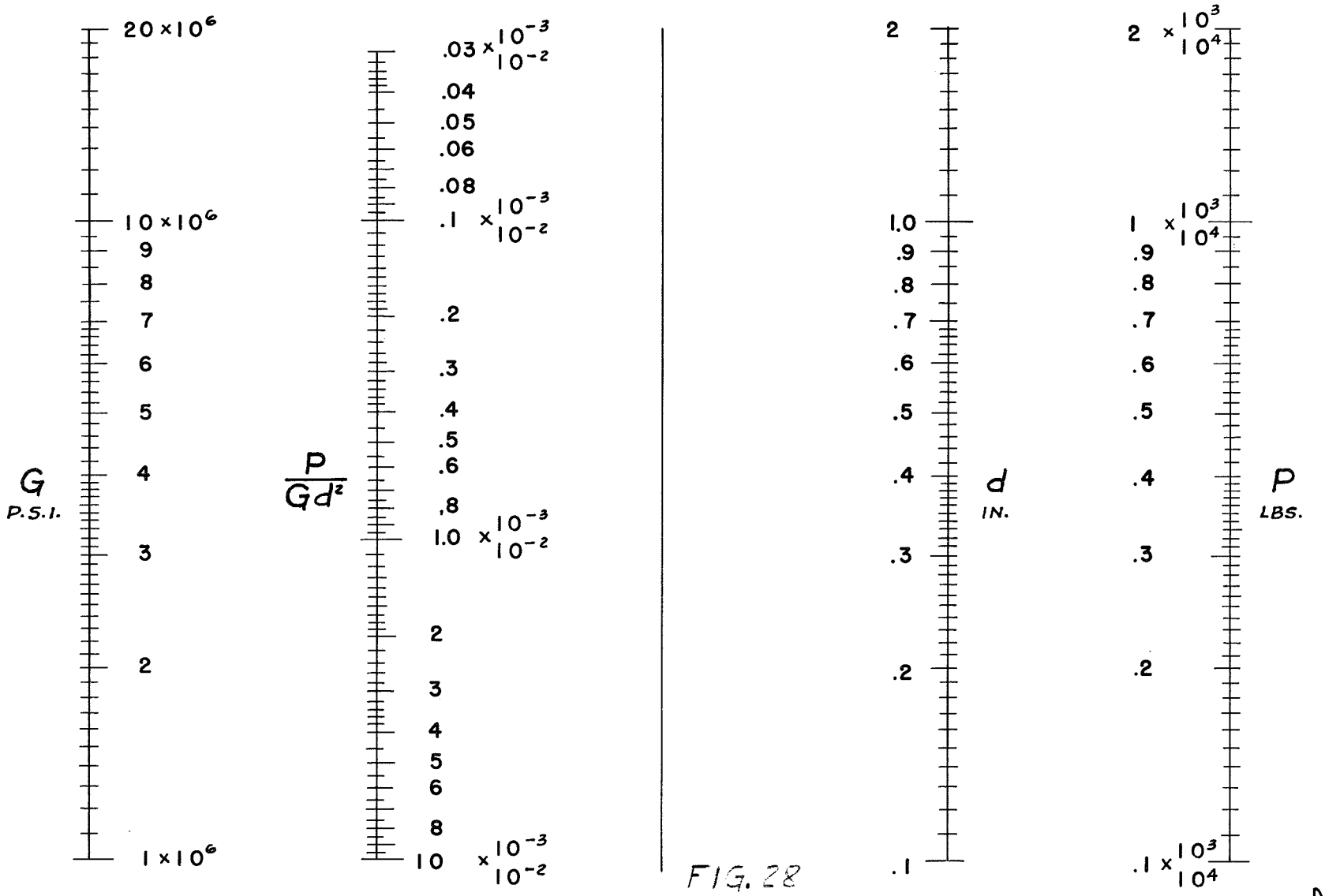
G
P.S.I.
20×10^6
10×10^6
9
8
7
6
5
4
3
2
1×10^6
P/Gd²
.03 ×10^-3 / 10^-2
.04
.05
.06
.08
.1 ×10^-3 / 10^-2
.2
.3
.4
.5
.6
.8
1.0 ×10^-3 / 10^-2
2
3
4
5
6
8
10 ×10^-3 / 10^-2
d
IN.
2
1.0
.9
.8
.7
.6
.5
.4
.3
.2
.1
P
LBS.
2 ×10^3 / 10^4
1 ×10^3 / 10^4
.9
.8
.7
.6
.5
.4
.3
.2
.1 ×10^3 / 10^4

FIG. 28

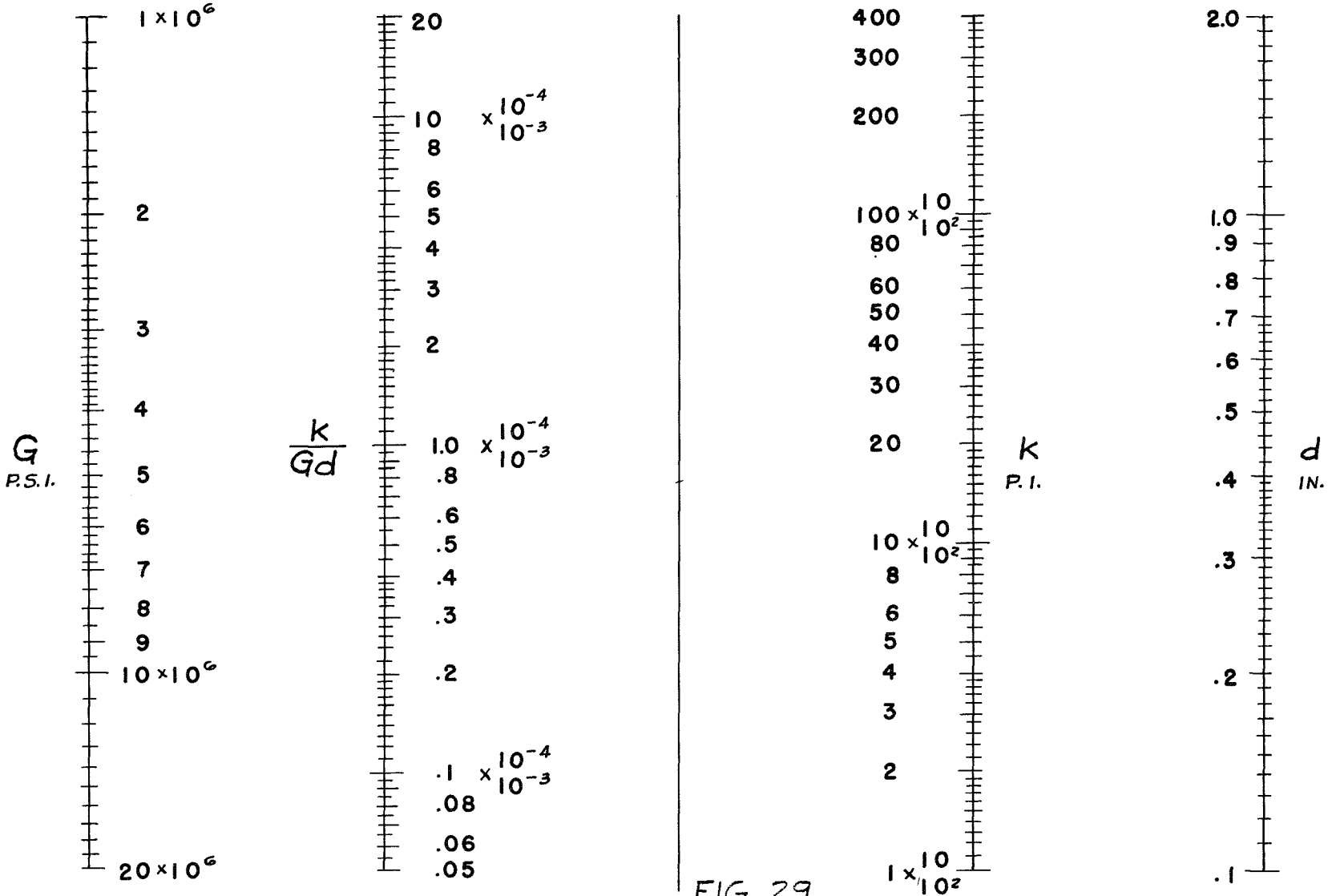
G
P.S.I.
1×10^6
2
3
4
5
6
7
8
9
10×10^6
20×10^6
k/Gd
20
10 ×10^-4 / 10^-3
8
6
5
4
3
2
1.0 ×10^-4 / 10^-3
.8
.6
.5
.4
.3
.2
.1 ×10^-4 / 10^-3
.08
.06
.05
400
300
200
100 ×10 / 10^2
80
60
50
40
30
20
10 ×10 / 10^2
8
6
5
4
3
2
1 ×10 / 10^2
k
P. I.
2.0
1.0
.9
.8
.7
.6
.5
.4
.3
.2
.1
d
IN.

FIG. 29

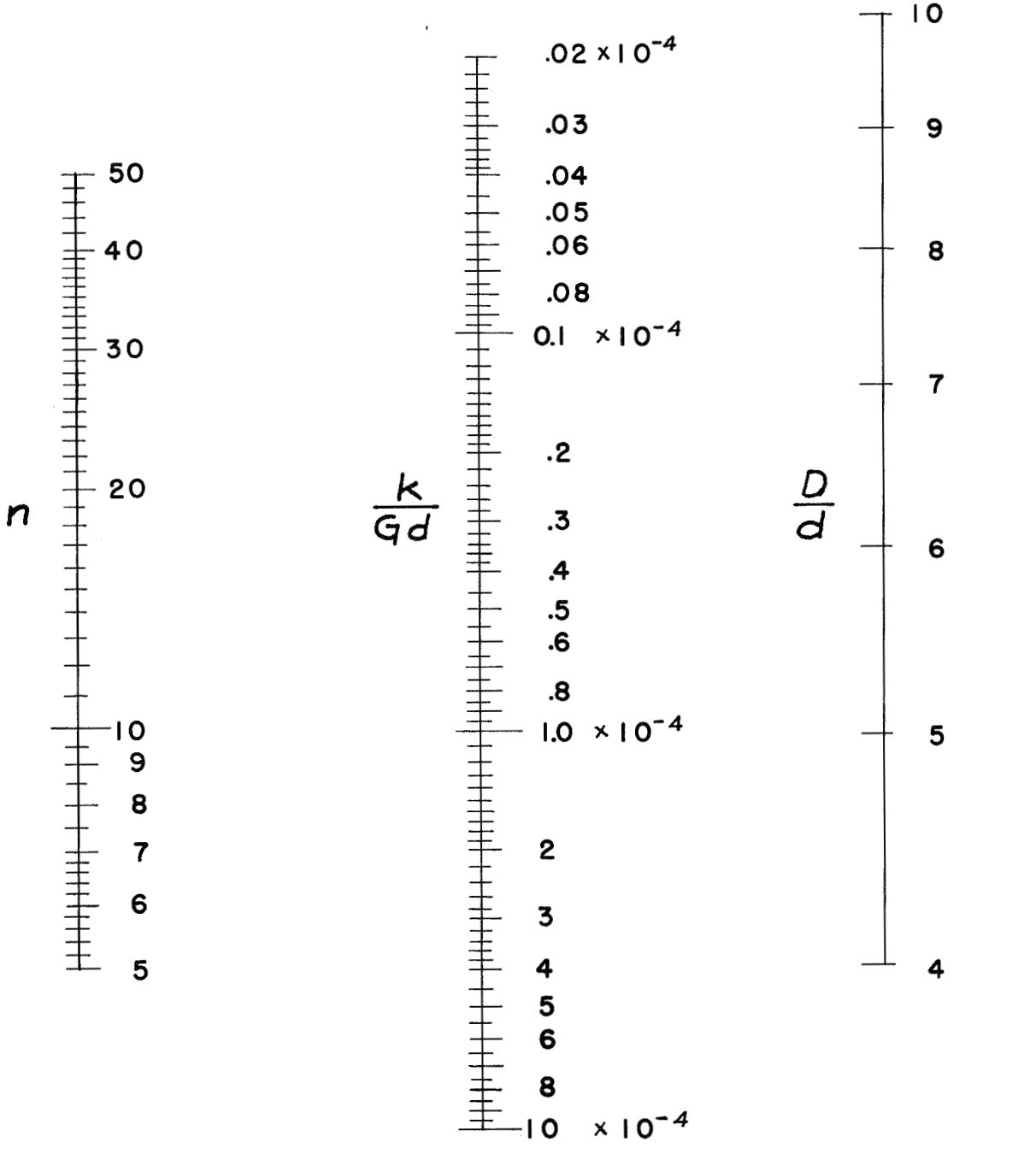
n
50
40
30
20
10
9
8
7
6
5
k/Gd
.02 ×10⁻⁴
.03
.04
.05
.06
.08
0.1 ×10⁻⁴
.2
.3
.4
.5
.6
.8
1.0 ×10⁻⁴
2
3
4
5
6
8
10 ×10⁻⁴
D/d
10
9
8
7
6
5
4

FIG. 30

$$\left.\begin{aligned} \tau_s &= \frac{GK_W}{\pi\left(\frac{D}{d}\right)^2}\left(\frac{p_F}{d} - 1\right) \\ P &= \frac{\left(\frac{\delta_P}{\delta_s}\right)Gd^2}{8\left(\frac{D}{d}\right)^3}\left(\frac{p_F}{d} - 1\right) \\ k &= \frac{Gd}{8n\left(\frac{D}{d}\right)^3} \end{aligned}\right\} \qquad (9\text{-}10)$$

are necessary and sufficient for designing or analyzing helical compression springs subjected to axial forces only. The stability considerations are not included. The nomographs, Figures 24, 27, 28, 29, and 30 will aid the designer in obtaining solutions for equations (9-10). The only consideration that need be given to the effect of the lateral deflection Δ, in the preliminary design for axial force only, is to assume a ratio $\frac{\delta_P}{\delta_s}$ that is relatively low so that there will be sufficient axial deflection remaining to prevent clashing of coils. A value of $\frac{\delta_P}{\delta_s}$ in the neighborhood of 0.5 is generally a good trial value especially for springs supporting heavy vibratory loading.

The problem of lateral buckling of compressed close-coiled helical springs is discussed in reference 3. The more general case for open-coiled springs will be developed

here. From equations (7-27) and (7-28), the critical load for a solid strut will equal

$$P_{CR} = \frac{CP_E}{1 + C\,\frac{NP_E}{GA}} \tag{9-11}$$

where

$$\left.\begin{aligned} C &= 1 \quad \text{hinged ends} \\ C &= 4 \quad \text{fixed ends} \end{aligned}\right\} \tag{1}$$

For a helical spring, using equation (7-19)

$$P_{CR} = \frac{\frac{C\pi^2(EI)_s}{L^2}}{1 + C\,\frac{N\pi^2(EI)_s}{L^2(GA)_s}} \tag{9-12}$$

also, the axial deflection due to the critical load will equal

$$\delta_{CR} = \frac{P_{CR}L}{(EA)_s} = L_F - L \tag{9-13}$$

or

$$P_{CR} = \frac{L_F - L}{L}(EA)_s \tag{9-14}$$

Combining equations (9-12) and (9-14), and using the equivalent rigidity factors expressed by equations (7-7), (7-8), and (7-9), there results

$$\left(\frac{L}{L_F}\right)^3 - \left(\frac{L}{L_F}\right)^2 + \left(1 + \frac{A_2}{A_1}\right)\frac{CA_1}{\left(\frac{L_F}{D}\right)^2}\left(\frac{L}{L_F}\right) - \frac{CA_1}{\left(\frac{L_F}{D}\right)^2} = 0 \qquad (9\text{-}15)$$

where

$$\left.\begin{aligned} A_1 &= \frac{\pi^2 G \cos\alpha}{2EF_M} \\ A_2 &= \frac{\pi^2 F_P}{2F_M} \end{aligned}\right\} \qquad (m)$$

Equation (9-15) has one real positive root which determines the ratio $\frac{L}{L_F}$ at which buckling of the spring occurs. Equation (9-14) may be written

$$P_{CR} = \frac{L_F - L}{L_F}(EA)_s\left(\frac{L_F}{L}\right)$$

or

$$\frac{P_{CR}}{(EA)_{sF}} = 1 - \left(\frac{L}{L_F}\right) \qquad (9\text{-}16)$$

where $(EA)_{sF}$ is the equivalent compressive rigidity for a helical spring for the free length condition which, from equation (7-7), will equal

$$(EA)_{sF} = \frac{Gd^2}{8\left(\frac{D}{d}\right)^3 F_P}\left(\frac{L_F}{nd}\right) \qquad (9\text{-}17)$$

Combining equations (9-13) and (9-16), there results

$$\frac{\delta_{CR}}{L_F} = \frac{P_{CR}}{(EA)_{sF}} = 1 - \left(\frac{L}{L_F}\right) \qquad (9\text{-}18)$$

where $\frac{L}{L_F}$ is determined from the cubic equation (9-15). For the open-coiled case, the critical buckling deflection δ_{CR} and the critical buckling force P_{CR} are dependent upon the coil pitch angle α as well as the physical and material characteristics of the spring.

If the spring material is carbon or alloy steel satisfying condition (f) and is within the range defined by condition (j), then, for all practical purposes, equations (9-7) will be valid. Using equations (9-7) and (m), equation (9-15) becomes

$$\left(\frac{L}{L_F}\right)^3 - \left(\frac{L}{L_F}\right)^2 + \frac{3.86C}{\left(\frac{L_F}{D}\right)^2}\left(\frac{L}{L_F}\right) - \frac{1.075C}{\left(\frac{L_F}{D}\right)^2} = 0 \qquad (9\text{-}19)$$

which is the case for close-coiled springs and conforms to the corresponding equation in reference 3. Also, using equations (1-7) and (9-7), equation (9-17) becomes

$$(EA)_{sF} = \frac{Gd^2}{8\left(\frac{D}{d}\right)^3}\left(\frac{p_F}{d}\right) \qquad (9\text{-}20)$$

For the close-coiled case, δ_{CR} and P_{CR} are determined from equations (9-18) and (9-19) and are dependent upon only the physical and material characteristics of the spring. Figure 31, included in reference 3, is a

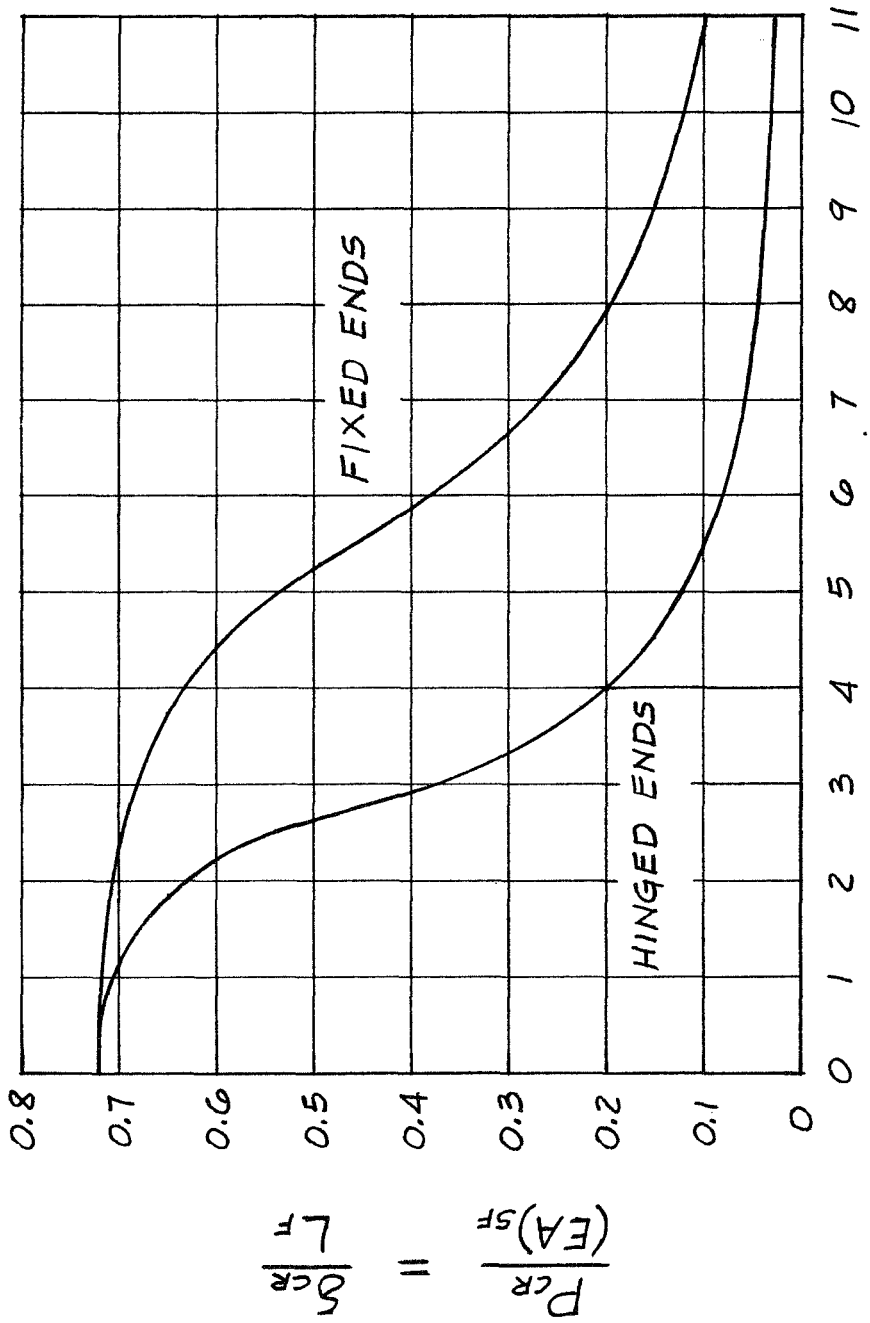
FIXED ENDS
HINGED ENDS
0.8
0.7
0.6
0.5
0.4
0.3
0.2
0.1
0
0 1 2 3 4 5 6 7 8 9 10 11
$\frac{L_F}{D}$
$\frac{P_{cr}}{(EA)_{SF}} = \frac{\delta_{cr}}{L_F}$

FIG. 31

graph of the combined equations (9-18) and (9-19). The fixed end condition of Figure 31 is included in reference 9.

From a safety standpoint, it is advisable to design the spring so that the critical load does not occur before solid compression. Assume that P_{CR} is equal to the load at solid compression P_s. Then, from equations (1-7), (1-10), and (9-18)

$$\frac{P_{CR}}{(EA)_{sF}} = \frac{P_s}{(EA)_{sF}} = \frac{\frac{p_F}{d} - 1}{\frac{p_F}{d}} \qquad (9\text{-}21)$$

and

$$n = \left(\frac{L_F}{D}\right)\frac{\frac{D}{d}}{\frac{p_F}{d}} \qquad (9\text{-}22)$$

Figure 32 is a graph of equations (9-21) and (9-22), plotted with the aid of Figure 31, for the particular values given in the table of Figure 26 and satisfying conditions (h) and (i).

The design requirements for helical springs, subjected to axial loading only, which will insure stability for the entire loading range, from free length to solid length, are determined by equations (9-21) and (9-22) and Figure 32. These requirements, rewritten as equations (9-23),

$P_{CR} = P_s$

$G = 10\,750\,000$ P.S.I.

$\tau_s = 80\,000$ P.S.I.

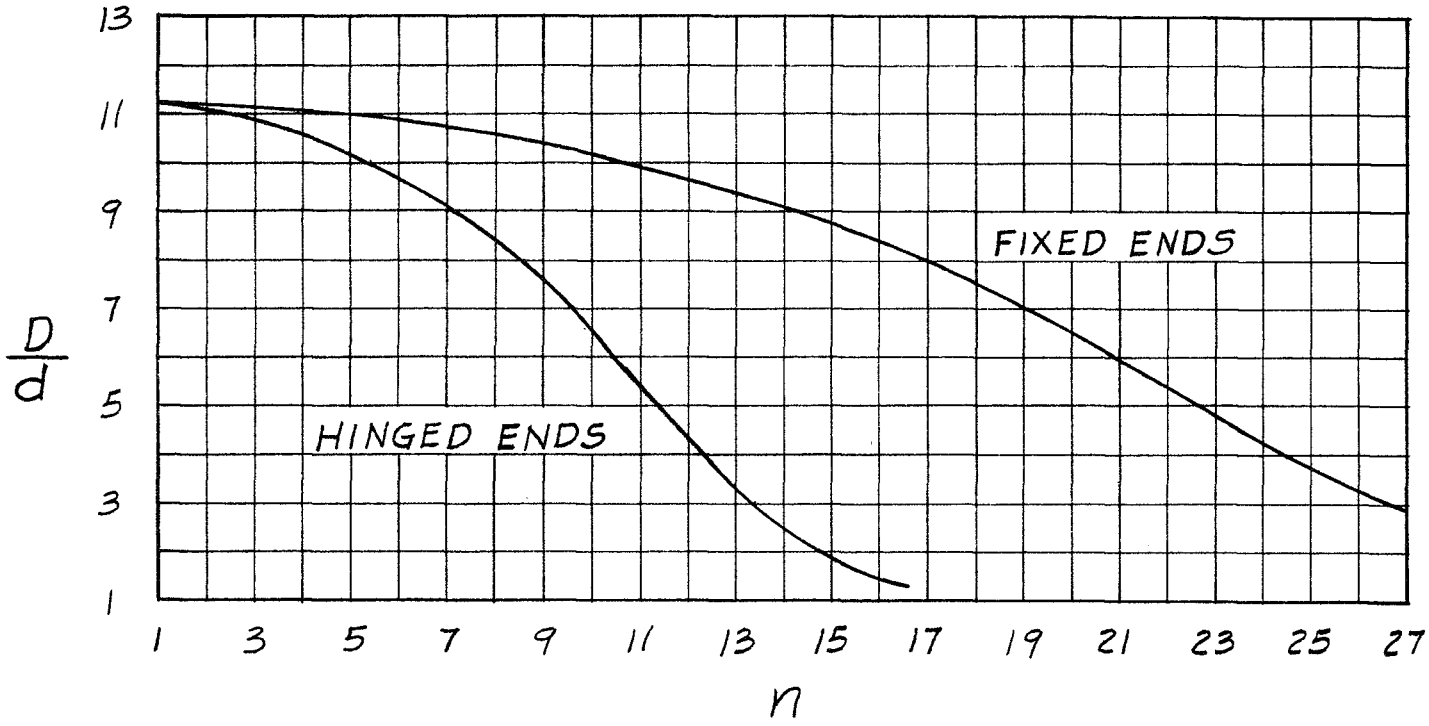

FIG. 32

$$\left.\begin{aligned} \frac{P_{CR}}{(EA)_{sF}} &= \frac{P_s}{(EA)_{sF}} = \frac{\frac{p_F}{d} - 1}{\frac{p_F}{d}} \\ &\text{Figure 32} \\ n &< \left(\frac{L_F}{D}\right)\frac{\frac{D}{d}}{\frac{p_F}{d}} \end{aligned}\right\} \qquad (9\text{-}23)$$

together with equations (9-10), are necessary and sufficient for the design and analysis of stable helical compression springs subjected to axial loading only or for the preliminary design of helical compression springs subjected to axial forces and a lateral deflection with the spring ends remaining nominally parallel to the original coil axis.

As indicated in Figures 31 and 32, there is a choice of two separate curves; the hinged end and the fixed end condition. If the seating of the spring against the base plates is square, and especially as indicated in Figure 2(b), the fixed end condition will be approximated. Reference 9 recommends the use of the fixed end condition.

In order to insure that the helical spring, subjected to axial compressive forces P, and a lateral deflection Δ, is always stable, it will be necessary to restrict the maximum Δ. The assumption will be made that the spring

ends are not clamped but that the axial force P is always sufficiently large so that the end cross sections are always in full contact with the loading plate. This assumption results in the same theory that applies to clamped or fixed ends with the exception that the limit of Δ is dependent upon P. The end conditions of the helical spring, represented analogously by a solid member with circular cross section of diameter D, are illustrated in Figure 33. Since the spring ends are not fixed, the end moments must result from the eccentric application of the axial forces and will equal

$$M = Pe \tag{n}$$

where e is the eccentricity. Using equations (7-13) and (n),

$$e = \frac{\Delta}{2} + \frac{HL}{2P} \tag{o}$$

In order for the end faces to be in full contact with the loading plates, the force P must be within the middle kern of the end faces. Considering the end faces of a coil spring to be a thin annulus, the boundaries of the middle kern will be $\frac{D}{4}$, so that

$$e \leq \frac{D}{4} \tag{p}$$

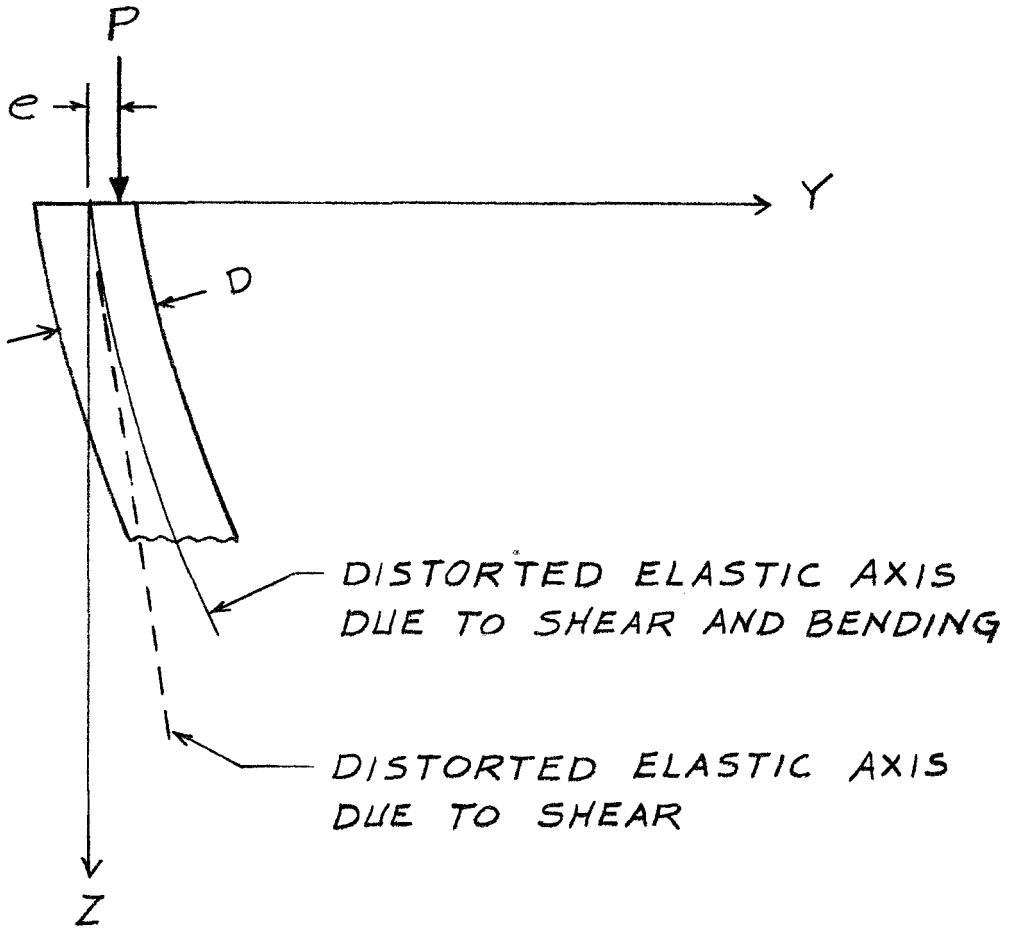
P
e
Y
D
DISTORTED ELASTIC AXIS
DUE TO SHEAR AND BENDING
DISTORTED ELASTIC AXIS
DUE TO SHEAR
Z

FIG. 33

and, from equation (o),

$$\frac{\Delta}{D} + \frac{HL}{PD} \leq \frac{1}{2} \tag{9-24}$$

or

$$\frac{\Delta}{D} S \leq \frac{1}{2} \tag{9-25}$$

where

$$S = 1 + \frac{HL}{P\Delta} \tag{9-26}$$

and, from equation (7-13),

$$S = \frac{2M}{P\Delta} = \frac{\frac{2M}{P_E \Delta}}{\frac{P}{P_E}} \tag{9-27}$$

Using equations (8-7) and (9-25), the stress amplification factor F becomes

$$F = 1 + \frac{\Delta}{D} S \leq \frac{3}{2} \tag{9-28}$$

which, for convenience, may be written

$$F = 1 + \frac{\frac{\Delta}{d}}{\frac{D}{d}} S \leq \frac{3}{2} \tag{9-29}$$

Figure 34 is a nomograph of equation (9-29).

The factor S, expressed by equation (9-27), is determined with the aid of equations (7-17), (7-18), and (7-30). Figures 35, 36, and 37 show, graphically, the

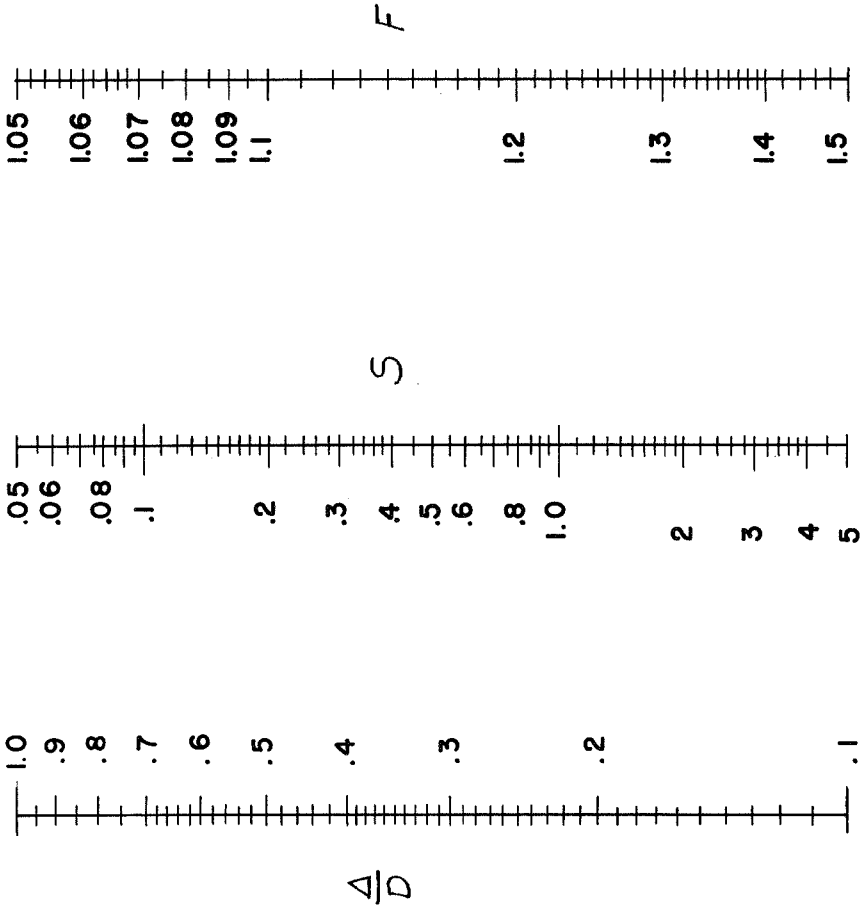
F
1.05 1.06 1.07 1.08 1.09 1.1 1.2 1.3 1.4 1.5
S
.05 .06 .08 .1 .2 .3 .4 .5 .6 .8 1.0 2 3 4 5
Q/D
1.0 .9 .8 .7 .6 .5 .4 .3 .2 .1
P/D
10 8 6 5 4 3 2 1 0.8 0.6 0.5 0.4
P/Q
10 9 8 7 6 5 4 3

FIG. 34

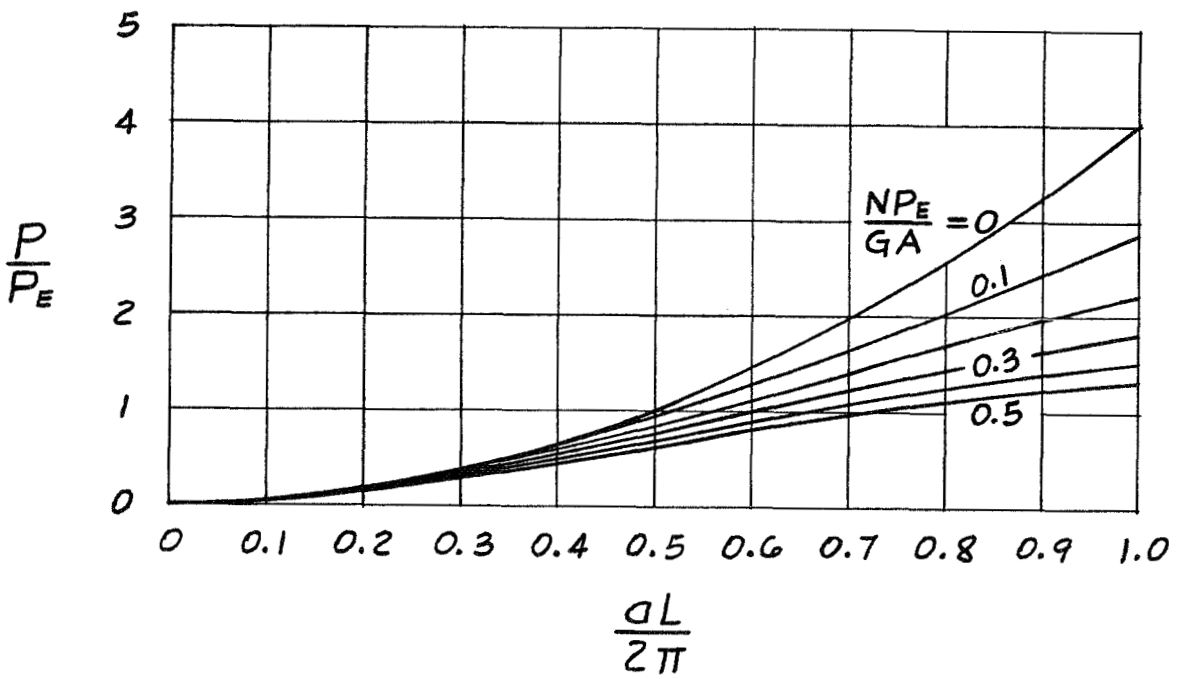

FIG. 35

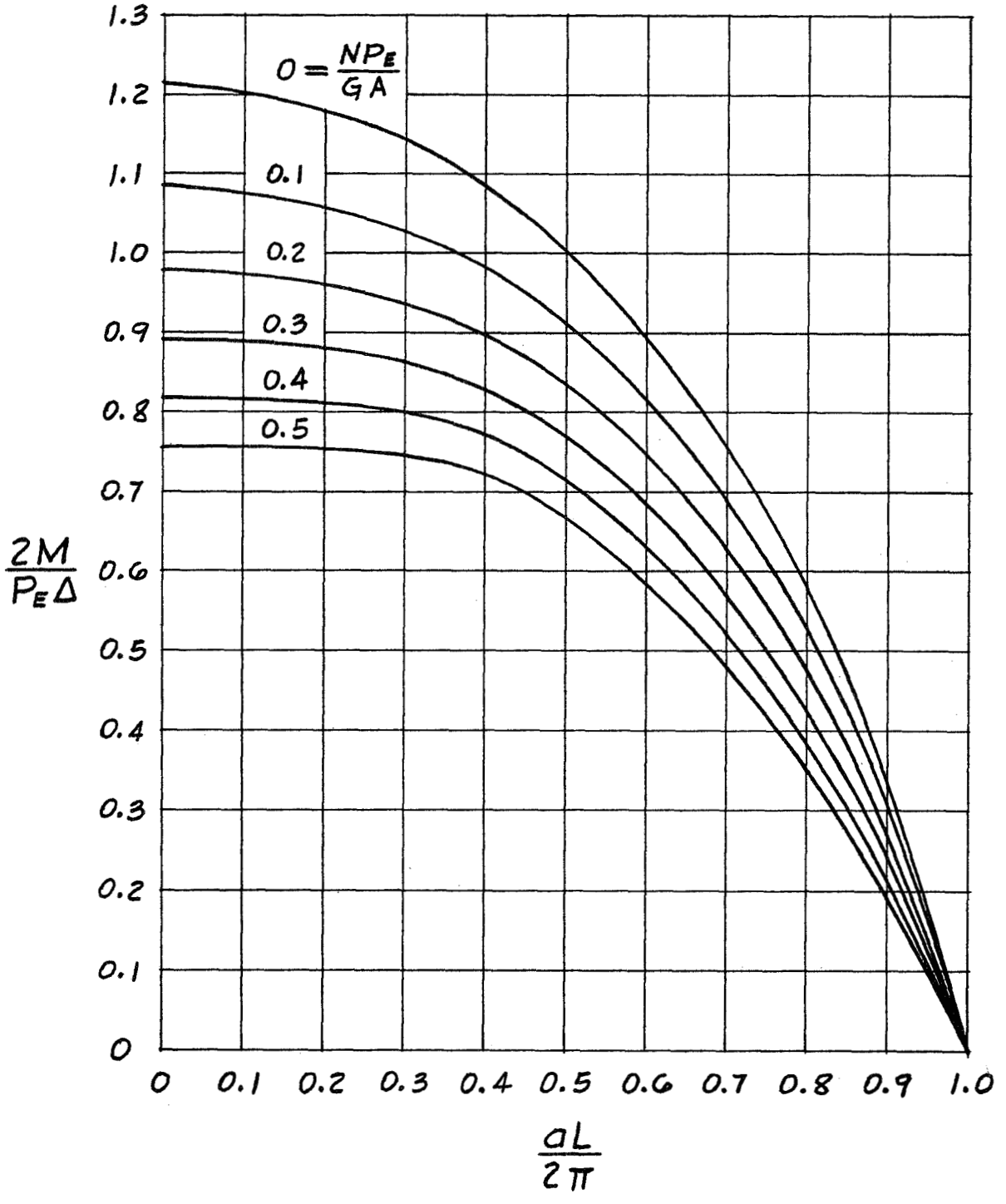
1.3
1.2
1.1
1.0
0.9
0.8
0.7
0.6
0.5
0.4
0.3
0.2
0.1
0
$0 = \frac{NP_E}{GA}$
0.1
0.2
0.3
0.4
0.5
$\frac{2M}{P_E \Delta}$
0
0.1
0.2
0.3
0.4
0.5
0.6
0.7
0.8
0.9
1.0
$\frac{aL}{2\pi}$

FIG. 36

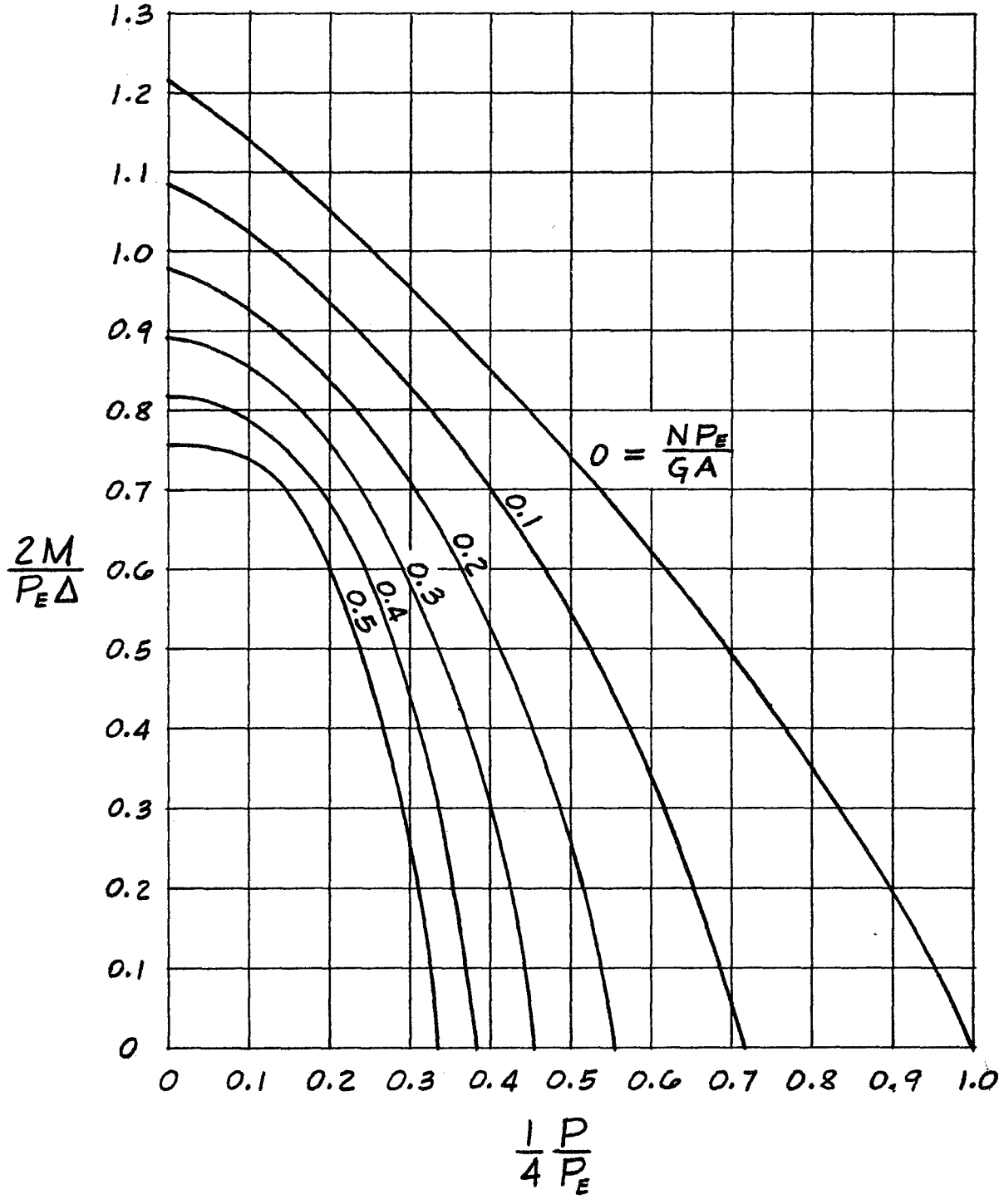
1.3
1.2
1.1
1.0
0.9
0.8
0.7
0.6
0.5
0.4
0.3
0.2
0.1
0
0 0.1 0.2 0.3 0.4 0.5 0.6 0.7 0.8 0.9 1.0
2M / PEΔ
1/4 P/PE
0 = NPE/GA
0.1
0.2
0.3
0.4
0.5

FIG. 37

relationship between the quantities $\frac{aL}{2\pi}$, $\frac{P}{P_E}$, $\frac{NP}{GA}$, and $\frac{2M}{P_E\Delta}$. If, for any particular application, the values of $\frac{P}{P_E}$ and $\frac{NP_E}{GA}$ are known, the value of $\frac{2M}{P_E\Delta}$ is obtained from Figure 37 and then S determined from equation (9-27). However, the quantities $\frac{P}{P_E}$ and $\frac{NP_E}{GA}$ are not readily available for they are interdependent with the loaded length L.

Using equations (7-8) and (7-19)

$$\frac{P}{P_E} = \left(\frac{16F_M}{\pi^2}\right)\frac{P}{Gd^2}\, n\left(\frac{D}{d}\right)\left(\frac{L}{d}\right) \qquad (9\text{-}30)$$

and, from equations (9-7),

$$\frac{P}{P_E} = 2.87n\left(\frac{D}{d}\right)\left(\frac{L}{d}\right)\frac{P}{Gd^2} \qquad (9\text{-}31)$$

Using equations (7-8), (7-9), and (7-19)

$$\frac{NP_E}{(GA)_s} = \left(\frac{\pi^2}{2F_M}\,\frac{G\cos\alpha}{E}\right)\frac{\left(\frac{D}{d}\right)^2}{\left(\frac{L}{d}\right)^2} \qquad (9\text{-}32)$$

and, from equations (f) and (9-7),

$$\frac{NP_E}{GA} = 1.075\,\frac{\left(\frac{D}{d}\right)^2}{\left(\frac{L}{d}\right)^2} \qquad (9\text{-}33)$$

The length of spring, under combined loading, will equal

$$L = L_F - \delta \tag{9-34}$$

and, from equation (7-22),

$$L = L_F - \delta_P - \delta_C \tag{q}$$

or

$$L = L_P - \delta_C \tag{r}$$

where

$$L_P = L_F - \delta_P \tag{s}$$

is the length of spring due to the action of the P load alone. From equation (7-31)

$$\delta_C = \frac{\Delta^2}{L} Z \tag{9-35}$$

where Z is defined by equation (7-32). Equation (r) may then be written

$$L^2 - L_P L + \Delta^2 Z = 0 \tag{9-36}$$

Figure 38 shows, graphically, the relationship between Z, $\frac{aL}{2\pi}$, and $\frac{NP_E}{GA}$ and it is apparent that Z is a function of L. If a value for Z could be assumed, reasonably close to its true value, then equation (9-36) would become, approximately,

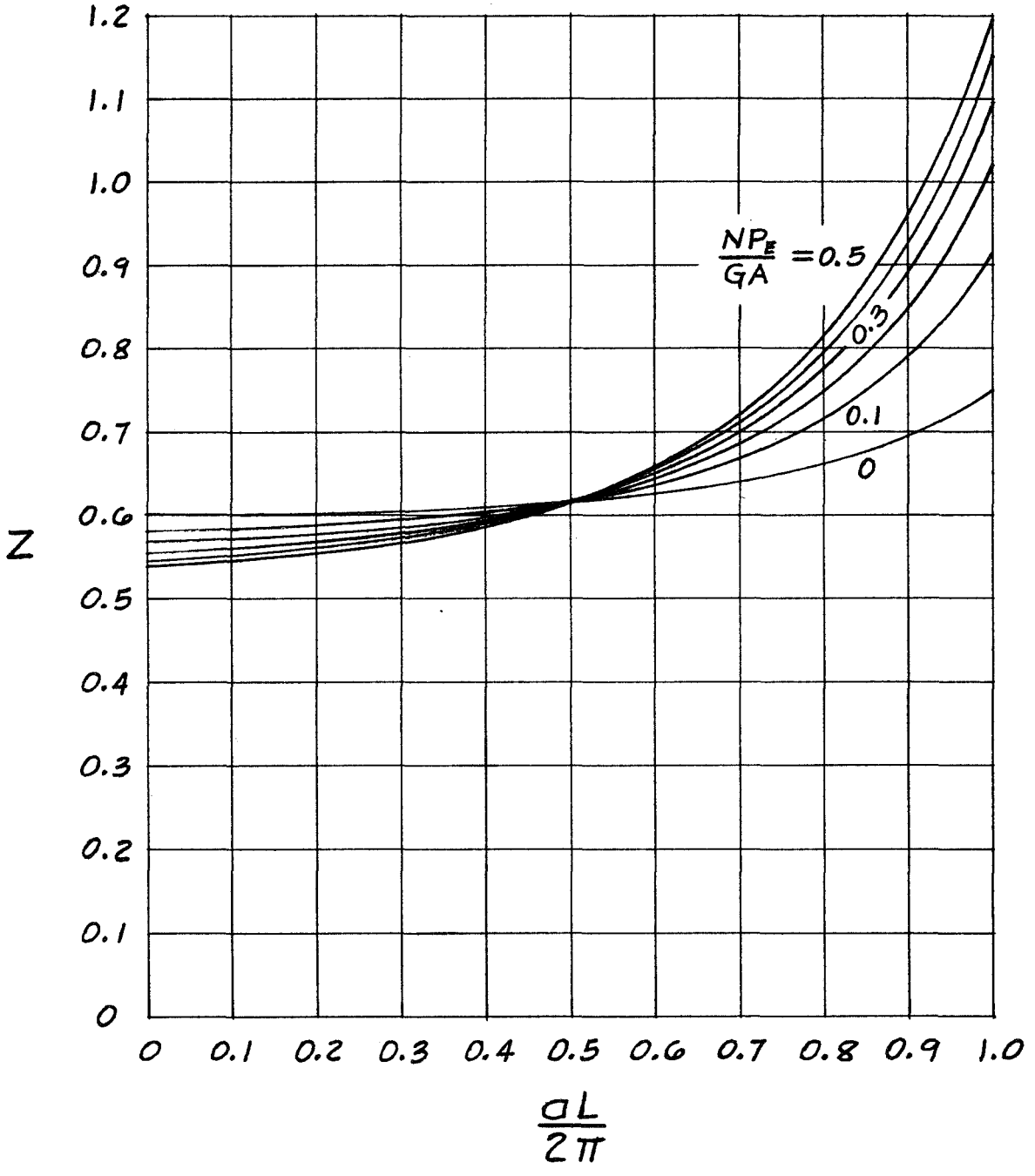
1.2
1.1
1.0
0.9
0.8
0.7
0.6
0.5
0.4
0.3
0.2
0.1
0
Z
$\frac{NP_E}{GA}$ =0.5
0.3
0.1
0
0 0.1 0.2 0.3 0.4 0.5 0.6 0.7 0.8 0.9 1.0
$\frac{aL}{2\pi}$

FIG. 38

$$\frac{L}{L_P} = \frac{1}{2} \pm \frac{1}{2}\left[1 - \left(\frac{2\Delta}{L_P}\right)^2 Z\right]^{1/2} \qquad (9\text{-}37)$$

which could be further approximated

$$\frac{L}{L_P} = \frac{1}{2} \pm \frac{1}{2}\left[1 - \frac{1}{2}\left(\frac{2\Delta}{L_P}\right)^2 Z\right] \qquad (9\text{-}38)$$

and using the positive sign

$$\frac{L}{L_P} = 1 - \left(\frac{\Delta}{L_P}\right)^2 Z \qquad (9\text{-}39)$$

or

$$\frac{L}{d} = \frac{L_P}{d}\left[1 - \frac{\left(\frac{\Delta}{d}\right)^2}{\left(\frac{L_P}{d}\right)^2} Z\right] \qquad (9\text{-}40)$$

Generally, the second term in the bracket of equation (9-40) will be small compared to unity so that

$$\frac{L}{d} \cong \frac{L_P}{d} = n\left(\frac{p_F}{d}\right) - \frac{P}{kd} \qquad (9\text{-}41)$$

A more accurate determination of equation (9-40), and hence equations (9-31) and (9-33), may be obtained by combining equation (9-41) with equations (9-31) and (9-33) to obtain first approximations. Using these first approximations and Figures 35 and 38, a first approximation of Z may be

obtained. Using this value and equation (9-40), a second approximation for $\frac{L}{d}$ will be obtained. The entire process can be repeated so that any degree of accuracy can be obtained. However, the use of the first approximation only, represented by equation (9-41), will usually provide a degree of accuracy commensurate with that inherent in the development of equation (8-7) and its ultimate result, equation (9-29).

The stability considerations for a helical spring subjected to combined loading will be developed in like manner to the case of a helical spring subjected to axial load only. For the fixed end condition

$$P_{CR} = \frac{4P_{ECR}}{1 + 4\frac{NP_{ECR}}{(GA)_{sCR}}} \tag{9-42}$$

where the subscripts CR denote the critical length condition. Equation (9-42) may be written

$$\frac{P_{CR}}{(EA)_{sF}} = \frac{4\frac{P_{ECR}}{(EA)_{sF}}}{1 + 4\frac{NP_{ECR}}{(GA)_{sCR}}} \tag{9-43}$$

where

$$\left.\begin{aligned} \frac{P_{ECR}}{(EA)_{sF}} &= \frac{A_2}{\left(\frac{L_{CR}}{L_F}\right)\left(\frac{L_F}{D}\right)^2} \\ \frac{NP_{ECR}}{(GA)_{sCR}} &= \frac{A_1}{\left(\frac{L_{CR}}{L_F}\right)^2\left(\frac{L_F}{D}\right)^2} \end{aligned}\right\} \qquad (9\text{-}44)$$

and where A_1 and A_2 are defined by equations (m). Using equations (9-44), equation (9-43) becomes

$$\frac{P_{CR}}{(EA)_{sF}} = \frac{4A_2\left(\frac{L_{CR}}{L_F}\right)}{\left(\frac{L_{CR}}{L_F}\right)^2\left(\frac{L_F}{D}\right)^2 + 4A_1} \qquad (9\text{-}45)$$

The spring length, for the critical condition, will equal

$$L_{CR} = L_F - \delta_{CR} \qquad (t)$$

and from equation (7-22)

$$L_{CR} = L_F - \delta_{PCR} - \delta_{CCR} \qquad (u)$$

where

$$\delta_{PCR} = \frac{P_{CR}L_{PCR}}{(EA)_{sPCR}} = \frac{P_{CR}L_F}{(EA)_{sF}} \qquad (v)$$

Combining equations (u) and (v), there results

$$\frac{P_{CR}}{(EA)_{sF}} = \left(1 - \frac{\delta_{CCR}}{L_F}\right) - \frac{L_{CR}}{L_F} \qquad (9\text{-}46)$$

Equating equations (9-45) and (9-46)

$$\left(\frac{L_{CR}}{L_F}\right)^3 - \left(1 - \frac{\delta_{CCR}}{L_F}\right)\left(\frac{L_{CR}}{L_F}\right)^2 + \frac{4(A_1 + A_2)}{\left(\frac{L_F}{D}\right)^2}\left(\frac{L_{CR}}{L_F}\right) -$$

$$\left(1 - \frac{\delta_{CCR}}{L_F}\right)\frac{4A_1}{\left(\frac{L_F}{D}\right)^2} = 0 \qquad (9\text{-}47)$$

which is similar in form to equation (9-15) and becomes identical when $\frac{\delta_{CCR}}{L_F}$ equals zero.

Equation (9-47) may be rewritten

$$\frac{\delta_{CCR}}{L_F} = 1 - \frac{\frac{L_{CR}}{L_F}\left[\left(\frac{L_{CR}}{L_F}\right)^2\left(\frac{L_F}{D}\right)^2 + 4(A_1 + A_2)\right]}{\left(\frac{L_{CR}}{L_F}\right)^2\left(\frac{L_F}{D}\right)^2 + 4A_1} \qquad (9\text{-}48)$$

and using equation (9-35)

$$\frac{\delta_{CCR}}{L_F} = \left(\frac{A}{L_F}\right)^2 \frac{Z_{CR}}{\left(\frac{L_{CR}}{L_F}\right)} \qquad (9\text{-}49)$$

From equation (7-32)

$$Z_{CR} = \frac{1}{4}\left[2 + (1 + J_{CR})^2\right] \tag{9-50}$$

and from equations (7-18), (9-43), and (9-44)

$$J_{CR} = \frac{4A_1}{\left(\frac{L_{CR}}{L_F}\right)^2\left(\frac{L_F}{D}\right)^2 + 4A_1} \tag{9-51}$$

or

$$\left(\frac{L_{CR}}{L_F}\right)^2\left(\frac{L_F}{D}\right)^2 = \frac{4A_1(1 - J_{CR})}{J_{CR}} \tag{9-52}$$

Equating equations (9-48) and (9-49), there results

$$\frac{L_{CR}}{L_F} = \frac{1 \pm \left[1 - 4Z_{CR}\left(1 + \frac{A_2}{A_1} J_{CR}\right)\left(\frac{\Delta}{L_F}\right)^2\right]^{1/2}}{2\left(1 + \frac{A_2}{A_1} J_{CR}\right)} \tag{9-53}$$

For close coiled springs composed of carbon or alloy steel, using equations (f) and (9-7),

$$\left.\begin{aligned} A_1 &= 1.075 \\ A_2 &= 2.79 \end{aligned}\right\} \tag{w}$$

then, using the positive sign, equation (9-53) becomes

$$\frac{L_{CR}}{L_F} = \frac{1 + \left[1 - 4Z_{CR}(1 + 2.59J_{CR})\left(\frac{\Delta}{L_F}\right)^2\right]^{1/2}}{2(1 + 2.59J_{CR})} \qquad (9\text{-}54)$$

Using equations (9-52), (w), and (9-54)

$$\frac{L_F}{D} = \frac{2(1 + 2.59J_{CR})\left[\frac{4.3(1 - J_{CR})}{J_{CR}}\right]^{1/2}}{1 + \left[1 - 4Z_{CR}(1 + 2.59J_{CR})\left(\frac{\Delta}{L_F}\right)^2\right]^{1/2}} \qquad (9\text{-}55)$$

Equations (9-54) and (9-55) give the relationship between $\frac{L_{CR}}{L_F}$, $\frac{L_F}{D}$, $\frac{\Delta}{L_F}$, and J_{CR} (Z_{CR} is a function of J_{CR}). Although J_{CR} is actually dependent upon both $\frac{L_{CR}}{L_F}$ and $\frac{L_F}{D}$, values for J_{CR} can be assumed and the relationship established between $\frac{L_{CR}}{L_F}$, $\frac{L_F}{D}$, and $\frac{\Delta}{L_F}$ from which solutions for equation (9-46) can be obtained. There are two limiting conditions for equations (9-54) and (9-55). When $\frac{\Delta}{L_F}$ equals zero, the condition of axial load only results represented by the fixed end condition of Figure 31. The maximum condition for $\frac{\Delta}{L_F}$ occurs when

$$\left(\frac{\Delta}{L_F}\right)_{max} = \left[\frac{1}{4Z_{CR}(1 + 2.59J_{CR})}\right]^{1/2} \qquad (9\text{-}56)$$

For any greater value, $\frac{L_{CR}}{L_F}$ and $\frac{L_F}{D}$ become imaginary.

Figures 39, 40, and 41 illustrate graphically the stability conditions for combined loading. It is apparent from Figure 41 that, for values of $\frac{L_F}{D}$ greater than about 5, there is greater stability for the combined loading condition than for the condition of axial load only. This effect seems rather unusual for from a physical conception of the problem it would seem that any given lateral deflection should produce a decrease in stability for the entire range of $\frac{L_F}{D}$, although for slenderer springs, represented by the larger values of $\frac{L_F}{D}$, the decrease in stability should become small. No explanation is offered for this phenomenon.

The design of a helical spring subjected to an axial compressive force and a lateral deflection with the spring ends remaining nominally parallel to the original coil axis differs from the usual case of an axial force only in two important respects. First, a factor F, expressed by equation (9-29) and determined with the aid of Figure 37, amplifies the stresses that result from the axial force only as indicated by equation (8-11) which, for convenience, may be written

$$\frac{\tau}{\tau_s} = \left(\frac{\delta_p}{\delta_s}\right)F \qquad (9\text{-}57)$$

Second, the stability restrictions of Figure 41 must not be exceeded.

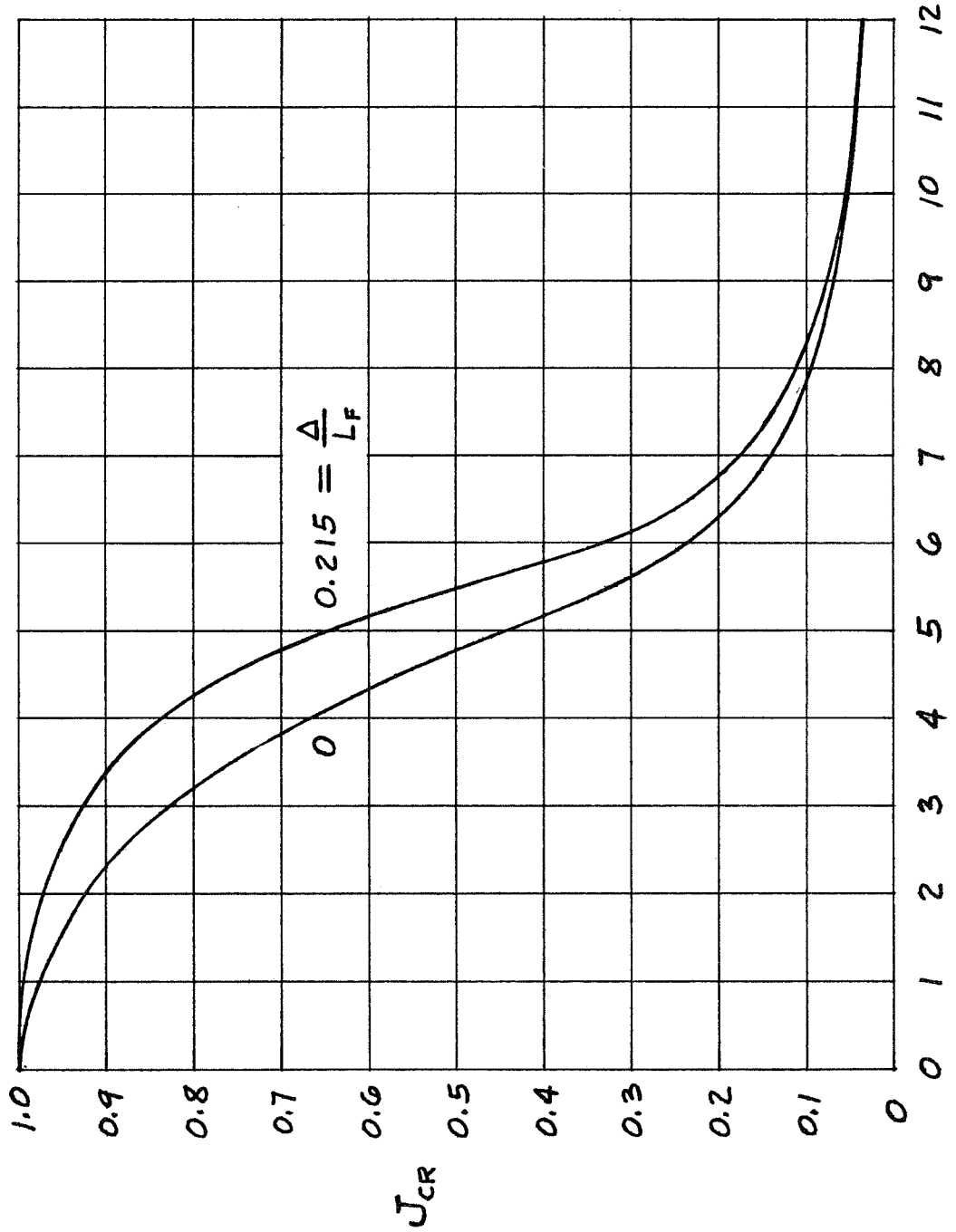
1.0
0.9
0.8
0.7
0.6
0.5
0.4
0.3
0.2
0.1
0
J_{CR}
0
1
2
3
4
5
6
7
8
9
10
11
12
$\frac{L_F}{D}$
$0.215 = \frac{\Delta}{L_F}$
0

FIG. 39

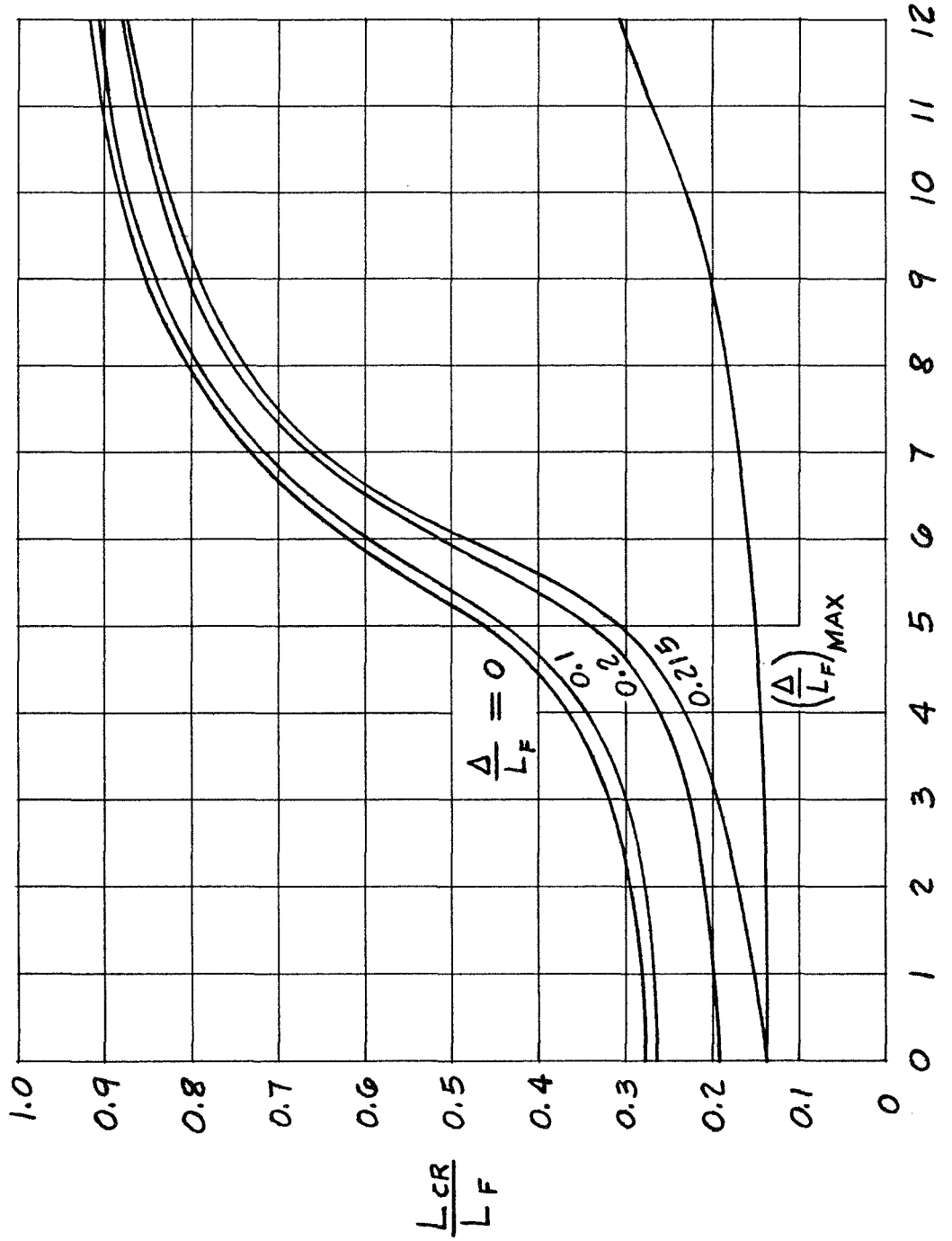
1.0
0.9
0.8
0.7
0.6
0.5
0.4
0.3
0.2
0.1
0
0 1 2 3 4 5 6 7 8 9 10 11 12
$\frac{L_{CR}}{L_F}$
$\frac{L_F}{D}$
$\frac{\Delta}{L_F} = 0$
0.1
0.2
0.215
$\left(\frac{\Delta}{L_F}\right)_{MAX}$

FIG. 40

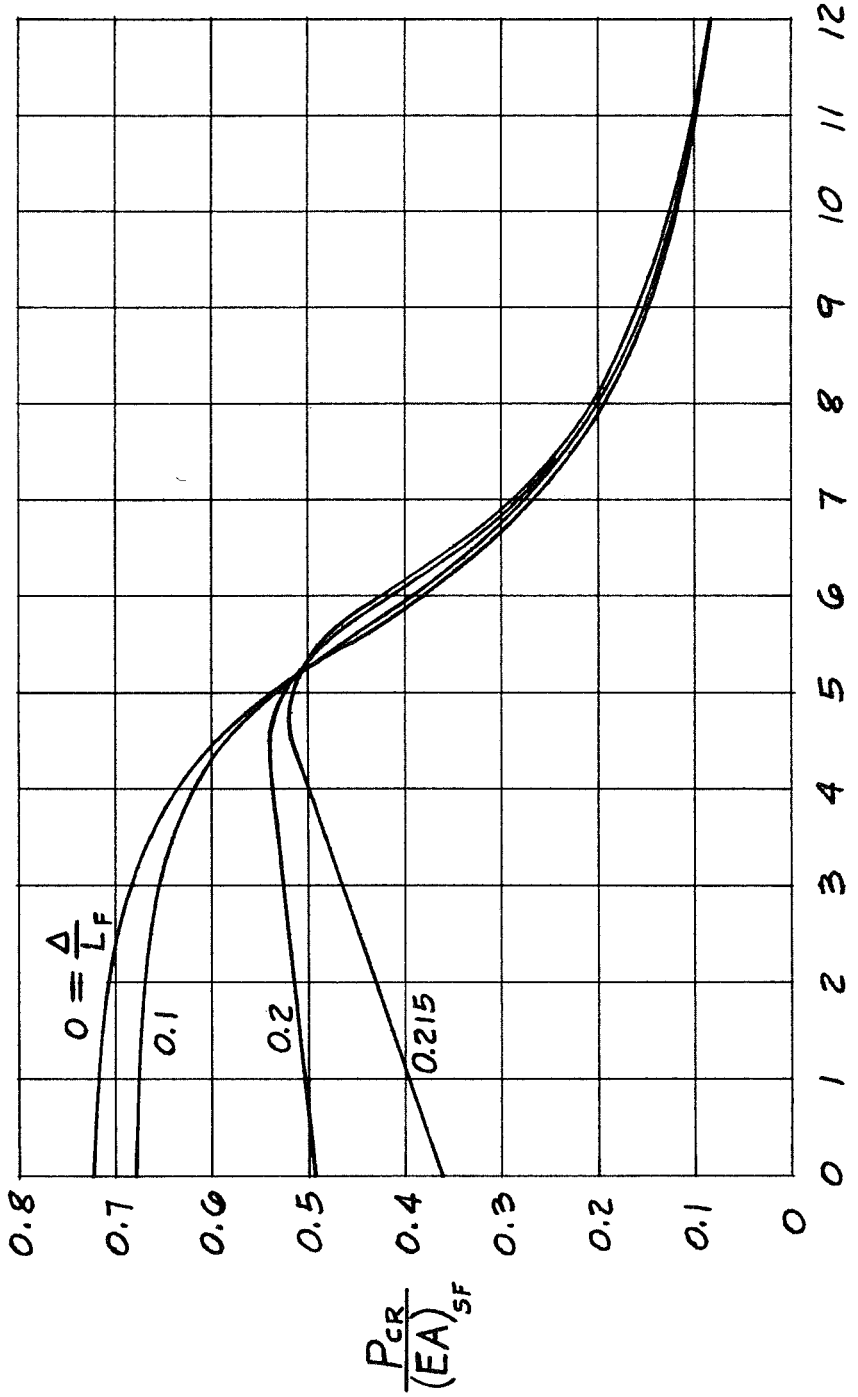
0.8
0.7
0.6
0.5
0.4
0.3
0.2
0.1
0
0 1 2 3 4 5 6 7 8 9 10 11 12
$\frac{P_{CR}}{(EA)_{SF}}$
$\frac{L_F}{D}$
$0 = \frac{\Delta}{L_F}$
0.1
0.2
0.215

FIG. 41

10. EXAMPLE

This section shall be devoted to an example illustrating the use of previously developed formulas and graphs for the design of a helical spring subjected to an axial force and a lateral deflection with the spring ends remaining nominally parallel to the original coil axis. Consider the basic requirements to be

$$\left.\begin{aligned} P &= 1750 \text{ lb} \\ k &= 800 \text{ lb/in.} \\ \Delta &= 2.25 \text{ in.} \end{aligned}\right\} \qquad (10\text{-}1)$$

Assume the wire material is hot wound carbon or alloy steel with

$$\left.\begin{aligned} G &= 10{,}750{,}000 \text{ psi} \\ \tau_s &= 80{,}000 \text{ psi} \end{aligned}\right\} \qquad (10\text{-}2)$$

Let the first trial quantity be

$$\frac{D}{d} = 4 \qquad (10\text{-}3)$$

then, from Figure 42

$$\frac{p_F}{d} = 1.267 \qquad (10\text{-}4)$$

which could be obtained from the table of Figure 26, since conditions (10-2) have been assumed. A value of the

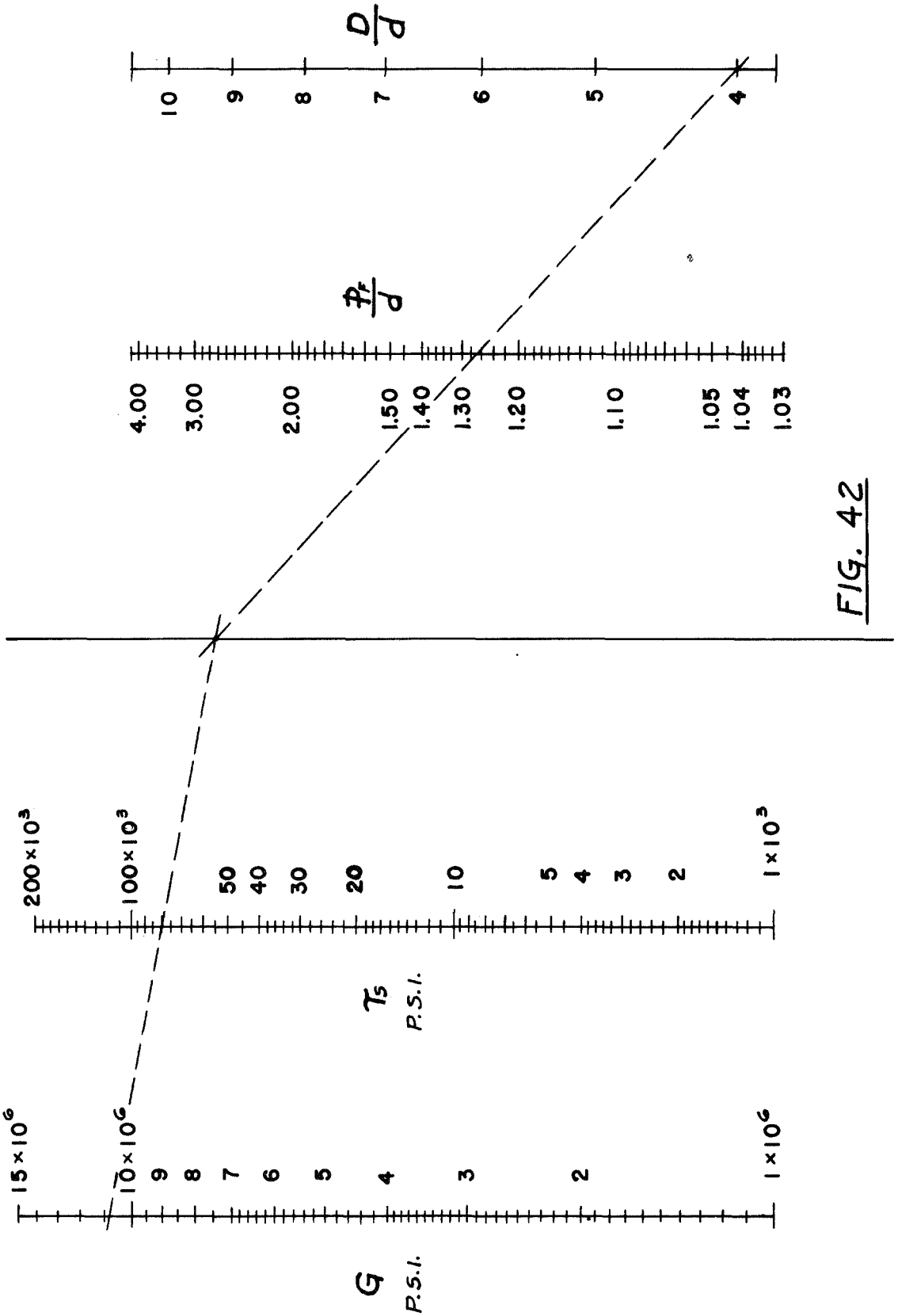
G
P.S.I.
15×10⁶
10×10⁶
9
8
7
6
5
4
3
2
1×10⁶
τs
P.S.I.
200×10³
100×10³
50
40
30
20
10
5
4
3
2
1×10³
Pf/d
4.00
3.00
2.00
1.50
1.40
1.30
1.20
1.10
1.05
1.04
1.03
D/d
10
9
8
7
6
5
4

FIG. 42

ratio $\frac{\delta_P}{\delta_s}$ in the neighborhood of 0.5 is generally desirable. From Figures 43 and 44

$$\left.\begin{aligned} P &= 1750 \\ d &= 0.75 \\ \frac{P}{Gd^2} &= 0.3 \times 10^{-3} \\ \frac{\delta_P}{\delta_s} &= 0.57 \end{aligned}\right\} \qquad (10\text{-}5)$$

then from Figures 45 and 46

$$\left.\begin{aligned} k &= 800 \\ \frac{k}{Gd} &= 1.02 \times 10^{-4} \\ n &= 20 \end{aligned}\right\} \qquad (10\text{-}6)$$

Sufficient information is now available so that the following results:

$$\frac{\Delta}{d} = \frac{2.25}{0.75} = 3 \qquad (10\text{-}7)$$

$$\begin{aligned} \frac{L_P}{d} &= n\left(\frac{p_F}{d}\right) - \frac{P}{kd} \\ &= 20 \times 1.267 - \frac{1750}{800 \times 0.75} = 22.42 \end{aligned} \qquad (10\text{-}8)$$

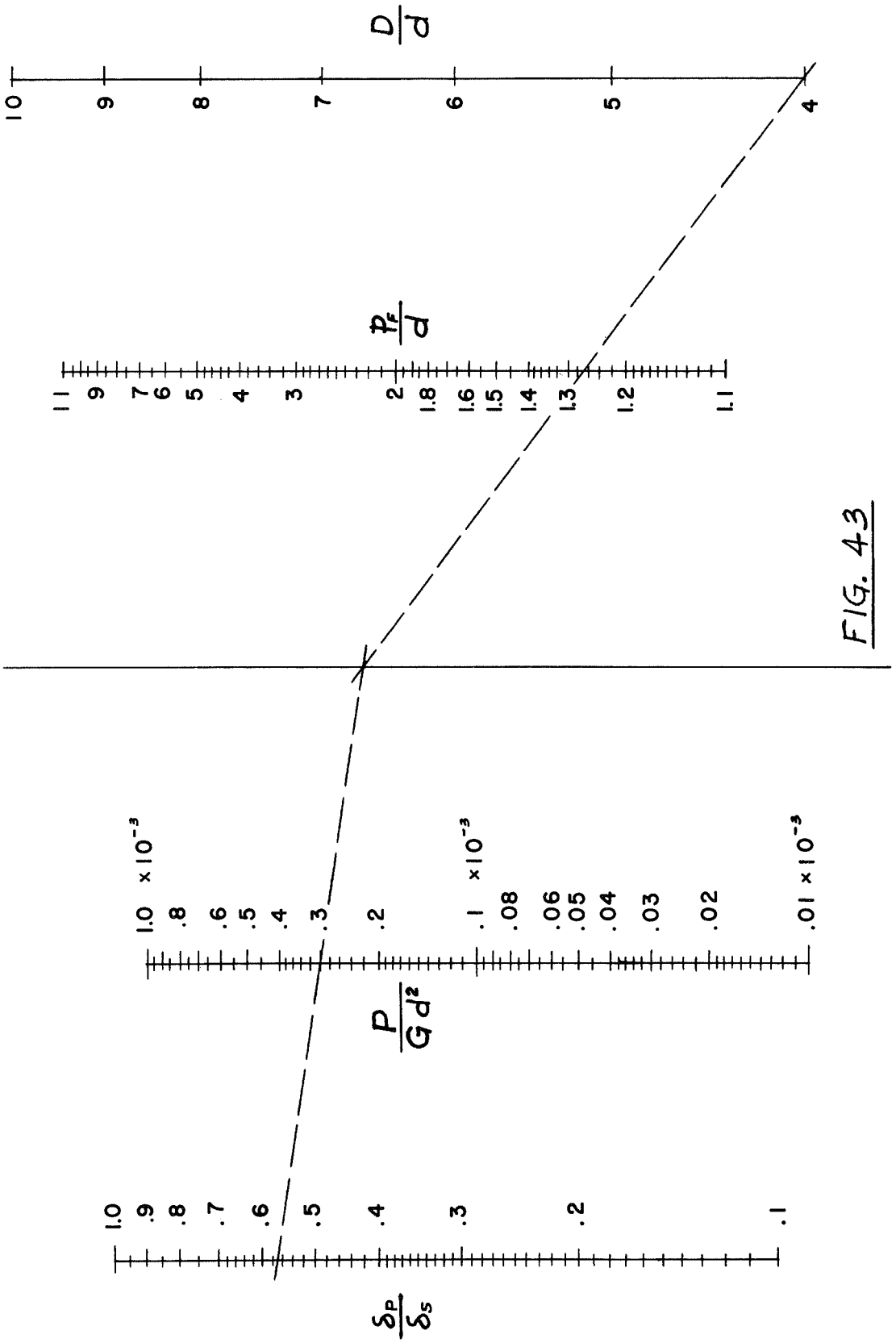
$\frac{\delta_P}{\delta_S}$
1.0 .9 .8 .7 .6 .5 .4 .3 .2 .1
$\frac{P}{Gd^2}$
1.0 ×10⁻³ .8 .6 .5 .4 .3 .2 .1 ×10⁻³ .08 .06 .05 .04 .03 .02 .01 ×10⁻³
$\frac{p_r}{d}$
11 9 7 6 5 4 3 2 1.8 1.6 1.5 1.4 1.3 1.2 1.1
$\frac{D}{d}$
10 9 8 7 6 5 4

FIG. 43

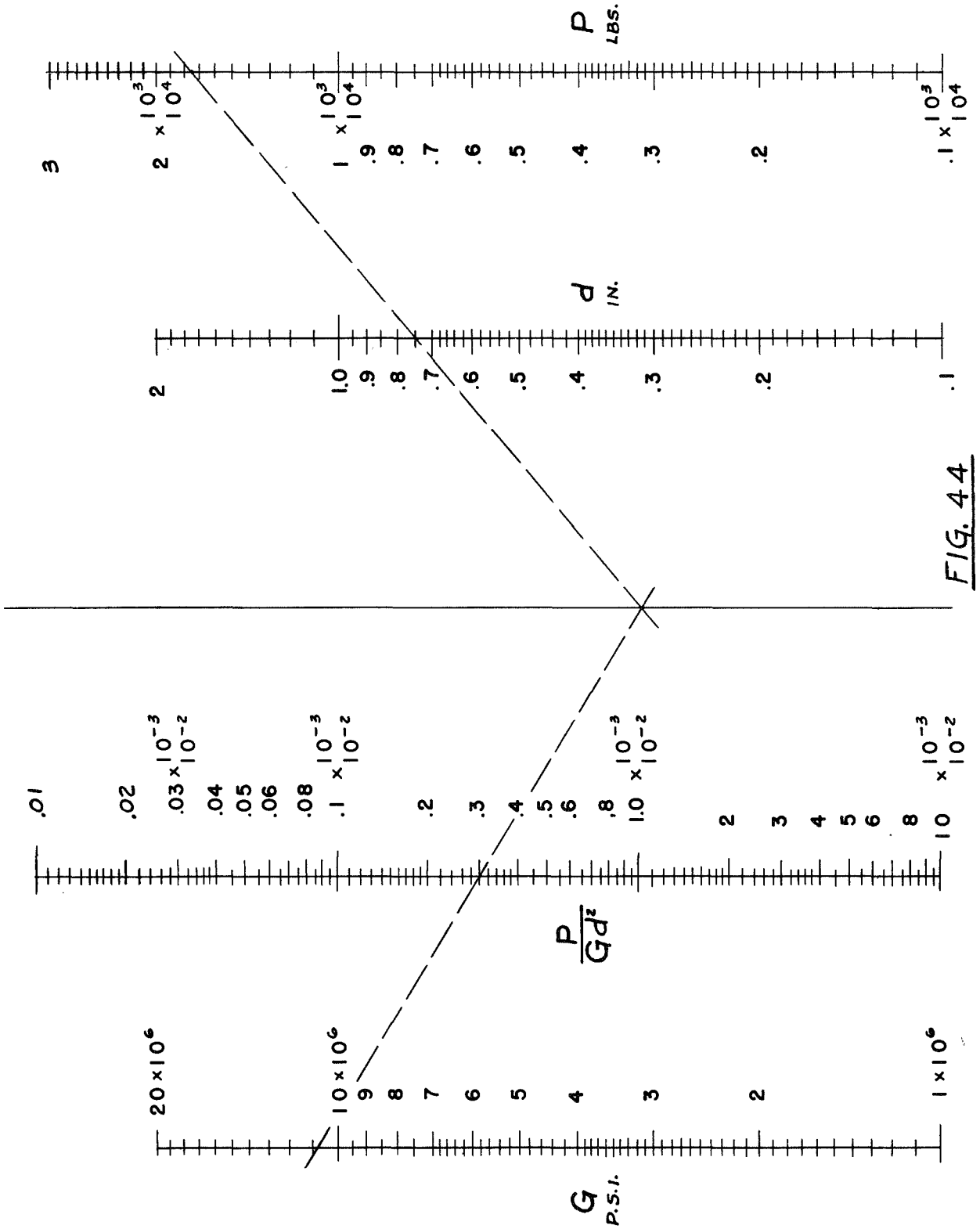

FIG. 44

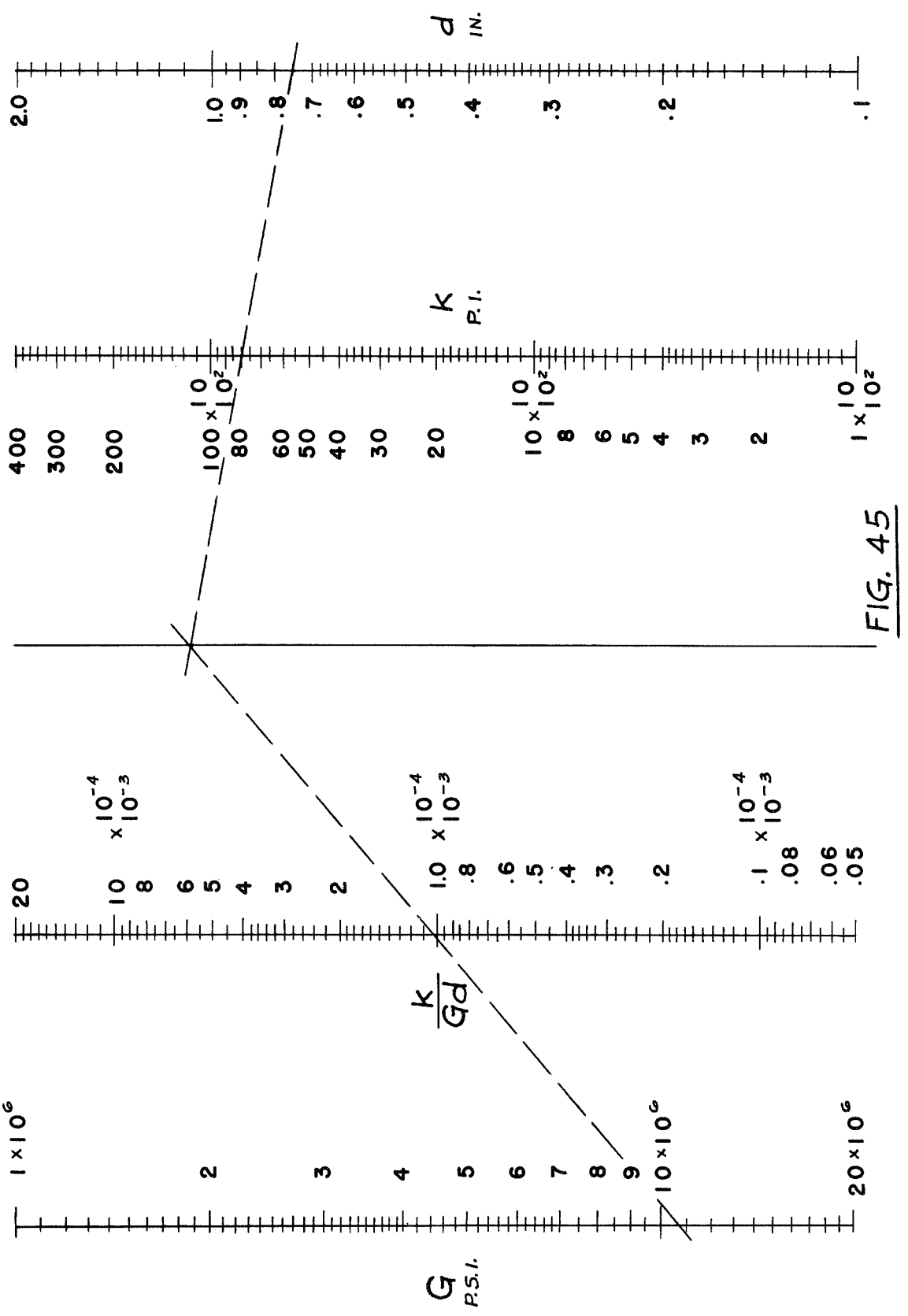
d
IN.
2.0
1.0
.9
.8
.7
.6
.5
.4
.3
.2
.1
K
P.I.
400
300
200
100 x 10^2
80
60
50
40
30
20
10 x 10^2
8
6
5
4
3
2
1 x 10^2
k/Gd
20
10
8
6
5
4
3
2
1.0 x 10^-3
.8
.6
.5
.4
.3
.2
.1 x 10^-3
.08
.06
.05
G
P.S.I.
1 x 10^6
2
3
4
5
6
7
8
9
10 x 10^6
20 x 10^6

FIG. 45

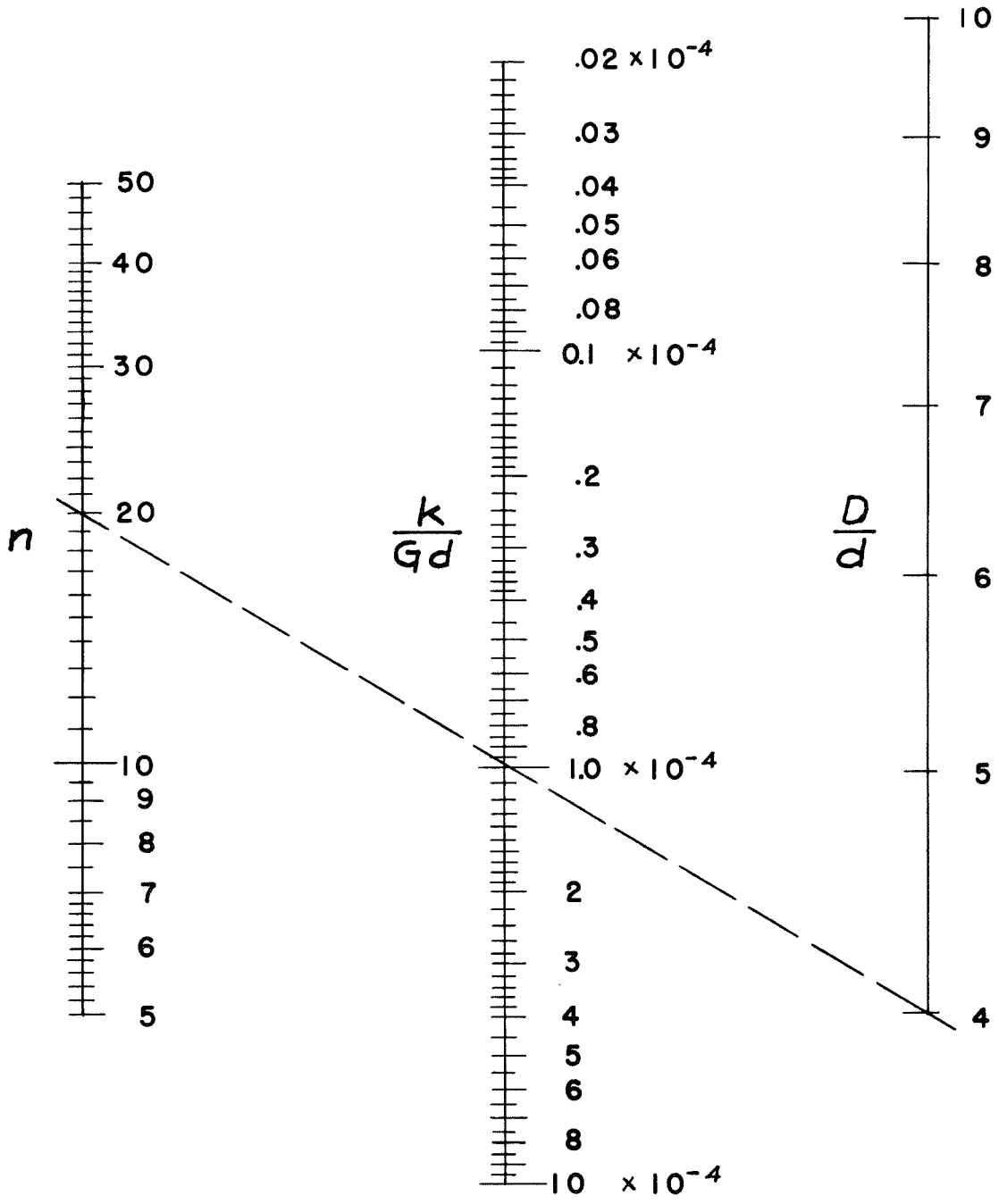
n
50
40
30
20
10
9
8
7
6
5
k/Gd
.02 x 10⁻⁴
.03
.04
.05
.06
.08
0.1 x 10⁻⁴
.2
.3
.4
.5
.6
.8
1.0 x 10⁻⁴
2
3
4
5
6
8
10 x 10⁻⁴
D/d
10
9
8
7
6
5
4

FIG. 46

$$\frac{L_F}{D} = n\frac{\frac{p_F}{d}}{\frac{D}{d}} = 20 \times \frac{1.267}{4} = 6.33 \qquad (10\text{-}9)$$

$$\frac{P}{(EA)_{sF}} = 8\frac{\left(\frac{D}{d}\right)^3}{\frac{p_F}{d}}\frac{P}{Gd^2}$$

$$= 8 \times \frac{64}{1.267} \times 0.3 \times 10^{-3} = 0.1212 \qquad (10\text{-}10)$$

$$\frac{\Delta}{L_F} = \frac{\frac{\Delta}{d}}{n\left(\frac{p_F}{d}\right)} = \frac{3}{20 \times 1.267} = 0.1185 \qquad (10\text{-}11)$$

If equation (10-8) is used as a first approximation, there results

$$\frac{P}{P_E} = 2.87n\left(\frac{D}{d}\right)\left(\frac{L}{d}\right)\frac{P}{Gd^2}$$

$$= 2.87 \times 20 \times 4 \times 22.42 \times 0.3 \times 10^{-3} = 1.545$$

$$\div 4$$

$$= 0.386 \qquad (10\text{-}12)$$

and

$$\frac{NP_E}{(GA)_s} = 1.075\frac{\left(\frac{D}{d}\right)^2}{\left(\frac{L}{d}\right)^2} = \frac{1.075 \times 16}{503} = 0.0342 \qquad (10\text{-}13)$$

Using Figure 35 and equations (10-12) and (10-13)

$$\frac{aL}{2\pi} = 0.63 \qquad (10\text{-}14)$$

and from Figure 38

$$Z = 0.67 \qquad (10\text{-}15)$$

then from equation (9-40)

$$\frac{L}{d} = 22.42\left(1 - \frac{9}{503} \times 0.67\right)$$
$$= 22.42 \times 0.988 = 22.15 \qquad (10\text{-}16)$$

It is seen that the first approximation, represented by equation (10-8), is sufficiently accurate. Therefore, using equations (10-12) and (10-13) with Figure 37

$$\frac{2M}{P_E\Delta} = 0.82 \qquad (10\text{-}17)$$

and

$$S = \frac{2M}{P\Delta} = \frac{\frac{2M}{P_E\Delta}}{\frac{P}{P_E}} = \frac{0.82}{1.545} = 0.532 \qquad (10\text{-}18)$$

From Figure 47

$$F = 1.39 \qquad (10\text{-}19)$$

then

$$\frac{\tau}{\tau_s} = \left(\frac{\delta_P}{\delta_s}\right)F = 0.57 \times 1.39 = 0.793 \qquad (10\text{-}20)$$

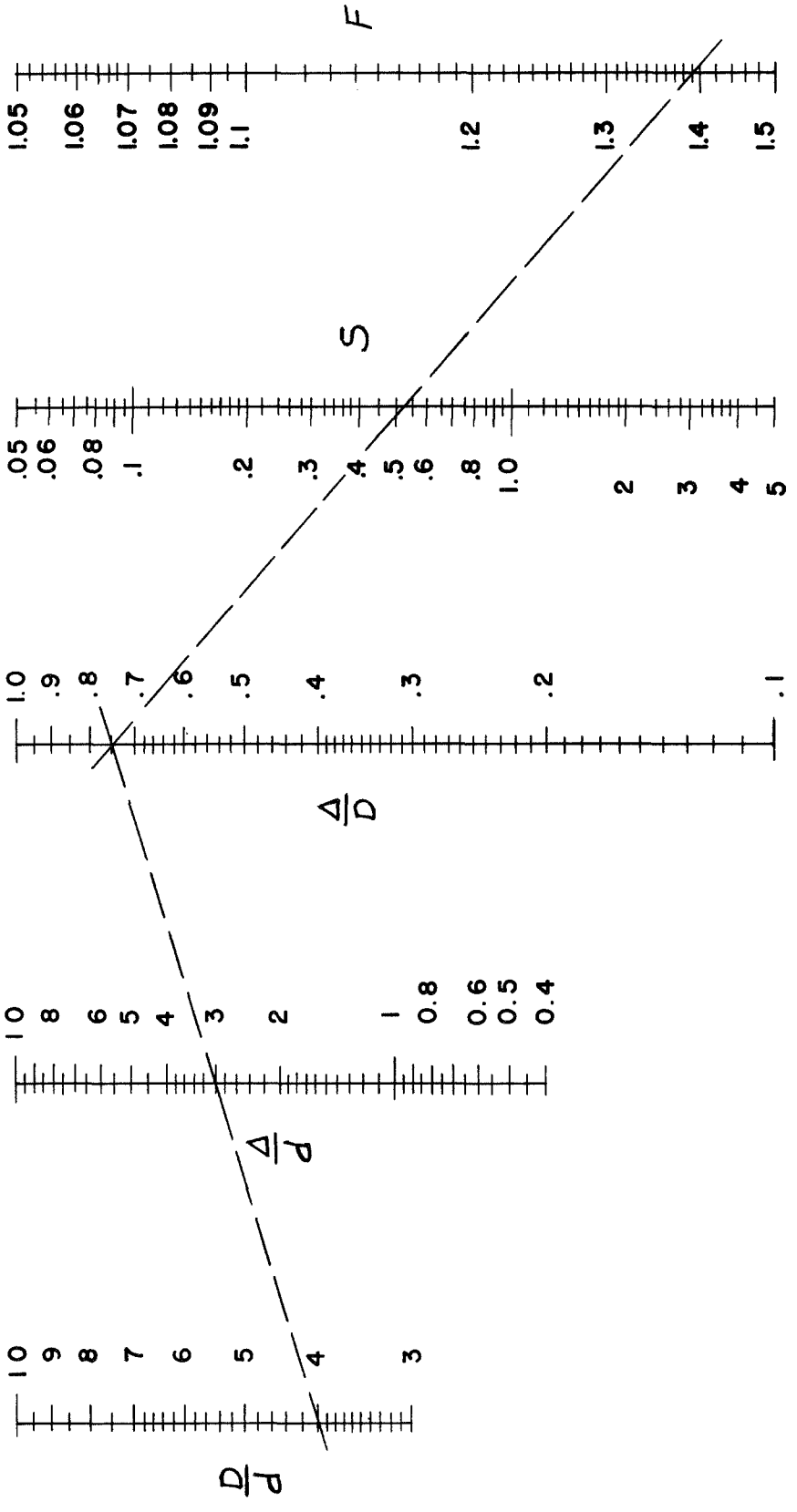
F
1.05
1.06
1.07
1.08
1.09
1.1
1.2
1.3
1.4
1.5
S
.05
.06
.08
.1
.2
.3
.4
.5
.6
.8
1.0
2
3
4
5
Δ/D
1.0
.9
.8
.7
.6
.5
.4
.3
.2
.1
P/Δ
10
8
6
5
4
3
2
1
0.8
0.6
0.5
0.4
P/D
10
9
8
7
6
5
4
3

FIG. 47

and

$$\tau = 0.793 \times 80{,}000 = 62{,}400 \text{ psi} \qquad (10\text{-}21)$$

Using equations (10-9) and (10-11) and Figure 41

$$\frac{P_{CR}}{(EA)_{sF}} = 0.35 \qquad (10\text{-}22)$$

The following physical characteristics, together with conditions (10-2), satisfy the basic requirements (10-1):

$$\left.\begin{aligned} d &= 0.75 \text{ in.} \\ D &= 3 \text{ in.} \\ n &= 20 \\ p_F &= 0.95 \text{ in.} \end{aligned}\right\} \qquad (10\text{-}23)$$

Furthermore, the stress under combined loading

$$\tau = 62{,}400 \text{ psi} < 80{,}000 \text{ psi} \qquad (10\text{-}24)$$

and

$$\frac{P}{(EA)_{sF}} = 0.1212 < 0.35 \qquad (10\text{-}25)$$